LA-UR-97-2905

Approved for public release; distribution is unlimited.

Title: Cascade-Exciton Model Detailed Analysis of Proton Spallation at Energies from 10 MeV to 5 GeV

Author(s): S. G. Mashnik, A. J. Sierk, O. Bersillon, T. Gabriel

Submitted to: http://t2.lanl.gov/publications/publications.html;
a much shorter version is published in:
Nucl. Instr. Meth. A (1998), v. 414, No. 1, p. 68-72;
E-print: nucl-th/9709014

CASCADE-EXCITON MODEL DETAILED ANALYSIS OF PROTON SPALLATION AT ENERGIES FROM 10 MeV TO 5 GeV

S. G. Mashnik* and A. J. Sierk
T-2, Theoretical Division, Los Alamos National Laboratory, Los Alamos, NM 87545

O. Bersillon
CEA, Centre d'Etude de Bruyères-le-Châtel, 91680, Bruyères-le-Châtel, France

and

T. Gabriel
Oak Ridge National Laboratory, Oak Ridge, Tennessee 37831

Abstract

An extended version of the Cascade-Exciton Model (CEM) of nuclear reactions is applied to analyze more than 600 excitation functions for interactions of protons with energies from 10 MeV to 5 GeV with nuclei ^{12}C, ^{14}N, ^{16}O, ^{27}Al, ^{31}P, ^{40}Ca, ^{54}Fe, ^{56}Fe, ^{57}Fe, ^{58}Fe, ^{nat}Fe, ^{59}Co, ^{90}Zr, ^{91}Zr, ^{92}Zr, ^{94}Zr, ^{96}Zr, ^{nat}Zr, and ^{197}Au. The relative roles of different reaction mechanisms and the effects of nuclear structure in the production of specific final nuclides are discussed. A comparison with results of two dozen other popular models and with predictions of several phenomenological systematics is given. Possible reasons for observed discrepancies between some theoretical results and experimental data and possible further improvements to the CEM and to other models are discussed.

*On leave of absence from Bogoliubov Laboratory of Theoretical Physics, Joint Institute for Nuclear Research, Dubna, Russia

Contents

1. Introduction

Precise nuclear data on excitation functions for reactions induced by nucleons, photons, pions, and other projectiles in the energy range up to several GeV are of great importance both for fundamental nuclear physics and for many applications. First, such data are necessary to understand the mechanisms of nuclear reactions, to study the change of properties of nuclei with increasing excitation energy, and to find out the effects of nuclear matter on properties of hadrons and their interactions [1, 2]. Excitation functions are more sensitive to mechanisms of nuclear reactions than are double differential cross sections of emitted particles or their integrals over energy and/or angles. Therefore, excitation functions are a convenient tool to test models of nuclear reactions.

Second, and perhaps more important today, expanded nuclear data bases in this intermediate energy range are required for several important applications [3]–[6]. Recently, one of the most challenging problems requiring reliable nuclear data files is Accelerator-Driven Transmutation Technology (ADTT) for elimination of nuclear waste [7]–[10]. To understand how this problem is important for any country with a strong commitment to commercial nuclear power, and especially for the USA and Russia with large stocks of weapons plutonium, it is sufficient to note that different aspects of transmutation of radioactive wastes were discussed at all recent international [3]–[5] and national (see, e.g. Japanese Meetings [11]–[18]) conferences on nuclear data; a dozen international meetings devoted solely to these problems were organized recently and are planned for the future in many countries (see, e.g. [19]–[28]); work on several ADTT projects is already going on in the nuclear centers of the USA, Europe, Russia, Japan, China, and Korea (see e.g., the recent reviews [7, 8, 29] and invited talks given at the last conference on ADTT held in Kalmar [20]). The problems of Accelerator Transmutation of Waste (ATW) are closely connected with Accelerator-Based Conversion (ABC) [30] aimed to complete the destruction of weapons plutonium, and with Accelerator-Driven Energy Production (ADEP) [9, 31, 32] which proposes to derive fission energy from thorium with concurrent destruction of the long-lived waste and without the production of weapons-usable material, though substantial differences among these systems do exist [30]. Precise nuclear data are needed for solving problems of radiation damage to microelectronic devices [33] and not only of radiation protection of cosmonauts and aviators or workers at nuclear installations, but also to estimate the radiological impact of radionuclides such as ^{39}Ar arising from the operation of fusion reactors or high-energy accelerators and the population dose from such radionuclides retained in the atmosphere so as to avoid possible problems of radiation health effects for the whole population (see, e.g. Ref. [34]). Another important new application which requires large nuclear data libraries at energies up to several hundreds of MeV is the radiation transport simulation of cancer radiotherapy used for selecting the optimal dose in clinical treatment planning systems [35]. Many excitation functions are needed for the optimization of commercial production of radioisotopes widely

used in different branches of nuclear medicine [36, 37], mining and industry [38]. Also, residual product nuclide yields in thin targets irradiated by medium- and high-energy projectiles are extensively used in cosmochemistry and cosmophysics, e.g. to interpret the production of cosmogenic nuclides in meteorites by primary galactic particles [39]–[42], etc.

Nuclear data needed for these purposes may be measured or evaluated using different theoretical models and phenomenological approximations. As of now, there is no sophisticated model or phenomenological systematics available to predict with good accuracy all the data required even for a single given projectile, target, and incident energy, suggesting that the best way to obtain these data may be to measure them.

As far as we know, the most precise and voluminous measurements of proton-induced spallation cross sections for a large range of target nuclei and proton energies up to 2.6 GeV have been performed recently by R. Michel et al. (see Refs. [43, 44] and references therein). A short but comprehensive review of experimental results obtained by 1976 may be found in Ref. [45]. To the best of our knowledge, the most complete compilation of experimental excitation functions is published in Ref. [46] and is available presently in an electronic version as an IBM PC code named NUCLEX [47]. Many data on experimental excitation functions are already included in the EXFOR compilations at the international nuclear data banks. Unfortunately, experiments to measure all necessary data are costly and there are a limited number of facilities available to make such measurements [48, 49]. In addition, most measurements have been performed on targets with the natural composition of isotopes for a given element and, what is more, often only cumulative yields of residual product nuclei are measured. In contrast, to study the physics of nuclear reactions and for many applications, independent yields obtained for isotopically separated targets are needed. Furthermore, only some 80–100 cross section values of residual product nuclei are normally determined in the experiments with heavy nuclei, whereas, according to calculations, over 1000 residual product nuclei are actually produced. Therefore, it turns out that reliable theoretical calculations are required to provide the necessary cross sections [48]–[53].

In some cases, it is more convenient to have fast-computing semiempirical systematics for various characteristics of nuclear reactions instead of using time-consuming, more sophisticated nuclear models. After many years of effort by many investigators, many empirical formulae are now available for spallation cross sections and excitation functions. Many current systematics on excitation functions have been reviewed recently by Koning [53]; most of the old systematics available in 1970 were analyzed in the monograph [54]; the majority of systematics for mass yields, charge dispersions, energy and angular distributions of fragments produced in pA and AA collisions at relativistic energies available in 1985 are presented in the review by Hüfner [55]; useful systematics for different hadron-nucleus interaction cross sections may be found in the recent review [56]. Below, we perform a comparison of some of our results with predictions of only those systematics in Refs. [57]–[60] and direct readers interested

in references on other phenomenological systematics to reviews [53]–[56] and to the recent work by Michel with co-authors [43]. The authors of Ref. [43] have performed a special analysis of predictabilities of different semiempirical systematics and have concluded that "Semiempirical formulas will be quite successful if binding energies are the crucial parameters dominating the production of the residual nuclides, i.e. for nuclides far from stability. In the valley of stability, the individual properties of the residual nuclei, such as level densities and individual excited states, determine the final phase of the reactions. Thus, the averaging approach of all semiempirical formulas will be inadequate." In this case, one has to perform calculations in the framework of reliable models of nuclear reactions. As was mentioned by Silberberg, Tsao, and Shapiro [61], there are also additional cases when Monte Carlo calculations should be used: (1) when it is essential to know the distributions in angle and energy for the ejected nucleons, (2) when the nuclear reaction is induced by neutrons, and (3) when the particles have relatively low energies ($E \leq 60$ MeV).

Different models of the statistical, preequilibrium and intranuclear cascade type or their combinations realized in many computer codes are presently available to calculate excitation functions in different regions of incident energy, targets, and projectiles. To test several available codes for calculation of isotope yields from nucleon-induced reactions at intermediate energies and to find the product nuclide yield domains where each of the codes is most effective, a benchmark calculation has been performed recently by the Theoretical Calculation Code Working Group of the Japanese Nuclear Data Committee [62, 63] and an attempt for intercomparison of some codes for the calculation of excitation functions in this region was done at NEA/OECD during the first step of the *International Code Comparison for Intermediate Energy Nuclear Data* for proton-induced reaction on thin ^{90}Zr and ^{208}Pb targets [48]. A more detailed analysis of predictions of 14 Groups from 12 Laboratories for spallation product yield A- and Z-distributions was performed during the second part *"The Thick Target Benchmark"* of this Intercomparison [64, 65]. As a third step, an *International Codes and Models Intercomparison for Intermediate Energy Activation Yield* which involves a larger number of popular codes was initiated recently [66], at the request of the NEA Nuclear Science Committee. After our work was completed, the report on this Intercomparison was published as an NEA OECD Document [67]. This report gives detailed information about the different models and codes used, surveys extensively the target element and product nuclide coverage of the different contributions, and gives information about the predictive power of models and codes when calculating cross sections for the production of residual nuclides from threshold up to 5 GeV. From this intercomparison it was concluded that "modeling calculations of intermediate energy activation yields on a predictive basis may at best have uncertainties of the order of a factor of two", therefore "there is need for major improvements of models and codes".

During the last two decades, several versions of the Cascade-Exciton Model (CEM) [68, 69] of nuclear reactions have been developed at JINR, Dubna (for an overview, see, e.g. [70]). A large variety of experimental data for reactions induced

by nucleons [71], pions [72], and photons [73] has been analyzed in the framework of the CEM and the general validity of this approach has been confirmed. The recent *International Code Comparison for Intermediate Energy Nuclear Data* [48] has shown that the CEM adequately describes nuclear reactions at intermediate energies and has one of the best predictive powers for double differential cross sections of secondary nucleons as compared to other available modern models (see Tabs. 5 and 6 in the Report [48] and Fig. 7 in Ref. [74]).

Recently, the CEM has been extended to calculate hadron-induced spallation [75] and used to study several excitation functions from reactions induced by protons on ^{12}C, ^{27}Al, ^{56}Fe, ^{59}Co, and ^{197}Au at incident energies up to 200 MeV [75], as well as to analyze the new measurements of yields of residual nuclei from ^{63}Cu, ^{65}Cu, ^{206}Pb, ^{207}Pb, ^{208}Pb, and ^{209}Bi irradiated by 1.5 GeV and 130 MeV protons and from ^{59}Co targets irradiated by 1.2 GeV protons [76]–[79]. Recently, the CEM has been applied successfully by Konshin [80] to calculate the production of several isotopes of U, Pa, Th, and Ac from p+^{238}U reactions at 0.34, 0.66, and 1.6 GeV, as well as to calculate yields of U, Pa, and Th isotopes from ^{235}U targets and yields of Pa, Th, and Ac isotopes from p+^{232}Th interactions at 0.68 GeV. Nevertheless, previously the CEM has not been applied to study all possible excitation functions in large ranges of incident energies and mass-numbers of targets; therefore, its predictive power and applicability to evaluate arbitrary spallation cross sections was unknown.

Here we apply the extended version of the CEM [75] to perform a detailed analysis of more than 600 reactions induced by protons from 10 MeV to 5 GeV on nuclei of ^{12}C, ^{14}N, ^{16}O, ^{27}Al, ^{31}P, ^{40}Ca, ^{54}Fe, ^{56}Fe, ^{57}Fe, ^{58}Fe, ^{nat}Fe, ^{59}Co, ^{90}Zr, ^{91}Zr, ^{92}Zr, ^{94}Zr, ^{96}Zr, ^{nat}Zr, and ^{197}Au with several aims: a) to determine the capability of the present version of the CEM realized in the code CEM95 to predict unknown excitation functions, b) to compare our results with calculations of other popular models and phenomenological systematics and with available experimental data, that may serve as an independent benchmark and a guidance for further evaluation of data files, and c) to study nuclear reaction mechanisms involved in the production of specific nuclides, to understand the dependence of our results on the physics incorporated in the code, on the values of input parameters and on the specific mode of calculation with the hope of identifying possible improvements to CEM95 and to other codes to improve their predictive powers. This last point was the major reason for our work.

2. Extended Version of the CEM Realized in the Code CEM95

A detailed description of the CEM may be found in Refs. [68, 69]; therefore, only its basic assumptions and the differences of the extended version used here from the standard one [68] will be outlined below. The CEM assumes that the reactions occur in three stages. The first stage is the intranuclear cascade in which primary and secondary particles can be rescattered several times prior to absorption by, or escape from the nucleus. The excited residual nucleus remaining after the emission of the cascade particles determines the particle-hole configuration that is the starting point for the second, preequilibrium stage of the reaction. The subsequent relaxation of the nuclear excitation is treated in terms of the exciton model of preequilibrium decay which includes the description of the equilibrium evaporative third stage of the reaction.

In a general case, the three components may contribute to any experimentally measured quantity. In particular, for the inclusive cross sections to be discussed later, we have

$$\sigma(p)dp = \sigma_{in}[N^{cas}(p) + N^{prq}(p) + N^{eq}(p)]dp \ . \tag{1}$$

The inelastic cross section σ_{in} is not taken from the experimental data or independent optical model calculations, but is calculated within the cascade model itself by the Monte Carlo method and is equal to the geometrical cross section of the targer nucleus σ_{geom} times the ratio of the total number of inelastic interactions N_{in} to the total number of elastic N_{el} and inelastic N_{in} simulated events: $\sigma_{in} = \sigma_{geom}N_{in}/(N_{in}+N_{el})$; $\sigma_{geom} = \pi R^2$, where R is the radius of the last zone of the target nucleus (for details, see [54]).

The cascade stage of the interaction is described by the standard version of the Dubna intranuclear cascade model (ICM) [54]. All the cascade calculations are carried out in a three-dimensional geometry. The nuclear matter density $\rho(r)$ is described by a Fermi distribution with two parameters taken from the analysis of electron-nucleus scattering, namely

$$\rho(r) = \rho_p(r) + \rho_n(r) = \rho_0\{1 + exp[(r-c)/a]\} \ , \tag{2}$$

where $c = 1.07A^{1/3}$ fm, A is the mass number of the target, and $a = 0.545$ fm. For simplicity, the target nucleus is divided by concentric spheres into seven zones in which the nuclear density is considered to be constant. The energy spectrum of the target nucleons is estimated in the perfect Fermi gas approximation with the local Fermi energy $T_F(r) = \hbar^2[3\pi^2\rho(r)]^{2/3}/(2m_N)$, where m_N is the nucleon mass. The influence of intranuclear nucleons on the incoming projectile is taken into account by adding to its laboratory kinetic energy an effective real potential V, as well as by considering the Pauli principle which forbids a number of intranuclear collisions and effectively increases the mean free path of cascade particles inside the target. For incident nucleons $V \equiv V_N(r) = T_F(r) + \epsilon$, where $T_F(r)$ is the corresponding

Fermi energy and ϵ is the mean binding energy of the nucleons ($\epsilon \simeq 7$ MeV [54]). For pions, in the Dubna ICM one usually uses [54] a square-well nuclear potential with the depth $V_\pi \simeq 25$ MeV, independently of the nucleus and pion energy. The interaction of the incident particle with the nucleus is approximated as a series of successive quasifree collisions of the fast cascade particles (N or π) with intranuclear nucleons:

$$\begin{aligned} NN \to NN, \qquad NN \to \pi NN, \qquad NN \to \pi_1, \cdots, \pi_i NN \ , \\ \pi N \to \pi N, \qquad \pi N \to \pi_1, \cdots, \pi_i N \qquad (i \geq 2) \ . \end{aligned} \tag{3}$$

To describe these elementary collisions, one uses experimental cross sections for the free NN and πN interactions, simulating angular and momentum distributions of secondary particles using special polynomial expressions with energy-dependent coefficients [54] and one takes into account the Pauli principle.

The Pauli exclusion principle at the cascade stage of the reaction is handled by assuming that nucleons of the target occupy all the energy levels up to the Fermi energy. Each simulated elastic or inelastic interaction of the projectile (or of a cascade particle) with a nucleon of the target is considered forbidden if the "secondary" nucleons have energies smaller than the Fermi energy. If they do, the trajectory of the particle is traced farther from the forbidden point and a new interaction point, a new partner and a new interaction mode are simulated for the traced particle, etc., until the Pauli principle is satisfied or the particle leaves the nucleus. Besides the elementary processes (3), the Dubna ICM also takes into account pion absorption on nucleon pairs

$$\pi NN \to NN. \tag{4}$$

The momenta of two nucleons participating in the absorption are chosen randomly from the Fermi distribution, and the pion energy is distributed equally between these nucleons in the center-of-mass system of the pion and nucleons participating in the absorption. The direction of motion of the resultant nucleons in this system is taken as isotropically distributed in space. The effective cross section for absorption is related (but not equal) to the experimental cross sections for pion absorption by deuterons.

In the standard version of the Dubna ICM used in the code CEM95 the kinetic energy of cascade particles is increased or decreased as they move from one potential region (zone) to another, but their directions remain unchanged. That is, in our calculations, refraction or reflection of cascade nucleons at potential boundaries is neglected.

The standard version of the Dubna ICM does not take into account the so-called "trawling" effect [54]. That is, in the beginning of the simulation of each event, the nuclear density distributions for the protons and neutrons of the target are calculated according to Eq. (2) and a further decrease of the nuclear density with the emission of cascade particles is not taken into account. Our detailed analysis (see, e.g. [71, 72] and references therein) of different characteristics of nucleon- and pion-induced

reactions for targets from C to Am has shown that this effect may be neglected at incident energies below about 5 GeV. At higher incident energies the progressive decrease of nuclear density with the development of the intranuclear cascade has a strong influence on the calculated characteristics and this effect has to be taken into account [54]. Therefore, to use the CEM approach at incident energies higher than about 5 GeV, the standard version of Dubna ICM has to be replaced by a version which includes the non-linear trawling effect of the local reduction of the nuclear density during the development of the cascade [54]. The standard version of the Dubna ICM is described in detail in the monograph [54] and more briefly, in the review [81] and in the recent book by Iljinov, Kazarnovsky, and Paryev [82]. A detailed comparison of the Dubna ICM with the well known Bertini ICM developed at Oak Ridge National Laboratory [83] and with the popular version developed at Brookhaven National Laboratory and Columbia University by Chen et al. [84] is made in Ref. [85].

An important point of the CEM is the condition for transition from the intranuclear cascade stage to preequilibrium processes. In a conventional cascade-evaporation model, cascade nucleons are traced down to some minimal energy, the cut-off energy T_{cut} being about 7–10 MeV, below which particles are considered to be absorbed by the nucleus. Calculations [54] show that a reasonable variation of the value T_{cut} does not significantly change the average number of particles in a nuclear collision. As a zero-order approximation to the CEM, this "sharp cut-off" method for passing to preequilibrium nuclear decay was also considered in Refs. [68, 69] and we show an example of this case below, in Figs. 1 and 2. In a real case, the cut-off is expected to be somewhat smoothed [68]. Moreover, when we move towards lower energies, the relative contributions of particles captured by peripheral and interior regions of a nucleus are changed. But this fact is completely outside the scope of the sharp cut-off approximation. Therefore, in the CEM [68], it was proposed to relate the condition for a cascade particle to be captured by the nucleus to the similarity of the imaginary part of the optical potential calculated in the cascade model $W_{opt.mod.}(r)$ to its experimental value $W_{opt.exp.}(r)$ obtained from analysis of data on particle-nucleus elastic scattering. This was inspired by a comparison of the classical kinetic equation describing the intranuclear cascade with its quantum-mechanical form in which the particle transport through nuclear matter is governed by the optical potential (for more details, see Ref. [68]).

In the "weak-coupling" approximation, the imaginary part of the optical potential can be expressed in terms of the cross section σ for scattering of a particle on target nucleons

$$W_{opt}(r) = -\frac{\hbar}{2} < \sigma(v_{rel}) v_{rel} > \rho^T(r) \ . \tag{5}$$

Here, the averaging is carried out over the spectrum of target nucleons and includes the Pauli exclusion principle. Practically, in the version of the CEM realized in the code CEM95, for $\sigma(v_{rel})$ we take the average of 50 proton-proton and 50 proton-neutron scattering cross sections calculated by the Monte Carlo simulation method

and introduce a factor η effectively taking into account the Pauli principle exactly as is done in the Fermi-gas model (see, e.g. [86])[1]

$$\sigma(v_{rel}) = \frac{1}{2}[\sigma_{pp}(v_{rel}) + \sigma_{pn}(v_{rel})]\eta(T_F/T) \ , \text{ where} \tag{6}$$

$$\eta(x) = \begin{cases} 1 - \frac{7}{5}x, & \text{if } x \leq 0.5 \ , \\ 1 - \frac{7}{5}x + \frac{2}{5}x(2 - \frac{1}{x})^{5/2}, & \text{if } x > 0.5 \ . \end{cases} \tag{7}$$

Here, v_{rel} is the relative velocity of the cascade nucleon and the target nucleon in units of the speed of light and T is the kinetic energy of the cascade nucleon. The free-particle interaction cross sections $\sigma_{pp}(v_{rel})$ and $\sigma_{pn}(v_{rel})$ in Eq. (6) are estimated using the relations suggested by Metropolis et al. [87]

$$\begin{aligned} \sigma_{pp}(v_{rel}) &= \frac{10.63}{v_{rel}^2} - \frac{29.92}{v_{rel}} + 42.9 \ , \\ \sigma_{pn}(v_{rel}) &= \frac{34.10}{v_{rel}^2} - \frac{82.2}{v_{rel}} + 82.2 \ , \end{aligned} \tag{8}$$

where the cross sections are given in mb. Formula (5) is valid only at sufficiently high energies and for the nuclear interior. As is seen from Eq. (5) the radial behavior of the density $\rho^T(r)$ follows that of the optical potential. In a general case, the $\rho^T(r)$ function lags behind $W_{opt}(r)$ due to the finite radius of particle interactions and the non-linear relation of W_{opt} to ρ^T. Since at present these effects cannot be considered in a consistent manner, the imaginary part of the optical potential for cascade particles *is defined* in the CEM by relation (5). To allow for the effect of the non-linear relation between W_{opt} and ρ^T, in the CEM [68] it was suggested to use for $\rho^T(r)$ a two parameter Fermi distribution like Eq. (2), but with parameters corresponding to the volume part of the imaginary optical potential taken from the analysis of experimental data. In CEM95 this idea is implemented as: following Ref. [88] we use Eq. (2) to calculate $\rho^T(r)$, with $c \equiv R_I = 1.26A^{1/3}$ fm and $a \equiv a_I = 0.58$ fm for cascade neutrons, and $c \equiv R_I = 1.32A^{1/3}$ fm and $a \equiv a_I = 0.51 + 0.7(N - Z)/A$ fm for cascade protons. For the experimental values of the imaginary part of the optical potential $W_{opt.exp.}(r)$, in CEM95 one employs the results of Becchetti and Greenlees [88] for protons and neutrons with $T \leq 25$ MeV, and at higher energies, the potential by Menet et al. [89] for protons and by Marshak et al. [90] for neutrons. Such a realization serves only as one possible approach from other possibilities. It should be added that the conditions for validity of the cascade and optical models do not coincide [68]; the cascade model considers the scattering from bound nucleons rather than from a potential well as the optical model does. Thus, the agreement between $W_{opt.mod.}$ and $W_{opt.exp.}$ is assumed to occur when the proximity parameter

$$\mathcal{P} = \mid (W_{opt.mod.} - W_{opt.exp.})/W_{opt.exp.} \mid \tag{9}$$

[1] Unfortunately, formulae (5) and (7) were published in Ref. [68] with some misprints; in the previous publication [69], they are printed correctly.

becomes small enough. In CEM95, we use a fixed value $\mathcal{P} = 0.3$ extracted from the analysis [68]–[72] of experimental proton- and pion-nucleus data at low and intermediate energies.

From a physical point of view, such a smooth transition from the cascade stage of the reaction seems to be more attractive than the "sharp cut-off" method. In addition, as was shown in Ref. [68], this improves the agreement between the calculated and experimental spectra of secondary nucleons, especially for low incident energies and backward angles of the detected nucleons (see e.g. Fig. 11 of Ref. [68]).

Let us note here that in the CEM the initial configuration for the preequilibrium decay (number of excited particles and holes, i.e. excitons $n_0 = p_0 + h_0$, excitation energy E_0^*, linear momentum $\boldsymbol{P}_0$ and angular momentum $\boldsymbol{L}_0$ of the nucleus) differs significantly from that usually postulated in exciton models. Our calculations [68, 74, 91] have shown that the distributions of residual nuclei remaining after the cascade stage of the reaction, i.e. before the preequilibrium emission, with respect to n_0, p_0, h_0, E_0^*, $\boldsymbol{P}_0$, and $\boldsymbol{L}_0$ are rather broad.[2]

As an example, Fig. 1 shows distributions of residual nuclei remaining after the cascade stage of the reaction p(1 GeV)+^{94}Mo that serve as input for the second, preequilibrium stage of the CEM with respect to mass A and charge Z numbers, excitation energy E^*, momentum $|\boldsymbol{P}_0|$ and angular momentum $|\boldsymbol{L}_0|$, numbers of excitons n_0, exciton-particles p_0, and exciton-holes h_0 calculated as proposed in the CEM (solid histograms) and using the "sharp cut-off" method as in a conventional ICM (dashed histograms). One can see that all distributions calculated in both the CEM and ICM approaches are very broad. Let us note here that as a rule, the smooth method of the CEM leads to an earlier completion of the cascade stage as compared to that of the ICM. As a result of this, the distributions with respect to A, Z, n_0, and especially with respect to p_0 and h_0, calculated by the CEM are narrower than those of the ICM. The distributions with respect to $|\boldsymbol{P}_0|$ and $|\boldsymbol{L}_0|$ calculated by both methods are very similar, while the distribution with respect to E_0^* of the CEM is broader than that of the ICM. Our calculations show that the difference in the distributions of residual nuclei calculated by the CEM and ICM increases with decreasing incident energy of the projectile and vice versa. Fig. 2 shows angle-integrated energy spectra of all secondary particles emitted from this reaction calculated in the CEM using both methods of finishing the cascade stage of the reaction. One can see that for this incident energy of 1 GeV the spectra of

[2]Unfortunately, this fact was misunderstood by the authors of the code HETC-3STEP [92]. In spite of the fact that it has been stressed explicitly, and figures with distributions of excited nuclei after the cascade stage of a reaction with respect to the number of excitons and other characteristics were shown in a number of publications (see, e.g. Fig. 5 in Ref. [68], Fig. 1 in Ref. [91], p. 109 in Ref. [74], p. 706 in Ref. [71]), the authors of Ref. [92] misstated this fact as *"Gudima et al. assumed the state of two particles and one hole at the beginning $\cdots$ Hence, their assumption is not valid for the wide range of incident energy"*, claiming this as a weakness of the CEM and a priority of the code HETC-3STEP, where smooth distributions of excited nuclei after the cascade stage of reactions with respect to n_0 are used. This had already been suggested and used in the CEM [68, 69].

nucleons calculated by both methods are almost the same. Let us note again that at incident energies below ~ 100 MeV the difference between nucleon spectra calculated by these methods is larger. As one can see from Figs. 3 and 11 of Ref. [68], the CEM approach gives a better agreement with the experimental data. The spectra of pions are just the same, as both methods of finishing the cascade do not deal at all with pions. But the spectra of composite particles calculated with the CEM method are significantly higher and broader than those of the ICM. This is caused mainly by the difference in the distributions of residual nuclei with respect to p_0 and h_0 (see Fig. 1).

The subsequent interaction stages (preequilibrium and equilibrium) of nuclear reactions are considered in the CEM in the framework of an extension of the modified exciton model [93, 94]. At the preequilibrium stage of a reaction we take into account all possible nuclear transitions changing the number of excitons n with $\Delta n = +2, -2$, and 0, as well as all possible multiple subsequent emissions of n, p, d, t, ^{3}He, and ^{4}He. The corresponding system of master equations describing the behavior of a nucleus at the preequilibrium stage is solved by the Monte Carlo technique [68, 69].

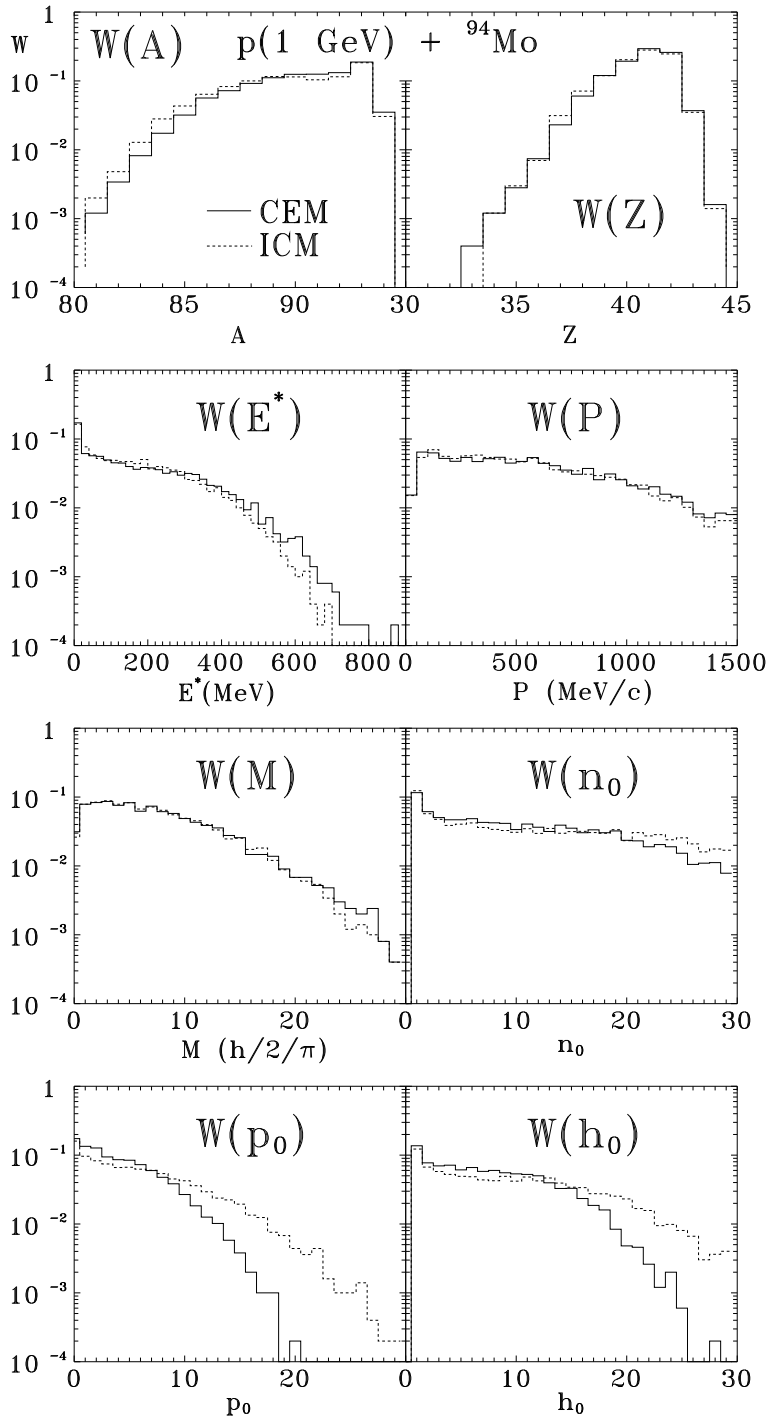

Fig. 1. Distributions of excited residual nuclei remaining after the cascade stage of the reaction p(1 GeV)+^{94}Mo with respect to the mass A and charge Z numbers, excitation energy E^*, momentum $|\boldsymbol{P}_0|$ and angular momentum $|\boldsymbol{L}_0|$ (labeled in the plot as P and M), number of excitons n_0, exciton-particles p_0, and exciton-holes h_0. Solid histograms correspond to a completion of the cascade as proposed in the CEM [67,68], dashed histograms are calculated in the "sharp cut-off" approximation in which a cascade particle is absorbed when its energy falls below a fixed value.

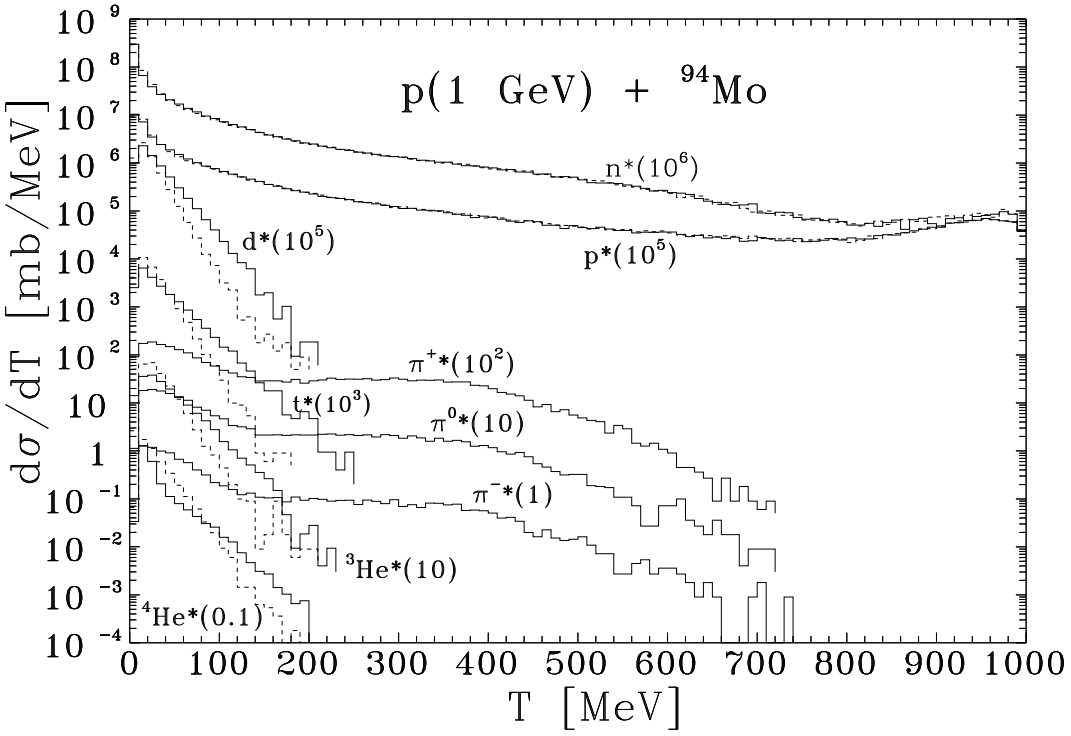

Fig. 2. Angle-integrated energy spectra of secondary particles from the reaction p(1 GeV)+^{94}Mo. As in Fig. 1, solid and dashed histograms are calculated with the completion of the cascade stages of the reactions according to the CEM [68, 69] and to a conventional ICM, respectively. The pion spectra are identical for both models.

For a preequilibrium nucleus with excitation energy E and number of excitons $n = p + h$, the partial transition probabilities changing the exciton number by Δn are

$$\lambda_{\Delta n}(p,h,E) = \frac{2\pi}{\hbar}|M_{\Delta n}|^2 \omega_{\Delta n}(p,h,E) \ . \tag{10}$$

The emission rate of a nucleon of the type j into the continuum is estimated according to the detailed balance principle

$$\begin{aligned} \Gamma_j(p,h,E) &= \int\limits_{V_j^c}^{E-B_j} \lambda_c^j(p,h,E,T)dT \ , \\ \lambda_c^j(p,h,E,T) &= \frac{2s_j+1}{\pi^2\hbar^3}\mu_j \Re_j(p,h)\frac{\omega(p-1,h,E-B_j-T)}{\omega(p,h,E)} T\sigma_{inv}(T) \ , \end{aligned} \tag{11}$$

where s_j, B_j, V_j^c, and μ_j are the spin, binding energy, Coulomb barrier, and reduced mass of the emitted particle, respectively. The factor $\Re_j(p,h)$ ensures the condition for the exciton chosen to be the particle of type j and can easily be calculated by the Monte Carlo technique.

Assuming an equidistant level scheme with the single-particle density g, we have the level density of the n-exciton state as [95]

$$\omega(p,h,E) = \frac{g(gE)^{p+h-1}}{p!h!(p+h-1)!} \ . \tag{12}$$

This expression should be substituted into Eq. (11). For the transition rates (10), one needs the number of states taking into account the selection rules for intranuclear exciton-exciton scattering. The appropriate formulae have been derived by Williams [96] and later corrected for the exclusion principle and indistinguishability of identical excitons in Refs. [97, 98]:

$$\begin{aligned}
\omega_+(p,h,E) &= \frac{1}{2}g\frac{[gE-\mathcal{A}(p+1,h+1)]^2}{n+1}\left[\frac{gE-\mathcal{A}(p+1,h+1)}{gE-\mathcal{A}(p,h)}\right]^{n-1} \ , \\
\omega_0(p,h,E) &= \frac{1}{2}g\frac{[gE-\mathcal{A}(p,h)]}{n}[p(p-1)+4ph+h(h-1)] \ , \\
\omega_-(p,h,E) &= \frac{1}{2}gph(n-2) \ ,
\end{aligned} \tag{13}$$

where $\mathcal{A}(p,h) = (p^2+h^2+p-h)/4 - h/2$. By neglecting the difference of matrix elements with different Δn, $M_+ = M_- = M_0 = M$, we estimate the value of M for a given nuclear state by associating the $\lambda_+(p,h,E)$ transition with the probability for quasi-free scattering of a nucleon above the Fermi level on a nucleon of the target nucleus. Therefore, we have

$$\frac{<\sigma(v_{rel})v_{rel}>}{V_{int}} = \frac{\pi}{\hbar}|M|^2\frac{g[gE-\mathcal{A}(p+1,h+1)]}{n+1}\left[\frac{gE-\mathcal{A}(p+1,h+1)}{gE-\mathcal{A}(p,h)}\right]^{n-1} \ . \tag{14}$$

Here, V_{int} is the interaction volume estimated as $V_{int} = \frac{4}{3}\pi(2r_c + \lambda/2\pi)^3$, with the De Broglie wave length $\lambda/2\pi$ corresponding to the relative velocity $v_{rel} = \sqrt{2T_{rel}/m_N}$. A value of the order of the nucleon radius is used for r_c in CEM95: $r_c = 0.6$ fm.

The averaging in the left-hand side of Eq. (14) is carried out over all excited states taking into account the Pauli principle in the approximation

$$<\sigma(v_{rel})v_{rel}> \simeq <\sigma(v_{rel})><v_{rel}> \ . \tag{15}$$

The averaged cross section $<\sigma(v_{rel})>$ is calculated according to Eqs. (6–8). The relative kinetic energy of colliding particles necessary to calculate $<v_{rel}>$ and the factor η in Eqs. (6,7) is estimated in the so-called "right-angle collision" approximation [93], i.e. as a sum of the mean kinetic energy of an excited particle (exciton) measured from the bottom of the potential well $T_p = T_F + E/n$ plus the mean kinetic energy of an intranuclear nucleon partner $T_N = 3T_F/5$, that is $T_{rel} = T_p + T_N = 8T_F/5 + E/n$. Combining (10), (12) and (14), we get finally for the transition rates:

$$\lambda_+(p,h,E) = \frac{<\sigma(v_{rel})v_{rel}>}{V_{int}} \ ,$$

$$\lambda_0(p,h,E) = \frac{<\sigma(v_{rel})v_{rel}>}{V_{int}}\frac{n+1}{n}\Big[\frac{gE-\mathcal{A}(p,h)}{gE-\mathcal{A}(p+1,h+1)}\Big]^{n+1}\frac{p(p-1)+4ph+h(h-1)}{gE-\mathcal{A}(p,h)} ,$$

$$\lambda_-(p,h,E) = \frac{<\sigma(v_{rel})v_{rel}>}{V_{int}}\Big[\frac{gE-\mathcal{A}(p,h)}{gE-\mathcal{A}(p+1,h+1)}\Big]^{n+1}\frac{ph(n+1)(n-2)}{[gE-\mathcal{A}(p,h)]^2} . \quad (16)$$

To economize on computing time, in the version of CEM95 used here the calculations are performed with the approximation $\mathcal{A}(p,h)=0$. Our experience with many years of calculations in the framework of the CEM shows that at incident energies of about 100 MeV and above the use of such an approach does not significantly change the final results but allows us to reduce significantly the computing time.

The CEM predicts forward peaked (in the laboratory system) angular distributions for secondary particles. Primarily, this is due to the high asymmetry of the cascade component (for ejected nucleons and pions). Another possibility for forward peaked distributions of nucleons and composite particles emitted during the preequilibrium interaction stage is related to retention of some memory of the projectile's direction. It means that along with energy conservation we need to take into account the conservation of linear momentum $\boldsymbol{P}_0$ at each step when a nuclear state is getting complicated. In a phenomenological approach this can be realized in different ways [68, 69]. The simplest way consists in sharing an incoming momentum $\boldsymbol{P}_0$ (similarly to energy E_0^*) between an ever-increasing number of excitons interacting in the course of equilibration of the nuclear system. In other words, the momentum $\boldsymbol{P}_0$ should be attributed only to n excitons rather than to all A nucleons. Then, particle emission will be symmetric in the rest frame of the n-exciton system, but will have some forward peaking in both the laboratory and center-of-mass reference frames.

In another approach to the asymmetry effect for the preequilibrium component, the nuclear state with a given excitation energy E^* should be specified not only by the exciton number n but also by the momentum direction Ω. Following Ref. [99], the master equation (11) from Ref. [68] can be generalized for this case provided that the angular dependence for the transition rates λ_+, λ_0, and λ_- (Eq. (16) is factorized. In accordance with Eqs. (14) and (15), in the CEM it is assumed that

$$<\sigma> \rightarrow <\sigma> F(\Omega) ,$$

where

$$F(\Omega) = \frac{d\sigma^{free}/d\Omega}{\int d\Omega' d\sigma^{free}/d\Omega'} .$$

The scattering cross section $d\sigma^{free}/d\Omega$ is assumed to be isotropic in the reference frame of the interacting excitons, thus resulting in an asymmetry in the laboratory frame. This calculational scheme is easily realized by the Monte Carlo technique. Calculations [68, 69] have shown that both methods give rise to similar distributions for preequilibrium particles. In comparing with experiment, the details of these distributions become more obscured due to the contribution of cascade and evaporative (equilibrium) components. In CEM95 we use the second method to allow for the asymmetry of a particle emitted at the preequilibrium interaction stage.

Complex particles can be produced in nucleon-nucleus reactions at different interaction stages and due to many mechanisms. These may include fast processes like direct knock-out, pick-up reactions or final state interactions resulting in coalescence of nucleons into a complex particle. CEM95 neglects all these processes at the cascade interaction stage. Therefore, fast complex particles can appear in our approach only due to preequilibrium processes. We assume that in the course of a reaction p_j excited particles are able to condense with probability γ_j forming a complex particle which can be emitted during the preequilibrium state. A modification of Eq. (11) for the complex particle emission rates is described in detail in Refs. [68, 69]. The "condensation" probability γ_j is estimated as the overlap integral of the wave function of independent nucleons with that of the complex particle (cluster)

$$\gamma_j \simeq p_j^3 (V_j/V)^{p_j - 1} = p_j^3 (p_j/A)^{p_j - 1} \ . \tag{17}$$

This is a rather crude estimate and we will see below that it does not provide a good prediction of emission of preequilibrium α-particles. In the usual way the values γ_j are taken from fitting the theoretical preequilibrium spectra to the experimental ones, which gives rise to an additional, as compared to (17), dependence of the factor γ_j on p_j and excitation energy (see, e.g. Refs. [100, 101]). In virtue of the variety of complex particle emission mechanisms mentioned above, we do not see a physical justification for such a fitting procedure [68, 69]. Therefore, the condensation probability γ_j *was defined* in the CEM by the relation (17) just as a first approximation. The single-particle density g_j for complex particle states is found in the CEM by assuming the complex particles move freely in the uniform potential well whose depth is equal to the binding energy of this particle in a nucleus [68]

$$g_j(T) = \frac{V(2s_j + 1)(2\mu_j)^{3/2}}{4\pi^2 \hbar^3} (T + B_j)^{1/2} \ . \tag{18}$$

As we stated previously, this is a crude approximation. Another approach is to assume preformed alpha clusters, whose preformation probability is adjusted to fit observed alpha particle spectra [102, 103]. The clusters are assumed to be single excitons with a level density $g_\alpha = g/4$.

The angular distributions of preequilibrium complex particles are assumed [68] to be similar to those for the nucleons in each nuclear state. However, the angular distributions summed up over all populated nuclear states will certainly differ, because the branching ratios for different particles depend in detail on the decaying nuclear states.

By "preequilibrium particles" we mean particles which have been emitted after the cascade stage of the reaction but before achieving statistical equilibrium at a time t_{eq}, which is fixed by the condition $\lambda_+(n_{eq}, E) = \lambda_-(n_{eq}, E)$ from which we get $n_{eq} \simeq \sqrt{2gE}$. At $t \geq t_{eq}$ (or $n \geq n_{eq}$), the behavior of the remaining excited compound nucleus is described in the framework of both the Weisskopf-Ewing statistical theory of particle evaporation [104] and fission competition according to the Bohr and Wheeler theory [105].

In the initial version of the CEM [68, 69], which was used mainly to describe spectra of secondary particles from interactions of nucleons with not too heavy targets at energies of about 100 MeV and below, several effects such as pairing energy, angular momentum of preequilibrium and evaporated particles and rotational energies of compound and precompound nuclei, as well as fission of compound nuclei were not taken into account and calculations were performed with constant values for the level density parameters $a = Const \cdot A$.[3] Such an approach was quite justified for those problems that have been solved in the framework of that version [68, 69]. It is well known from the literature that excitation functions are more sensitive to the physics of any model and to the values of input parameters than are inclusive spectra of secondary particles.

To be able to analyze reactions with heavy targets and to describe accurately excitation functions over a wider range of incident particle energy, the CEM has been extended recently [75]. The extended version incorporates the competition between evaporation and fission of compound nuclei, takes into account pairing energies, considers the angular momentum of preequilibrium and evaporated particles and the rotational energy of excited nuclei, and can use more realistic nuclear level densities (with Z, N, and E^* dependences of the level density parameter). In the version of the CEM realized in the code CEM95, the following models for the level density parameters are incorporated: Malyshev's [106] systematics for $a = a(Z, N)$ and 8 parameter sets for $a = a(Z, N, E^*)$; two from Ignatyuk et al. [107, 108], two from Cherepanov and Iljinov [109], and four from Iljinov et al. [110]. The possibility of calculating with $a = a_0 A$, where a_0 is a constant input value (as in the earlier versions) is also provided. In CEM95, it is possible to calculate with three different shell and pairing corrections, namely those due to Cameron [111], Truran, Cameron and Hilf [112], and Myers and Swiatecki [113]. A comprehensive comparison of level density parameters (and of level densities themselves, for several excited compound nuclei) calculated in the framework of these models with the available experimental data may be found in the recent review [114].

The following models for fission barriers are incorporated in CEM95: the phenomenological approach of Barashenkov et al. [115], the semiphenomenological approach of Barashenkov and Gereghi [116], the liquid-drop model (LDM) with Myers and Swiatecki's parameters [113], the LDM with Pauli and Ledergerber's parameters [117], the single-Yukawa modified LDM of Krappe and Nix [118], the Yukawa-plus-exponential modified LDM of Krappe, Nix, and Sierk [119], the subroutine BARFIT of Sierk [120] which provides macroscopic fission barriers of rotating nuclei in the Yukawa-plus-exponential modified LDM [119], double-humped fission barriers for transuranium nuclides as proposed in Ref. [121], giving a fixed input value for single-humped fission barriers B_f, and giving fixed input values B_f^A and B_f^B for double-humped fission barriers.

[3] Here and everywhere below, the level density parameter a is defined in units of 1/MeV, but for the sake of brevity we do not explicitly write this unit.

CEM95 allows one to calculate both without taking into account the dependence of B_f on the excitation energy E^* and with the dependences $B_f(E^*)$ proposed by Barashenkov et al. [122] and by Sauer, Chandra, and Mosel [123].

With CEM95 one may calculate either without taking into account the dependence of B_f on the angular momentum L of a fissioning nucleus, or with the dependences $B_f(L)$ estimated by a phenomenological approach with the values for the moment of inertia of a nucleus at the nonrotating saddle-point from Ref. [124] or from [125], or by using the subroutine BARFIT of Sierk [120]. To calculate B_f, three different models [111]–[113] for ground-state shell and pairing corrections may be used.

A detailed comparison of these different fission barriers and an analysis in the framework of the extended version of the CEM of nuclear fissilities and fission cross sections for several nuclei, including a comparison with available experimental data, are given in the recent review [126]. An example of the dependence of calculated ^{238}U proton-induced fission cross sections on these different models for fission barriers and level density parameters may be found in Ref. [80].

Every model for fission barriers, shell and pairing corrections, and level density parameter a incorporated in the code CEM95 may be selected by input switches that permit one to perform calculations either with "the best" set of parameters for predictions in a wide range of incident energy and/or target nuclei, or to choose a specific model to analyze a specific characteristic in a special case.

We used in our recent extension of the CEM [75, 114, 126] many results of Iljinov et al. [110], [127]–[129], who realized similar schemes in their cascade-evaporation models. In the Weisskopf-Ewing statistical theory of particle emission [104] and Bohr and Wheeler theory of fission [105], the partial widths Γ_j for the emission of a particle j ($j \equiv$ n, p, d, t, ^{3}He, ^{4}He) and Γ_f for fission are expressed by the approximate formulas (units: $\hbar = c = 1$; see, e.g., [110, 129]):

$$\Gamma_j = \frac{(2s_j+1)m_j}{\pi^2\rho_c(U_c)} \int\limits_{V_j}^{U_j-B_j} \sigma_{inv}^j(E)\rho_j(U_j-B_j-E)EdE \ , \tag{19}$$

$$\Gamma_f = \frac{1}{2\pi\rho_c(U_c)} \int\limits_{0}^{U_f-B_f} \rho_f(U_f-B_f-E)dE \ . \tag{20}$$

Here ρ_c, ρ_j, and ρ_f are the level densities of the compound nucleus, the residual nucleus produced after the emission of the j-th particle, and of the fissioning nucleus at the fission saddle point, respectively; m_j, s_j and B_j are the mass, spin and the binding energy of the j-th particle, respectively, and B_f is the fission barrier height. The code CEM95 calculates the binding energies of particles using the Cameron formulas [111], and $\sigma_{inv}^j(E)$ is the inverse cross-section for absorption of the j-th particle with kinetic energy E by the residual nucleus. The approximation proposed

by Dostrovsky et al. [130] is used,

$$\sigma_{inv}^{j}(E) = \sigma_{geom}^{j}\alpha_j \left(1 + \frac{\beta_j}{E}\right) \ , \tag{21}$$

where

$$\sigma_{geom}^{j} = \pi R_j^2 \ ; \ R_j = \tilde{r}_0 A_{fj}^{1/3} \ ; \ \tilde{r}_0 = 1.5 \text{ fm} \ ; \tag{22}$$

$$\alpha_n = 0.76 + 2.2 A_{fj}^{-1/3} \ ;$$

$$\beta_n = (2.12 A_{fj}^{-2/3} - 0.05)/\alpha_n \ .$$

For charged particles $\beta_j = -V_j$, where V_j is the effective Coulomb barrier and the constants α_j are calculated for a given nucleus by interpolating the values of Ref. [130]. Following Refs. [127, 128], the angular momentum dependence of the level density is approximated by $\rho(E^*, L) = \rho(U, 0)$, where $U = E^* - E_R$ and E_R are the "thermal" and rotational energies of the nucleus, respectively;

$$U_c = E^* - E_R^c - \Delta_c \ ; \ U_j = E^* - E_R^j - \Delta_j \ ; \ U_f = E^* - E_R^f - \Delta_f \ .$$

Here, E^* is the total excitation energy of the compound nucleus; E_R^c, E_R^j, and E_R^f are the rotational energies for the compound, residual, and fissioning nucleus at the saddle point, respectively, and they are determined as:

$$E_R^{gs} = \frac{L(L+1)\hbar^2}{2J_{rb}},$$

$$E_R^{sp} = \frac{L(L+1)\hbar^2}{2J_{sp}}, \tag{23}$$

$$J_{rb} = 0.4 m_N r_0^2 A^{5/3}. \tag{24}$$

Here, L is the angular momentum of the nucleus, m_N is the nucleon mass, and the values calculated and plotted in [124] or tabulated in [125] are used for the moment of inertia of a nucleus at the saddle-point J_{sp}.

Following Ref. [110], the pairing energies of the compound nucleus Δ_c, of the residual nucleus Δ_j, and of the fission saddle point Δ_f are estimated as:

$$\Delta_c = \chi_c \cdot 12/\sqrt{A_c} \ ; \ \Delta_j = \chi_j \cdot 12/\sqrt{A_{fj}} \ ; \text{ and } \Delta_f = \chi_c \cdot 14/\sqrt{A_c} \text{ (in MeV)}. \tag{25}$$

$A_{fj} = A_c - A_j$, where A_c and A_j are the mass numbers of the compound nucleus and of the j-th particle, and $\chi_k = 0$, 1, or 2 for odd-odd, odd-even, or even-even nuclei, respectively.

Particle emission and fission widths (19,20) are obtained within the Fermi-gas approach to the nuclear level density

$$\rho(E^*) \simeq Const \cdot exp\{2\sqrt{aE^*}\} \ .$$

The fission cross section σ_f is determined by the ratio of the number N_f of fission events to the total number $N_t = N_{el} + N_{in}$ of Monte Carlo simulations in CEM95,

$$\sigma_f = \sigma_{in} P_f = \sigma_{in} \frac{N_f}{N_{in}} = \sigma_{geom} \frac{N_f}{N_t} \ . \tag{26}$$

Here P_f is the fissility of nucleus. In the case of low-fissility nuclei (e.g., gold) $N_f << N_t$, and, as a consequence, a large number of cascades should be calculated to obtain the value of σ_f with sufficient statistical accuracy, so that the calculation of σ_f becomes extremely time-consuming. Therefore, besides the direct calculation of the fission cross section via the expression (26), we have incorporated in CEM95 (following Barashenkov et al. [122]) a Monte Carlo calculation by means of the statistical functions $W_n = \prod_{i=1}^{N} w_{ni}$ and $W_f = 1 - W_n$. Here, W_n is the probability of the nucleus to "drop" the excitation energy E^* by a chain (cascade) of N successive evaporations of particles; W_f is the probability for the nucleus to fission at one of the chain stages; $w_{ni} = 1 - w_{fi}$ is the probability of particle emission at the i-th stage of the evaporative cascade; w_{fi} is the corresponding fission probability which is easy to determine using the formulae (19,20) for the widths Γ_j and Γ_f. After the subsequent averaging of W_f over the total number N_{in} of the cascades followed, and after multiplication of the result by the corresponding total inelastic cross section σ_{in}, we obtain the following expression for the fission cross section:

$$\sigma_f = \frac{\sigma_{in}}{N_{in}} \sum_{i=1}^{N_{in}} (W_f)_i \ . \tag{27}$$

The intranuclear cascade model [54] considers angular momenta of emitted particles as classical vectors $\boldsymbol{m}_i^{cas} = [\boldsymbol{r}_i \boldsymbol{p}_i]$, where $\boldsymbol{r}_i$ is the radius vector at the exit of the cascade particle i from the nucleus and $\boldsymbol{p}_i$ is its momentum. Following Ref. [127], angular momenta of preequilibrium and evaporation particles are also considered as classical vectors, since $| \sum_i \boldsymbol{m}_i^{cas} | \gg 1$. In CEM95, angular momenta of preequilibrium and evaporated particles m_j are estimated in the sharp cut-off approximation, as was proposed by Iljinov et al. [127]. In this approach, the distribution of m_j satisfies the expression

$$P(m_j) dm_j \sim m_j dm_j; \qquad 0 \le m_j \le m_j^{max} = \sqrt{2\mu_j (E_j - V_j)} R_j / \hbar \ .$$

Here R_j is the radius of the interaction of the jth emitted particle with the residual nucleus, E_j, V_j, and μ_j are the energy in the center-of-mass system, Coulomb barrier, and reduced mass of the particle, respectively. Following Ref. [127], the spins of the emitted particles are not taken into account when estimating the angular momentum of the residual nuclei, though they are taken into account in the corresponding statistical factors of the emission rates (19). Angular momenta of residual nuclei are calculated in CEM95 without taking into account the spin of the initial target nucleus and of intermediate nuclei during consecutive emission of particles.

Let us note that in CEM95 nuclear structure is taken into account at the preequilibrium and evaporation stages of reactions through the level density parameters, nuclear masses, pairing energies, and binding energies of secondary particles. As was mentioned above, CEM95 uses nuclear masses from Ref. [111] while pairing energies are calculated according to Eq. (25). To take into account shell effects on level densities and their decrease with increasing excitation energy, we used in our calculations the third systematics for $a(Z,N,E^*)$ by Iljinov et al. [110] for all reactions except interactions with the lightest ^{12}C, ^{14}N, and ^{16}O targets, for which, to avoid some calculational difficulties, we used fixed values $a = 0.125A$. Recall that the authors of Ref. [110] have obtained this approximation for $a(Z,N,E^*)$ by fitting not only measurements on neutron resonances but also data at higher excitation energies (using the same Cameron's mass formulas [111]), in a functional form proposed by Ignatyuk et al. [108]

$$a(Z,N,E^*) = \tilde{a}(A)\left\{1 + \delta W_{gs}(Z,N)\frac{f(E^*-\Delta)}{E^*-\Delta}\right\}, \tag{28}$$

where

$$\tilde{a}(A) = \alpha A + \beta A^{2/3} B_s \tag{29}$$

is the asymptotic Fermi-gas value of the level density parameter at high excitation energies. Here, B_s is the ratio of the surface area of the nucleus to the surface area of a sphere of the same volume (for the ground state of a nucleus, $B_s \approx 1$), and

$$f(E^*) = 1 - exp(-\gamma E^*) \ . \tag{30}$$

For the parameters α, β, and γ, the authors of Ref. [110] have found different values from those of Ignatyuk et al. [108], namely

$$\alpha = 0.072; \quad \beta = 0.257; \quad \gamma = 0.052 \ \mathrm{MeV}^{-1} \ . \tag{31}$$

Let us note as well that in CEM95 collective effects are not taken into account explicitly. In Ref. [110], the values of parameters α, β, and γ (31) were fitted (also, without explicit collective terms) to the experimental resonance spacing and other data, therefore they include collective effects in a non-explicit, phenomenological way. Our experience shows that for the version of the CEM realized in the code CEM95 the systematics (28–31) for $a(Z,N,E^*)$ provides a good overall agreement with different experimental data, therefore we use it in our present study.

In CEM95, all other CEM parameter values are fixed and are the same as described in Refs. [68, 69].

At the end of this section we show a typical example of how the code CEM95 describes the inclusive spectra of secondary nucleons and fission cross sections. Fig. 3 shows a comparison of calculated and measured inclusive spectra of neutrons [131] and protons [132] from p(80 MeV)+^{90}Zr. To illustrate the relative role of the CEM nucleon production mechanisms, the cascade, preequilibrium, and evaporative components of angle-integrated energy spectra are shown separately in the upper part

of Fig. 3. In the lower part, only the sums of all three components are shown for double-differential cross sections for five laboratory angles. One can see that CEM95 reproduces well the absolute value and the change in the spectrum shape with increasing emission angle both for secondary protons and neutrons.

As an example, the incident energy dependence of experimental [133, 134] and calculated fission cross section for interaction of neutrons with ^{238}U is shown in Fig. 4. We performed these calculations with Krappe, Nix, and Sierk fission barriers [119], Cameron shell and pairing corrections [111], the third Iljinov et al. systematics for the level density parameters [110], with a dependence $B_f(L)$ estimated by a phenomenological approach (formulas (28–30) from Ref. [126]) with the value of the moment of inertia of a nucleus at the saddle-point J_{sp} from Ref. [124], without taking into account the dependence of B_f on excitation energy E^*, and with the value for the ratio $a_f/a_n = 1.02$. For comparison, two values of fission cross sections calculated in Ref. [135] with the well known code LAHET [136] are shown for $T_n = 100$ and 160 MeV. One can see that CEM95 describes correctly (and no worse than LAHET) the shape and the absolute value of the fission cross section at these intermediate incident energies.

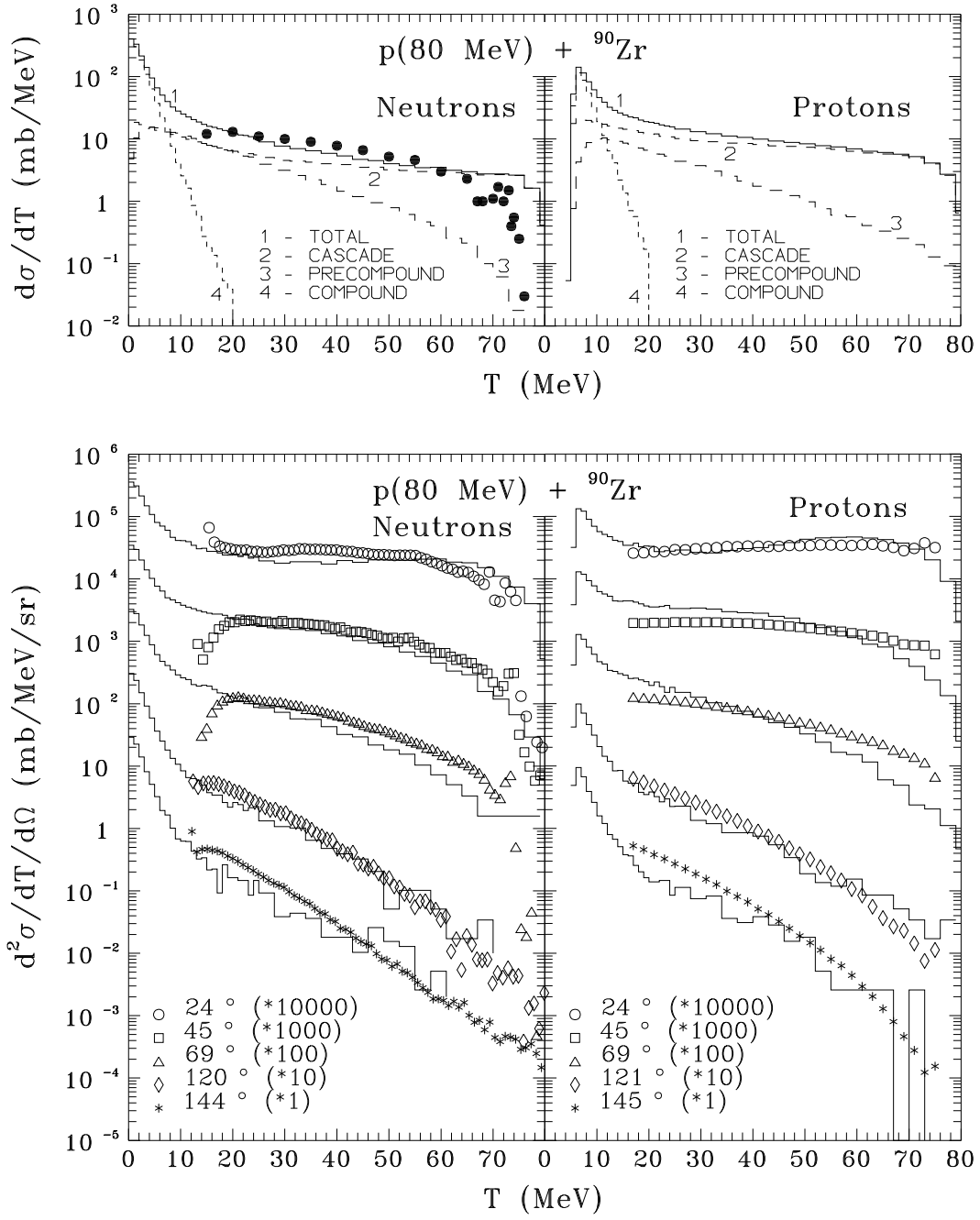

Fig. 3. Angle-integrated energy distributions (upper row) and double differential cross sections (lower row) of neutrons and protons from 80 MeV protons on ^{90}Zr. In the upper row, histograms 1, 2, 3, and 4 show the total spectra and contributions of cascade, pre-equilibrium, and evaporative components, respectively. In the lower row, different emission angles are drawn with different symbols, as indicated. The experimental data are from Ref. [131] for neutrons and from Ref. [132] for protons.

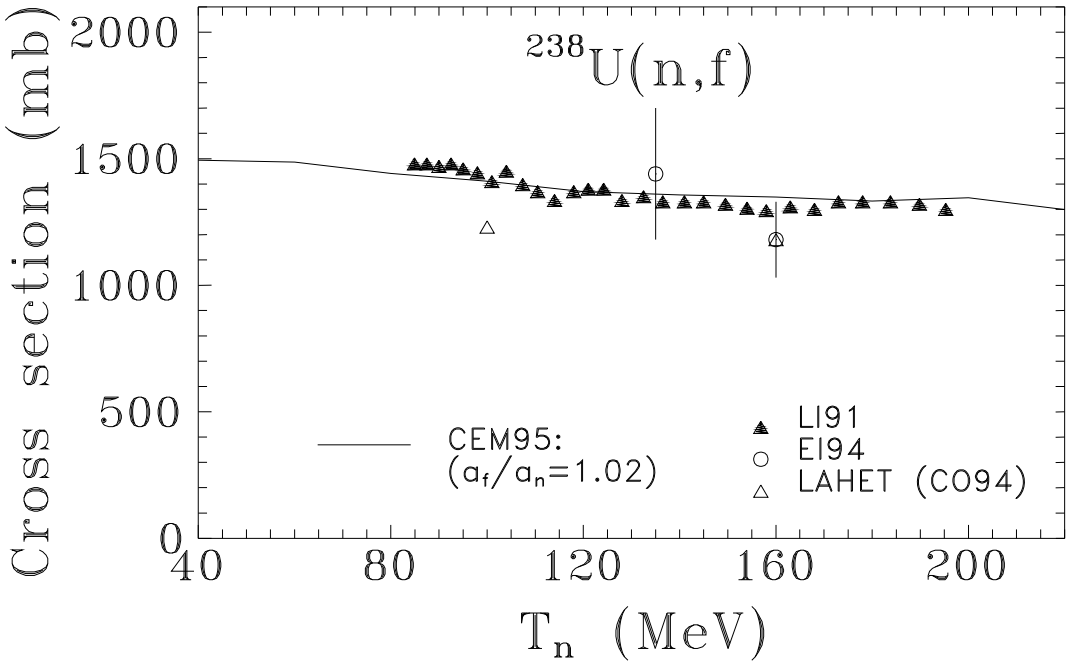

Fig. 4. Energy dependence of the neutron-induced fission cross section of ^{238}U. Calculations are performed with Krappe, Nix, and Sierk fission barriers [119], Cameron shell and pairing corrections [111], the third Iljinov et al. systematics for the level density parameters [110], with a dependence $B_f(L)$ estimated by a phenomenological approach (formulas (28–30) from Ref. [126]) with the value for the moment of inertia of a nucleus at the saddle-point J_{sp} from Ref. [124], without taking into account the dependence of B_f on excitation energy E^*, and with the value for the ratio $a_f/a_n = 1.02$. The experimental points are from Refs. [133, 134]. For comparison, two values of σ_f calculated at $T_n = 100$ and 160 MeV in Ref. [135] with the code LAHET [136] are shown by open triangles.

3. Sensitivity of Results to Details of Calculations and Input Parameters

Our previous analysis of excitation functions in the framework of the CEM has shown [75] that if one uses the usual "default" parameters, CEM95 describes satisfactorily (and no worse than other models) the majority of isotope yields in the spallation region. At the same time, for a few cases in the same spallation region where the model "has to work", it underestimates or overestimates some individual measured excitation functions, sometimes by a order of magnitude. Similar results have been obtained by many authors with other codes (see, e.g. Refs. [43, 62, 63, 137, 138]). To understand this situation, we first perform a detailed analysis of the dependence of calculated excitation functions on those input parameters of the CEM which can be changed without affecting the basis of the model. Moreover, such a study seems to be necessary, as to our knowledge there is not a common point of view in the literature on the question: "How do calculated excitation functions depend on the input values of the same parameters used in different models?"

Our first, trivial but necessary test was as follows. The voluminous and time-consuming calculations of this study were performed using different UNIX machines and DOS PCs at JINR (Dubna), ORNL (Oak Ridge), and CEA (Bruyères-le-Châtel). As we used different FORTRAN compilers on UNIX and DOS machines, it was important to check that the code would run without problems on all these different machines and that the results would be the same. As a test, the reaction p+^{59}Co has been calculated for the same incident energies on all the machines used. Within statistical errors, we have obtained the same results, serving as a convincing proof of the reliability of CEM95.

Our second test is done to understand how the extended version of the model [75], realized in the code CEM95, describes excitation functions as compared to the standard version of the CEM [68, 69]. We perform calculations with both versions of the CEM for several dozens of excitation functions for different target nuclei. As an example, Fig. 5 shows a comparison of experimental [40, 46, 47, 54, 60] excitation functions for the production of ^{27}Si, ^{26}Al, ^{24}Na, ^{22}Na, ^{4}He, ^{3}He, t, and d from p+^{27}Al with predictions of both versions of the CEM. Similar results are obtain for other targets. One can see that on the whole, the extended version [75] agrees better with experimental data than the standard CEM [68, 69] does.

Our next test was to analyze the dependence of calculated excitation functions on the inverse cross sections $\sigma^j_{inv}(E)$ used in calculations. In CEM95, inverse cross sections are used to calculate partial widths Γ_j for particle emission at preequilibrium stages of reactions according to Eq. (11), and at the evaporative stages, according to Eq. (19). We calculate $\sigma^j_{inv}(E)$ using the almost 40 year old approximation (21,22) by Dostrovsky et al. [130], which in principle should be replaced by a newer one, taking into account all available experimental data. To understand how our results depend on $\sigma^j_{inv}(E)$, we perform calculations with the Dostrovsky et al. [130] value for $\tilde{r}_0$ in Eq. (22) of 1.5 fm, and with $\tilde{r}_0 = 1.3$ fm. An example of such calculations

for the production of ^{55}Fe, ^{53}Mn, ^{49}Cr, ^{49}V, ^{43}K, and ^{36}Cl from p+^{56}Fe is shown in Fig. 6. Similar results are obtained for other reactions.

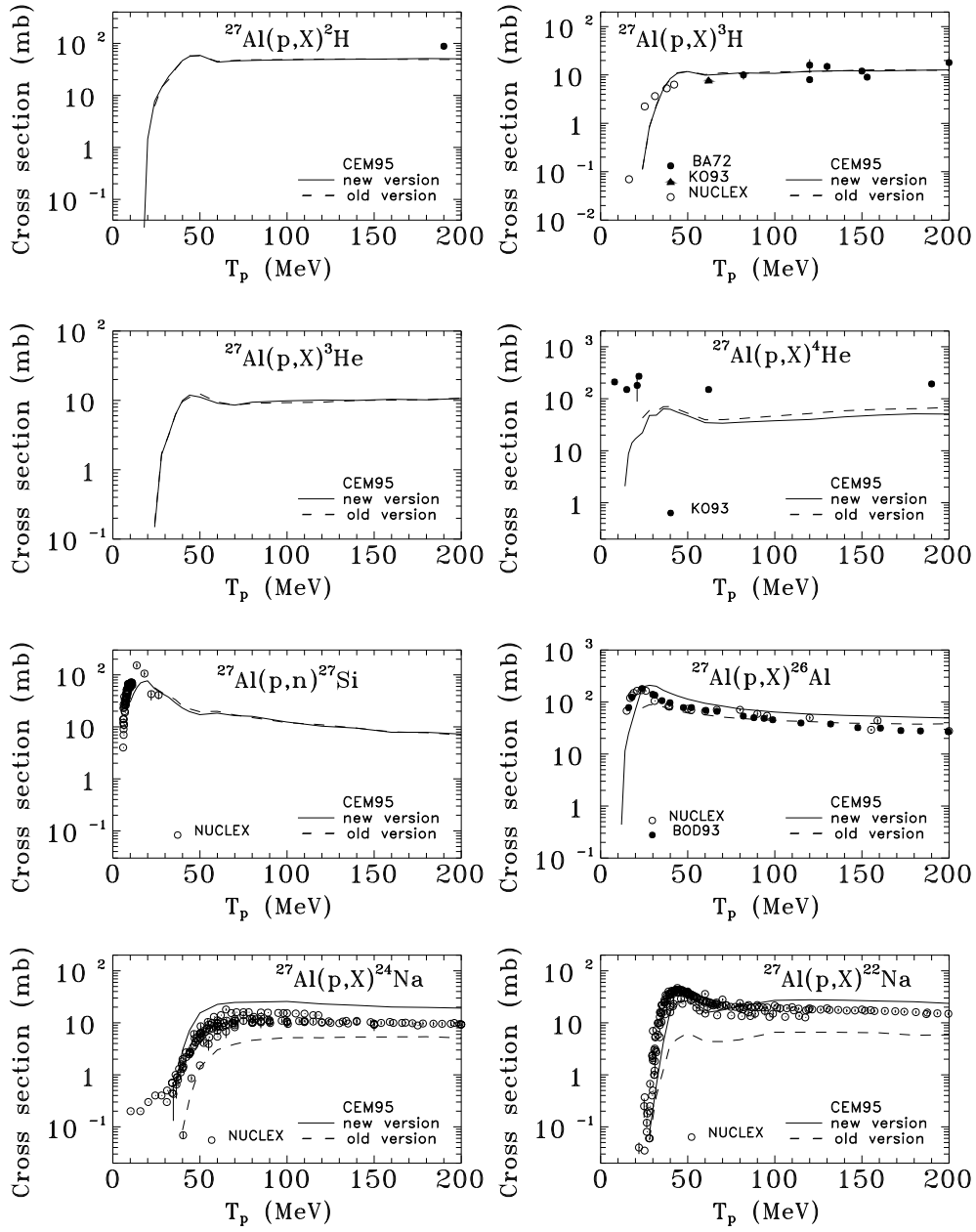

Fig. 5. Excitation functions for the production of d, t, ^{3}He, ^{4}He, ^{27}Si, ^{26}Al, ^{24}Na, and ^{22}Na from p+^{27}Al calculated with the extended version [75] of the CEM (solid lines) and with the standard version [68] with $a = 0.1A$ (dashed lines). Experimental data are labeled as: BA72 [54], KO93 [60], NUCLEX [46, 47], and BOD93 [40].

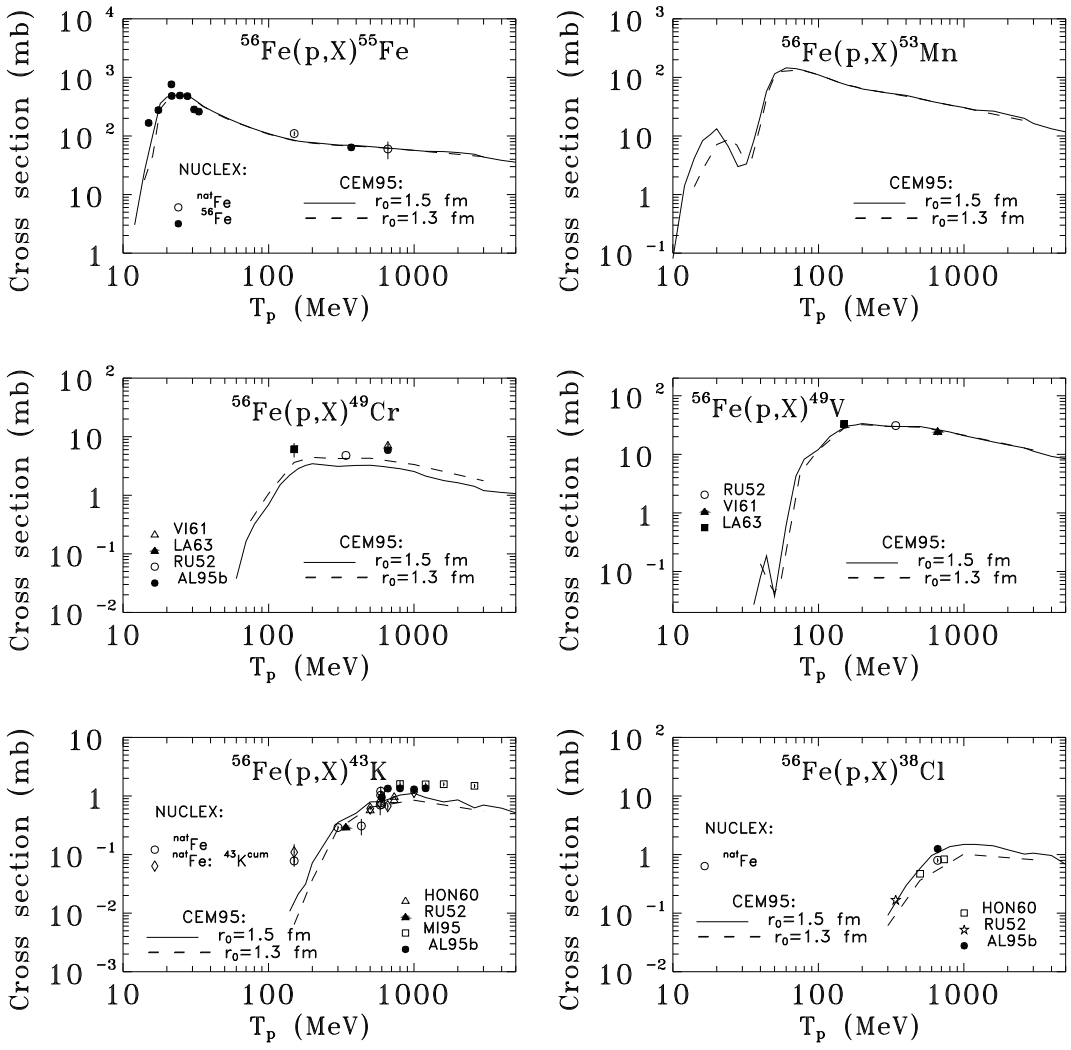

Fig. 6. Dependence of calculated excitation functions for the production of ^{55}Fe, ^{53}Mn, ^{49}Cr, ^{49}V, ^{43}K, and ^{36}Cl from p+^{56}Fe on the value of $\tilde{r}_0$ in Eq. (22) for the inverse cross sections; solid lines are calculated with $\tilde{r}_0 = 1.5$ fm and dashed lines with $\tilde{r}_0 = 1.3$ fm. Experimental data are labeled as: NUCLEX [46, 47], VI62 [139], LA63 [140], RU52 [141], AL95b [142], and HON60 [143].

One can see that our excitation functions are not very sensitive to the inverse cross sections used in the calculations. Only in a few cases, and at not too high incident energies, do excitation functions calculated with $\tilde{r}_0 = 1.5$ fm differ from the ones calculated with $\tilde{r}_0 = 1.3$ fm by a factor of two. So, we can conclude that the few previously mentioned large discrepancies between experimental data and some excitation functions calculated with CEM95 observed in Ref. [75] are not connected with the old inverse cross sections used in the calculations. However, as one can see from Fig. 6, inverse cross sections do affect results in some cases up to a factor of about 2, so we should use the best possible values of $\sigma^j_{inv}(E)$.

Our next test is to find out how excitation functions predicted by CEM95 depend on the level density parameter used in the calculations. The fact that at incident energies below $\sim$ 100 MeV nuclear structure effects on level density parameters are important and have to be properly taken into account in calculations of excitation functions is well known and is often discussed in the literature [144]–[146]. Nevertheless, there is no common point of view in the literature on this question. So, in Ref. [145], it was found that proton-induced excitation functions calculated with the code ALICE-92 [147] agree better with experimental data using level density parameters calculated in the framework of the generalized superfluid model of nuclei [148] as compared to the case of using of the Fermi-gas model value $a = A/9.0$ (the same conclusion was made in Ref. [144]), and just the opposite result was obtained in the case of α-induced reactions. At higher incident energies of about 1 GeV, where one may expect that the influence of level density parameters on calculated yields is of less importance, the situation is even more confused. Recently Fukahori has concluded [149] that isotope production cross sections calculated at these energies with the code ALICE-P are not sensitive to the level density parameter. The difference of results obtained with the Fermi-Gas Model, with Ramamurthy's method [150], and with the Liquid Drop Model for the level density parameter was only about 5% [149]. On the contrary, Nishida and Nakahara [151] have found that the distribution of some isotopes of the non-fission component from p+^{237}Np interactions at 500 MeV calculated with the code NUCLEUS [152] with the values for the level density parameter $a = A/30$, $A/20$, $A/10$, $A/5$, and calculated according to an expression derived by Le Couteur [153] differ both in shape and absolute value by about one order of magnitude (see Fig. 2 from Ref. [151]).

The influence of the level density parameter on excitation functions calculated by CEM95 was not studied previously and, as the information presented in the literature with other codes is contradictory, we perform a detailed analysis of this point here. In Ref. [75], it was found that the main CEM nuclide production mechanism in the spallation region is the successive emission of several nucleons, while emission of complex particles is of importance (and may even be the only mechanism for production of a given isotope in a limited range of energy) only at low incident energies, near the threshold, while with increasing energy its relative role quickly decreases. Taking this into account, one may try to obtain an overview of the question of how the level density parameter affects excitation functions predicted by CEM95 in the spallation region from a study of the influence of the level density parameter on the mean multiplicities (or yields) of emitted particles. As an example, Table I summarizes the ratios of mean multiplicities of n, p, d, t, ^{3}He, and ^{4}He emitted from p+^{59}Co interactions at 50, 500, and 5000 MeV calculated with $a = 0.15A$, $0.10A$, and $0.05A$ to the ones calculated using the third Iljinov et al. [110] systematics (28–31) for $a(Z, N, E^*)$. Fig. 7 shows the yields of n, p, d, t, ^{3}He, and ^{4}He calculated with these four level density parameters for proton incident energies from 10 MeV to 5 GeV. One can see that the yields of neutrons and protons predicted by CEM95 depend very weakly on the value of the level density parameter a: The biggest difference of the

ratios for nucleons shown in Table I, may be seen for neutrons, at an incident energy of 50 MeV when one passes from $a = 0.15A$ to $a = 0.05A$, and it is only about 13%; which is consistent with the conclusion of Fukahori [149] and does not agree with the results of Nishida and Nakahara [151]. The yields of complex particles predicted by CEM95 depend more strongly on the level density parameter; the biggest difference for the ratios shown in Table I is for emission of t at 50 MeV, where it is about 72%.

TABLE I

Ratios of mean multiplicities of secondary particles emitted from p+^{59}Co interactions at 50, 500, and 5000 MeV calculated with the code CEM95 with $a = 0.15A$, $0.10A$, and $0.05A$ to the ones calculated using the third Iljinov et al. [110] systematics (28–31) for $a(Z, N, E^*)$ (figures in parenthesis in the last row show the corresponding mean multiplicities themselves)

T_p (MeV)	Part.	$a = 0.15A$	$a = 0.10A$	$a = 0.05A$	$a = a(Z, N, E^*)$ [110]
50	n	1.07	1.02	0.94	1. (0.791)
	p	0.94	0.96	1.00	1. (0.580)
	d	1.10	0.86	0.54	1. (0.0391)
	t	1.16	0.88	0.44	1. (0.00687)
	^{3}He	0.98	0.86	0.40	1. (0.00377)
	^{4}He	1.13	0.75	0.57	1. (0.0347)
500	n	1.02	1.02	0.99	1. (1.66)
	p	0.99	1.00	1.00	1. (1.41)
	d	1.03	0.87	0.63	1. (0.134)
	t	1.05	0.79	0.53	1. (0.0407)
	^{3}He	1.05	0.85	0.63	1. (0.0265)
	^{4}He	0.97	0.72	0.88	1. (0.0812)
5000	n	1.00	1.01	0.95	1. (6.74)
	p	1.02	1.03	0.96	1. (5.59)
	d	0.96	1.04	1.23	1. (0.714)
	t	0.96	0.86	0.96	1. (0.334)
	^{3}He	0.93	0.86	1.07	1. (0.261)
	^{4}He	0.87	0.75	0.73	1. (0.532)

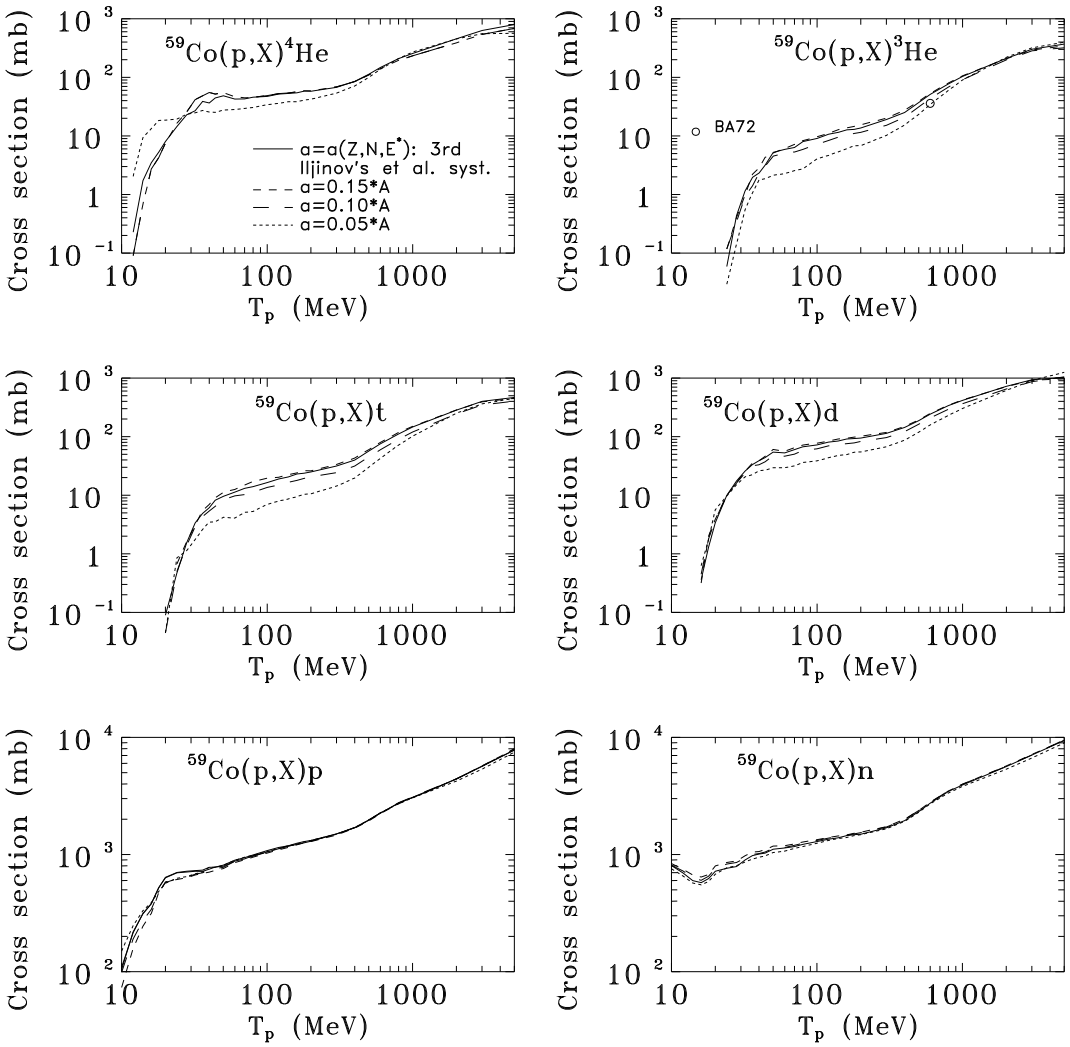

Fig. 7. Excitation functions for the production of ^{4}He, ^{3}He, t, d, p, and n from p+^{59}Co calculated with the third Iljinov et al. systematics for $a(Z,N,E^*)$ (solid lines) and with fixed values $a = 0.15A$, $a = 0.10A$, and $a = 0.05A$ (dashed lines), as indicated.

This is much lower than the corresponding differences of about two orders of magnitude shown in Table I of the work by Nishida and Nakahara [151]. Therefore, we may expect, as was concluded by Fukahori [149], that isotope yield production in the spallation region for these incident energies is not sensitive to the level density parameter. This inference can also be drawn from Fig. 8, where mass-yield distributions from p+^{59}Co at 50, 200, 600, and 1200 MeV calculated with CEM95 using the four values cited above for the level density parameter are shown together with the available experimental data [42, 43, 137, 138]. (Note that the experimental points in Fig. 8 show the yields of only the several measured nuclides indicated in the figure, while the calculated histograms represent sums over all produced isobars, therefore an exact comparison between them is not possible, and we show the experimental data only as a guide.)

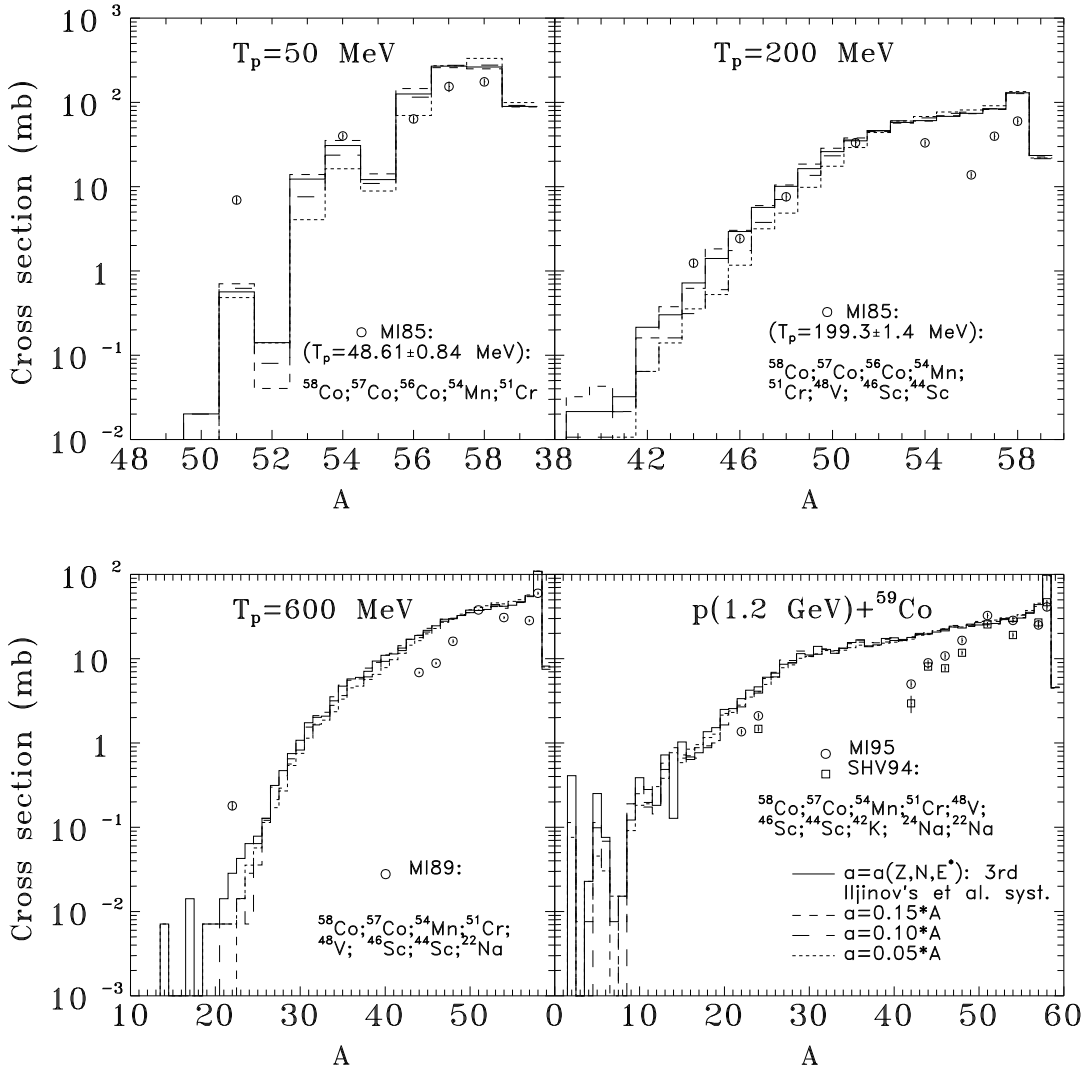

Fig. 8. Mass-yield distributions from p+^{59}Co at 50, 200, 600, and 1200 MeV calculated with the third Iljinov et al. systematics for $a(Z, N, E^*)$ (solid lines) and with fixed values $a = 0.15A$, $a = 0.10A$, and $a = 0.05A$ (dashed lines), as indicated. Experimental data for incident energies and nuclides shown in the figure are labeled as: MI85 [137], MI89 [42], MI95 [43], and SHV94 [138].

One can see that for all these incident energies, mass-yield distributions calculated with different values of a are very close to each other, especially in the spallation region. Only for final isobars far away from the target nucleus do the differences of calculated yields increase slightly, but still remain within a factor of two. Similar results are obtained for charge-yield distributions. Such results suggest to us that on the whole, excitation functions calculated with the CEM95 in the spallation region are not very sensitive to the level density parameter.

A more detailed analysis of all possible excitation functions shows that such a conclusion is not exactly correct. We perform calculations of all possible excitation

functions for interactions of protons with energies from 10 MeV up to 5 GeV with ^{59}Co using the four values of a cited above. Figs. 9–12 show our results for the production of all nuclides for which we are able to find experimental data, as well as for ^{59}Ni, the simplest reaction channel.

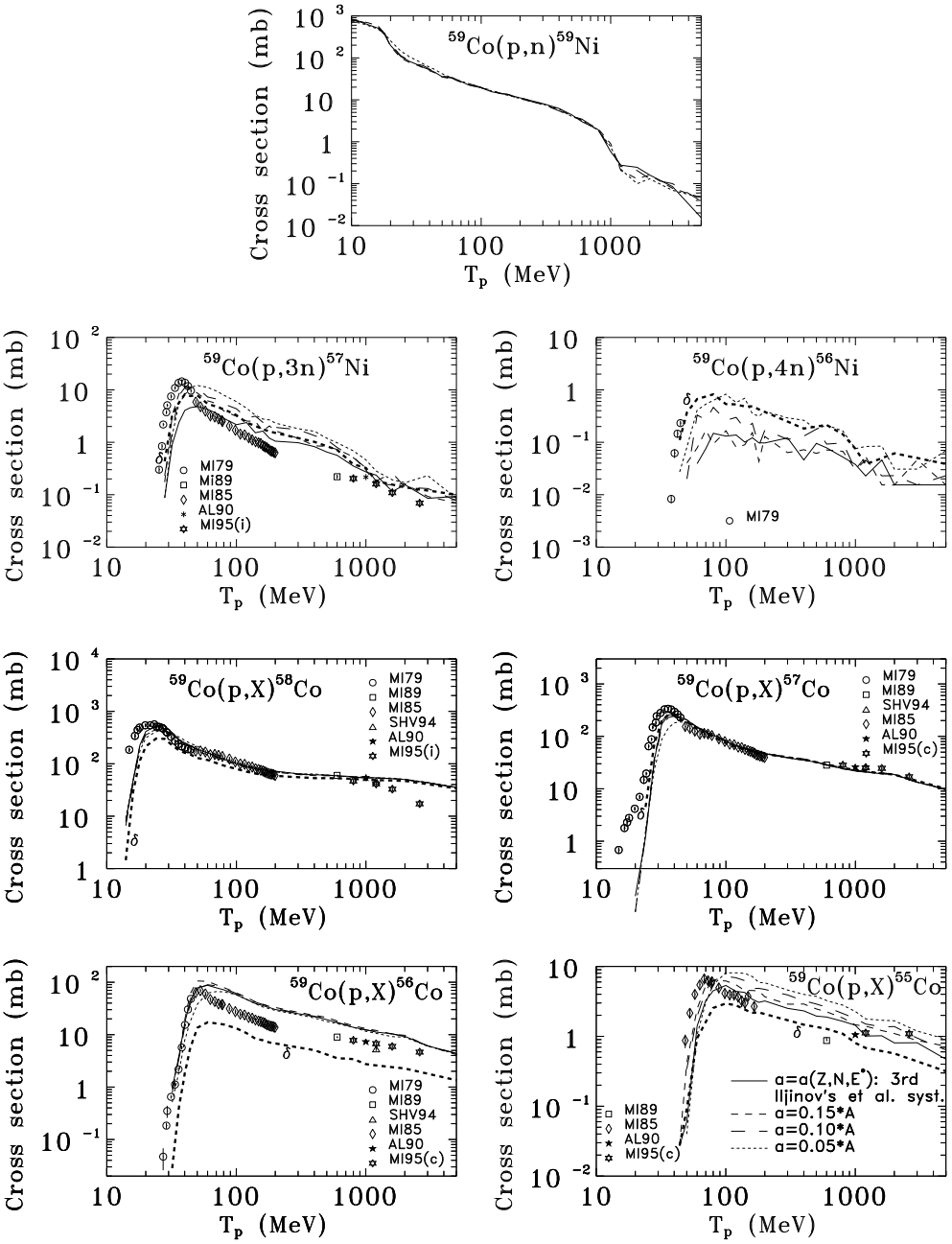

Fig. 9. Excitation functions for the production of ^{59}Ni, ^{57}Ni, ^{56}Ni, ^{58}Co, ^{57}Co, ^{56}Co, and ^{55}Co from p+^{59}Co calculated with the third Iljinov et al. systematics for $a(Z,N,E^*)$ (solid lines) and with fixed values $a = 0.15A$, $a = 0.10A$, and $a = 0.05A$ (dashed lines), as indicated. The thick short dashed lines marked with a δ are calculated as the solid ones but with six times smaller pairing energies: $\Delta_c = \chi_c \cdot 2/\sqrt{A_c}$ and $\Delta_j = \chi_j \cdot 2/\sqrt{A_{fj}}$ (see Eq. (25)). Experimental data are labeled as: MI79 [155], MI89 [42], MI85 [137], AL90 [156], MI95 [43], and SHV94 [138]. Here and in all following figures, an (i) or (c) indicates whether the experimental cross sections are given as independent or cumulative, respectively.

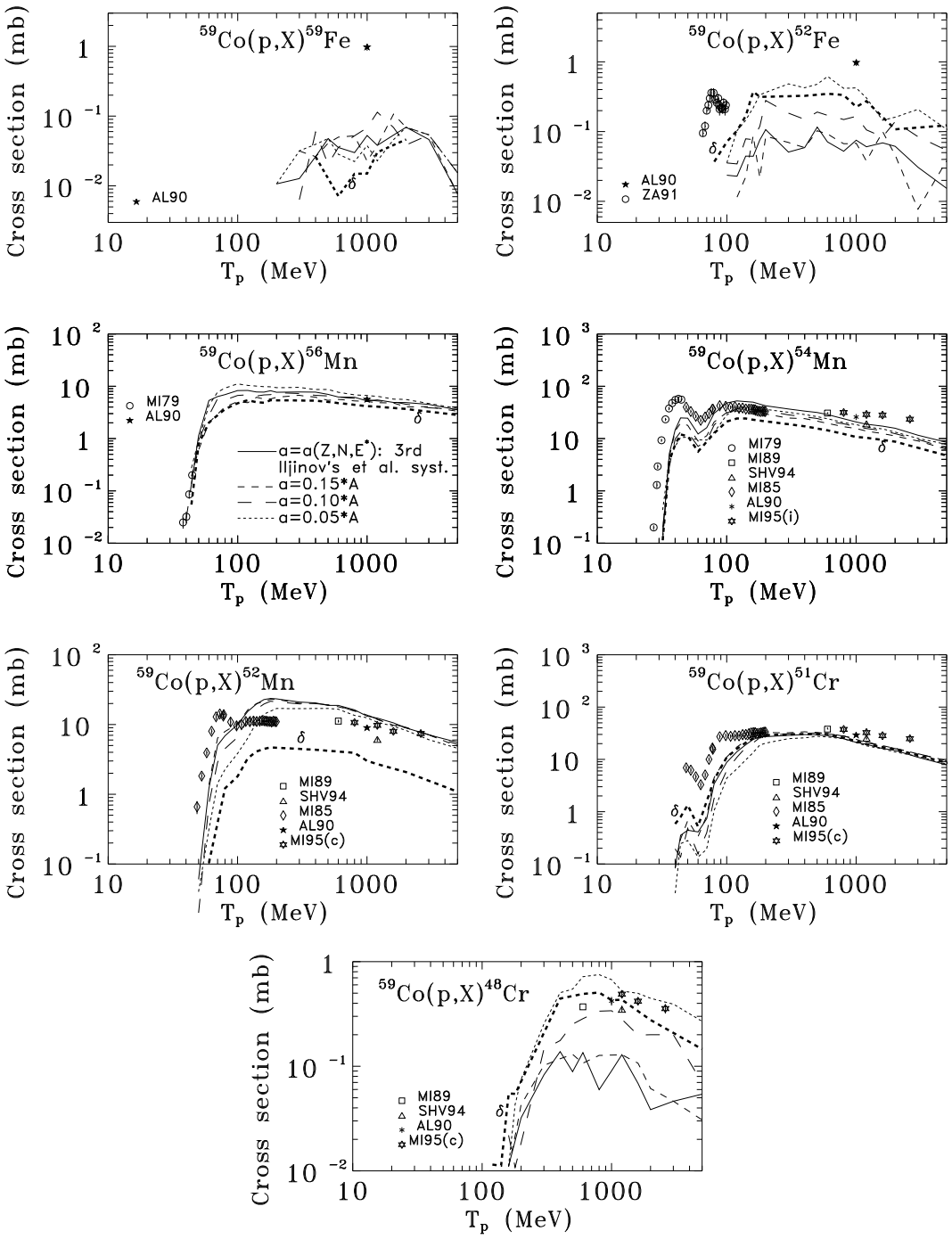

Fig. 10. The same as Fig. 9 but for the production of ^{59}Fe, ^{52}Fe, ^{56}Mn, ^{54}Mn, ^{52}Mn, ^{51}Cr, and ^{48}Cr. Experimental data are labeled as: AL90 [156], ZA91 [157], MI79 [155], MI89 [42], SHV94 [138], MI85 [137], and MI95 [43].

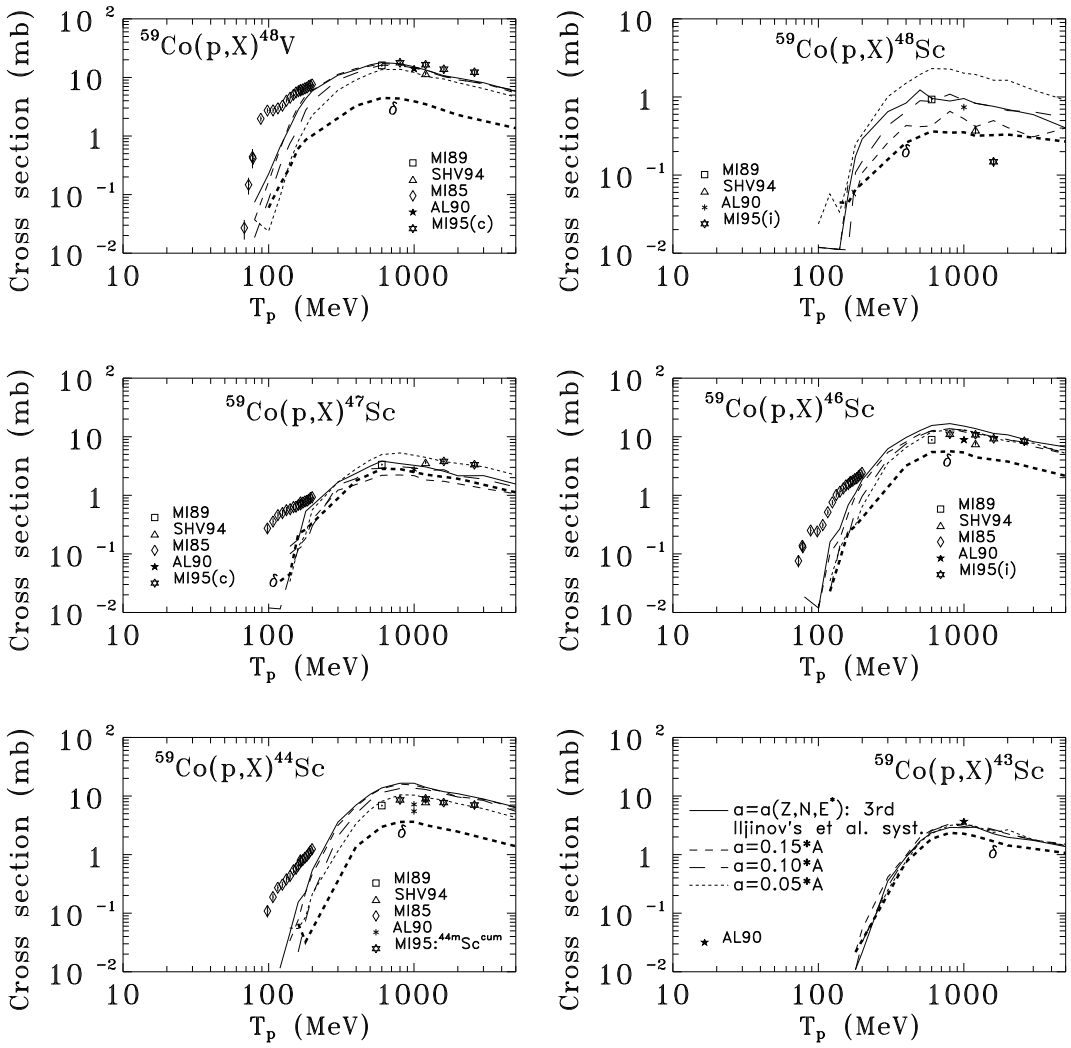

Fig. 11. The same as Fig. 9 but for the production of ^{48}V, ^{48}Sc, ^{47}Sc, ^{46}Sc, ^{44}Sc, and ^{43}Sc. Experimental data are labeled as: MI89 [42], SHV94 [138], MI85 [137], AL90 [156], and MI95 [43].

One can see that the majority of excitation functions calculated with these different values for a are very similar. This is true both for the production of most nuclides near the target nucleus and for nuclides far away from it, especially for nuclides with large yields. However, for some nuclides with low production cross sections, the influence of a on calculated excitation functions is significant. Sometimes results obtained with different values of a differ up to a factor of 10. Unfortunately, our results for such nuclides are less precise due to poorer statistics in the Monte Carlo simulation for these rare events; but the observed differences are greater than would be explained by the statistical errors of the calculations. We obtain such results for the production of several nuclides near the target nucleus: ^{56}Ni and ^{55}Co (Fig. 9), ^{59}Fe and ^{52}Fe (Fig. 10); for nuclides in the spallation region: ^{48}Cr (Fig. 10), ^{48}Sc (Fig. 11), ^{43}K and ^{42}K (Fig. 12); and for nuclides in the fragmentation region, far away of the target: ^{28}Mg and ^{7}Be (Fig. 12).

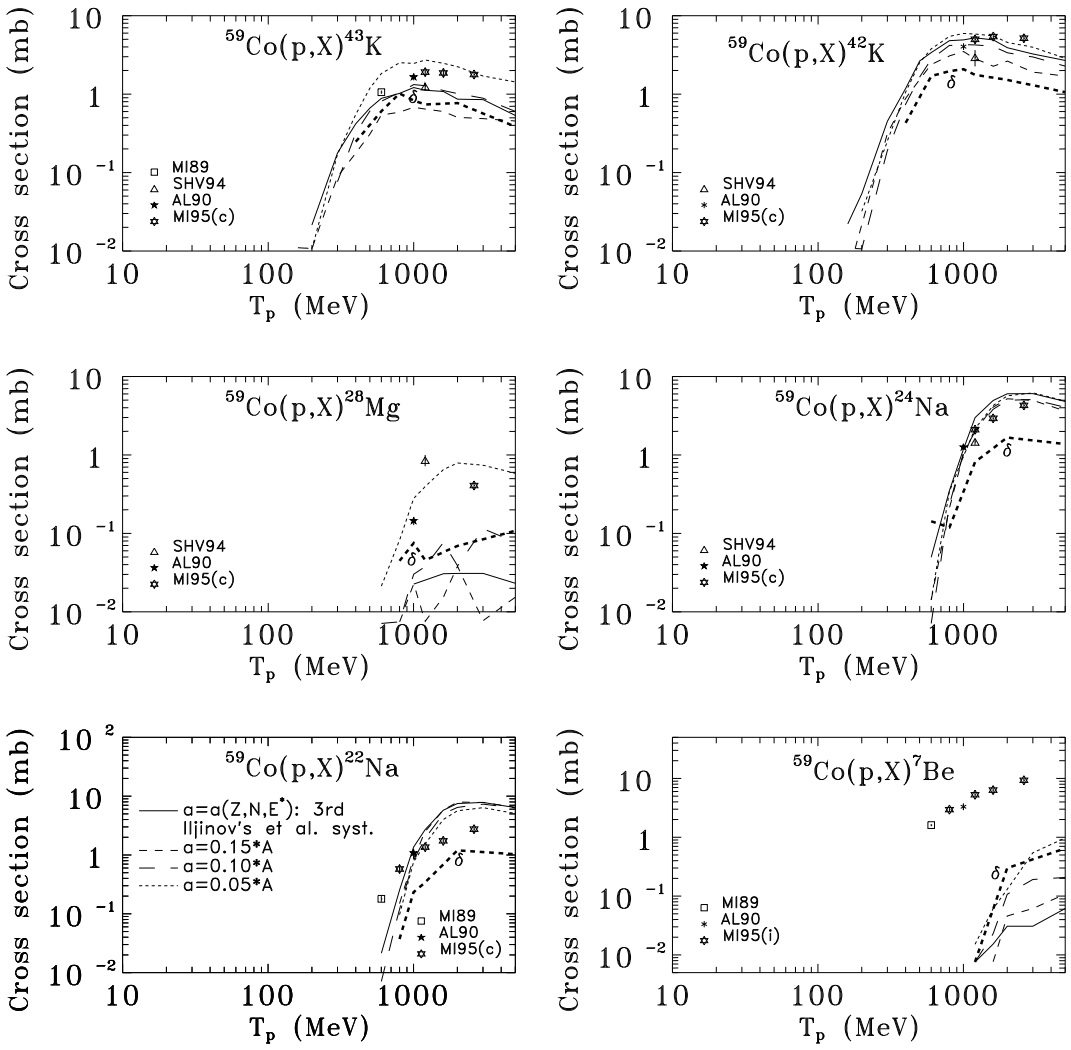

Fig. 12. The same as in Fig. 9 but for the production of ^{43}K, ^{42}K, ^{28}Mg, ^{24}Na, ^{22}Na, and ^{7}Be. Experimental data are labeled as: MI89 [42], SHV94 [138], AL90 [156], and MI95 [43].

Let us note that the CEM does not contain a special mechanism for nuclear fragmentation and does not pretend to describe the production of light fragments like ^{7}Be from intermediate and heavy targets. But at high incident energies of about 1 GeV and above, a deep spallation with emission of a large number of nucleons from the target nucleus takes place, and as a result, for not too heavy targets, we have events when residual nuclei at the end of all stages of reactions are just fragments. This is only a small part of the total fragment production measured in experiments, but as one can see from Fig. 12 its cross section depends also strongly on the value of level density parameter a. Summarizing all results shown in Figs. 7–12, we can conclude that the mean multiplicity of nucleons predicted by the CEM does not depend significantly on the level density parameter used in calculation, and as a result of this, the mass-yield and charge-yield distributions of residual nuclei as

well as excitation functions for the production of nuclides with large production cross sections are not very sensitive to the level density parameter. But excitation functions of some nuclides with small yields are more sensitive to the value of a. Therefore, to be able to predict correctly the production of arbitrary nuclides, it is necessary to perform calculations with reliable values for the level density parameter.

Although the level density parameter influences the calculated nuclide yields, we do not think that those large discrepancies between some theoretical and experimental excitation functions observed in Ref. [75] were caused by use of an inappropriate value of a: we used in those calculations [75] the third Iljinov et al. [110] systematics (28–31) for $a(Z, N, E^*)$, which was tested to be "the best" set for CEM95. We think that such large discrepancies between some calculated and experimental excitation functions are connected mainly with the energetics of reactions, i.e., with the calculation of nuclear masses, binding energies and consequent Q-values, and with the shell and pairing corrections used. The fact that excitation functions are very sensitive to the nuclear masses and shell corrections used in calculations is well known in the literature and this problem was analyzed in a number of recent works [40, 149, 154]. To our knowledge, the influence of pairing energies on excitation functions calculated at energies of about 1 GeV and above has not been previously discussed. To understand how pairing corrections influence excitation functions calculated with CEM95, we perform calculations for the reaction p+^{59}Co with six times smaller pairing energies $\Delta_c = \chi_c \cdot 2/\sqrt{A_c}$ and $\Delta_j = \chi_j \cdot 2/\sqrt{A_{fj}}$, as compared to "the standard" values defined by Eq. (25). The corresponding results are shown in Figs. 9–12 by thick short-dashed lines which should be compared with the solid lines in the same figures. One can see that excitation functions for the production of some nuclides are rather sensitive to the values of pairing energies used in calculations. This result is unexpected: our experience shows that such characteristics of nuclear reactions as inclusive spectra of secondary particles, their integrals over energy and/or angles, mass-yield or charge-yield distributions of residual nuclei essentially do not depend on the values of the pairing energy used in the CEM calculations at these incident energies. As one can see from Figs. 9–12, some excitation functions calculated with different values of pairing energies differ by fairly large factors and these differences even increase with increasing incident energy. To be able to predict arbitrary excitation functions it is necessary to use values for the pairing energies which are reliable and well tested for the whole range of incident energies.

Several special calculations show that our conclusions from analysis of p+^{59}Co interactions are also valid for other reactions. As an example, Figs. 13–14 show a comparison of experimental data with theoretical total inelastic cross section and excitation functions for the production of ^{15,14}O, ^{13}N, ^{14,11}C, ^{11,10}B, ^{10,9,7}Be, ^{9,6}Li, and ^{3}H from p+^{16}O calculated in the framework of the standard version of the CEM [68] with the value for $\tilde{r}_0$ in Eq. (22) of 1.5 fm with fixed values for the level density parameter $a = 0.125A$ (thick solid curves labeled as 1) and $a = 0.100A$ (thick dashed curves labeled as 2) as well as to those calculated with the extended

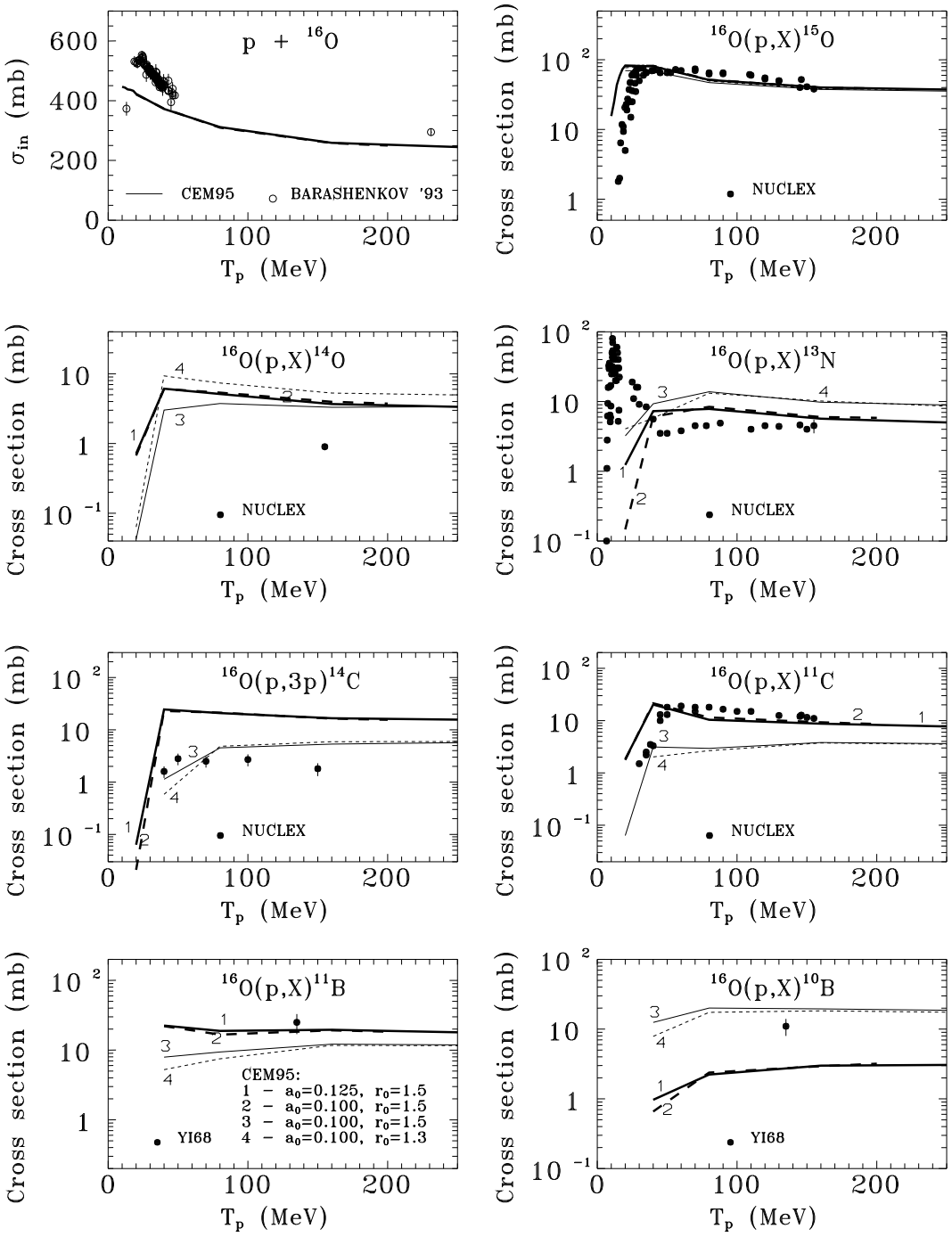

Fig. 13. Total inelastic cross section and excitation functions for the production of ^{15}O, ^{14}O, ^{13}N, ^{14}C, ^{11}C, ^{11}B, and ^{10}B from p+^{16}O calculated in the standard version of the CEM [68] with $a = 0.125A$ (curves 1) and $a = 0.100A$ (curves 2), and in the extended version [75] for $a = 0.100A$ with $\tilde{r}_0 = 1.5$ fm (curves 3) and $\tilde{r}_0 = 1.3$ fm (curves 4). Experimental data are labeled as: BARASHENKOV'93 [158], NUCLEX [46, 47], and YI68 [159].

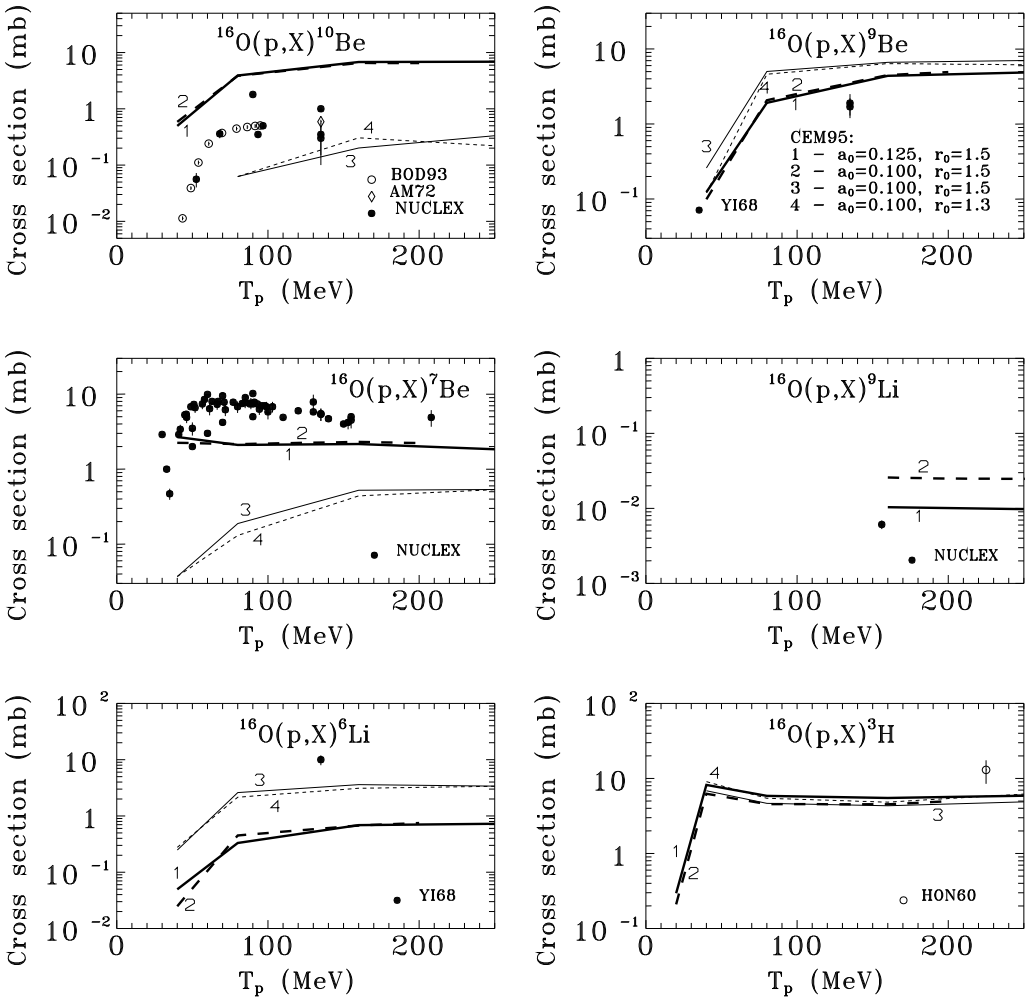

Fig. 14. Excitation functions for the production of ^{10}Be, ^{9}Be, ^{7}Be, ^{9}Li, ^{6}Li, and ^{3}H from p+^{16}O. Experimental data are labeled as: BOD93 [40], AM72 [160], NUCLEX [46, 47], YI68 [159], and HON60 [143]. The rest of the notation is the same as in Fig. 13.

version [75] with $a = 0.100A$ for $\tilde{r}_0 = 1.5$ fm (thin solid curves labeled as 3) and $\tilde{r}_0 = 1.3$ fm (thin dashed curves labeled as 4).

Although these calculations are performed for a smaller number of incident energies (therefore the curves connecting the calculated points are not smooth), one can see that these excitation functions are not very sensitive either to a reasonable variation of the level density parameter a (compare curves 1 and 2) or to the inverse cross sections (compare curves 3 and 4). But one can see large differences (compare curves 1 and 3) between results obtained with the original version of the CEM [68] and those from the extended version [75]. Just as in the case of ^{59}Co, we see that excitation functions generally are very sensitive to the energetics (shell and pairing energies and Q-values) of the reactions and much less so to the level density parameters and the inverse cross sections used in calculations.

Let us dwell now on two important details of the calculation and comparison with measured data. Many experimental data are obtained for targets of natural isotopic composition. Our experience shows that such characteristics of nuclear reactions as total inelastic cross sections, spectra and multiplicities of secondary particles, etc. are not very sensitive to the values of mass-number A of the target used in CEM calculations. For example, for interactions of protons of 500 MeV with iron, spectra of secondary particles calculated with CEM95 separately for the stable isotopes ^{54}Fe, ^{56}Fe, ^{57}Fe, and ^{58}Fe and then summed up with the corresponding weights of each isotope in the target are practically the same as results obtained from a single calculation of the p+^{56}Fe reaction. In the case of excitation functions, the situation is different: As an example, Fig. 15 shows available experimental data together with excitation functions predicted by CEM95 for the production of ^{58}Co, ^{57}Co, ^{56}Co, ^{55}Co, and ^{54}Mn from interactions of protons with energies from 10 MeV up to 5 GeV with ^{54}Fe, ^{56}Fe, ^{57}Fe, ^{58}Fe, and ^{nat}Fe. One can see that both experimental and calculated excitation functions depend critically on the mass number of the target isotope. Excitation functions for the production of the same nuclides from different target isotopes differ both in the shape and magnitude up to an order of magnitude and more in the whole region of incident energies. Therefore, to predict unknown excitation functions from a target with a natural composition of isotopes, it is necessary to perform calculations for all isotopes of the target taking into account the percentage of each. Similar problems arise when we would like to compare calculated and experimental excitation functions: for an accurate comparison it is necessary to know the exact isotopic composition of experimental samples and to perform calculations for the same composition, otherwise we may obtain large discrepancies only because we compare different things.

The next problem for an accurate comparison between experimental and theoretical excitation functions is connected with the so called "individual" and "cumulative" yields. All theoretical models give "individual" cross sections for the production of specific nuclides at "zero time" after a nuclear reaction. On the contrary, the gamma-spectrometry method used in the majority of current measurements provides only "cumulative" yields, i.e., the "measured" cross sections contain contributions from all radioactive precursors which through their decay chains lead to the production of the detected nuclides. Only if there are no radioactive precursors contributing to a given nuclide will the measured cross section be "independent". For many nuclides, especially those produced from heavy targets, the cumulative yields may be an order of magnitude or more larger than the independent ones. Therefore, one should be very careful when comparing measured and calculated excitation functions, as one may obtain false differences of orders of magnitude simply due to comparison of different things. This point is especially important for models and codes which can allow only a limited number of nucleons to be emitted from targets.

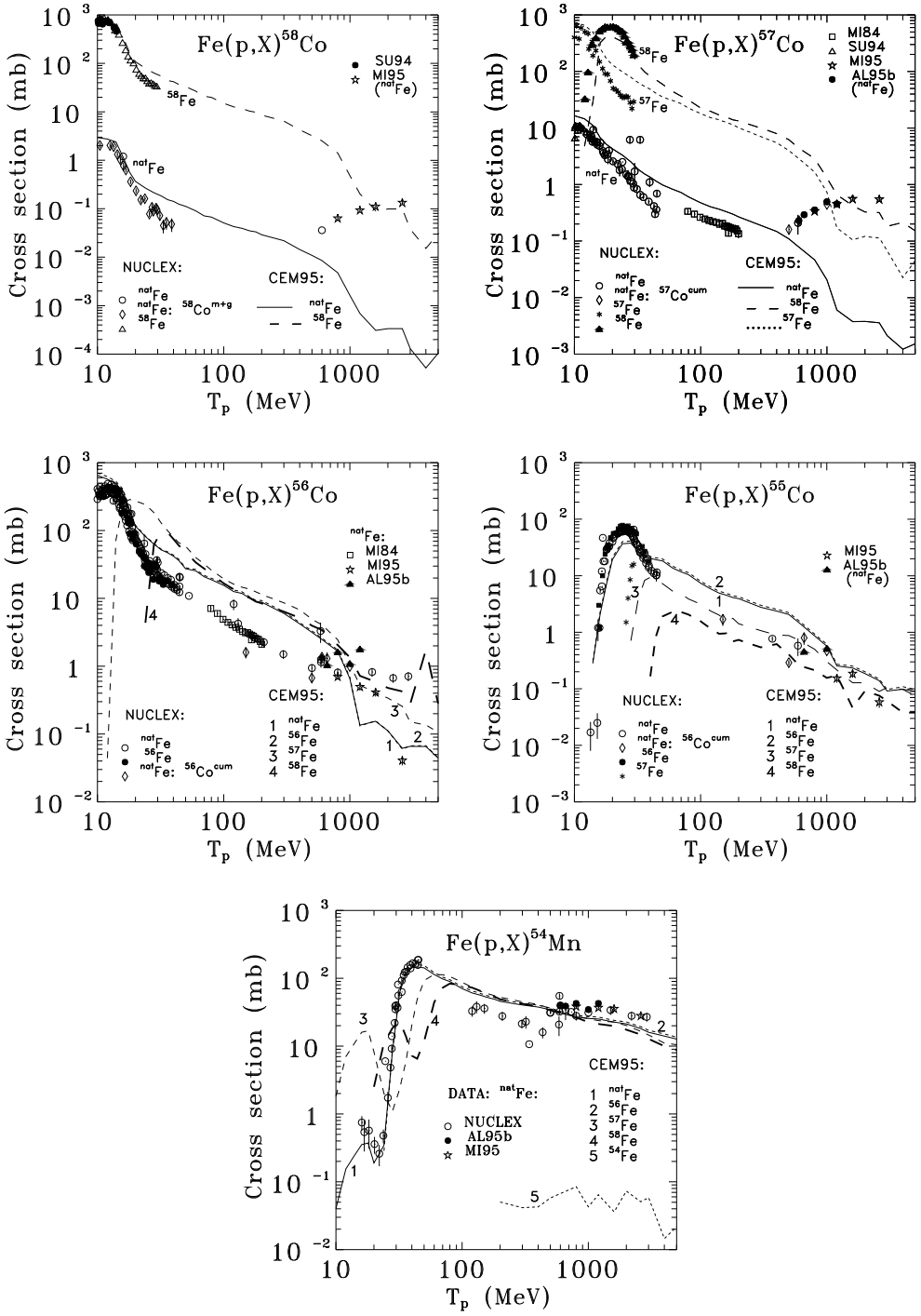

Fig. 15. Excitation functions for the production of ^{58}Co, ^{57}Co, ^{56}Co, ^{55}Co, and ^{54}Mn from interaction of protons with different isotopes of iron, as indicated. Experimental data are labeled as: SU94 [161], MI95 [43], MI84 [41], AL95b [142], and NUCLEX [46, 47].

Let us denote the "independent" yield of a nuclide (A, Z) by $\sigma^i(A, Z)$ and the "cumulative" yield, by $\sigma^{cum}(A, Z)$. From the definition of cumulative yields we have [162]

$$\sigma^{cum}(A, Z) = \sigma^i(A, Z) + \sum_{(A',Z')} b(A', Z' \to A, Z)\sigma^i(A', Z') \ , \tag{32}$$

where $b(A', Z' \to A, Z)$ is the fraction of decays of (A', Z') that go to (A, Z). For a decay chain

$$(A_1, Z_1) \to (A_2, Z_2) \to \cdots \to (A_n, Z_n)$$

defined by decay constants λ_j, half-lives $T^j_{1/2} = \ln 2/\lambda_j$, and branching ratios r_j the cumulative yield of a nth nuclide in the $\lambda_j \gg \lambda_n$ case can be calculated [77, 163] as:

$$\sigma^{cum}_n(A_n, Z_n) = \sigma^i_n(A_n, Z_n) + \frac{\lambda_{n-1}}{(\lambda_{n-1} - \lambda_n)} \sum_j \sigma^i_j(A_j, Z_j) r_j \ . \tag{33}$$

For the majority of cumulative yields calculated in the present work, the factors $\lambda_{n-1}/(\lambda_{n-1} - \lambda_n)$ in Eq. (33) and $b(A', Z' \to A, Z)$ in Eq. (32) are very close to one. For all targets and incident energies regarded here, we perform at the beginning calculations of individual yields for all possible nuclides, then, from these numerical files, calculate the corresponding cumulative yields. To simplify this work, we take into account in our calculations only precursors "k" with branching rations r_k nearly equal to one, and estimate cumulative yields approximately, as:

$$\sigma^{cum}(A, Z) = \sigma^i(A, Z) + \sum_k \sigma^i(A_k, Z_k) \ . \tag{34}$$

All precursors included in the calculations of each cumulative yield are shown explicitly in the figures and tables with our results in the following section. We use the radioactive decay chains and corresponding branching rations published in Refs. [163, 164].

4. Results and Discussion

In this section we present results of calculation and analysis of 597 excitation functions for reactions induced by protons from 10 MeV to 5 GeV on ^{12}C, ^{14}N, ^{16}O, ^{27}Al, ^{31}P, ^{40}Ca, ^{54}Fe, ^{56}Fe, ^{57}Fe, ^{58}Fe, ^{nat}Fe, ^{59}Co, ^{90}Zr, ^{91}Zr, ^{92}Zr, ^{94}Zr, ^{96}Zr, ^{nat}Zr, and ^{197}Au. To some extent, this study was inspired by the present *International Codes and Model Intercomparison for Intermediate Energy Activation Yields* [66]. Therefore we have included in our analysis target elements of ^{16}O, ^{27}Al, ^{nat}Fe, ^{59}Co, ^{nat}Zr, and ^{197}Au recommended by the Intercomparison as different types of materials which are important for technological applications [66]. Oxygen is a main constituent of ambient air and shielding concrete; aluminum is a structural material and one of the best investigated target nuclei being the most often used for monitoring purposes; iron and zirconium are structural materials also well investigated experimentally; cobalt was selected in order to test the model when calculating nuclide production near closed shells; and gold was chosen to represent the heavy target elements. For these targets, we include in our work not only the excitation functions required by the Intercomparison [66], but also all other excitation functions for which we found reliable experimental data. Furthermore, apart from the recommended targets of ^{nat}Fe and ^{nat}Zr of natural isotopic composition, we have included in our study also reactions on all isotopes of iron and zirconium, in order to analyze how excitation functions for the production of the same nuclides from different target isotopes depend on the isotopic spin of the target and how well CEM95 reproduces this effect. In addition to the targets recommended by the Intercomparison [66], we have included in our study also reactions with nuclei of human tissue ^{12}C, ^{14}N, ^{31}P, and ^{40}Ca, for which reliable data files are needed for dosage calculation in radiation oncology. For all targets considered in this work, we calculate excitation functions for the production of all possible nuclides in the framework of the extended version of the CEM [75] using the third systematics for $a(Z, N, E^*)$ by Iljinov et al. [110], except for interactions with the lightest ^{12}C, ^{14}N, and ^{16}O targets, for which, to avoid some computational troubles, we use the fixed value $a = 0.125A$ and perform calculations with the standard version of the CEM [68, 69]. Below we show results for the production of those nuclides for which we found reliable experimental data, and as a prediction, several excitation functions that are not measured yet, but are interesting for understanding mechanisms of nuclear reactions and for some applications.

Let us show our results starting with the lightest target ^{12}C and moving successively to heavier ones, up to ^{197}Au.

4.1. Targets ^{12}C, ^{14}N, and ^{16}O

These lightest targets are just "the most difficult" for us, as the CEM, similarly to other Monte Carlo statistical models, is not well justified for light nuclei. None of the three stages of nuclear reactions considered by the CEM is well justified physically

for such light targets. The separation energies of nucleons from light nuclei differ significantly from the mean value of binding energy of 7 MeV used at the cascade stage of a reaction, the "trawling" effect mentioned in Section 2 is more important for light targets, but is not taken into account in CEM95, it is difficult to justify a division of a nucleus having only 12 nucleons into 7 potential zones, etc. It is also difficult to justify a process of statistical equilibration with possible emission of particles at the preequilibrium stage of reactions when after emission of several cascade nucleons we may have a system with less than 10 nucleons. It is even less well justified to evaporate particles at the last stage of reaction from a residual nucleus with only a few nucleons, when the assumptions of the evaporation model lose their validity. It probably makes more sense to use for the description of de-excitation of such light excited nuclei the Fermi breakup model, at least for relatively high values of excitation energy (see a detailed discussion of these questions, e.g., in Refs. [54, 82]), but this model is not incorporated into the CEM.

Taking all these points into account, it is questionable to expect a good description by the CEM of nuclide yields from such light targets. Nevertheless, our previous calculations [71] have shown that the CEM satisfactorily predicts spectra of secondary particles even for ^{12}C. It is interesting to check its applicability for a description of excitation functions from such targets. Due to a lack of better grounded and suitable models for incident energies of $\sim$ 1 GeV and above, similar statistical Monte Carlo approaches as implemented, e.g., in the codes HETC/KFA2 [165], DISCA2 [166], CASCADE [167] are often used [39, 60, 168, 169] to calculate excitation functions from such light targets.

The total inelastic cross section σ_{in} and excitation functions for the production of ^{12}N, $^{11;10}$C, $^{10;7}$Be, $^{9;8}$Li, $^{6;4;3}$He, t, d, p, n, π^+, π^0, and π^- from p+^{12}C calculated in our present work are shown in Figs. 16 and 17 together with available experimental data [40, 43, 46, 47, 54, 60, 158, 160, 170]. To understand the mechanisms of production of final isotopes predicted by the CEM, for ^{11}C and ^{10}C (Fig. 16), the contributions from the channels (p,d), (p,np), and (p,nd) to the total yields are shown separately. For ^{4}He, ^{3}He, t, d, p, and n, the contributions to the total production cross sections from preequilibrium emission, evaporation, and the cascade stage of the reaction (for nucleons), as well as the contribution of residual nuclei remaining after all three stages of the reactions are shown also in Fig. 17. For comparison, predictions of the phenomenological systematics by Korovin et al. [60] for the production of ^{4}He, ^{3}He, and t, are shown in Fig. 17 as well. CEM95 cross sections for the production of ^{3}He shown in Fig. 17 for ^{12}C, and in the following figures for other targets, are independent, without a contribution from the progenitor t.

Figs. 18 and 19 show a comparison of calculated σ_{in} and excitation functions for the production of ^{14}O, ^{13}N, $^{11;10}$C, $^{10;7}$Be, $^{9;8}$Li, $^{4;3}$He, $^{3-1}$H, n, and $\pi^{+;0;-}$ from p+^{14}N with available experimental data [40, 43, 46, 47, 54, 158, 160]. For the production of ^{8}Li, independent and cumulative yields calculated according to Eq. (34) are shown separately.

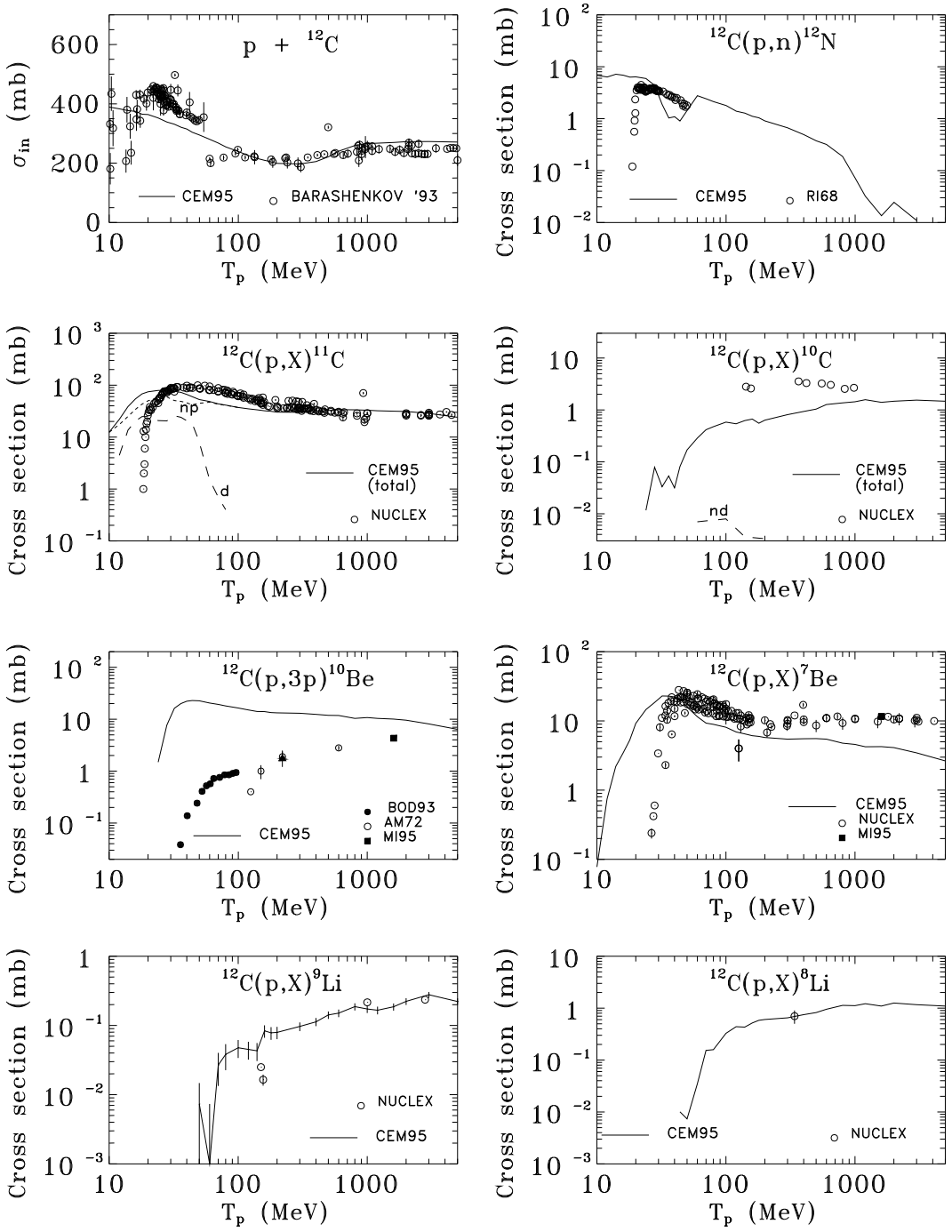

Fig. 16. Total inelastic cross section and excitation functions for the the production of ^{12}N, ^{11}C, ^{10}C, ^{10}Be, ^{7}Be, ^{9}Li, and ^{8}Li from p+^{12}C. For ^{11}C and ^{10}C, dashed lines show contributions from the channels (p,d), (p,np), and (p,nd) to the total yields, as indicated. Experimental data are labeled as: BARASHENKOV'93 [158], RI68 [170], NUCLEX [46, 47], BOD93 [40], AM72 [160], and MI95 [43].

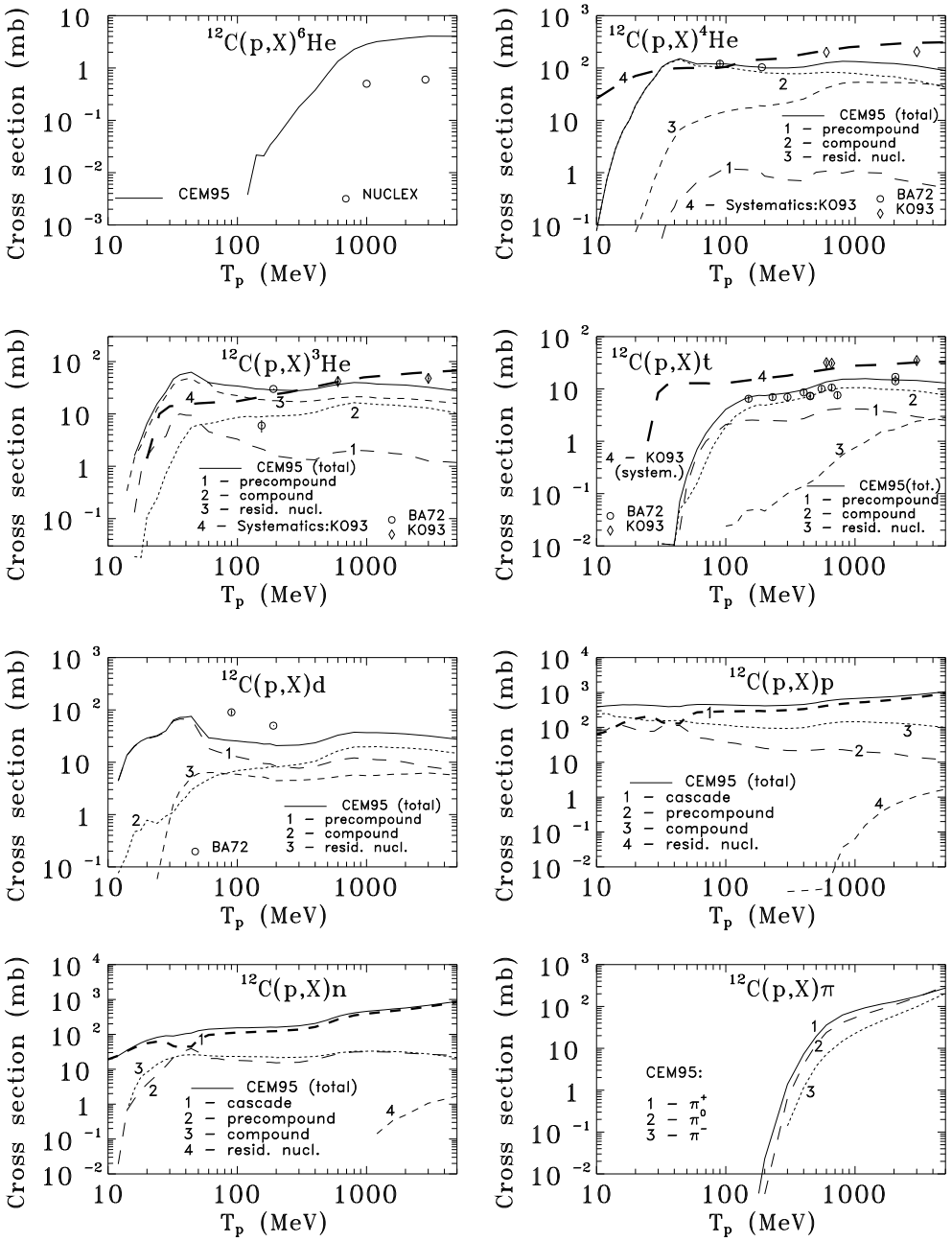

Fig. 17. Excitation functions for the the production of ^{6}He, ^{4}He, ^{3}He, t, d, p, n, π^+, π^0, and π^- from p+^{12}C. The contribution to the total yields of nucleons and complex particles from preequilibrium emission, evaporation, and the cascade stage of the reaction (for nucleons), as well as the contribution of residual nuclei remaining after all three stages of the reactions to the total CEM95 yields are shown separately by dashed lines, as indicated. Experimental data are labeled as: NUCLEX [46, 47], BA72 [54], and KO93 [60]. For ^{4}He, ^{3}He, and t, predictions of the phenomenological systematics by Korovin et al. [60] are shown by thick long dashed lines labeled by 4.

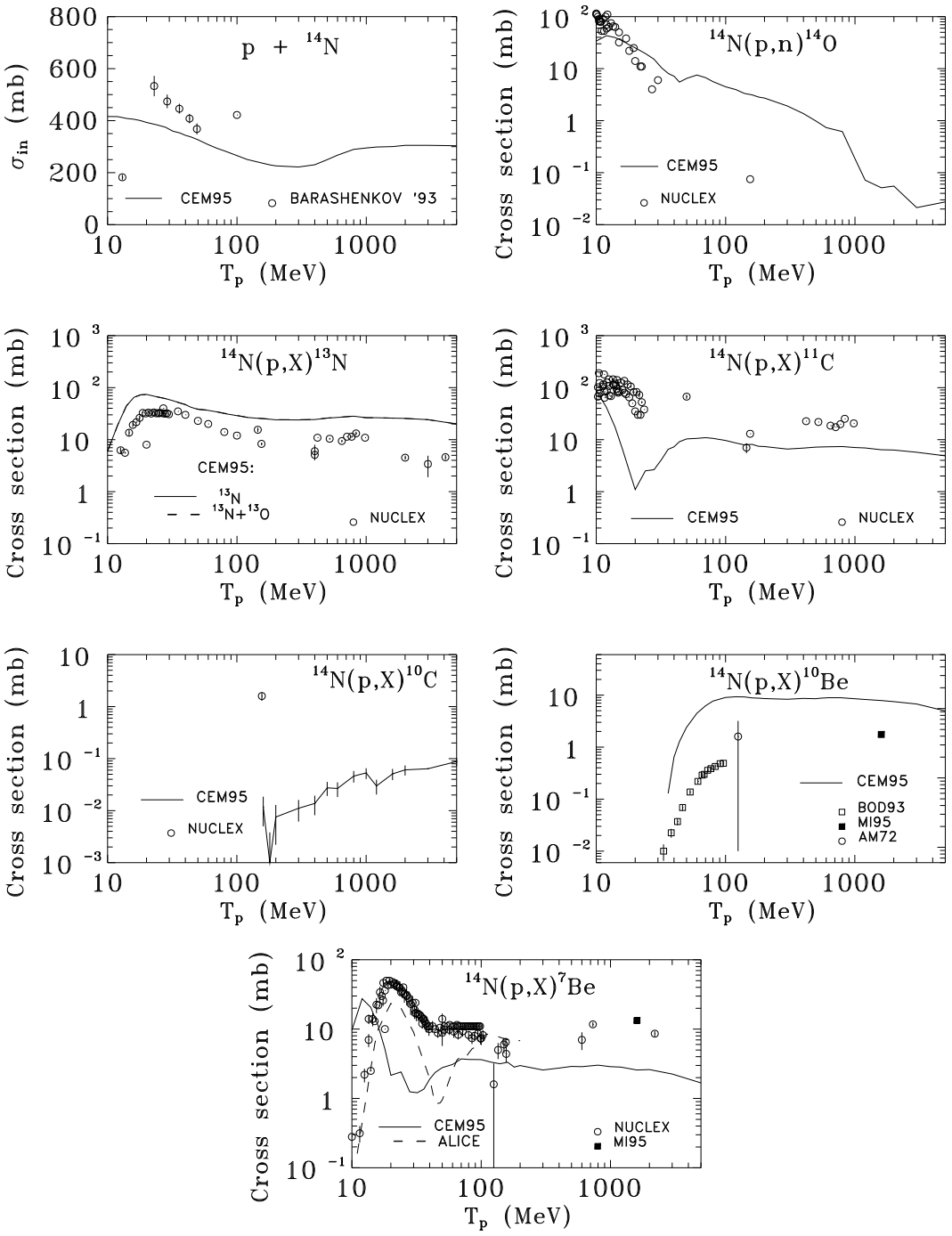

Fig. 18. Total inelastic cross section and excitation functions for the production of ^{14}O, ^{13}N, ^{11}C, ^{10}C, ^{10}Be, and ^{7}Be from p+^{14}N. For ^{7}Be, the dashed line shows the results obtained in Ref. [40] with the hybrid model code ALICE LIVERMORE 87 [171] using the Myers and Swiatecki mass formula [113] (see Fig. 3 and details in Ref. [40]). Experimental data are labeled as: BARASHENKOV'93 [158], NUCLEX [46, 47], BOD93 [40], MI95 [43], and AM72 [160].

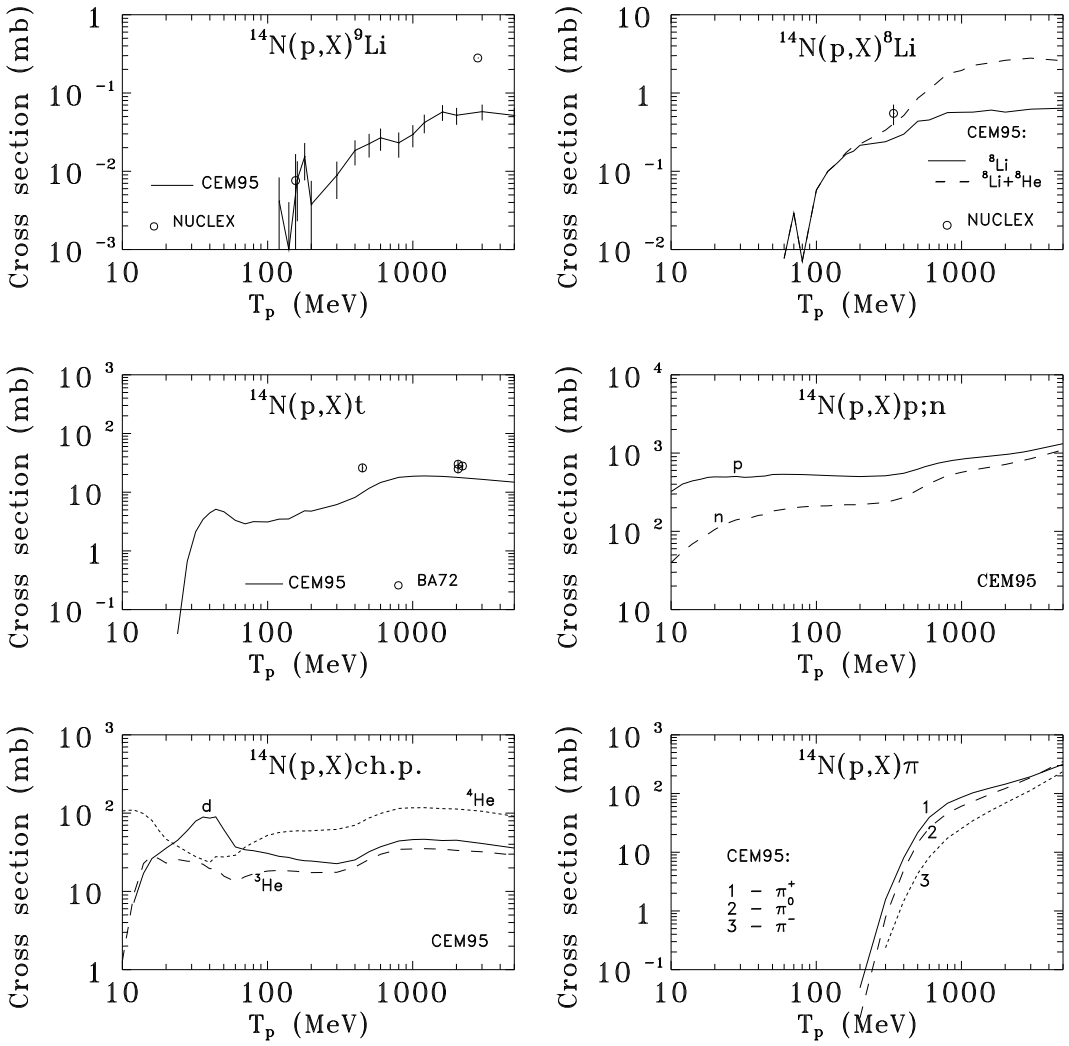

Fig. 19. Excitation functions for the production of ^{9}Li, ^{8}Li, ^{4}He, ^{3}He, t, d, p, n, π^+, π^0, and π^- from p+^{14}N. For ^{8}Li, the independent and cumulative yields are shown by solid and dashed lines, respectively. Experimental data are labeled as: NUCLEX [46, 47] and BA72 [54].

The results of calculation of σ_{in} and of excitation functions for the production of $^{15;14}$O, ^{13}N, $^{14;11;10}$C, $^{11;10}$B, $^{10;9;7}$Be, $^{9;7;6}$Li, $^{4;3}$He, $^{3-1}$H, n, and $\pi^{+;0;-}$ from p+^{16}O are compared in Figs. 20–22 with available experimental data [40, 43, 46, 47, 143, 158, 159, 160], with results of calculations of ^{10}Be yield using the codes ALICE LIVERMORE 87 [171] and HETC/KFA2 [165] from Ref. [169] in Fig. 21, and with the predictions of the phenomenological systematics from Ref. [60] for the production of t in Fig. 22.

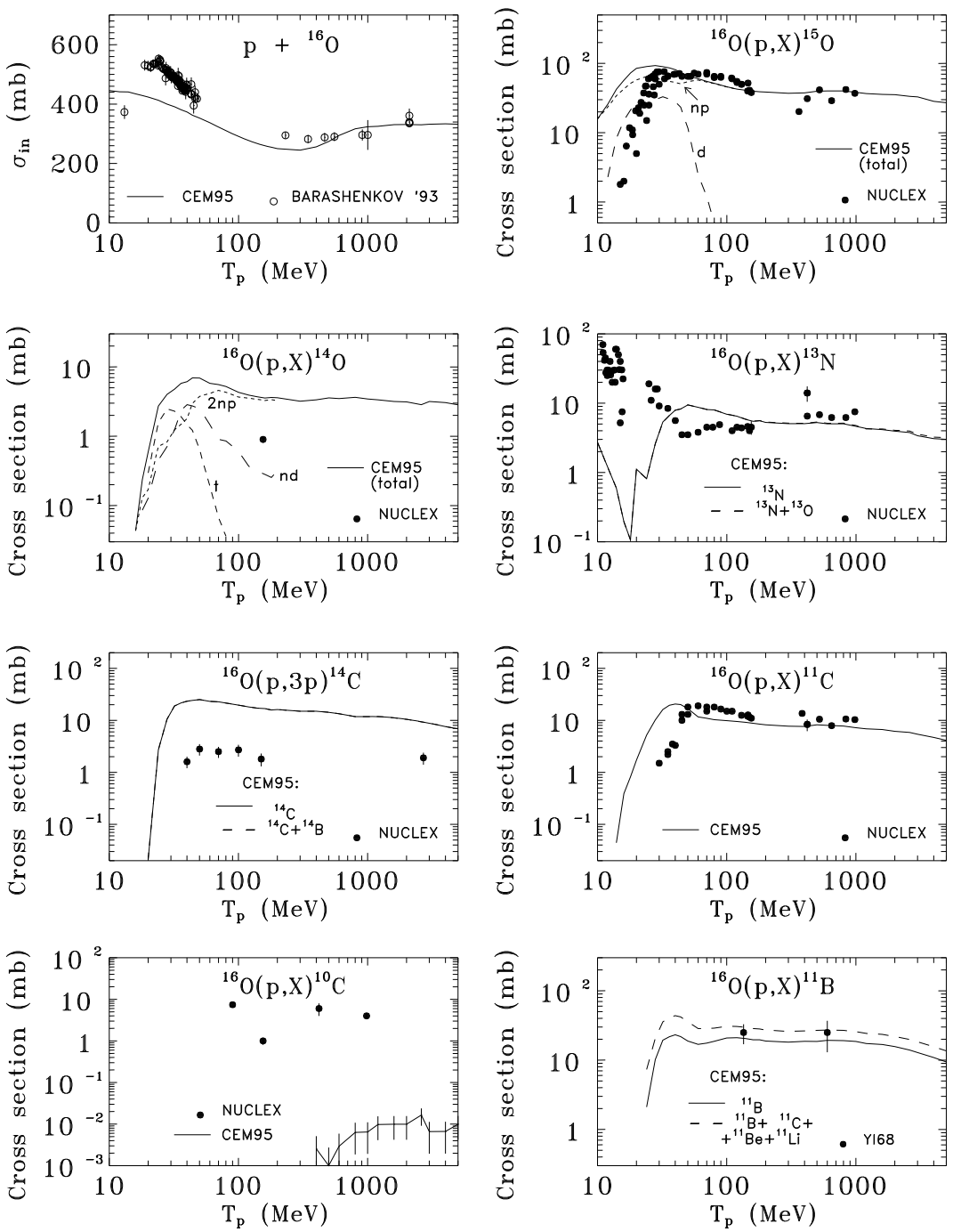

Fig. 20. Total inelastic cross section and excitation functions for the production of ^{15}O, ^{14}O, ^{13}N, ^{14}C, ^{11}C, ^{10}C, and ^{11}B from p+^{16}O. For ^{15}O and ^{14}O, dashed lines show the contributions from the channels (p,d), (p,np), (p,t), (p,nd), and (p,2np) to the total yields, as indicated. For ^{13}N, ^{14}C, and ^{11}B, the independent and cumulative yields are shown by solid and dashed lines, respectively (for ^{13}N and ^{14}C, they are practically the same). Experimental data are labeled as: BARASHENKOV'93 [158], NUCLEX [46, 47], and YI68 [159].

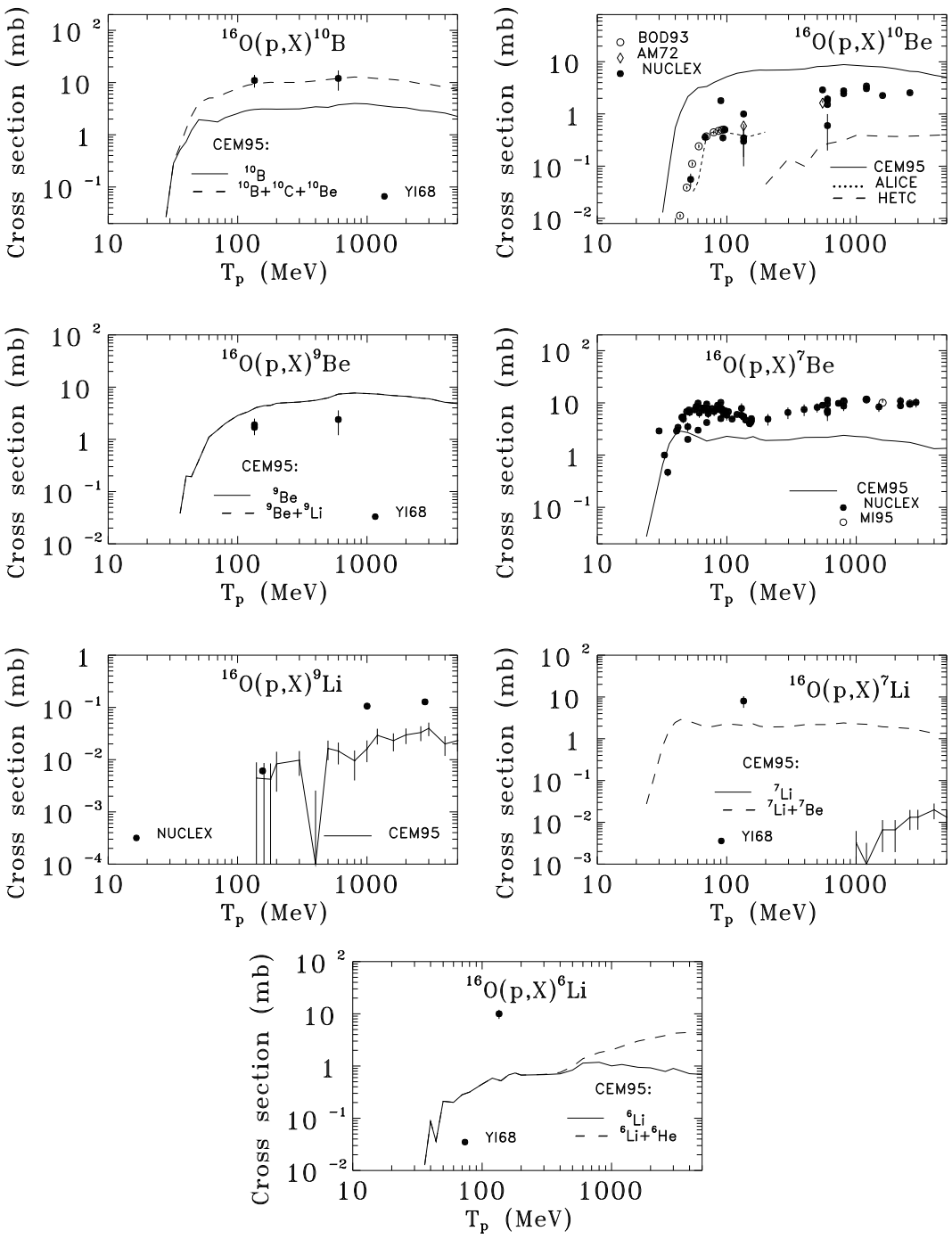

Fig. 21. Excitation functions for the production of ^{10}B, ^{10}Be, ^{9}Be, ^{7}Be, ^{9}Li, ^{7}Li, and ^{6}Li from p+^{16}O. For ^{10}Be, the results from Fig. 1 of Ref. [169] calculated with the codes ALICE LIVERMORE 87 [171] and HETC/KFA2 [165] are shown by dotted and dashed lines, respectively. Experimental data are labeled as: YI68 [159], BOD93 [40], AM72 [160], NUCLEX [46, 47], and MI95 [43]. The rest of the notation is the same as in Fig. 20.

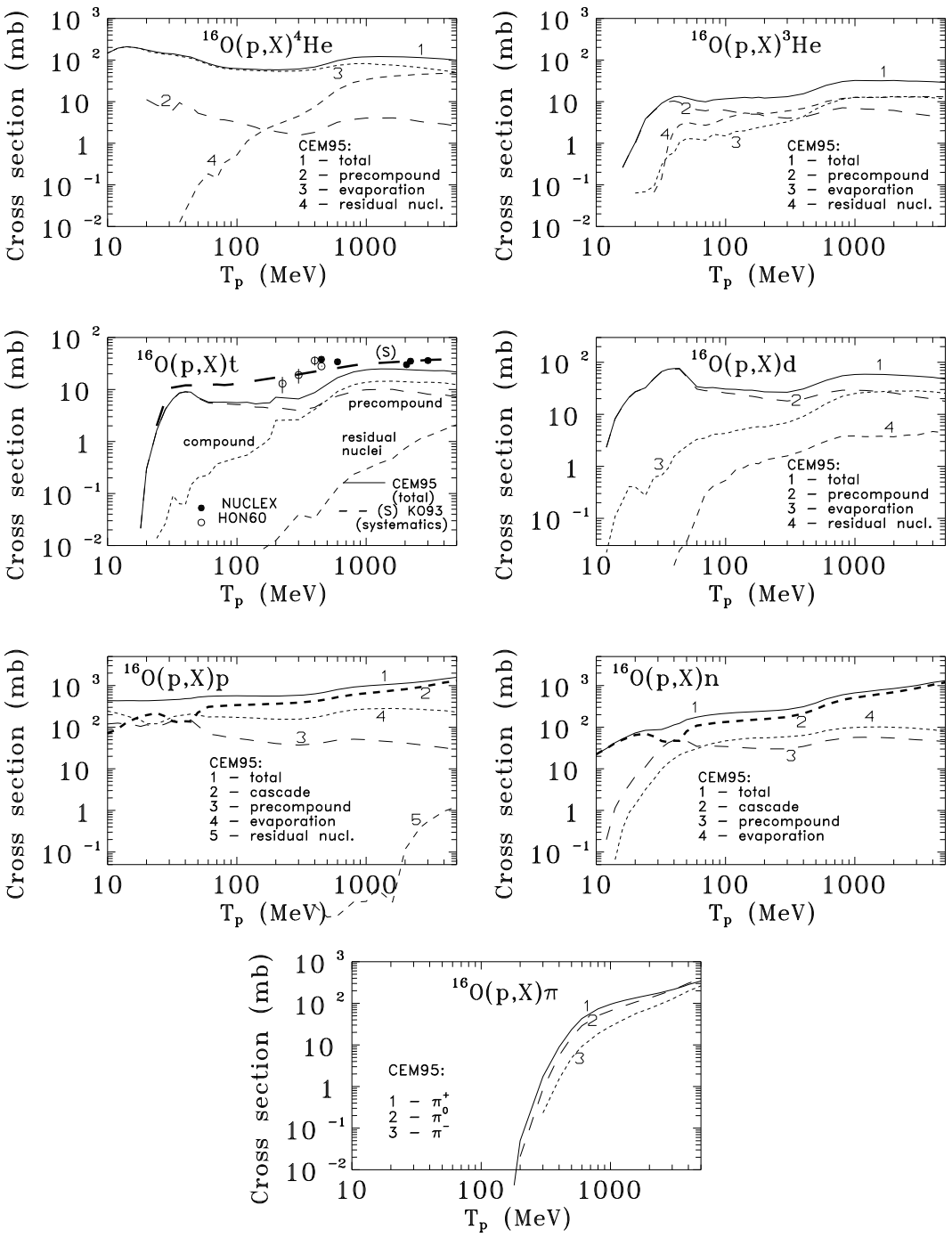

Fig. 22. Excitation functions for the production of ^{4}He, ^{3}He, t, d, p, n, π^+, π^0, and π^- from p+^{16}O. The contribution to the total yields from cascade, preequilibrium, evaporation emission, and from residual nuclei after all three stages of the reaction are shown separately by dashed lines, as indicated. For t, the prediction of phenomenological systematics from Ref. [60] is shown by a thick long dashed line marked with an (s). Experimental data are labeled as: NUCLEX [46, 47] and HON60 [143].

Contributions from the channels (p,d), (p,np), (p,t), (p,nd), and (p,2np) to the total yields are shown in Fig. 20 for the production of ^{15}O and ^{14}O, and from cascade, preequilibrium, evaporation emissions, and from residual nuclei, are shown in Fig. 22 for ^{4}He, ^{3}He, t, d, p, and n, respectively.

One can see that, on the whole, the agreement between calculations and experimental data is poor for these light targets. Sometimes, the CEM reproduces the shapes, and for some reactions, the absolute values of measured excitation functions for not too low incident energies. But for several reactions, like ^{12}C(p,3p)^{10}Be, ^{14}N(p,x)^{11}C, ^{14}N(p,x)^{7}Be, ^{16}O(p,x)^{13}N, the CEM fails to reproduce correctly the form of experimental data. For other reactions, like ^{12}C(p,x)^{7}Be, ^{14}N(p,x)^{13}N, ^{16}O(p,x)^{10}Be, the form of experimental excitation functions are reproduced satisfactorily but the difference in the absolute values is too large.

As discussed above, there are many aspects of the CEM not appropriate to such light targets and there are many causes of the observed discrepancies. Nevertheless, taking into account the results presented in Section 3, we think that such serious discrepancies are caused mainly by poor nuclear masses, binding energies, and consequent Q-values used in CEM95 for these nuclides. First, we calculate the binding energies of preequilibrium and evaporative particles using the Cameron formula [111]. This formula is old and fails to describe correctly the masses of some nuclides. It is preferable to use for this purpose the recent experimental mass tables [172] and where they are absent, some new and more reliable mass formulas, e.g., from Ref. [173]. This has been done in a newer version of the CEM, and its effect will be discussed in a separate paper. A more serious problem for light nuclides are masses and binding energies used at the cascade stage of reactions. The Dubna ICM [54] used as the first stage of reactions in the CEM is a purely classical approach which does not use any nuclear structure effects. The mass of a nucleus is calculated in the ICM simply as the atomic mass number times the mean mass of a nucleon, and a mean separation energy for nucleons $B_N \simeq 7$ MeV is used for all nuclides. The last point is partially justified only for medium and heavy nuclei, but for light targets, it is often strongly violated. So, if ^{10}Be is produced in the reaction ^{12}C(p,3p)^{10}Be via a consecutive emission of three protons, the experimental separation energies for these protons are [172] 1.943551, 15.9570, and 11.2276 MeV, respectively, which differ significantly from the value of 7 MeV used in the CEM. In the case of the production of ^{14}C from p+^{16}O, the experimental separation energies of the three consecutively emitted protons are [172] 0.560, 12.12747, and 10.20736 MeV, which also differ greatly from 7 MeV. We think that this is one of the weaker points of CEM95 and of all codes using fixed values for the mean nucleon binding energy B_N of cascade nucleons, if one wishes to describe with these codes yields of nuclides from light targets. This includes all modifications of HETC [174] using the standard Bertini ICM [83] with $B_N = 7$ MeV, HETC-3STEP [92] ($B_N = 8$ MeV), NUCLEUS [152] ($B_N = 7$ MeV), and INUCL [175] ($B_N = 5$–7 MeV). Probably it is necessary to use in CEM95 and other codes experimental mass tables augmented by new and reliable mass formulas for the cascade stage of reactions, as is already done in some codes, like DISCA2 [166]

or CASCADE [167].

For comparison, the results of Michel's group for the production of ^{7}Be from ^{14}N obtained in Ref. [40] with the hybrid model code ALICE LIVERMORE 87 [171] using the Myers and Swiatecki mass formula [113] are shown in Fig. 18, and the yields of ^{10}Be from ^{16}O calculated with the codes ALICE LIVERMORE 87 [171] and HETC/KFA2 [165] from Ref. [169] are shown in Fig. 21. One can see that HETC/KFA2 [165] also fails to reproduce the excitation function ^{16}O(p,x)^{10}Be, while ALICE LIVERMORE 87 [171] reproduces correctly the production of ^{10}Be from ^{16}O but fails to describe the reaction ^{14}N(p,x)^{7}Be.

As the CEM reasonably describes the spectra of nucleons, pions and composite particles from such light targets [71], the corresponding excitation functions for the production of ^{4}He, ^{3}He, t, and d agree better with the scarce available experimental data and with predictions of phenomenological systematics by Korovin et al. [60] (Figs. 17, 19, and 22) than do those for production of heavier nuclei. We do not know of any experimental data for yields of nucleons and pions from these targets, so our results shown in Figs. 17, 19, and 22 for these cross sections may serve as predictions.

When our study was completed, two new papers by Michel's group were published [176, 44]. They contain new measurements for these and other targets considered in our work, as well as results of calculations with the codes HETC/KFA2 [165] and AREL [177] which is a relativistic version of the popular hybrid model code ALICE. As a detailed comparison with these new data and calculations is not included in the present paper, let us note only that neither HETC/KFA2 [165] nor AREL [177] are able to reproduce correctly the production of ^{10}Be and ^{7}Be from carbon, nitrogen and oxygen, although AREL shows better results for energies below $\sim$ 200 MeV.

4.2. Target ^{27}Al

Excitation functions from p+^{27}Al are some of the best measured and most widely investigated theoretically. Our results for production of $^{27;26}$Si, ^{26}Al, $^{27;23}$Mg, and $^{25;24;22}$Na are shown in Fig. 23; for $^{24-20}$Ne, $^{20;18}$F, and ^{19}O, in Fig. 24; for $^{17;13}$N and $^{16;11}$C, in Fig. 25, and for $^{10;7}$Be, ^{9}Li, $^{6;4;3}$He, and t, in Fig. 26. The CEM independent yields are shown by solid lines, with the corresponding cumulative yields by dashed lines. For some nuclides like ^{26}Al, ^{23}Mg, $^{25;24;22}$Na, $^{23;21}$Ne, and $^{20;18}$F, cumulative and independent yields are so close that the corresponding lines on our plots practically coincide. But for several nuclides like ^{22}Ne and ^{20}Ne, cumulative yields (shown on plots by thick dashed lines) are about one order of magnitude higher that the independent ones, indicating a careful consideration of the proper yield calculations is necessary.

^{27}Al is not as light as the previous targets and is already more suitable to be calculated with the CEM. One can see that on the whole, the agreement of calculations with measured data is much better than for C, N, and O, although some large

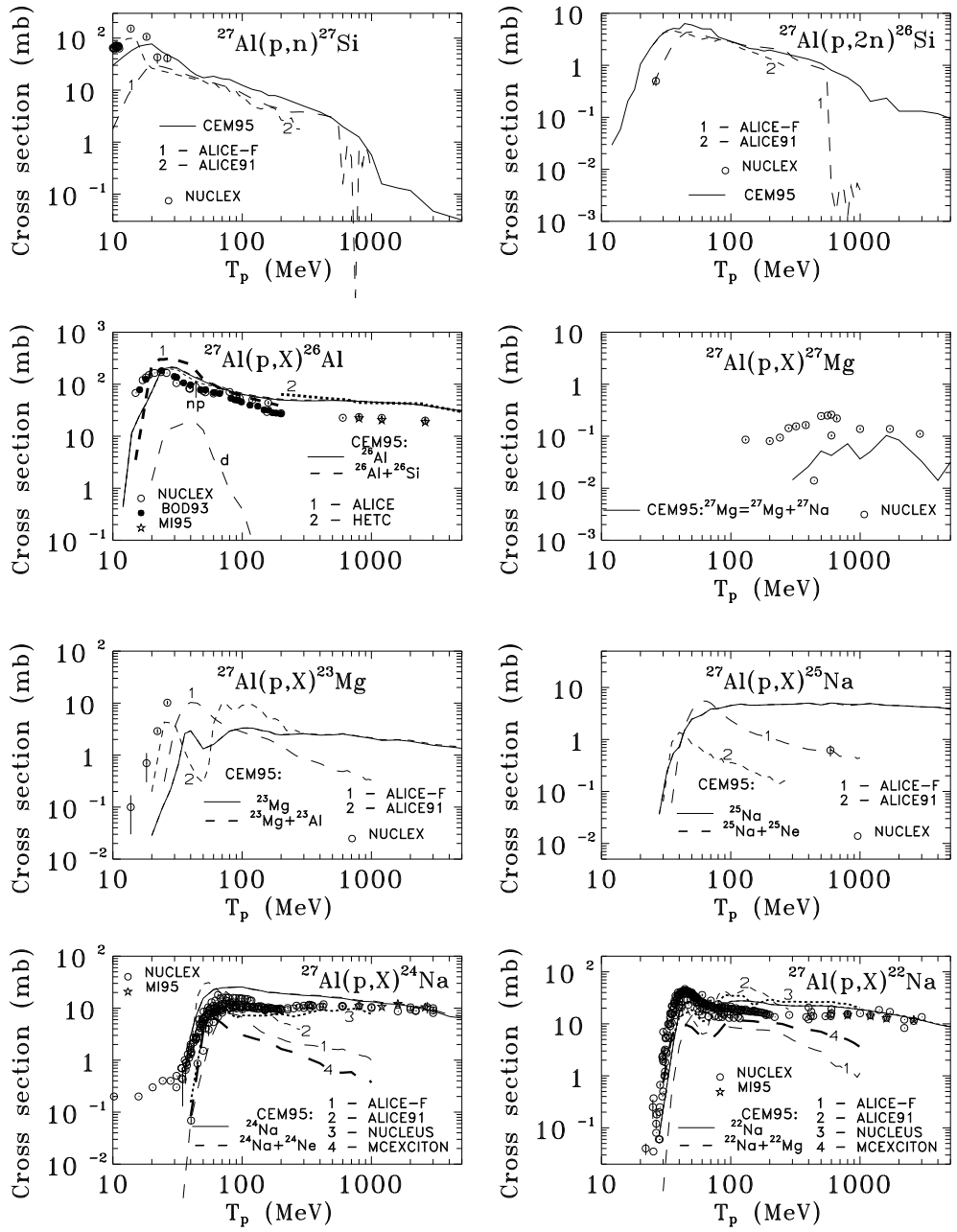

Fig. 23. Excitation functions for the production of ^{27}Si, ^{26}Si, ^{26}Al, ^{27}Mg, ^{23}Mg, ^{25}Na, ^{24}Na, and ^{22}Na from p+^{27}Al. For comparison, the results [178] of the recent JAERI Benchmark [62, 63] obtained with the codes ALICE-F [179], ALICE91 [180], NUCLEUS [152], and MCEXCITON [181] are shown by dashed lines 1, 2, 3, and 4, respectively. For ^{26}Al, the results from Fig. 3 of Ref. [169] calculated with the codes ALICE LIVERMORE 87 [171] and HETC/KFA2 [165] are shown by dashed lines 1 and 2, as indicated. The independent and cumulative CEM95 yields are plotted by solid and dashed lines which for these reactions are very close to each other. For ^{26}Al, the contributions to the total CEM95 yield from the channels (p,d) and (p,np) are shown separately by dashed lines, as indicated. Experimental data are labeled as: NUCLEX [46, 47], BOD93 [40], and MI95 [43].

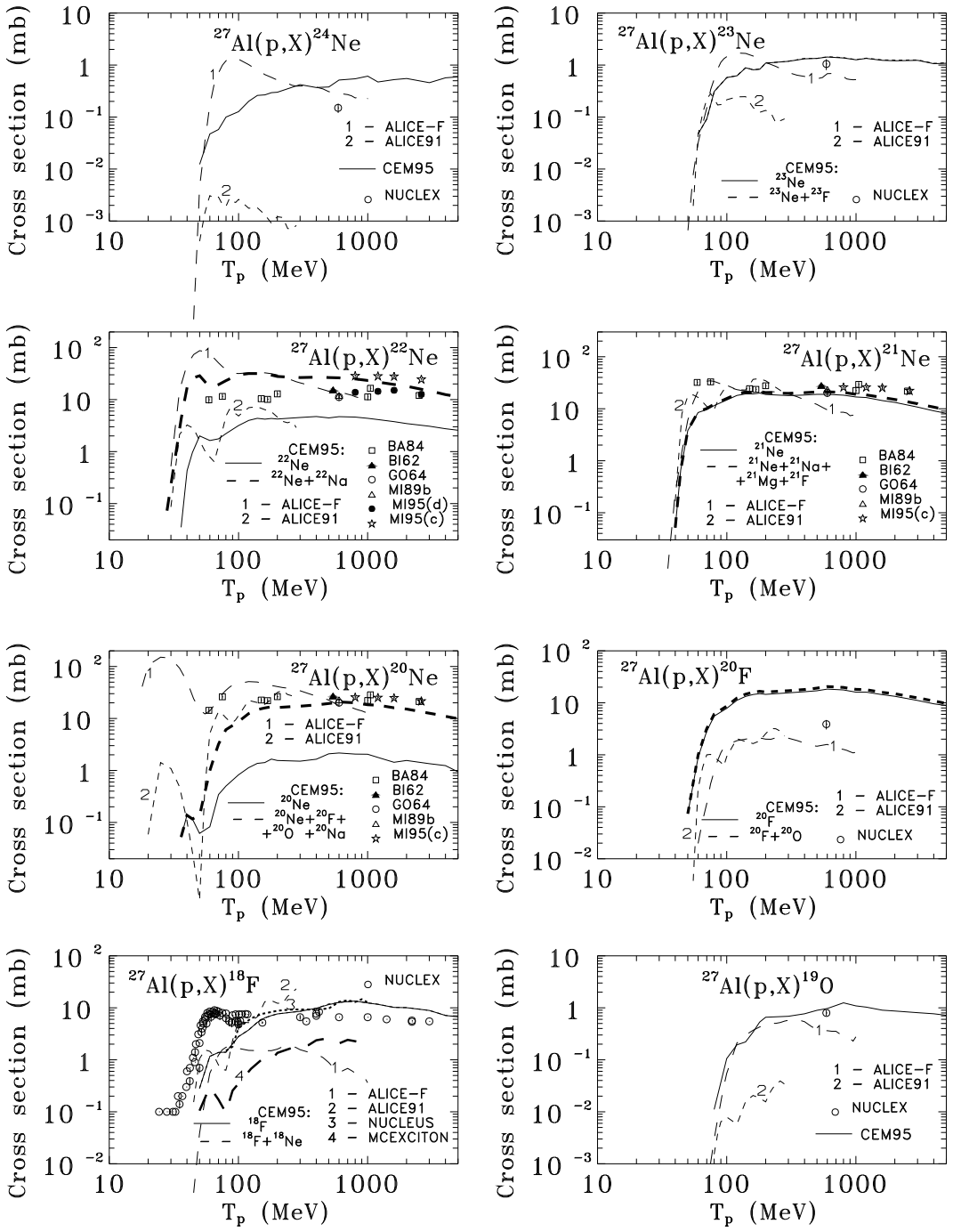

Fig. 24. Excitation functions for the production of ^{24}Ne, ^{23}Ne, ^{22}Ne, ^{21}Ne, ^{20}Ne, ^{20}F, ^{18}F, and ^{19}O from p+^{27}Al. For comparison, the results [178] of the recent JAERI Benchmark [62, 63] obtained with the codes ALICE-F [179], ALICE91 [180], NUCLEUS [152], and MCEXCITON [181] are shown by dashed lines 1, 2, 3, and 4, respectively. Experimental data are labeled as: NUCLEX [46, 47], BA84 [182], BI62 [183], GO64 [184], MI89b [185], and MI95 [43].

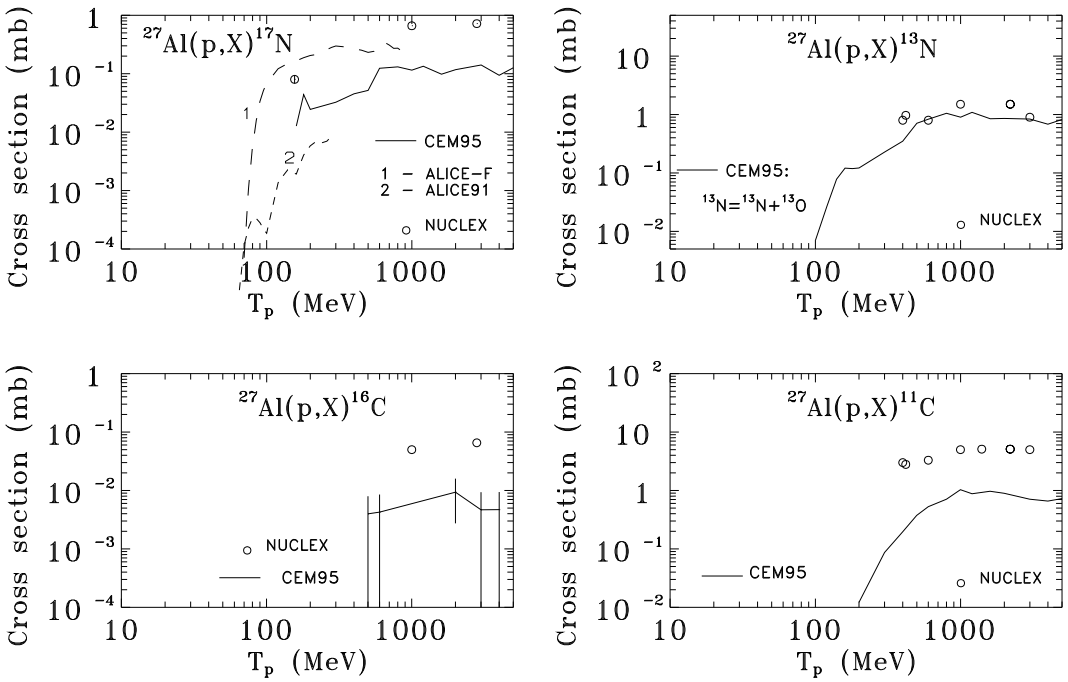

Fig. 25. Excitation functions for the production of ^{17}N, ^{13}N, ^{16}C, and ^{11}C from p+^{27}Al. The results [178] of the recent JAERI Benchmark [62, 63] obtained with the codes ALICE-F [179] and ALICE91 [180] are shown by dashed lines 1 and 2, respectively. Experimental data are labeled as NUCLEX [46, 47].

systematic discrepancies for several nuclides still occur. We believe these discrepancies result mainly from two different causes. First, the strong overestimation of the production of ^{26}Si, ^{25}Na, ^{24}Ne, ^{20}F, and the underproduction of $^{27;23}$Mg and ^{17}N are probably caused by the inaccurate masses and binding energies used in CEM95. For example, the separation energies of the two neutrons emitted in the reaction ^{27}Al(p,2n)^{26}Si are equal to 17.179 and 13.312 MeV in the experimental mass tables [172], much different from the value 7 MeV used in CEM95 for cascade neutrons.

The underproduction of ^{16}C and ^{11}C may be partly be caused for the same reason, as well as by a second and separate one, which may be seen more obviously for fragments ^{10}Be, ^{7}Be, and ^{9}Li (Fig. 26). The CEM does not contain a mechanism of fragmentation and does not take into account evaporation and preequilibrium emission of complex particles with $A > 4$. All light fragments predicted by the CEM are only residual nuclei remaining after all three stages of reactions. This is only a small part of the total production of fragments, and it is significant only for light enough targets and high incident energies. To be able to reproduce the production of fragments, the CEM has to be extended by incorporating mechanisms of fragmentation of heavy nuclei, Fermi breakup of highly excited light nuclei, evaporation, and preequilibrium emission of fragments with $A > 4$ from medium and heavy nuclei.

For comparison, the results [178] of the recent JAERI Benchmark [62, 63] obtained with the codes ALICE-F [179], ALICE91 [180], NUCLEUS [152], and MCEXCITON [181] are shown in Figs. 23–26 for several nuclides, and the results for ^{26}Al from Ref. [169] calculated with the codes ALICE LIVERMORE 87 [171] and HETC/KFA2 [165] are shown in Fig. 23 as well. One can see that on the whole, for these reactions, our calculations agree with experimental data better than results obtained with these codes. Let us note also that the total inelastic cross sections predicted (and used for normalization of all excitation functions) by different codes differ up to 25% at low incident energies (see the lower-right plot in Fig. 26).

To understand the CEM production mechanisms for ^{26}Al (Fig. 23), the contributions to the total yield from the channels (p,d) and (p,np) and for ^{4}He, ^{3}He, and t (Fig. 26), the contributions from preequilibrium emission, evaporation, and from residual nuclei are shown separately. We will discuss these results later in this section, making a comparison with other targets.

For production of ^{4}He and t, the prediction of phenomenological systematics by Korovin et al. [60] is shown in Fig. 26 for comparison. One can see that the yields of ^{3}He and t calculated with the CEM95 agree well with the experimental data and with systematics [60]. But for ^{4}He, the CEM underestimates the experimental data and results from Ref. [60]. The underproduction of ^{4}He is another serious problem of the CEM (just as it is for almost all other similar models) which we will discuss later.

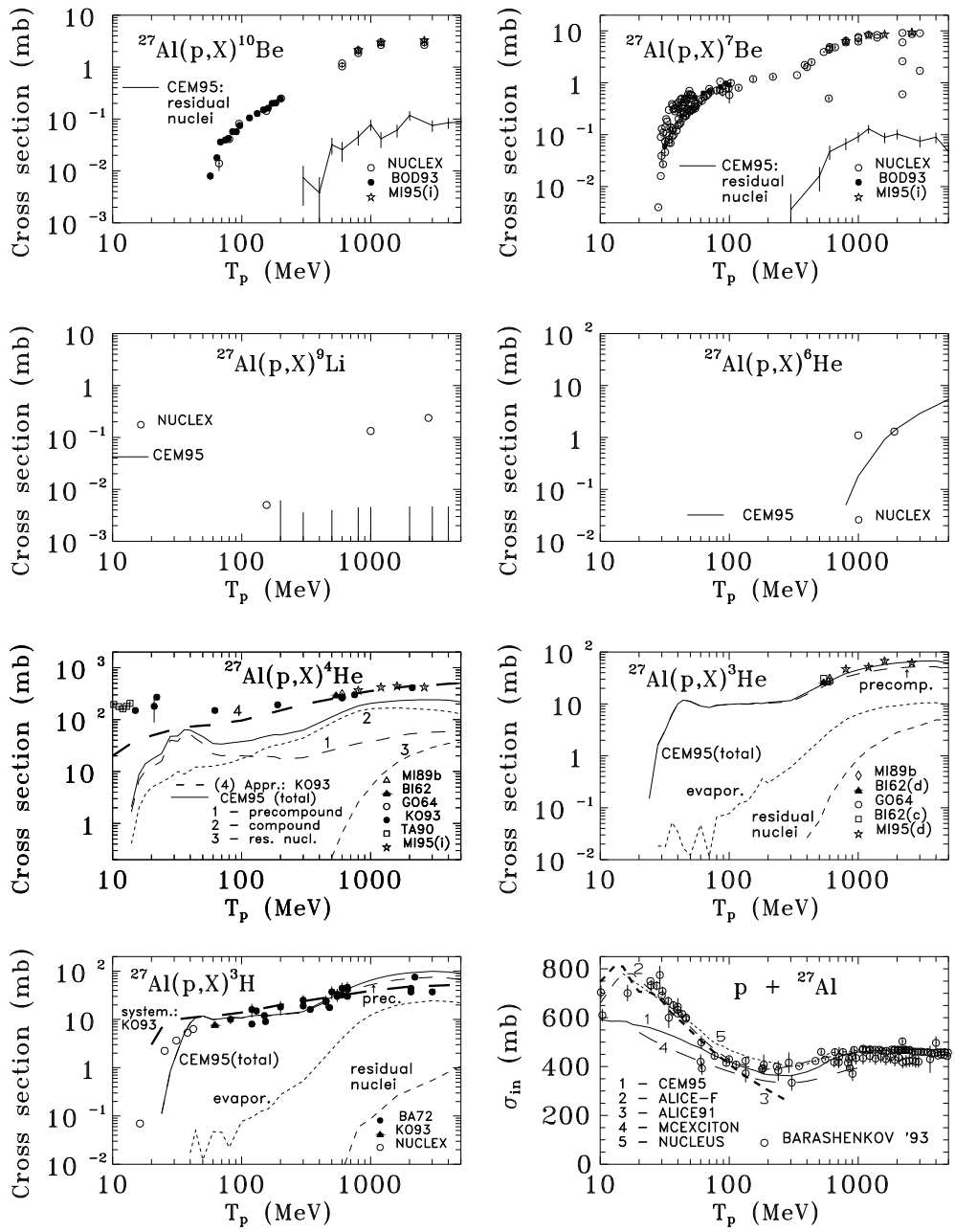

Fig. 26. Total inelastic cross section and excitation functions for the production of ^{10}Be, ^{7}Be, ^{9}Li, ^{6}He, ^{4}He, ^{3}He, and t from p+^{27}Al. Contributions to the total CEM95 yields of ^{4}He, ^{3}He, and t from preequilibrium emission, evaporation, and from residual nuclei are shown separately by dashed lines, as indicated. Inelastic cross sections calculated with the codes ALICE-F [179], ALICE91 [180], and MCEXCITON [181] are taken from files [178] of the recent JAERI Benchmark [62, 63]; σ_{in} calculated with the code NUCLEUS [152] is taken from Fig. 13 of Ref. [63]. For production of ^{4}He and t, the prediction of phenomenological systematics from Ref. [60] is shown by a thick long dashed line marked as KO93. Experimental data are labeled as: NUCLEX [46, 47], BOD93 [40], MI95 [43], MI89b [185], BI62 [183], GO64 [184], KO93 [60], TA90 [186], BA72 [54], and BARASHENKOV'93 [158].

4.3. Targets ^{31}P and ^{40}Ca

To our knowledge, these targets are less well investigated both experimentally and theoretically. A few more experimental data for the target element calcium and a calculation of the excitation function Ca(p,x)^{36}Cl with the codes HETC/KFA2 [165] and AREL [177] have been presented in a recent paper [176] published after our study was completed; these results are not included here.

Our prediction for σ_{in} and excitation functions for production of ^{30}P, ^{28}Mg, $^{24;22}$Na, $^{4;3}$He, t, d, p, n, π^+, π^0, and π^- from ^{31}P are shown in Fig. 27 together with experimental data from Refs. [46, 47].

Figs. 28–30 show a comparison of our results for σ_{in} and for excitation functions of production of ^{38}K, $^{39-36}$Ar, ^{36}Cl, ^{28}Mg, $^{24;22}$Na, $^{22-20}$Ne, ^{17}N, ^{16}C, ^{9}Li, $^{4;3}$He, $^{3-1}$H, n, and $\pi^{+;0;-}$ from p+^{40}Ca with available experimental data [43, 46, 47, 158, 182].

The general agreement of our results with these data and possible causes of some disagreements are the same as for the target ^{27}Al discussed above. Let us mention only the "dramatic" disagreement between the data and calculations that may be seen for ^{40}Ca(p,x)^{39}Ar. In reality, this is a false disagreement and a good example of the necessity to take into account in calculations the exact isotopic composition of the target measured. Above, we compared our calculations for ^{12}C, ^{14}N, and ^{16}O with the data not mentioning that the real measurements were performed on targets with natural isotopic composition. For carbon, nitrogen and oxygen this was reasonably justified, as the percentage of ^{12}C in carbon [187] is 98.892% (and only 1.108% for ^{13}C). For nitrogen and oxygen the corresponding percentage [187] is also appropriate: ^{14}N 99.635% and ^{15}N 0.365%; ^{16}O 99.759%, ^{17}O 0.0371%, and ^{18}O 0.2039%. Therefore the comparisons made in Figs. 16–22 were quite justified, although some discrepancies could be partly caused by isotopes of the targets which were not taken into account in our calculations.

In the case of calcium, a comparison of calculations for ^{40}Ca with data obtained for ^{nat}Ca is less justified as the percentage of ^{40}Ca in natural calcium is lower: ^{40}Ca 96.941%, ^{42}Ca 0.647%, ^{43}Ca 0.135%. ^{44}Ca 2.086%, ^{46}Ca 0.004%, and ^{48}Ca 0.187%.

^{39}Ar can be produced from p+^{40}Ca interactions only through the rare channel (p,2pπ^+), or through even more rare channels (p,np2π^+) and (p,2n3π^+). Therefore our calculated excitation function ^{40}Ca(p,x)^{39}Ar is different from zero only at energies above the pion production threshold and is small in value. The measured yield of ^{39}Ar comes mainly from interactions of incident protons with heavier isotopes of calcium, therefore it is already significant at 20 MeV and it is much higher than our results obtained from ^{40}Ca.

Another large discrepancy between experimental data and our calculations is also shown in Fig. 28, for ^{37}Ar. It probably occurs for the same reason just discussed for ^{40}Ca(p,x)^{39}Ar.

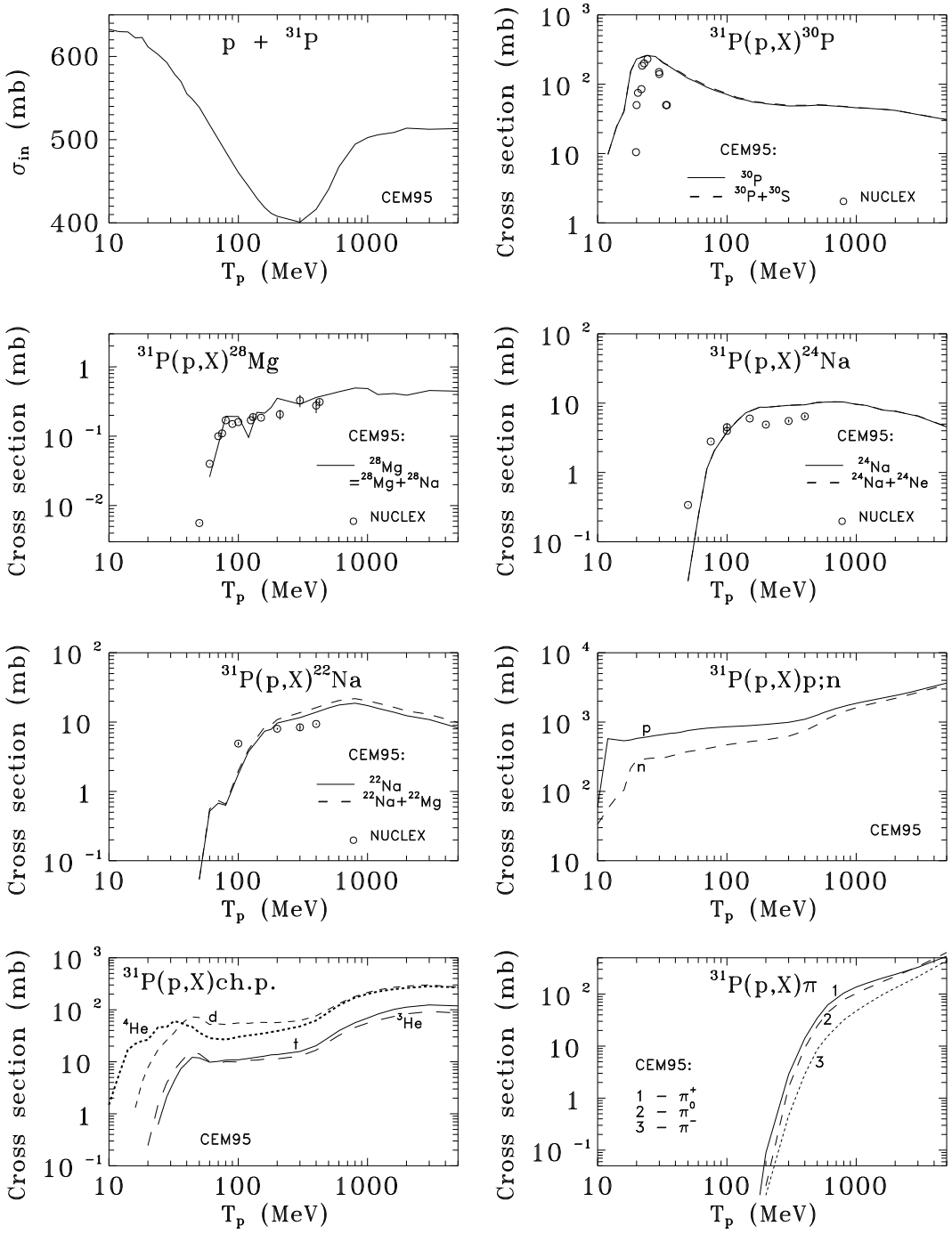

Fig. 27. Total inelastic cross section and excitation functions for the production of ^{30}P, ^{28}Mg, ^{24}Na, ^{22}Na, ^{4}He, ^{3}He, t, d, p, n, π^+, π^0, and π^- from p+^{31}P. Experimental data labeled as NUCLEX are from Refs. [46, 47].

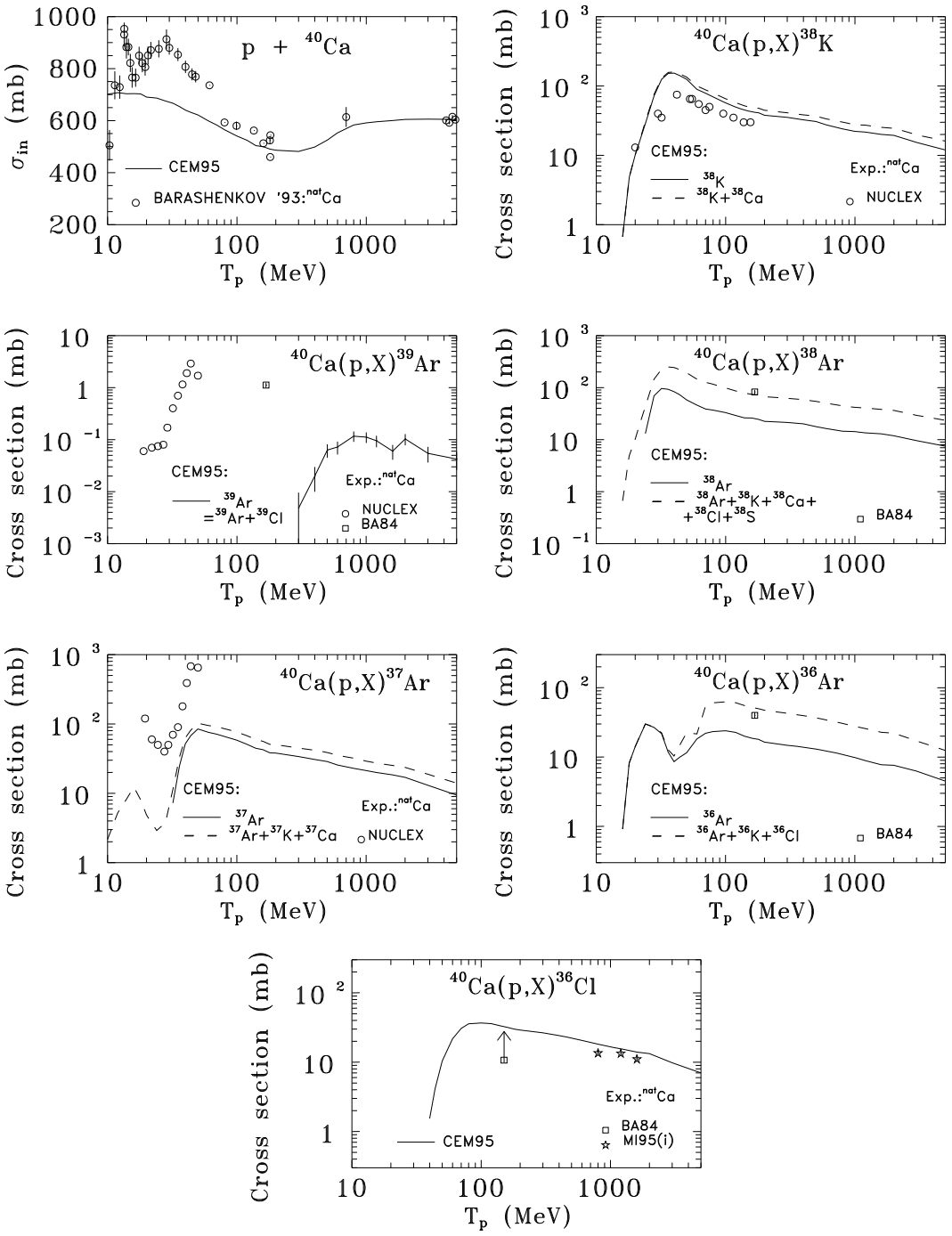

Fig. 28. Total inelastic cross section and excitation functions for the production of ^{38}K, ^{39}Ar, ^{38}Ar, ^{37}Ar, ^{36}Ar, and ^{36}Cl from p+^{40}Ca. Experimental data are labeled as: BARASHENKOV'93 [158], NUCLEX [46, 47], BA84 [182], and MI95 [43].

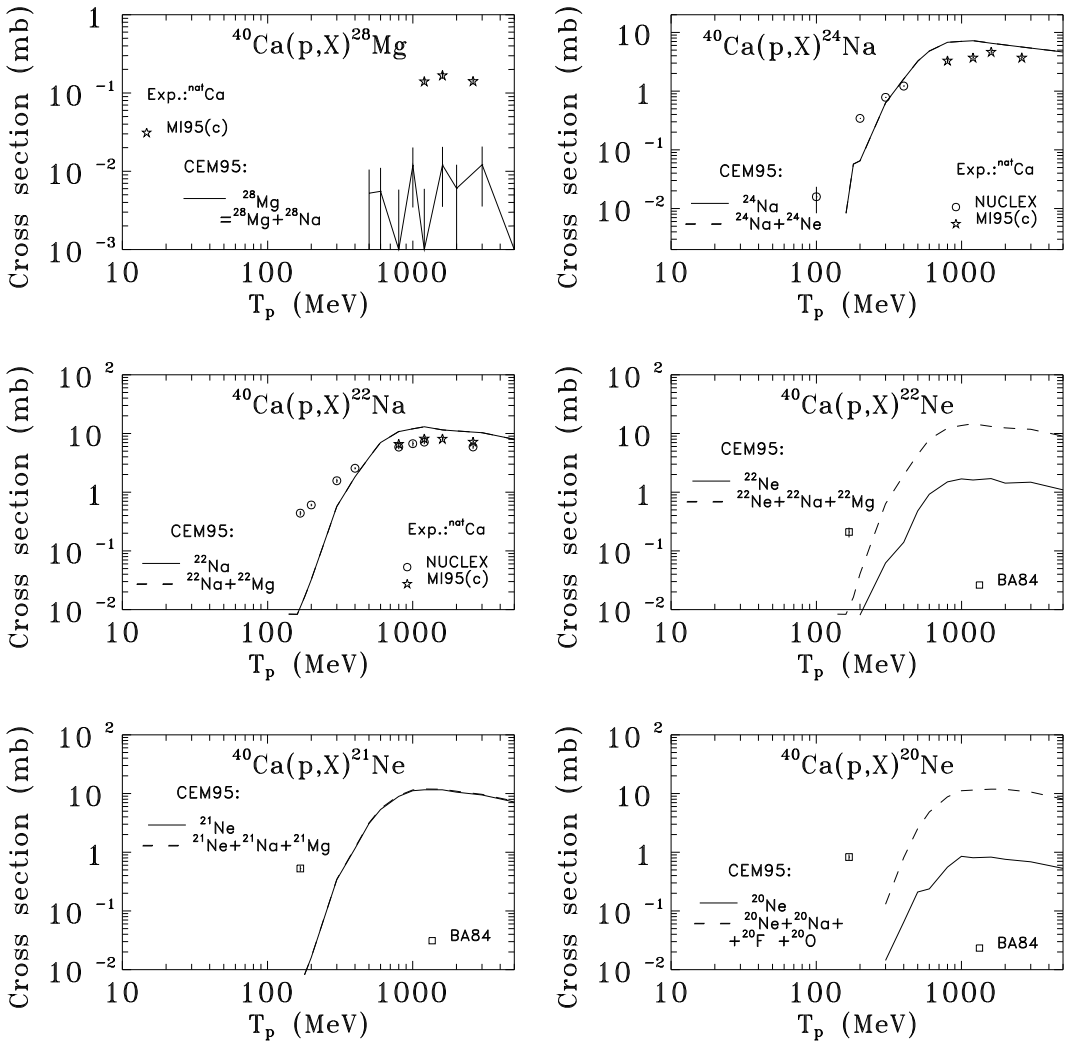

Fig. 29. Excitation functions for the production of ^{28}Mg, ^{24}Na, ^{22}Na, ^{22}Ne, ^{21}Ne, and ^{20}Ne from p+^{40}Ca. Experimental data are labeled as: MI95 [43], NUCLEX [46, 47], and BA84 [182].

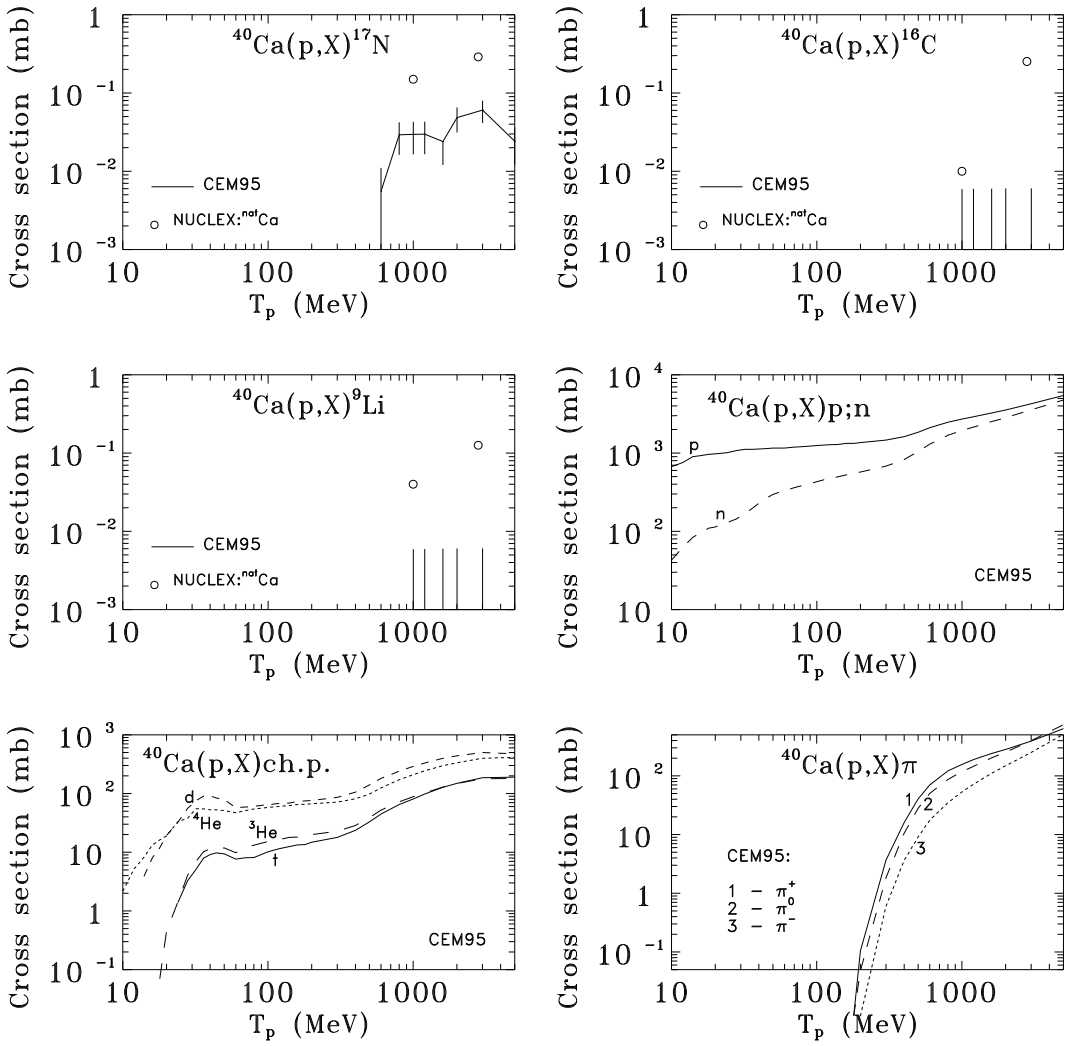

Fig. 30. Excitation functions for the production of ^{17}N, ^{16}C, ^{9}Li, ^{4}He, ^{3}He, t, d, p, n, π^+, π^0, and π^- from p+^{40}Ca. Experimental data labeled as NUCLEX are from Refs. [46, 47].

4.4. Targets ^{58}Fe, ^{57}Fe, ^{56}Fe, ^{54}Fe, and ^{nat}Fe

Excitation functions from iron are also very intensively studied. The majority of measurements were performed on targets with a natural composition of iron, therefore most experimental excitation functions were obtained for ^{nat}Fe. Nevertheless, measurements were performed on targets enriched with given isotopes of iron, and in several measurements with ^{nat}Fe, the yields from different isotopes were deduced taking into account the isotopic composition of target and the estimated cross sections for the competing reactions. Because of this, many data on excitation functions for many nuclides from ^{nat}Fe are available in the literature, while not so many, only for incident energies below $\sim$ 40 MeV, and for only a few nuclides are available for the separate isotopes of iron.

Our results for excitation functions for production of $^{58-56}$Co and ^{54}Mn from ^{58}Fe are compared with experimental data [46, 47, 161] in Fig. 31. Fig. 32 shows a comparison of calculated and measured excitation functions for production of $^{57-55}$Co and $^{56;54}$Mn from ^{57}Fe, as well as of ^{51}Mn from ^{54}Fe. Our results for production of $^{56;55}$Co, ^{55}Fe, and $^{54;52}$Mn from ^{56}Fe are compared in Fig. 33 with experimental data from Refs. [46, 47] and with results of the recent JAERI Benchmark [62, 63] obtained with the codes ALICE-F [179], ALICE91 [180], NUCLEUS [152], and MCEXCITON [181]. To understand the relative role of different channels in the production of several nuclides, the contributions from the channels (p,nα) (Figs. 31 and 33), from (p,α) and (p,npd) (Fig. 32), and from (p,np), (p,d), (p,n2p), (p,pd), (p,^{3}He) (Fig. 33) are shown separately.

One can see that the effect of the target isotopic spin on nuclide yields is very strong (see, also Fig. 15); excitation functions for production of the same nuclides from different target isotopes differ in shape and magnitude up to an order of magnitude or more. CEM95 describes quite well all available data (except the production of ^{54}Mn from ^{58}Fe and ^{57}Fe, and ^{51}Mn from ^{54}Fe) and reproduces correctly the isotope effect. As one can see from Fig. 33, the agreement of our results with all experimental data is a little bit better than that of calculations with the codes ALICE-F [179], ALICE91 [180], NUCLEUS [152], and MCEXCITON [181].

The serious disagreement between our results and data for ^{58}Fe(p,x)^{54}Mn, ^{57}Fe(p,x)^{54}Mn, and ^{54}Fe(p,x)^{51}Mn is connected with an old problem of the CEM: the model underestimates emission of ^{4}He (see, e.g., [71, 75]). We encounter similar disagreements in a limited region of incident energies for all excitation functions where emission of α-particles is an important, or even the only mechanism for production of a given nuclide. Unfortunately, this is a problem not only of the CEM, but of almost all other codes being used for evaluation of nuclear data at intermediate energies; therefore it is one of the most important problems which needs to be solved. A similar, but smaller underestimation related to this problem can also be seen for ^{56}Fe(p,x)^{52}Mn (Fig. 33). One can see that the codes ALICE-F [179], ALICE91 [180], and MCEXCITON [181] underestimate this excitation function even more than CEM95 does. Fortunately, as one can see from Figs. 31–33 and from

Figs. 16, 20, and 23 discussed above, the role of complex particle emission in the production of nuclides in the spallation region is important only at low incident energies, near the corresponding thresholds, where this mechanism in a region of incident energies may be the main channel. With increasing incident energy the importance of this channel decreases, and the main mechanism for production of nuclides in the spallation region becomes a successive emission of several nucleons. Therefore, at incident energies above $\sim$ 200 MeV this problem is no longer of great importance.

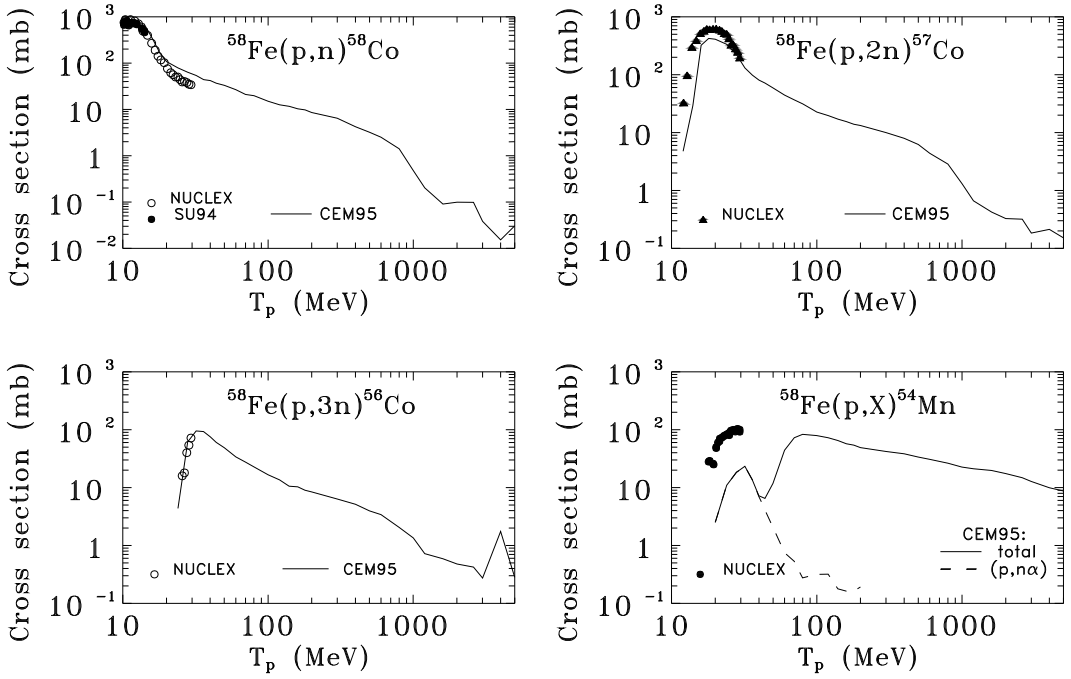

Fig. 31. Excitation functions for the production of ^{58}Co, ^{57}Co, ^{56}Co, and ^{54}Mn from p+^{58}Fe. For ^{54}Mn, the contribution to the total CEM95 yield from the channel (p,nα) is shown by a dashed line. Experimental data are labeled as: NUCLEX [46, 47] and SU94 [161].

Our results for σ_{in} and for excitation functions for production of $^{58-55}$Co, $^{55;53;52}$Fe, $^{56;54-51}$Mn, $^{51;49;48}$Cr, $^{49-47}$V, $^{45;44}$Ti, $^{48-46;44;43}$Sc, $^{47;45;41}$Ca, $^{45-38}$K, $^{42;41;39-36}$Ar, $^{39;38;36;34}$Cl, $^{38;35}$S, $^{33;32}$P, $^{32;31}$Si, ^{26}Al, ^{28}Mg, $^{24;22}$Na, $^{22-20}$Ne, ^{18}F, ^{11}C, $^{10;7}$Be, $^{4;3}$He, $^{3-1}$H, n, and $\pi^{+;0;-}$, from ^{nat}Fe are compared in Figs. 34–43 with the available experimental data as well as with the results of calculations [192] with Rudstam's semiempirical systematics [57] (Figs. 34–38 and 41), revised results of JAERI calculations [191] obtained with the codes NUCLEUS [152] and HETC-3STEP [92] (Fig. 34–37), results of calculation for ^{36}Cl with the code HETC/KFA2 [165] from Ref. [168] (Fig. 40), results of calculations with the code HETC/KFA2 [165] for ^{26}Al from Ref. [169] and for ^{22}Na from Ref. [203] (Fig. 41), results of calculations of t yield with the codes DISCA2 [166], CASCADE [167], NUCLEUS [152], and HETC/KFA2 [165] from Ref.

[60] (Fig. 43), and with predictions of phenomenological systematics by Korovin et al. [60] for $^{4;3}$He and t (Fig. 43).

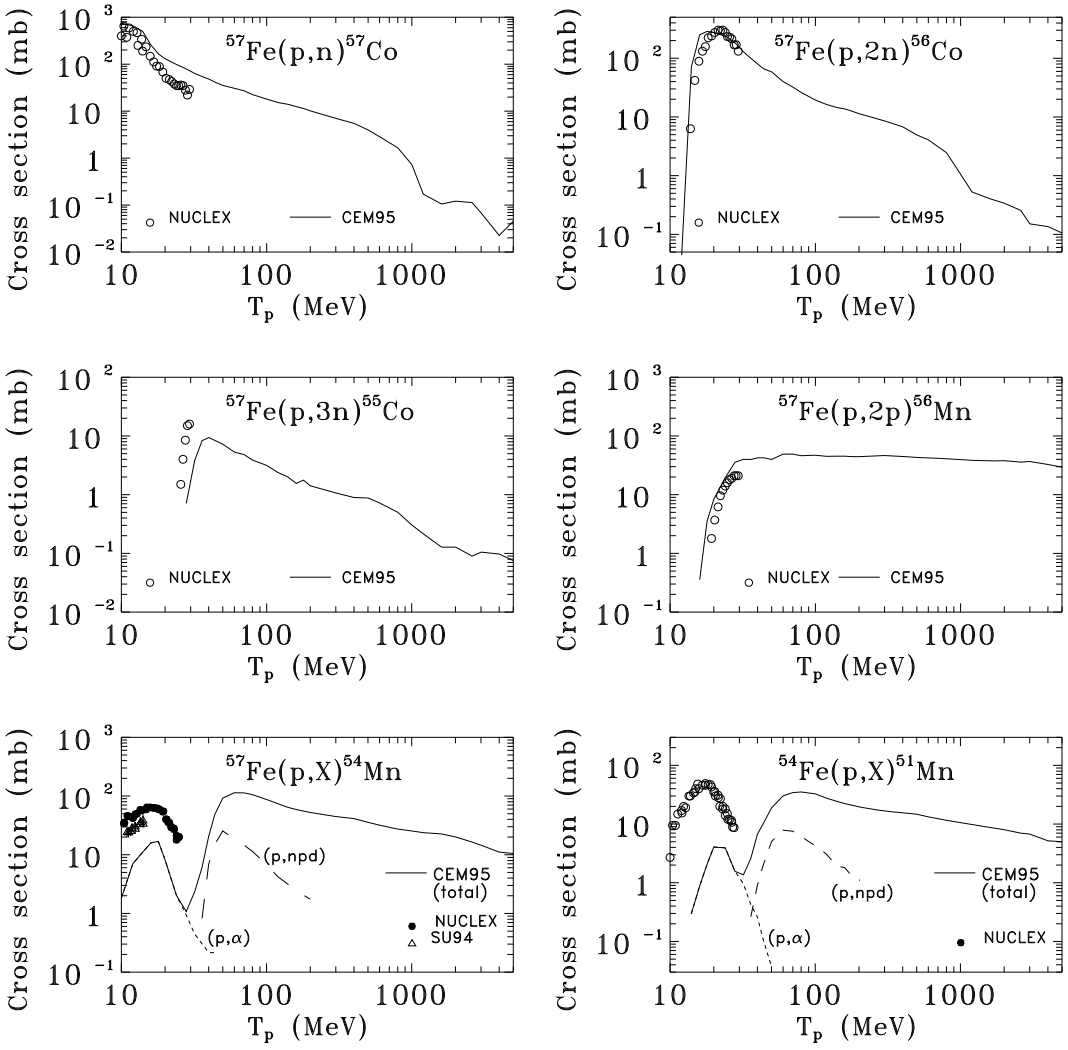

Fig. 32. Excitation functions for the production of ^{57}Co, ^{56}Co, ^{55}Co, ^{56}Mn, and ^{54}Mn from p+^{57}Fe, and for the production of ^{51}Mn from p+^{54}Fe. For ^{54}Mn and ^{51}Mn, the contributions to the total CEM95 yields from the channels (p,α) and (p,npd) are shown by dashed lines, as indicated. Experimental data are labeled as: NUCLEX [46, 47] and SU94 [161].

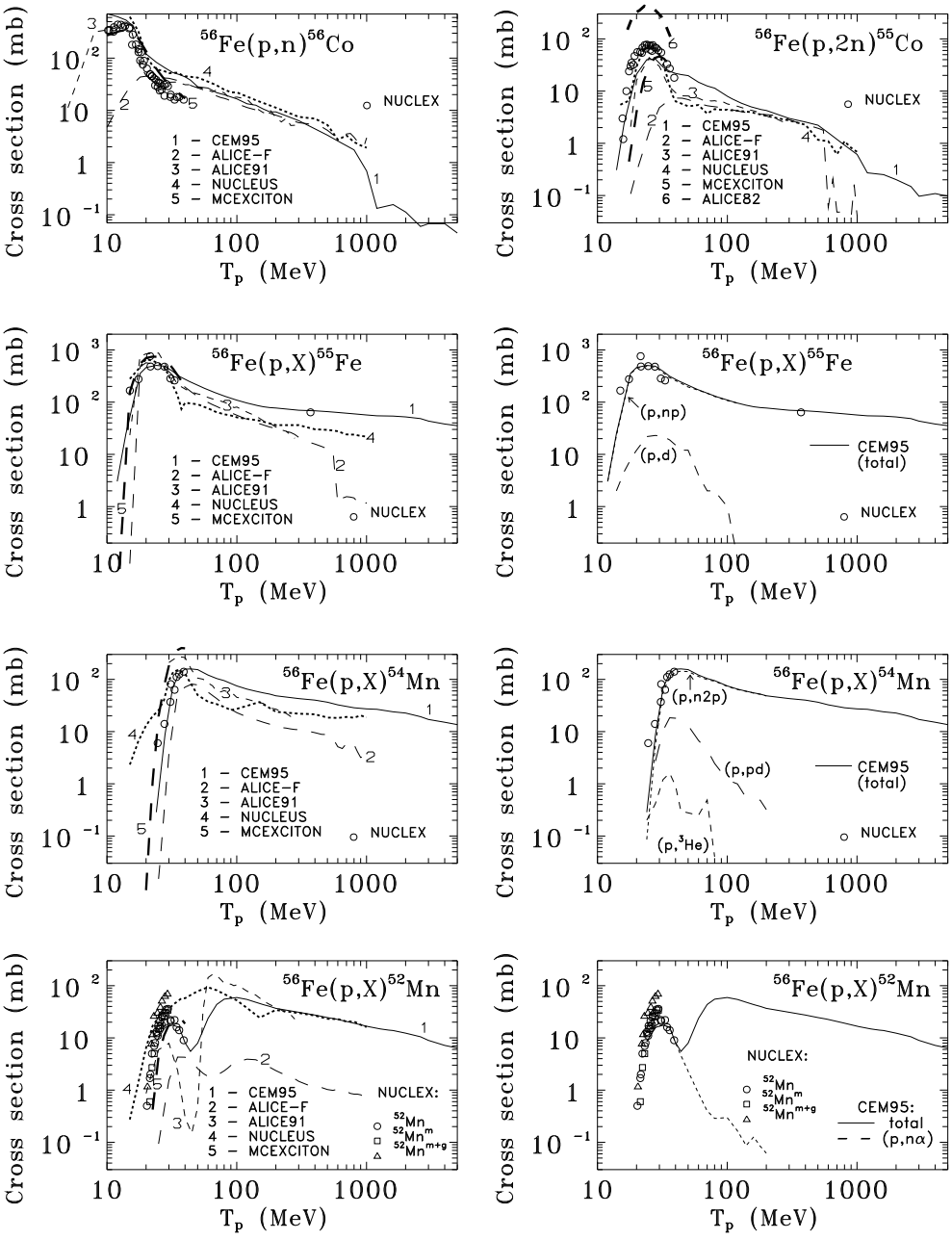

Fig. 33. Excitation functions for the production of ^{56}Co, ^{55}Co, ^{55}Fe, ^{54}Mn, and ^{52}Mn from p+^{56}Fe. Lines labeled as 2, 3, 4, and 5 are plotted from files [178] with results of the recent JAERI Benchmark [62, 63] obtained with the codes ALICE-F [179], ALICE91 [180], NUCLEUS [152], and MCEXCITON [181], respectively. For production of ^{55}Fe, ^{54}Mn, and ^{52}Mn, on the three lower right plots, the contributions to the total CEM95 yields from the channels (p,np), (p,d), (p,n2p), (p,pd), (p,^{3}He), and (p,nα) are shown by dashed lines, as indicated. On the upper right plot, the thick-dashed line 6 labeled as ALICE82 shows the results obtained in Ref. [188] with the code ALICE82 [189]. Experimental data labeled as NUCLEX are from Refs. [46, 47].

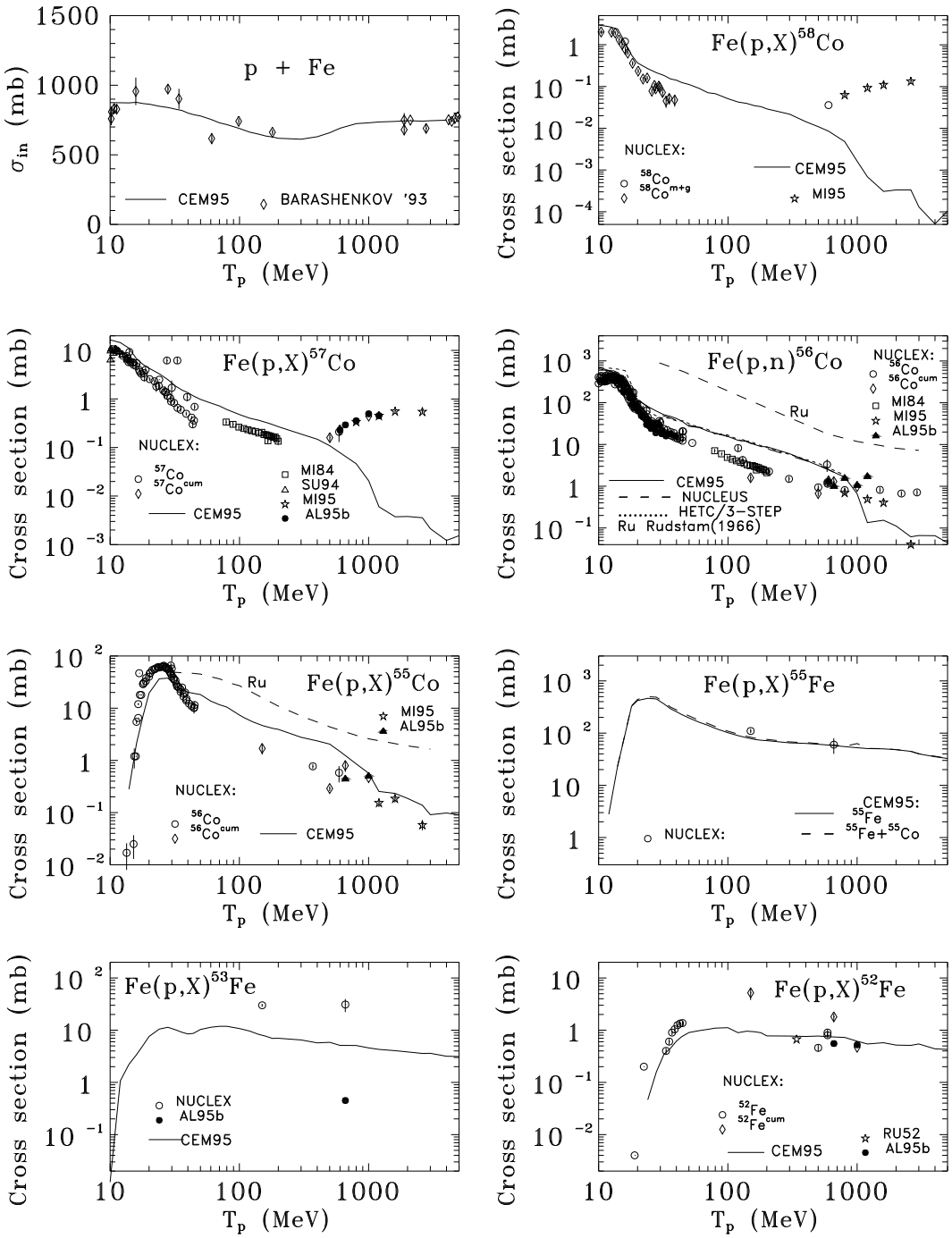

Fig. 34. Total inelastic cross section and excitation functions for the production of ^{58}Co, ^{57}Co, ^{56}Co, ^{55}Co, ^{55}Fe, ^{53}Fe, and ^{52}Fe from p+^{nat}Fe. Dashed curves labeled as NUCLEUS and HETC/3-STEP are plotted from files with revised results of JAERI calculations [191] obtained with the codes NUCLEUS [152] and HETC-3STEP [92]. Here and in all following figures, dashed lines marked with "Ru" show results of calculations [192] with Rudstam's semiempirical systematics [57]. Experimental data are labeled as: BARASHENKOV'93 [158], MI95 [43], MI84 [41], SU94 [161], AL95b [142], NUCLEX [46, 47], and RU52 [141].

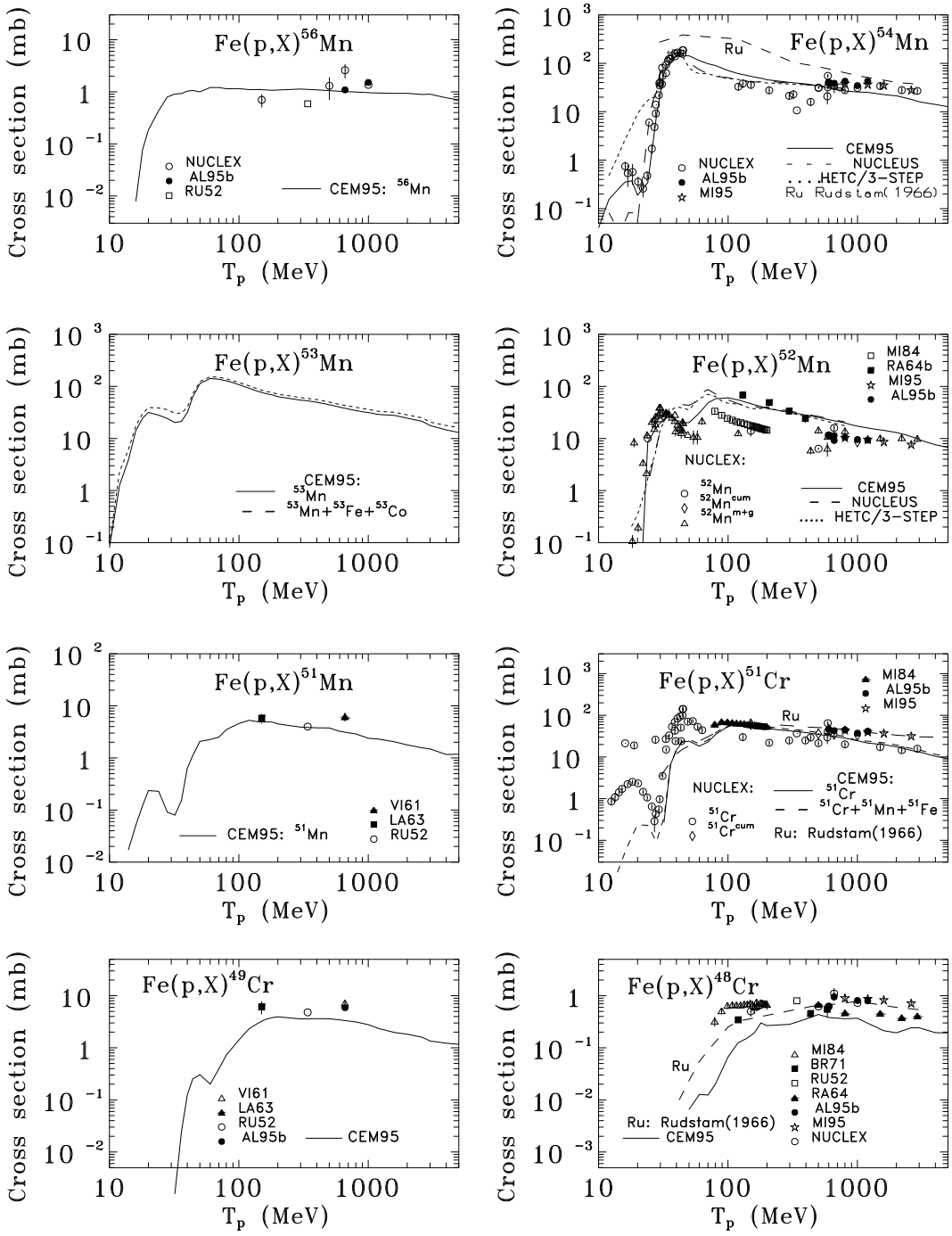

Fig. 35. Excitation functions for the production of ^{56}Mn, ^{54}Mn, ^{53}Mn, ^{52}Mn, ^{51}Mn, ^{51}Cr, ^{49}Cr, and ^{48}Cr from p+^{nat}Fe. Experimental data are labeled as: NUCLEX [46, 47], AL95b [142], RU52 [141], MI95 [43], MI84 [41], RA64b [193], VI61 [139], LA63 [140], BR71 [192], and RA64 [194]. The rest of the notation is the same as in Fig. 34.

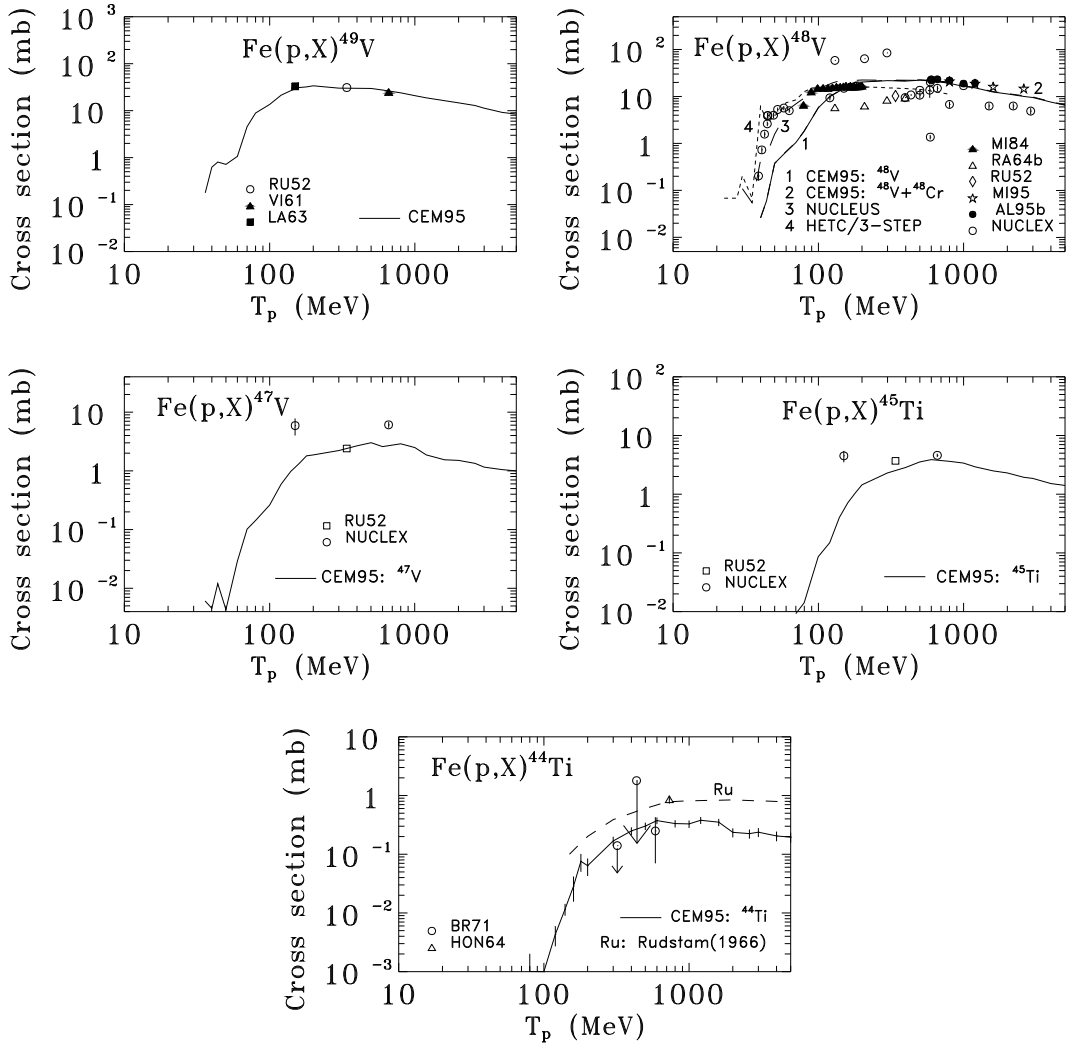

Fig. 36. Excitation functions for the production of ^{49}V, ^{48}V, ^{47}V, ^{45}Ti, and ^{44}Ti from p+^{nat}Fe. Experimental data are labeled as: RU52 [141], VI61 [139], LA63 [140], MI84 [41], RA64b [193], MI95 [43], AL95b [142], NUCLEX [46, 47], BR71 [192], and HON64 [195]. The rest of the notation is the same as in Fig. 34.

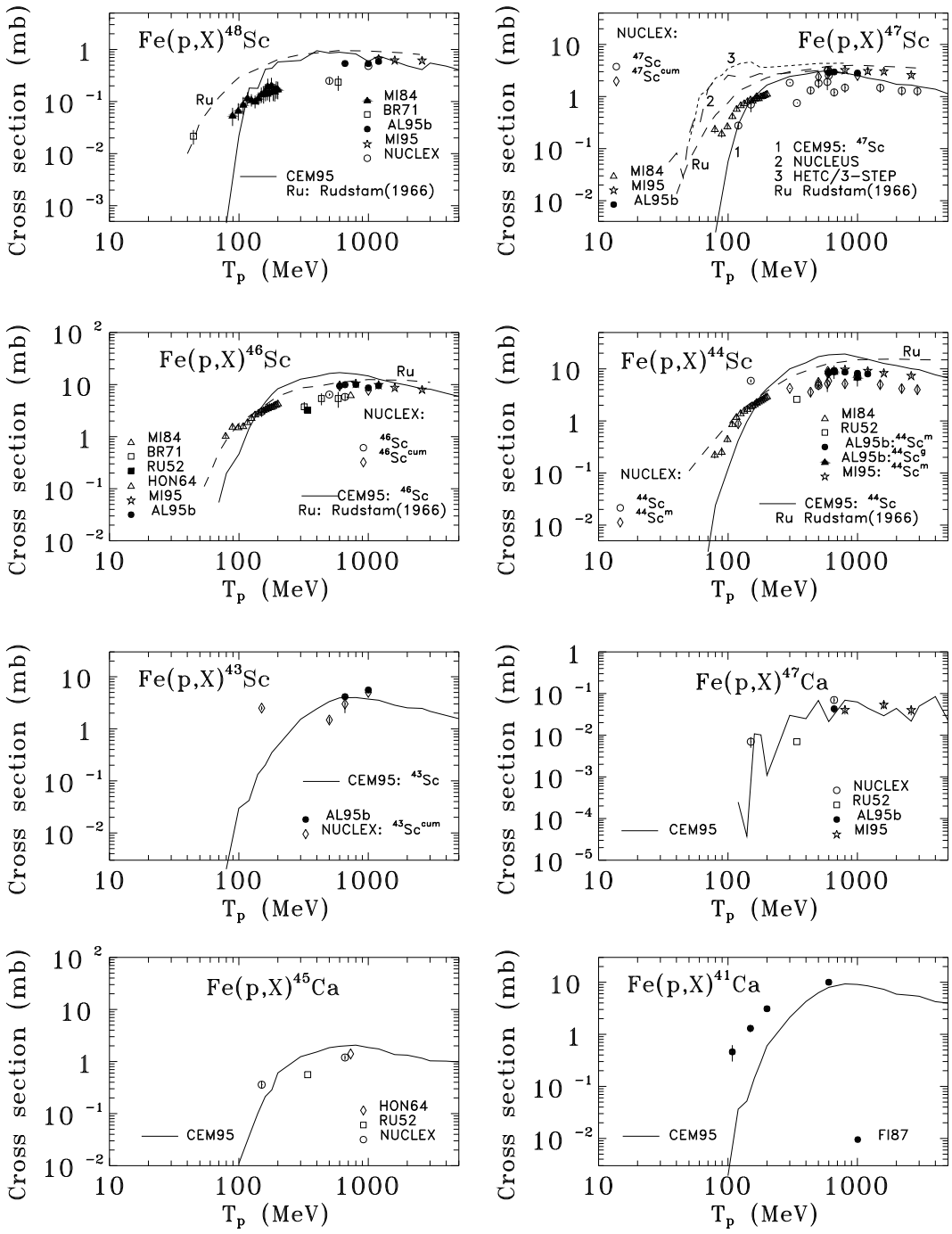

Fig. 37. Excitation functions for the production of ^{48}Sc, ^{47}Sc, ^{46}Sc, ^{44}Sc, ^{43}Sc, ^{47}Ca, ^{45}Ca, and ^{41}Ca from p+^{nat}Fe. Experimental data are labeled as: MI84 [41], BR71 [192], AL95b [142], MI95 [43], NUCLEX [46, 47], RU52 [141], HON64 [195], and Fi87 [196]. The rest of the notation is the same as in Fig. 34.

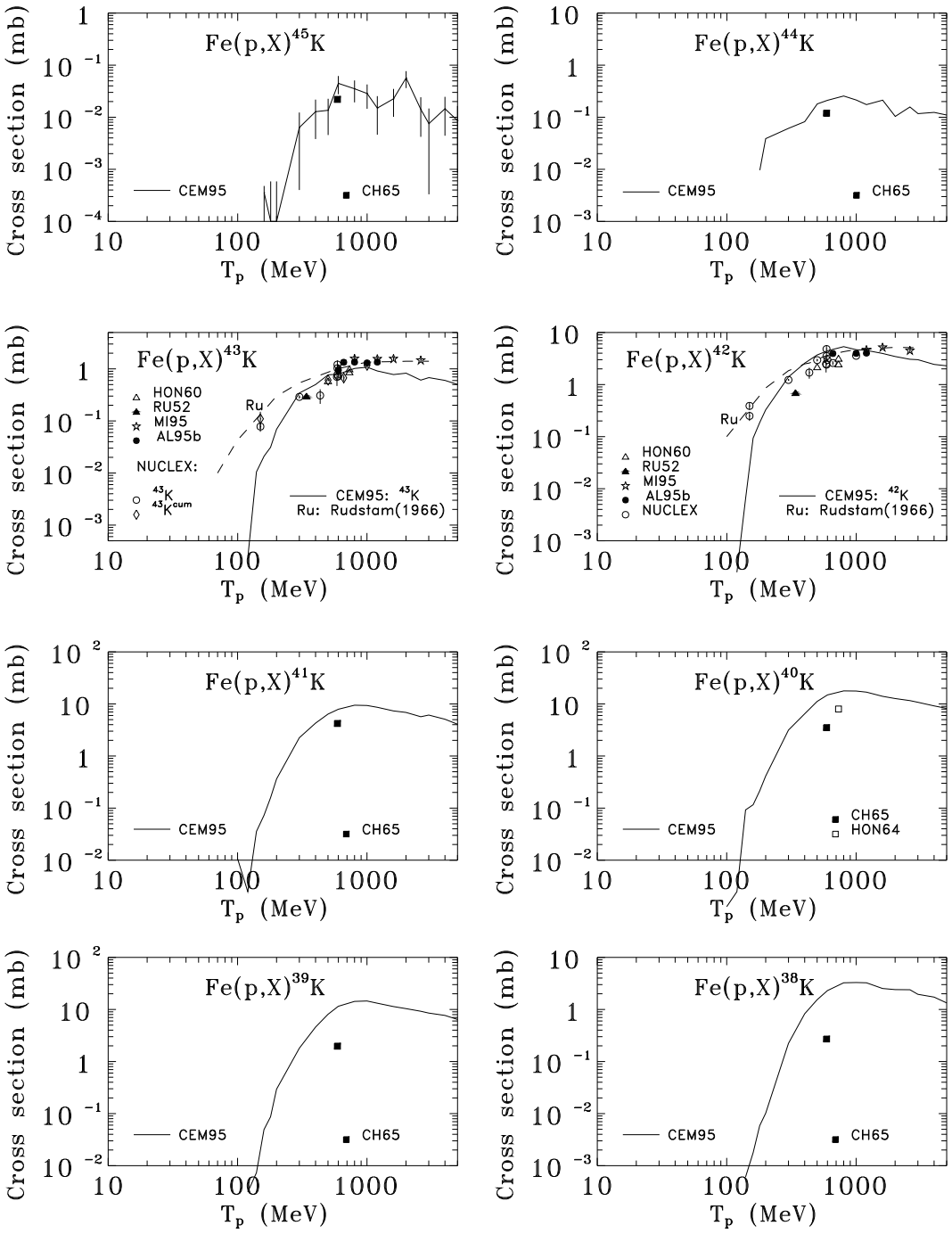

Fig. 38. Excitation functions for the production of ^{45}K, ^{44}K, ^{43}K, ^{42}K, ^{41}K, ^{40}K, ^{39}K, and ^{38}K from p+^{nat}Fe. Experimental data are labeled as: CH65 [197], HON60 [143], RU52 [141], MI95 [43], AL95b [142], NUCLEX [46, 47], and HON64 [195].

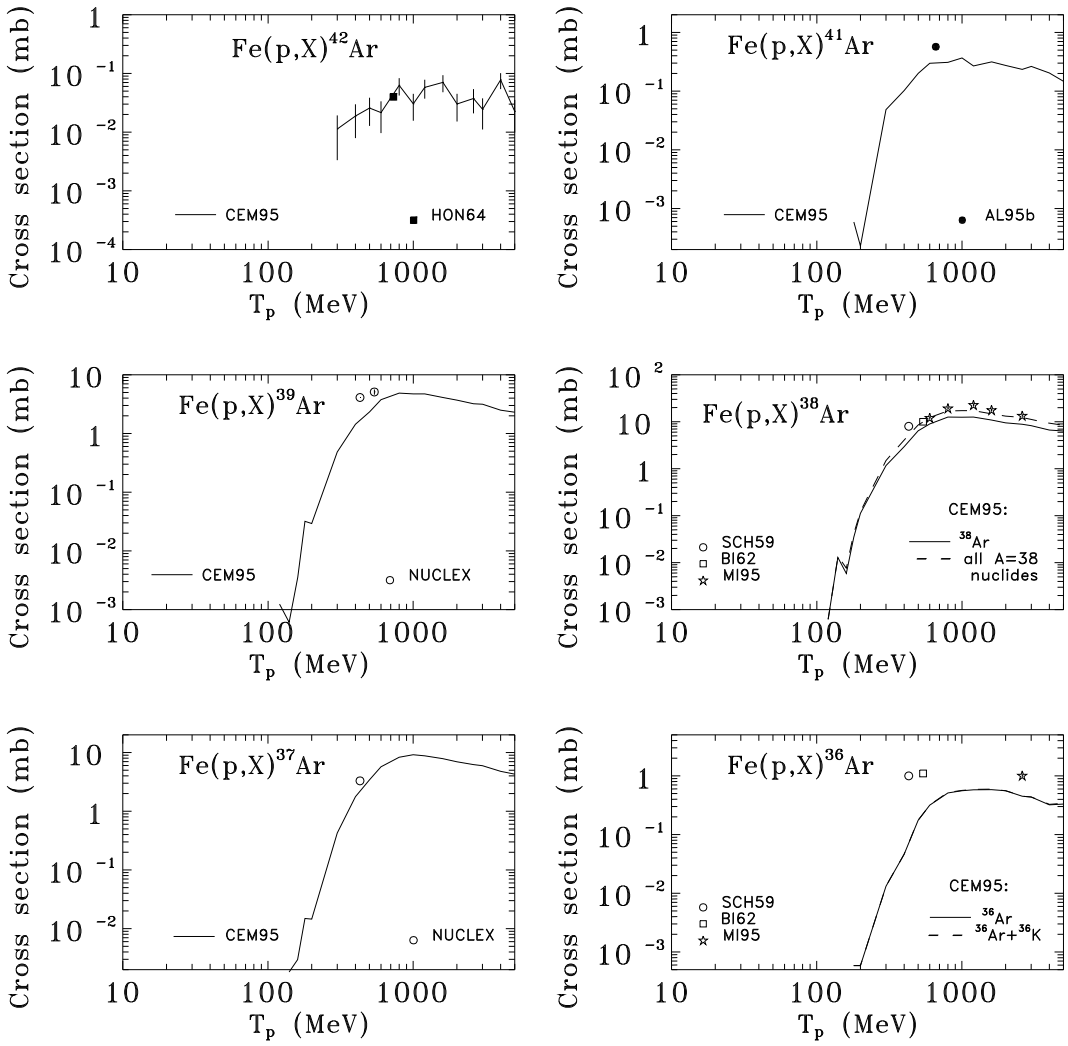

Fig. 39. Excitation functions for the production of ^{42}Ar, ^{41}Ar, ^{39}Ar, ^{38}Ar, ^{37}Ar, and ^{36}Ar from p+^{nat}Fe. Experimental data are labeled as: HON64 [195], AL95b [142], NUCLEX [46, 47], SCH59 [198], BI62 [183], and MI95 [43].

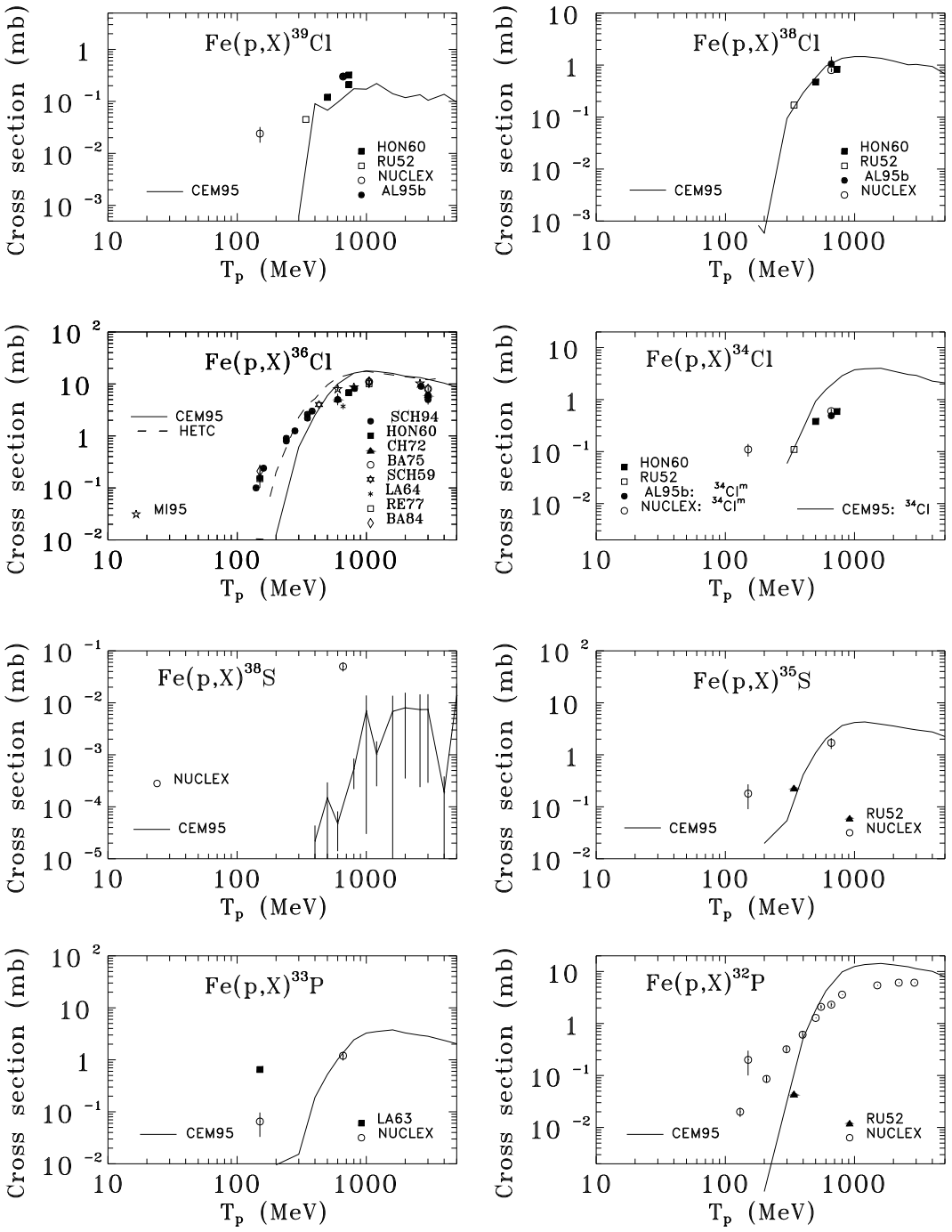

Fig. 40. Excitation functions for the production of ^{39}Cl, ^{38}Cl, ^{36}Cl, ^{34}Cl, ^{38}S, ^{35}S, ^{33}P, and ^{32}P from p+^{nat}Fe. The dashed line for ^{36}Cl shows results of calculations with the code HETC/KFA2 [165] from Ref. [168]. Experimental data are labeled as: HON60 [143], RU52 [141], NUCLEX [46, 47], AL95b [142], SCH94 [168], CH72 [199], BA75 [200], SCH59 [198], LA64 [202], RE77 [201], BA84 [182], and LA63 [140].

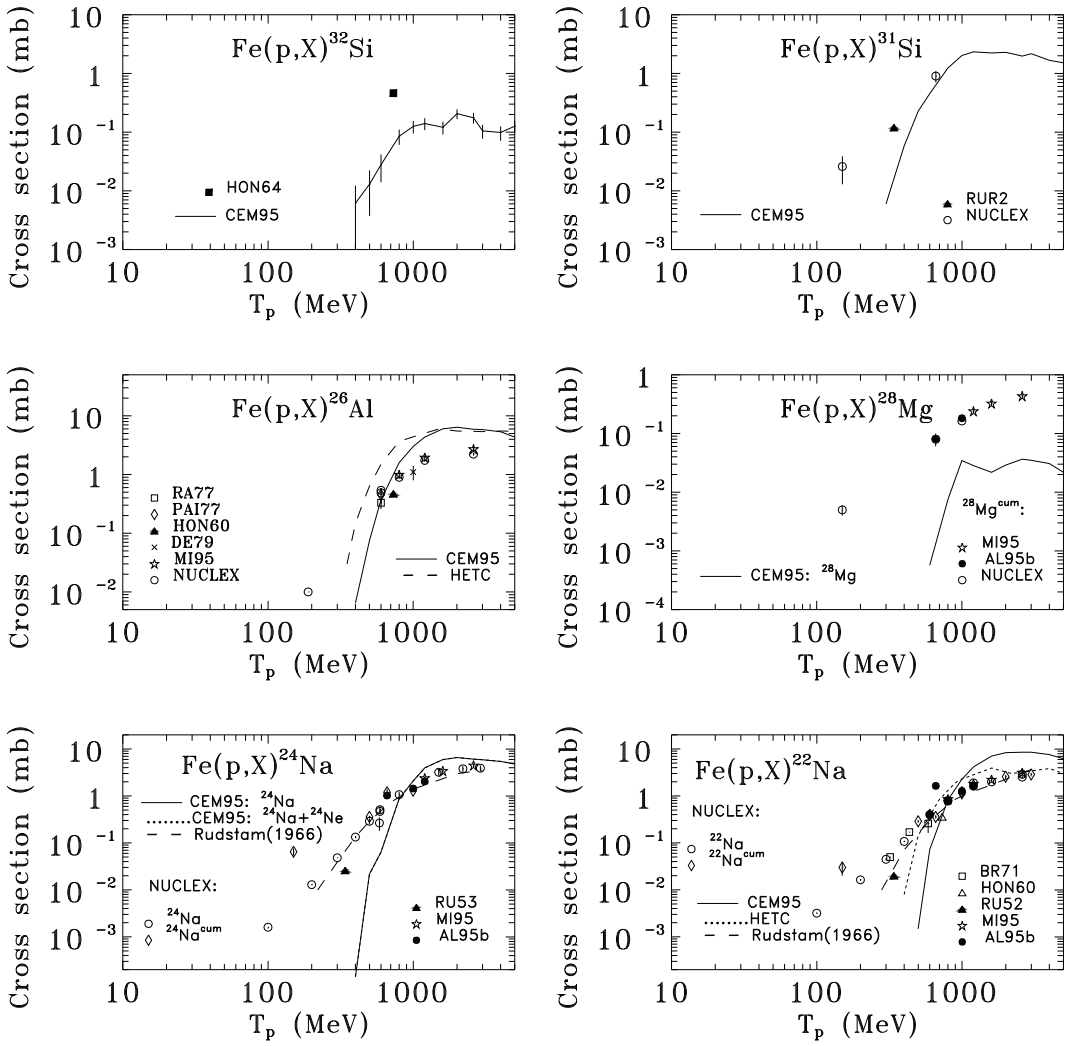

Fig. 41. Excitation functions for the production of ^{32}Si, ^{31}Si, ^{26}Al, ^{28}Mg, ^{24}Na, and ^{22}Na from p+^{nat}Fe. The results of calculations with the code HETC/KFA2 [165] are shown with a dashed line for ^{26}Al (from Ref. [169]) and with a dotted line for ^{22}Na (from Ref. [203]). For ^{24}Na and ^{22}Na, dashed lines show the results of calculations [192] with Rudstam's semiempirical systematics [57]. Experimental data are labeled as: HON64 [195], RUR2 [141], NUCLEX [46, 47], RA77 [204], PAI77 [205], HON60 [143], DE79 [206], MI95 [43], AL95b [142], RU53 [141], BR71 [192], and RU52 [141].

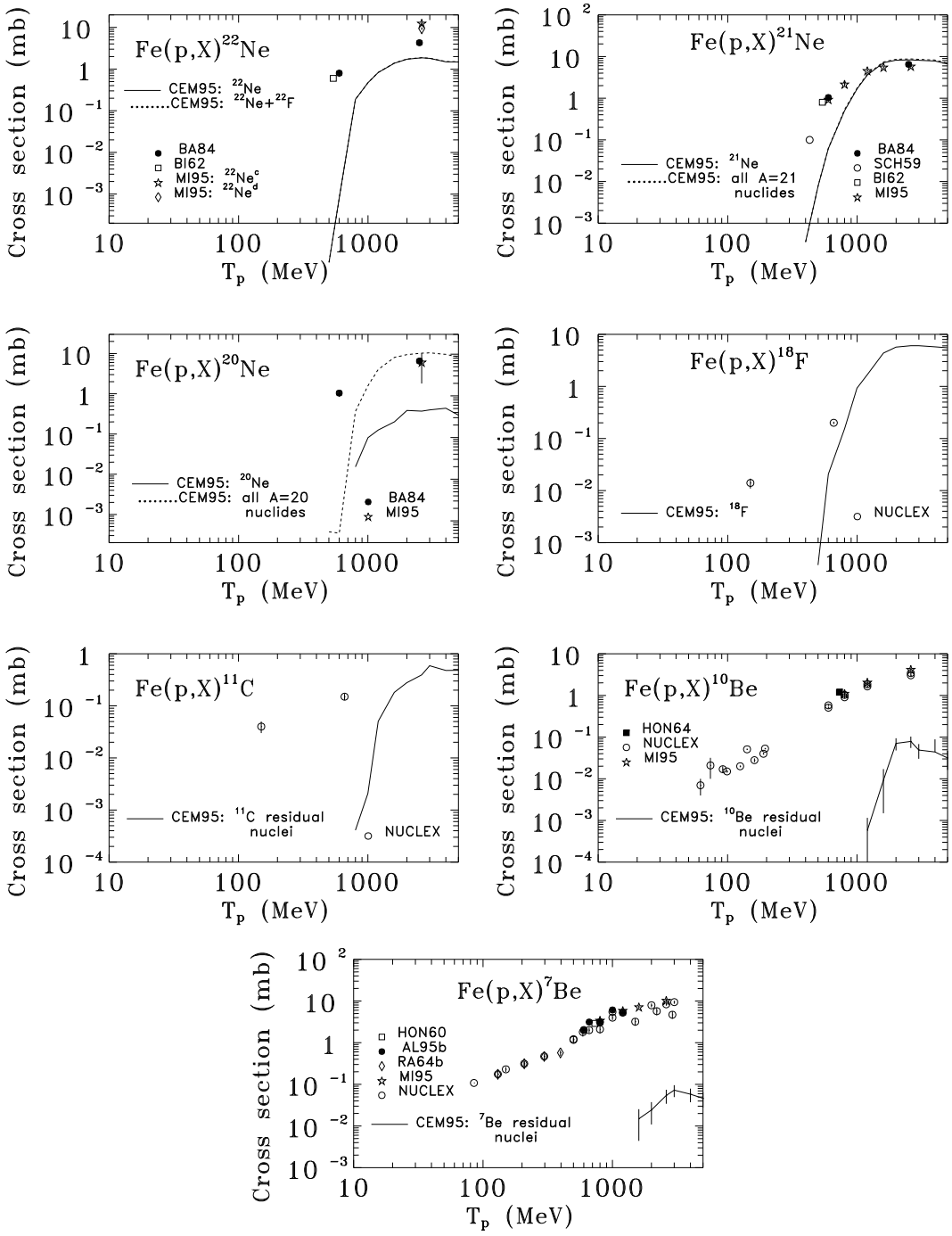

Fig. 42. Excitation functions for the production of ^{22}Ne, ^{21}Ne, ^{20}Ne, ^{18}F, ^{11}C, ^{10}Be, and ^{7}Be from p+^{nat}Fe. Experimental data are labeled as: BA84 [182], BI62 [183], MI95 [43], SCH59 [198], NUCLEX [46, 47], HON64 [195], AL95b [142], and RA64b [193].

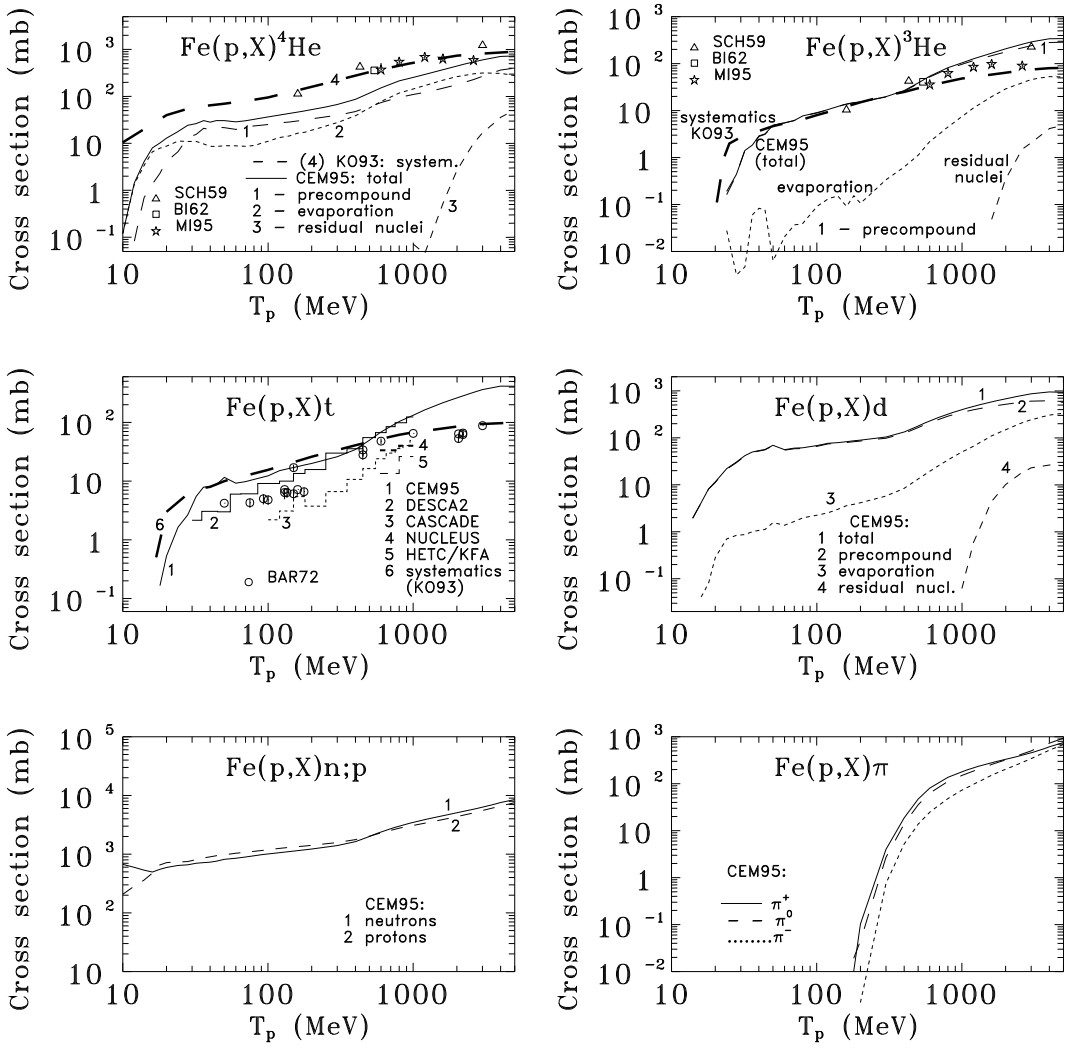

Fig. 43. Excitation functions for the production of ^{4}He, ^{3}He, t, d, p, n, π^+, π^0, and π^- from p+^{nat}Fe. For ^{4}He, ^{3}He, and t, predictions of the phenomenological systematics by Korovin et al. [60] are shown by thick long dashed lines labeled as KO93. For production of t, the results of calculations with the codes DISCA2 [166], CASCADE [167], NUCLEUS [152], and HETC/KFA2 [165] from Ref. [60] are shown by dashed histograms 2, 3, 4, and 5, respectively. For ^{4}He, ^{3}He, and d, contributions from preequilibrium emission, evaporation, and from residual nuclei to the total CEM95 yields are shown by dashed lines, as indicated. Experimental data are labeled as: SCH59 [198], BI62 [183], MI95 [43], and BAR72 [54].

One can see that on the whole, CEM95 reproduces the experimental data in the spallation region quite well, and no worse than the codes cited above or Rudstam's semiempirical systematics [57]. There are nevertheless some disagreements for several nuclides in this region caused for the same reasons discussed above for previous targets. One should note that some experimental data shown in these figures are also

questionable (see a good discussion of the experimental situation for iron in Ref. [43]). But one can also see some serious systematic discrepancies for light nuclides produced in the fragmentation region. As was mentioned above, CEM95 does not contain a mechanism of fragmentation and does not take into account evaporation and preequilibrium emission of complex particles with $A > 4$, or even coalescence of fragments from emitted particles, as we did in a former version of the CEM (see, e.g. [71]). All fragments calculated in the present work are only residual nuclei remaining after all three stages of reactions; therefore, for these medium-mass targets, they represent only a very small part of the total fragment production.

As one can see from Fig. 43, CEM95 describes production of ^{3}He and t no worse than phenomenological systematics by Korovin et al. [60], or than the codes DISCA2 [166], CASCADE [167], NUCLEUS [152], and HETC/KFA2 [165] do for t. For ^{4}He, our results are again below the experimental data and prediction of the systematics [60]. This is the old problem of the CEM underestimating α-particle emission as discussed above.

4.5. Target ^{59}Co

Since ^{59}Co is the single stable isotope of cobalt, it is particularly suitable [137] for testing model calculations of nuclear reactions, especially as a target for production of doubly magic ^{56}Ni and magic ^{57}Ni nuclides providing a test of the capability of models to describe nuclide production near closed shells [66]. We used in our study all experimental excitation functions for ^{59}Co. Let us note here that a recent paper by Michel's group [176] (published after our calculations were completed, and not discussed here) contains many new experimental data for ^{59}Co as well as results of calculations with the codes HETC/KFA2 [165] and AREL [177].

Our results for σ_{in} and for excitation functions for production of $^{59;57;56}$Ni, $^{58-55}$Co, $^{59;52}$Fe, $^{56;54;52}$Mn, $^{51;48}$Cr, ^{48}V, $^{48-46;44;43}$Sc, $^{43;42}$K, ^{28}Mg, $^{24;22}$Na, ^{7}Be $^{4;3}$He, $^{3-1}$H, n, and $\pi^{+;0;-}$ are compared in Figs. 44–48 with available experimental data and with results of calculations with the codes: ALICE75 [207], for $^{59;57}$Ni and ^{52}Fe from Ref. [157] (Figs. 44 and 45); ALICE82 [189], for ^{57}Ni from Ref. [188] (Fig. 44); ALICE-LIVERMORE-82 [208], for ^{58}Co (Fig. 44), ^{52}Mn, ^{51}Cr (Fig. 45), ^{48}V and ^{46}Sc (Fig. 46) from Ref. [137]; HETC/KFA2 [165], for ^{46}Sc from Ref. [43] (Fig. 46). The contributions from the channels (p,d), (p,np), (p,t), (p,nd), (p,2np), (p,nt), (p,2nd), (p,3np), (p,n3p), and (p,2pd) to the total CEM95 yields of ^{58}Co, ^{57}Co, ^{56}Co, and ^{56}Mn are shown separately in Figs. 44 and 45.

On the whole, CEM95 reproduces satisfactorily the shapes of the majority of measured excitation functions, and at incident energies above $\sim$ 100–200 MeV, it reproduces correctly the absolute values of most data and agrees with experiment no worse than other codes. But at lower energies, especially near the thresholds, CEM95 tends to underestimate the data systematically. This is for two different reasons. First, CEM95 underestimates practically all measured excitation functions for p+^{59}Co at low energies. This indicates that the total inelastic cross section of this

reaction is also underestimated by the model. The few experimental data shown in Fig. 44 that we were able to find for σ_{in} in Barashenkov's compilation [158] confirm this. At energies below $\sim$ 80 MeV, CEM95 underestimates the experimental σ_{in} from 10 to 30%. This is a result of the model employing a geometrical approximation for the total cross section. Often, it is only important to know the relative cross sections of the various inelastic channels. For other cases, when one needs to know the absolute cross sections, it is possible to calculate the partial cross sections at each incident energy with σ_{in} provided by the model, then to perform renormalization of all partial cross sections using more precise values of σ_{in} either from measurements, from independent optical model calculations, or from systematics.

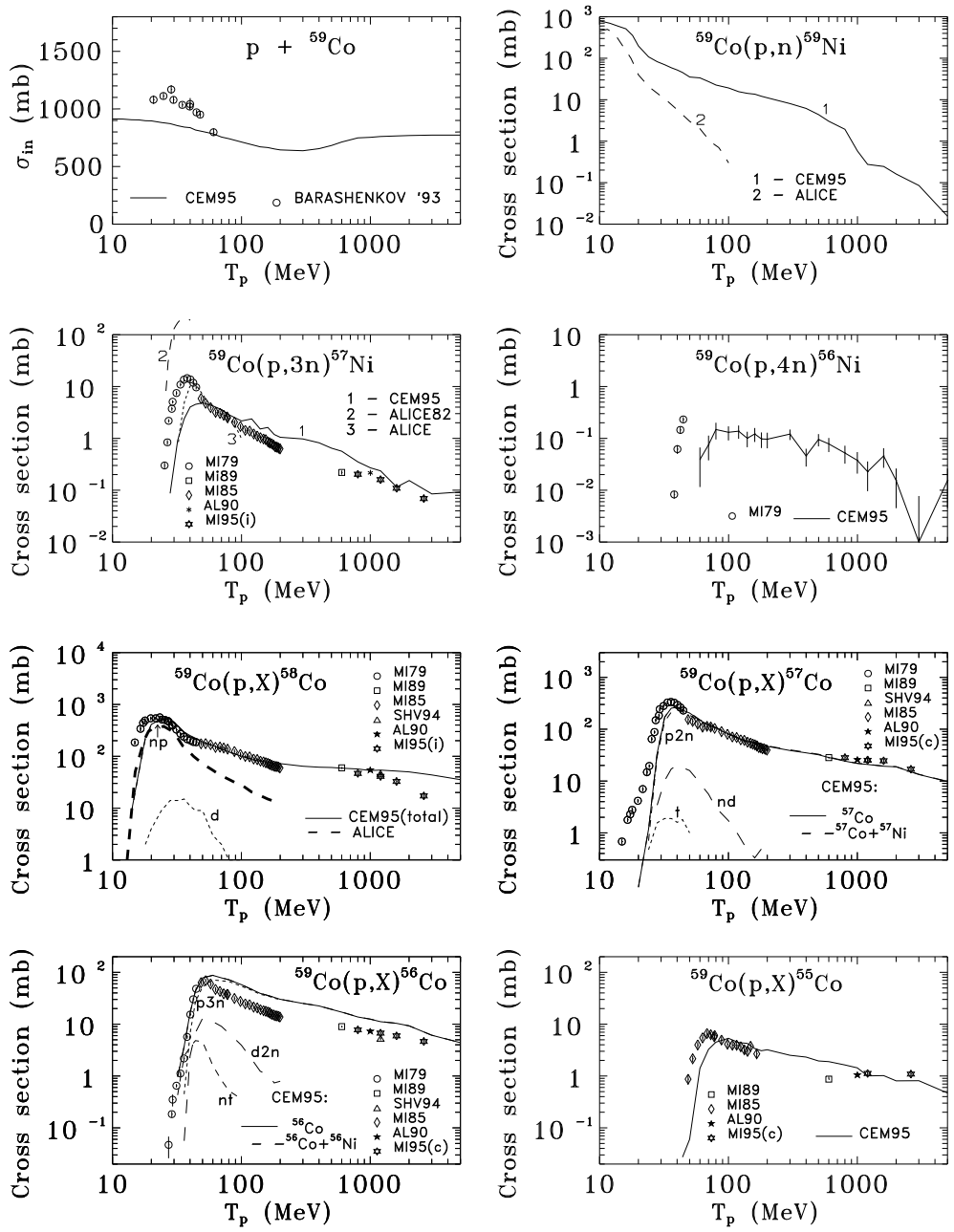

Fig. 44. Total inelastic cross section and excitation functions for the production of ^{59}Ni, ^{57}Ni, ^{56}Ni, ^{58}Co, ^{57}Co, ^{56}Co, and ^{55}Co from p+^{59}Co. For ^{59}Ni and ^{57}Ni, predictions of the code ALICE [207] from Ref. [157] are shown by lines 2 and 3 labeled as "ALICE". For ^{57}Ni, results of the code ALICE82 [189] from Ref. [188] are shown by the dashed line 2. Results of calculations with the code ALICE-LIVERMORE-82 [208] from Ref. [137] are shown for ^{58}Co by a dashed line labeled as ALICE. For ^{58}Co, ^{57}Co, and ^{56}Co, contributions from the channels (p,d), (p,np), (p,t), (p,nd), (p,2np), (p,nt), (p,2nd), and (p,3np) are shown by dashed lines, as indicated. Experimental data are labeled as: BARASHENKOV'93 [158], MI79 [155], MI89 [42], MI85 [137], AL90 [156], MI95 [43], and SHV94 [138].

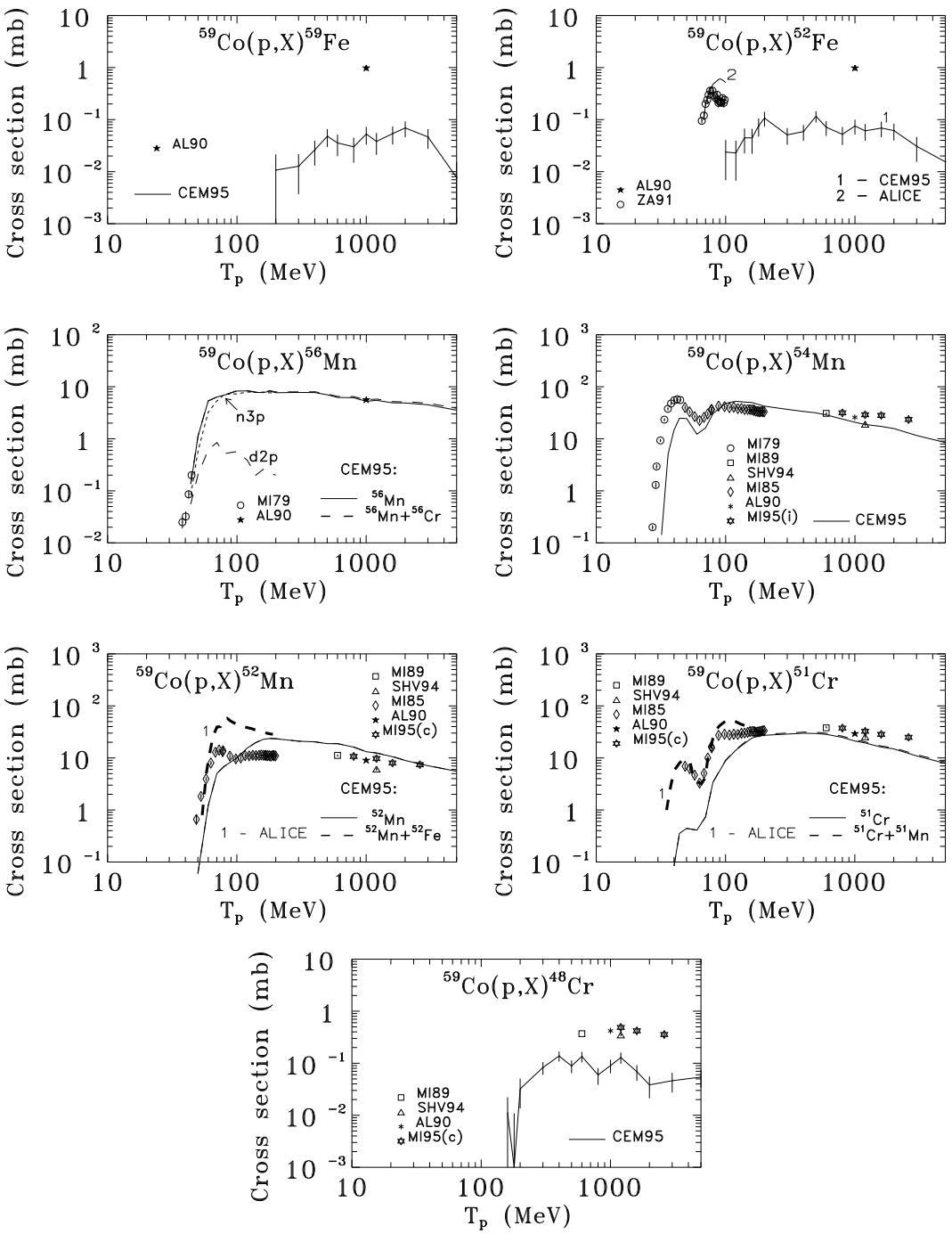

Fig. 45. Excitation functions for the production of ^{59}Fe, ^{52}Fe, ^{56}Mn, ^{54}Mn, ^{52}Mn, ^{51}Cr, and ^{48}Cr from p+^{59}Co. Dashed lines labeled as ALICE show results of the hybrid model calculations with a version of the code ALICE75 [207] for ^{52}Fe (from Ref. [157]) and with the code ALICE-LIVERMORE-82 [208] for ^{52}Mn and ^{51}Cr (from Ref. [137]). The contributions from channels (p,n3p) and (p,2pd) to the total CEM95 yield of ^{56}Mn are shown by dashed lines, as indicated. Experimental data are labeled as: AL90 [156], ZA91 [157], MI79 [155], MI89 [42], SHV94 [138], MI85 [137], and MI95 [43].

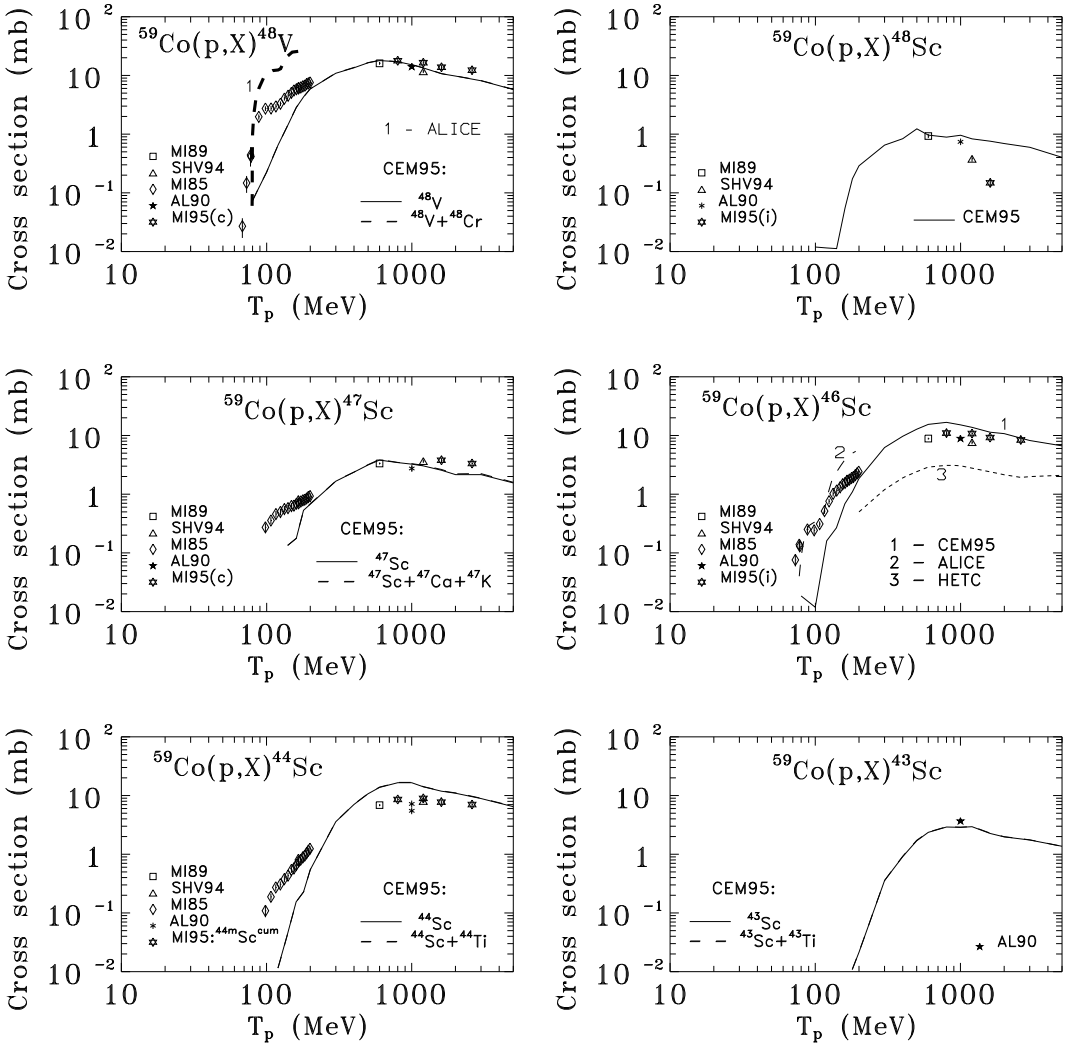

Fig. 46. Excitation functions for the production of ^{48}V, ^{48}Sc, ^{47}Sc, ^{46}Sc, ^{44}Sc, and ^{43}Sc from p+^{59}Co. For ^{48}V and ^{46}Sc, dashed lines labeled as ALICE show results of calculations with the code ALICE-LIVERMORE-82 [208] from Ref. [137]. For ^{46}Sc, the dotted line 3 labeled as HETC shows results of calculations with the code HETC/KFA2 [165] from Ref. [43]. Experimental data are labeled as: MI89 [42], SHV94 [138], MI85 [137], AL90 [156], and MI95 [43].

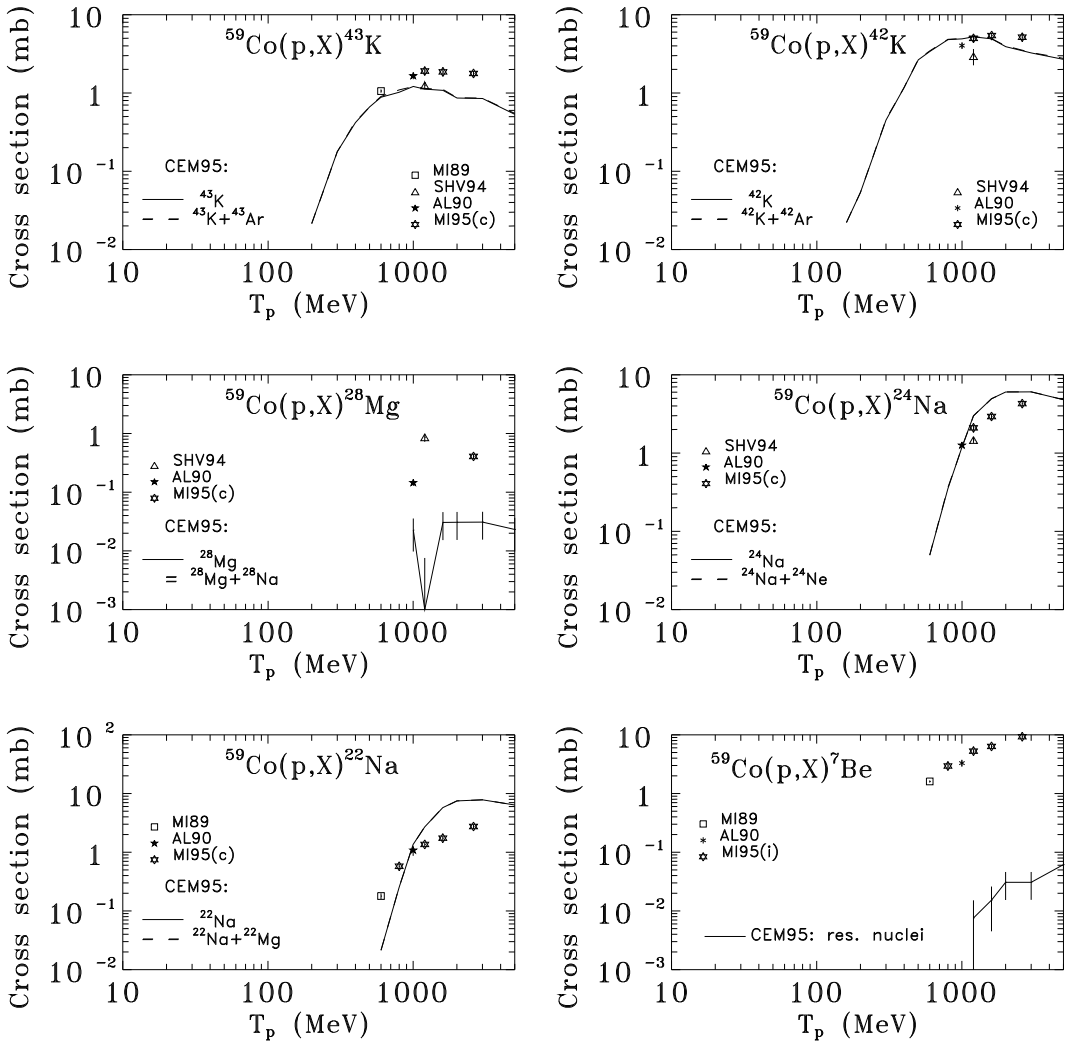

Fig. 47. Excitation functions for the production of ^{43}K, ^{42}K, ^{28}Mg, ^{24}Na, ^{22}Na, and ^{7}Be from p+^{59}Co. Experimental data are labeled as: MI89 [42], SHV94 [138], AL90 [156], and MI95 [43].

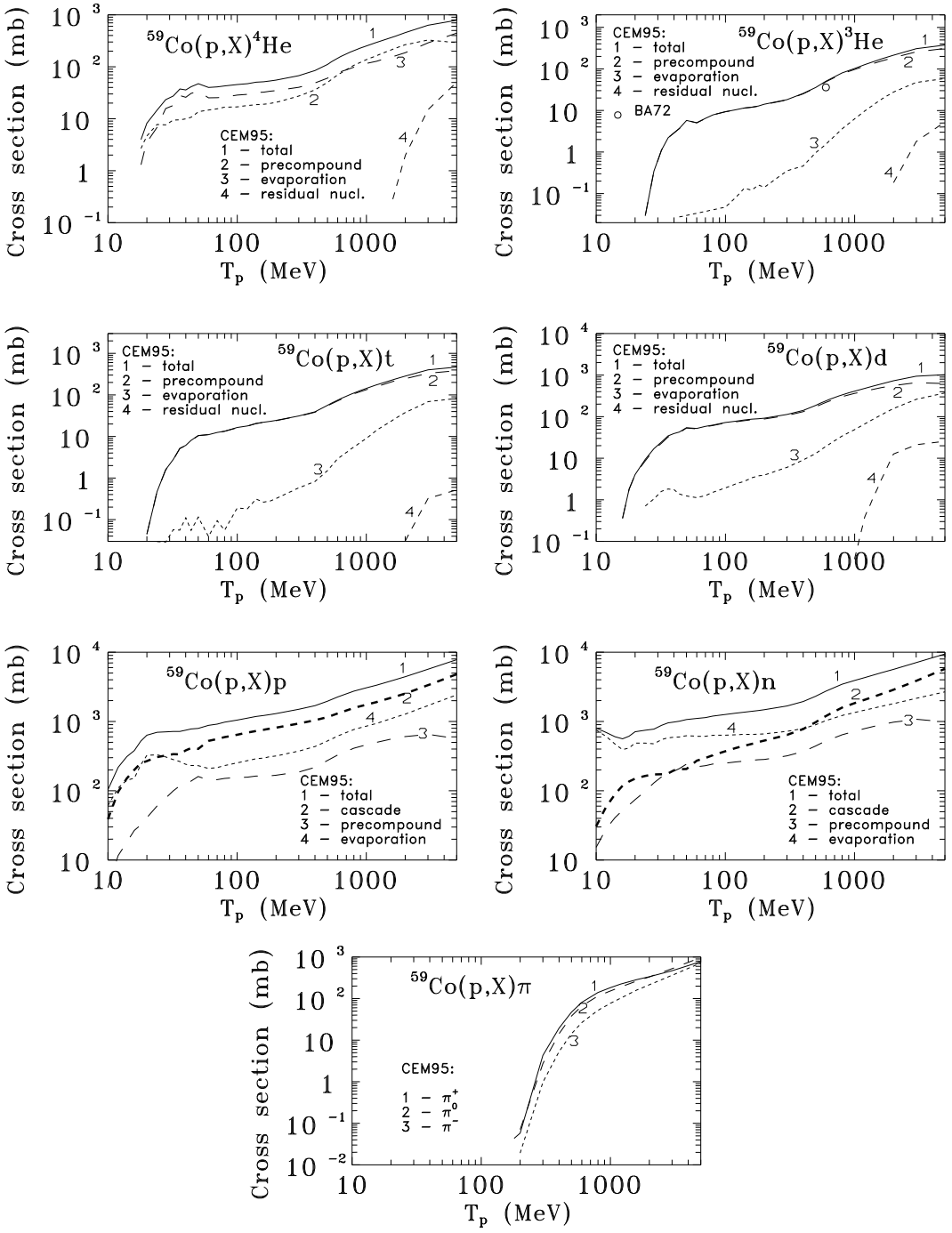

Fig. 48. Predictions of CEM95 for the production of ^{4}He, ^{3}He, t, d, p, n, π^+, π^0, and π^- from p+^{59}Co. The contributions to the total yields from cascade, preequilibrium emission, evaporation, and from residual nuclei are shown by dashed lines, as indicated. The experimental point for ^{3}He labeled as BA72 is taken from Ref. [54].

The second, and more serious reason for the large underestimation of the yields of several nuclides, like ^{48}V, $^{47;46;44}$Sc (Fig. 46) at low energies, is connected with a poor calculation by CEM95 of nuclear masses and binding energies. In the production of these nuclides from p+^{59}Co via a consecutive emission of several particles, the excited nuclei at intermediate stages pass through or near the region of magic or doubly magic nuclei. Therefore their masses, shell and pairing energies, and their level densities have to be calculated appropriately. If the approaches used for such calculations at the preequilibrium and evaporation stages of reactions do not do this, the final results can be strongly affected. The main problem in the description of reactions involving nuclei near the closed shells comes from the ICM, which does not contain any shell and pairing effects and uses a fixed value for the mean binding energy, $B_N = 7$ MeV for all nuclei. A direct confirmation of this may be seen from comparison of our results with the hybrid model calculations. At low incident energies, the hybrid model, which does not use a classical approach like ICM, describes much better all excitation functions shown in Figs. 44–46. To be able to correctly describe such reactions, the classical ICM has to be extended by using real nuclear masses and shell and pairing corrections in the calculation of the binding energies of emitted nucleons.

Discrepancies of another type, that can be seen, e.g., for ^{52}Fe, ^{54}Mn, and ^{51}Cr in Fig. 45, are connected with the previously discussed underproduction of ^{4}He. The peaks of excitation functions for the production of these nuclides in the low energy region are probably caused by α-emission through the channels (p,4nα), (p,npα), and (p,n2α), respectively. CEM95 underestimates α-emission, and as a result, the corresponding peaks in these excitation functions are not reproduced correctly.

The reason for incorrectly predicting the production of ^{7}Be fragments (Fig. 48) was discussed previously.

A detailed comparison of our results for the production of different nuclides from p(1.2 GeV)+^{59}Co with the recent measurements [43, 138] and calculations [138] with the codes HETC [174] and INUCL [175], and with phenomenological systematics [58, 59] is given in Table II.

The cumulative yields for all nuclides are calculated using Eq. (34) taking into account the precursors shown in the first column of the table. To be able to compare adequately our results with predictions of the codes HETC and INUCL, we calculate here according to Eq. (34) the cumulative yields predicted by HETC and INUCL using independent yields given in Tabs. 1 and 2 of Ref. [138]. These values are marked with a (*).

TABLE II

Comparison of cross sections for the production of daughter nuclides from p(1.2 GeV)+^{59}Co measured in Refs. [43, 138] with predictions of CEM95, and calculations from Ref. [138], with the codes HETC [174] and INUCL [175], and systematics [58, 59]

Nuclide	Exp. [43]	Exp. [138]	CEM95	HETC	INUCL	[59]	[58]
^{57}Ni	0.160± 0.019		0.236± 0.0423	0.851± 0.114*	0.517± 0.137*		
^{58}Co	41.1± 4.1	46.8± 3.0	54.2± 0.642	53.8± 0.9	45.7± 1.6	31.5	24.8
^{57}Co (^{57}Ni)	25.1± 2.1	26.7± 1.8	21.136± 0.441	26.0± 0.7	17.7± 1.0	24.4	17.8
^{56}Co (^{56}Ni)	6.72± 0.56	5.35± 0.48	11.223± 0.305	21.77± 0.803*	9.8± 0.6	9.7	4.9
^{55}Co	1.12± 0.12		1.01± 0.0877	2.57± 0.198*	1.93± 0.271*		
^{54}Mn	28.9± 2.4	19.1± 1.4	18.8± 0.378	14.2± 0.5	22.9± 1.0	22.4	22.9
^{52}Mn (^{52}Fe)	9.72± 0.98	6.12± 0.42	12.461± 0.328	18.1± 0.527*	17.3± 1.0	9.3	7.8
^{51}Cr (^{51}Mn)	32.5± 2.5	25.5± 1.8	20.45± 0.473	21.9± 0.8	18.3± 1.1	18.0	22.9
^{48}Cr	0.488± 0.043	0.35± 0.03	0.129± 0.0313	0.62± 0.10	0.34± 0.11	0.30	0.11
^{48}V (^{48}Cr)	16.5± 1.3	11.75± 0.78	12.529± 0.350	18.5± 0.5	15.25± 0.925*	8.6	11.7
^{48}Sc		0.38± 0.04	0.828± 0.0794	0.64± 0.10	6.0± 0.5	0.94	0.35
^{47}Sc (^{47}Ca,^{47}K)		3.66± 0.25	3.058± 0.174	2.222± 0.222*	5.2345± 0.6127*	4.3	3.7
^{46}Sc	10.8± 0.9	7.69± 0.61	13.8± 0.324	4.8± 0.3	14.3± 0.8	10.1	15.2
^{44}Sc (^{44}Ti)	8.94± 0.67	8.08± 0.52	14.252± 0.361	13.9± 0.5	14.2± 0.8	7.7	17.1
^{43}K (^{43}Ar)	1.91± 0.14	1.25± 0.13	1.143± 0.105	0.53± 0.09	3.8± 0.4	2.4	1.9
^{42}K (^{42}Ar)	5.00± 0.42	2.95± 0.69	5.283± 0.219	2.36± 0.19	12.907± 0.8298*	6.53	10.0
^{28}Mg (^{28}Na)		0.86± 0.14		0.11± 0.05	0.48± 0.18	1.04	0.05
^{24}Na (^{24}Ne)	2.10± 0.16	1.47± 0.12	2.99± 0.151	1.11± 0.17	3.58± 0.44	2.66	0.71
^{22}Na (^{22}Mg)	1.36± 0.10		2.71± 0.143	3.27± 0.223*	2.03± 0.278*		
^{7}Be	5.28± 0.40		0.0076± 0.0076				

One can see that a general agreement between different calculations and the data exists. Nevertheless, on the whole, our results obtained with CEM95 are closer to experiment. To make the result of such a comparison visual, the ratio of cumulative yields predicted by CEM95, HETC, and INUCL for ^{58}Co, ^{57}Co,^{56}Co, ^{54}Mn, ^{52}Mn, ^{51}Cr, ^{48}V, ^{47}Sc, ^{44}Sc, ^{43}K, ^{42}K, ^{28}Mg, ^{24}Na, and ^{22}Na to experimental data [138] are plotted in Fig. 49 as a function of nuclide mass.

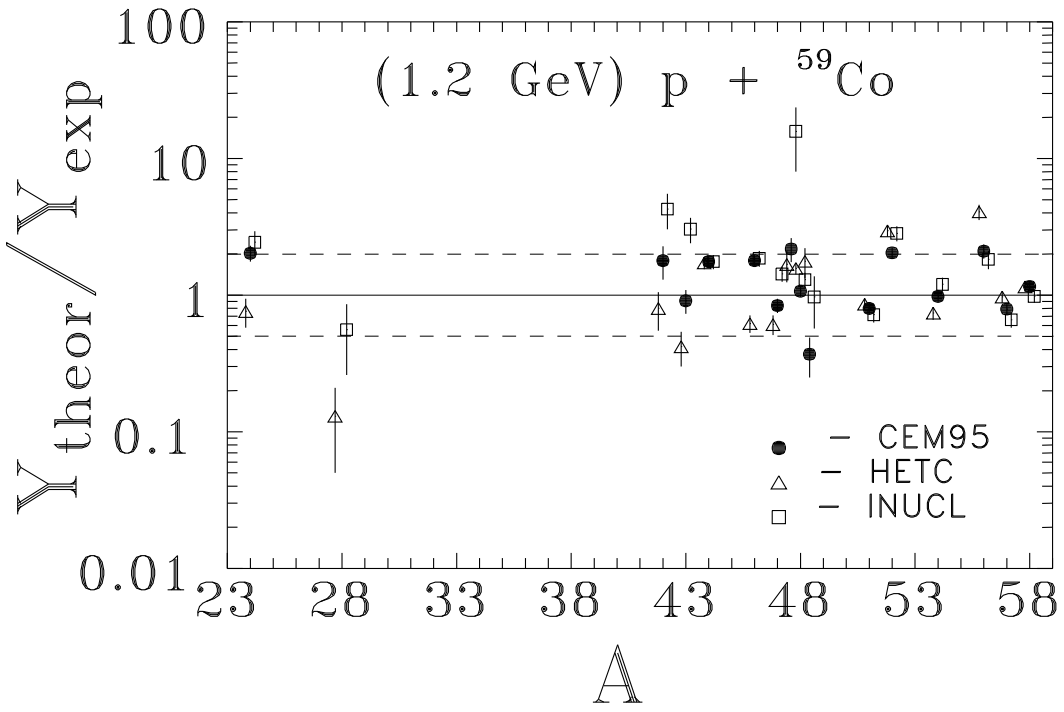

Fig. 49. Ratios of calculated to experimental [138] cumulative yields predicted by the codes CEM95, HETC [174, 138], and INUCL [175, 138] for the nuclides ^{58}Co, ^{57}Co, ^{56}Co, ^{54}Mn, ^{52}Mn, ^{51}Cr, ^{48}V, ^{47}Sc, ^{44}Sc, ^{43}K, ^{42}K, ^{28}Mg, ^{24}Na.

A more detailed comparison of results obtained using the CEM95, HETC, and INUCL codes with the recent measurements [76]–[79] of the yields of residual nuclides from interactions of protons of 130 MeV and 1.5 GeV with ^{63}Cu, ^{65}Cu, ^{206}Pb, ^{207}Pb, ^{208}Pb, and ^{209}Bi and from p(1.2 GeV)+^{59}Co may be found in Refs. [76]–[79]. Let us show here part of results from Ref. [77]. If the coincidence criterion between the experimental and calculated cross sections is taken to be $0.5 \leq \sigma_{cal}/\sigma_{exp} \leq 2.0$, the results of the comparison may be expressed by the ratio of the number of reactions that did "coincide" to the total number of reactions compared. Table III shows the results of such an analysis.

TABLE III
Statistics of coincidence (within a factor of 2) between calculated and experimental cross sections for the production of daughter nuclei in the spallation region (adapted from Ref. [77])

Target	T_p (MeV)	HETC	INUCL	CEM95
^{59}Co	1200	18/30	20/30	19/30
^{63}Cu	1500	12/22	12/22	17/22
	130	2/4	3/4	4/4
^{65}Cu	1500	10/22	10/22	17/22
	130	3/4	3/4	4/4
^{206}Pb	1500	5/10	3/10	3/10
	130	3/3	1/3	3/3
^{207}Pb	1500	8/11	3/11	5/11
	130	3/3	1/3	3/3
^{208}Pb	1500	6/11	4/11	6/11
	130	3/3	1/3	3/3
^{209}Bi	1500	10/16	5/16	8/16
	130	2/3	0/3	2/3
Average		68.6 %	45.7 %	74.2 %

One can see that the results of CEM95, when compared with all measured cross sections for all these targets and incident energies, agree within a factor of two with the experimental data for 74.2% of the reactions, the results of HETC agree for 68.6% of the reactions, and the results of INUCL agree for 45.7% of the reactions.

4.6. Targets ^{96}Zr, ^{94}Zr, ^{92}Zr, ^{91}Zr, ^{90}Zr, and ^{nat}Zr

Being an important structural material, zirconium is well investigated experimentally. At present, there are excitation functions available for many nuclides from each stable isotope of zirconium, and for ^{nat}Zr. To our knowledge, the majority of published experimental excitation functions were included in the compilation [46, 47]. There are also experimental data published in Refs. [211, 212], not covered by the compilation [46, 47]. We include in our analysis all these data. Many new experimental data for Zr were obtained recently by the group of Michel [44], but these measurements were reported after we finished our work. We have, however, included in our study several excitation functions required by the Intercomparison [66], whose measurement was subsequently reported in Ref. [44]. These results are thus a prediction of the CEM.

Our results for excitation functions for the production of $^{96;95}$Nb, ^{95}Zr, ^{95}Y, ^{72}Se, $^{74;72;71}$As, $^{73;72;67;66}$Ga, and ^{72}Zn from p+^{96}Zr are compared with experimental data in Figs. 50 and 51. Excitation functions for the production of $^{83;82}$Sr, $^{88-86}$Y, $^{89;88;86}$Zr, $^{90-88;86;84-76}$Rb, ^{77}Br, $^{75;73;72}$Se, and $^{74;72;71}$As from p+^{94}Zr are shown in Figs. 52–55, and yields of $^{92;90}$Nb and ^{88}Y from p+^{92}Zr are shown in Fig. 56.

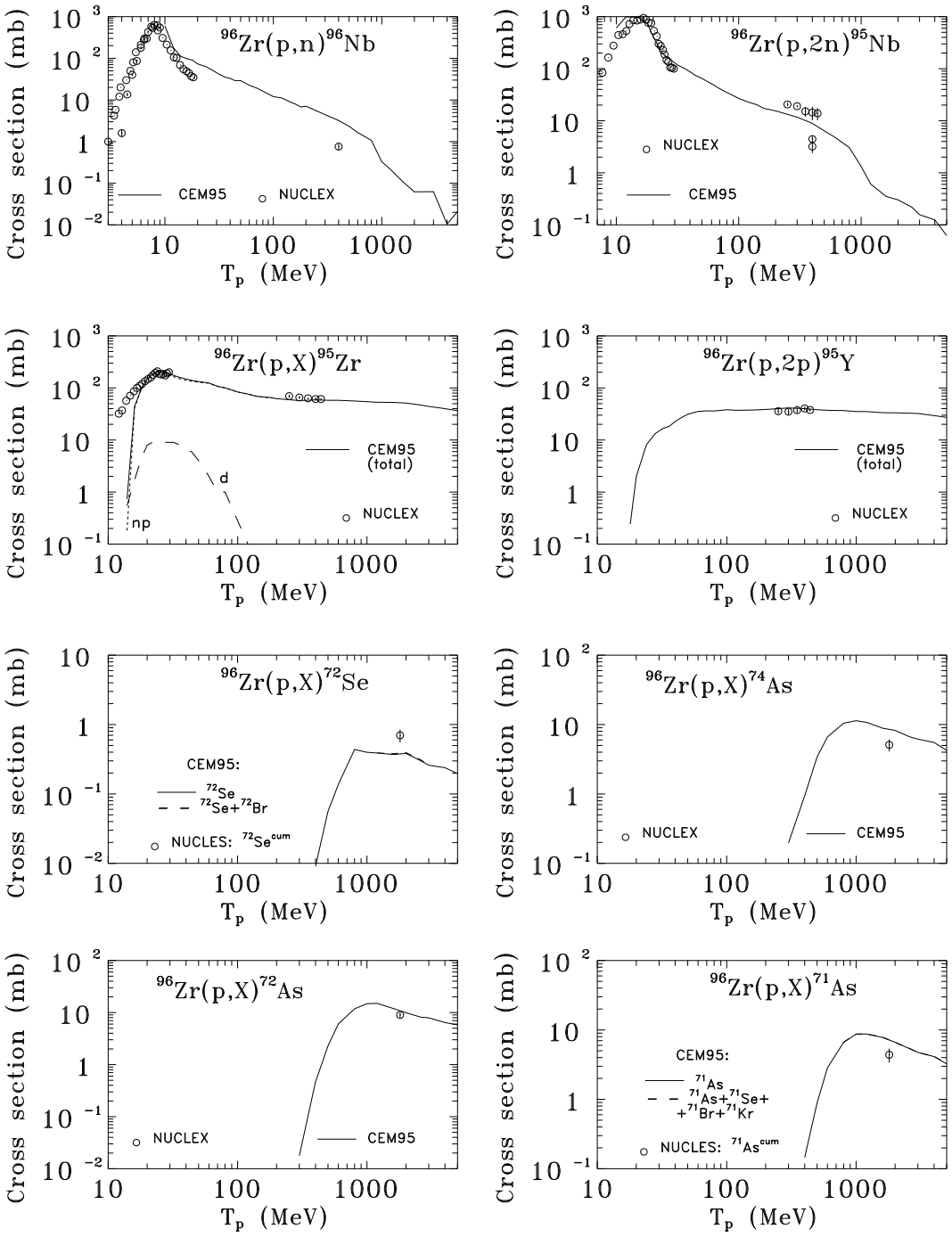

Fig. 50. Excitation functions for the production of ^{96}Nb, ^{95}Nb, ^{95}Zr, ^{95}Y, ^{72}Se, ^{74}As, ^{72}As, and ^{71}As from p+^{96}Zr. The contributions from the channels (p,d) and (p,np) to the total CEM95 yield of ^{95}Zr are shown by dashed lines, as indicated. Experimental data labeled as NUCLEX are from Refs. [46, 47].

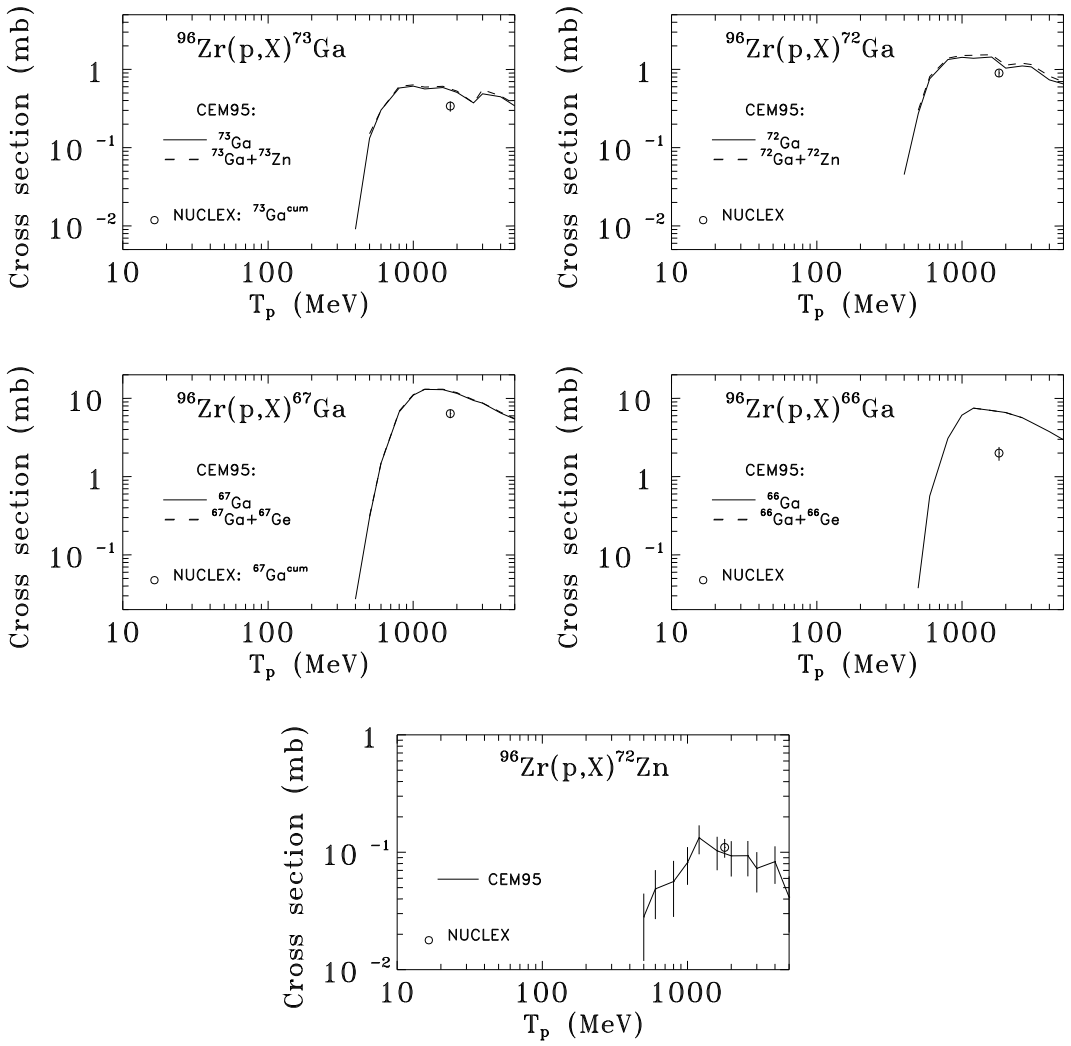

Fig. 51. Excitation functions for the production of ^{73}Ga, ^{72}Ga, ^{67}Ga, ^{66}Ga, and ^{72}Zn from p+^{96}Zr. Experimental data labeled as NUCLEX are from Refs. [46, 47].

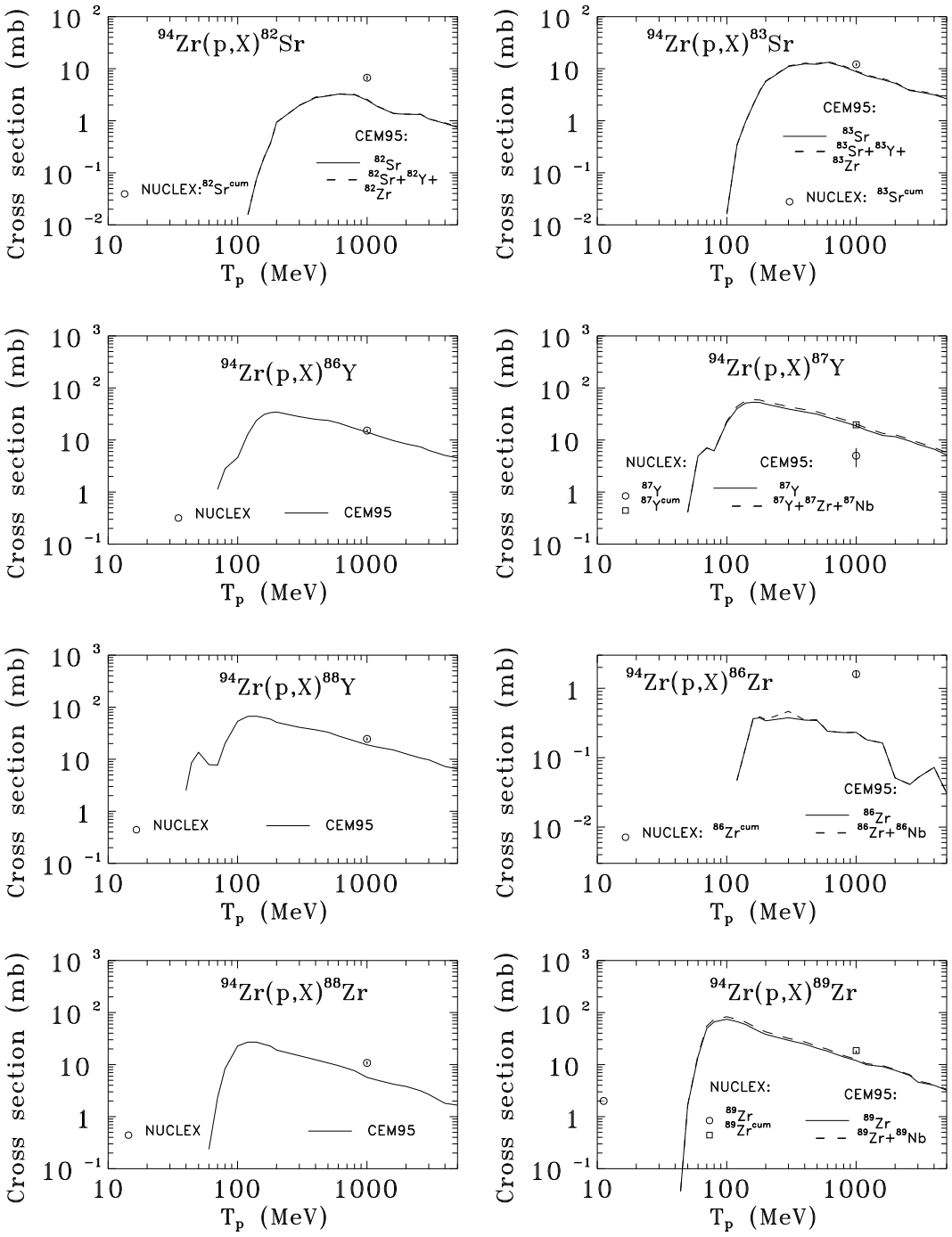

Fig. 52. Excitation functions for the production of ^{82}Sr, ^{83}Sr, ^{86}Y, ^{87}Y, ^{88}Y, ^{86}Zr, ^{88}Zr, and ^{89}Zr from p+^{94}Zr. Experimental data labeled as NUCLEX are from Refs. [46, 47].

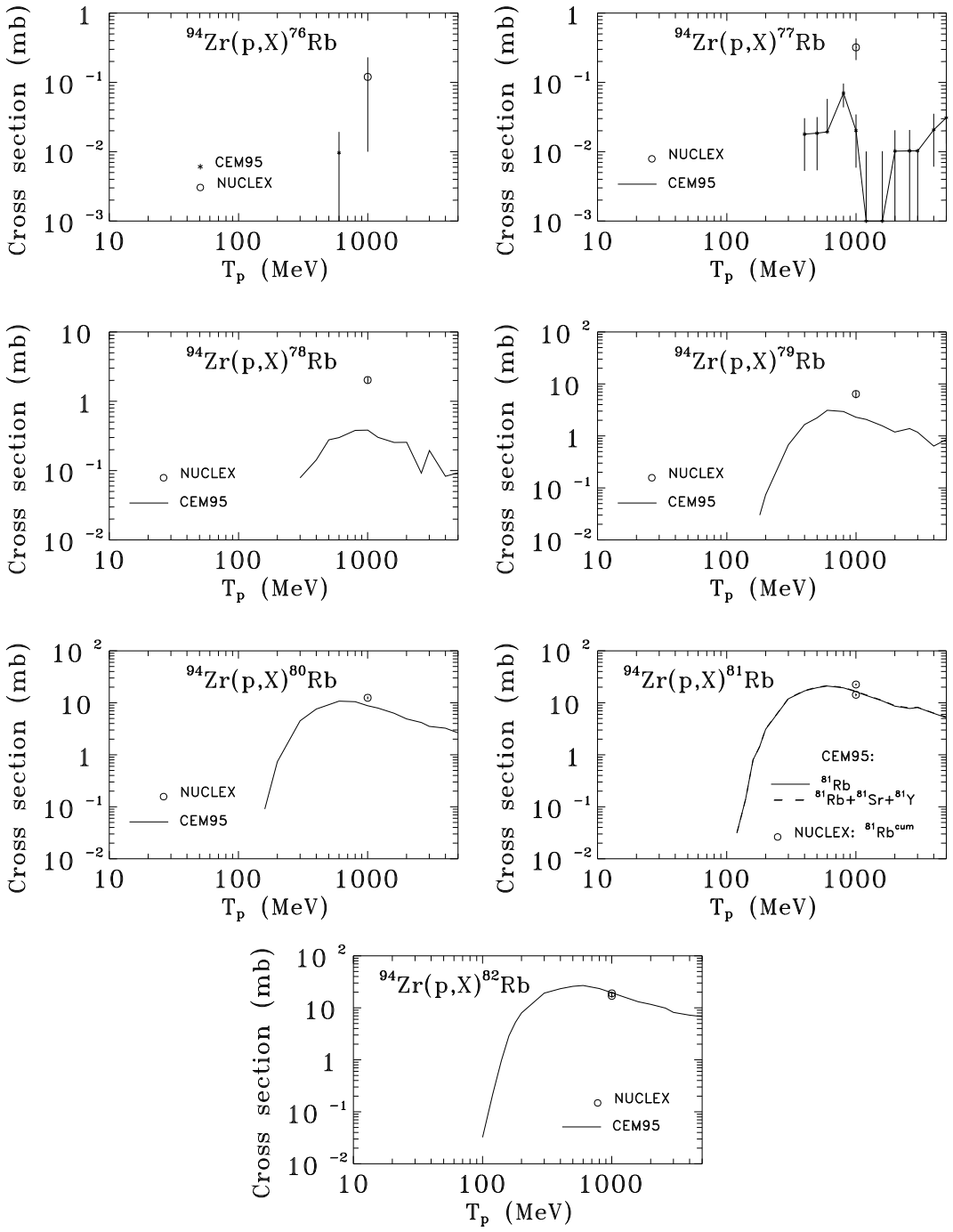

Fig. 53. Excitation functions for the production of ^{76}Rb, ^{77}Rb, ^{78}Rb, ^{79}Rb, ^{80}Rb, ^{81}Rb, and ^{82}Rb from p+^{94}Zr. Experimental data labeled as NUCLEX are from Refs. [46, 47].

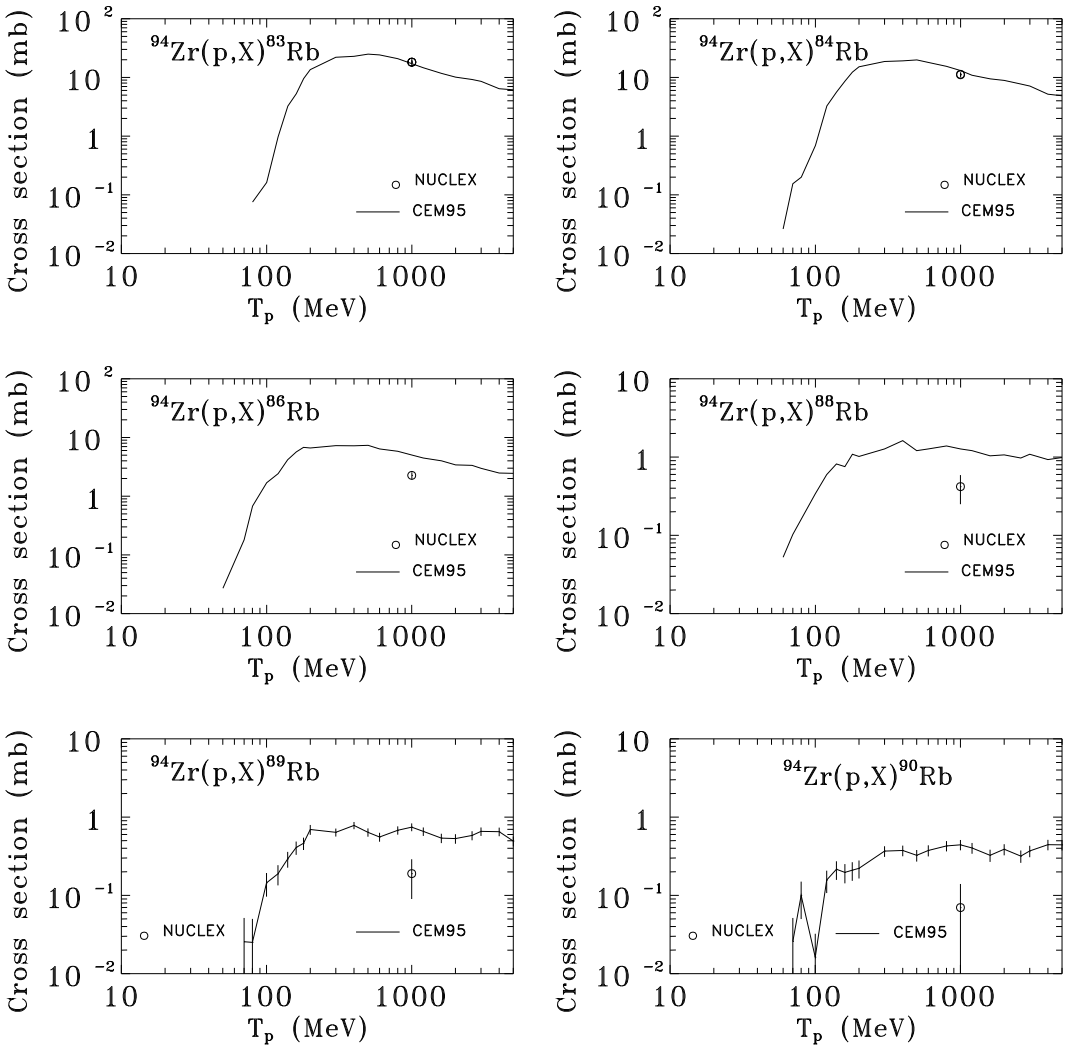

Fig. 54. Excitation functions for the production of ^{83}Rb, ^{84}Rb, ^{86}Rb, ^{88}Rb, ^{89}Rb, and ^{90}Rb from p+^{94}Zr. Experimental data labeled as NUCLEX are from Refs. [46, 47].

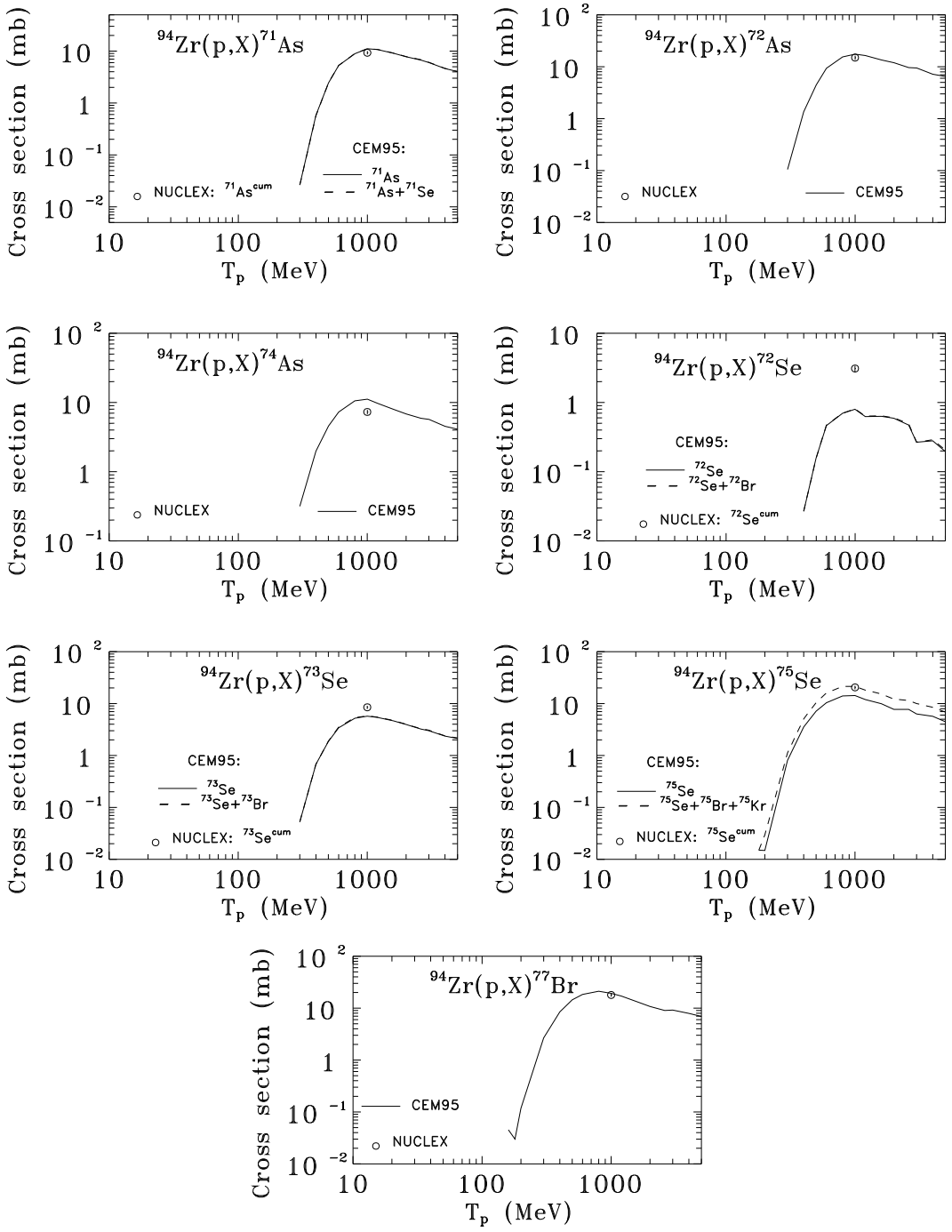

Fig. 55. Excitation functions for the production of ^{71}As, ^{72}As, ^{74}As, ^{72}Se, ^{73}Se, ^{75}Se, and ^{77}Br from p+^{94}Zr. Experimental data labeled as NUCLEX are from Refs. [46, 47].

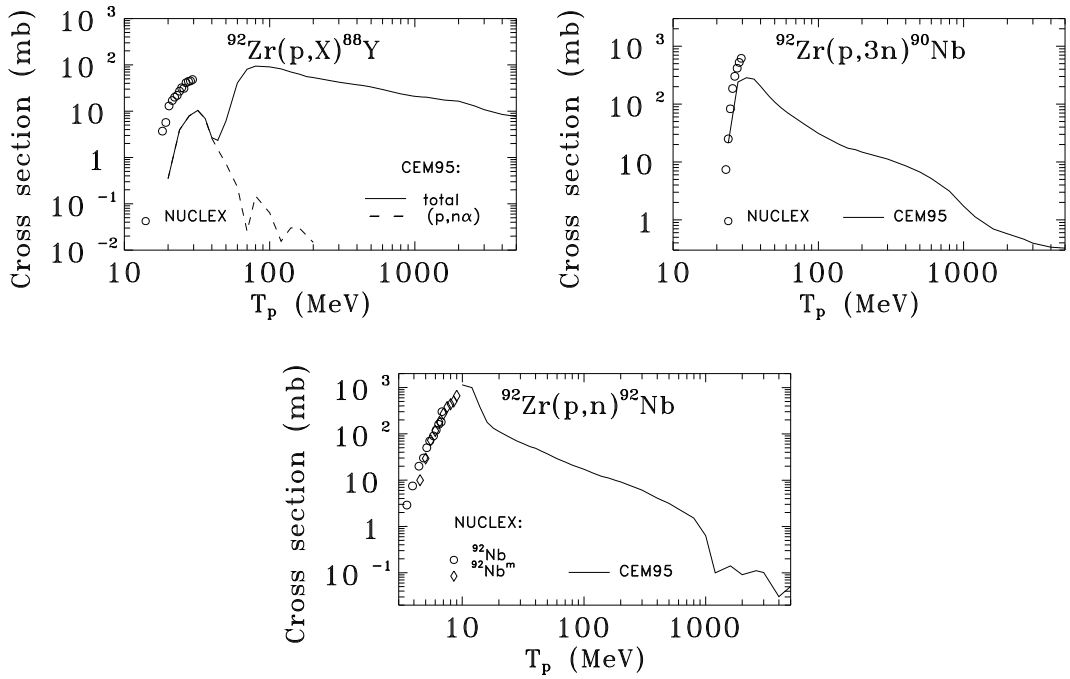

Fig. 56. Excitation functions for the production of ^{88}Y, ^{90}Nb, and ^{92}Nb from p+^{92}Zr. The contribution from the channel (p,nα) to the total CEM95 yield of ^{88}Y is shown by a dashed line. Experimental data labeled as NUCLEX are from the compilation [46, 47].

Our calculations for the the production of $^{91;90}$Nb, $^{89;88;86}$Zr, $^{88-86}$Y, $^{83;82}$Sr, $^{88;86;84-76}$Rb, $^{84-82;80;78-71}$Br, $^{75;73;72}$Se, and $^{74;72;71}$As from p+^{91}Zr are compared with experimental data in Figs. 57–62. Excitation functions for the production of $^{90;89}$Nb, $^{89;88;86}$Zr, $^{85;83;82}$Sr, $^{88-83}$Y, $^{86;84-76}$Rb, ^{77}Br, $^{75;73;72}$Se, and $^{74;72;71}$As, from p+^{90}Zr are shown in Figs. 63–66. Total inelastic cross section σ_{in} and excitation functions for the production of $^{96;95;92;90}$Nb, $^{95;89;88;86}$Zr, $^{91;88-86}$Y, $^{85-82}$Sr, $^{86;84;83;81}$Rb, $^{86-76}$Kr, $^{77;75}$Br, $^{75;73;72}$Se, $^{74;71;70}$As, ^{69}Ge, $^{67;66}$Ga, ^{65}Zn, $^{60;58-56}$Co, $^{54;52}$Mn, ^{51}Cr, ^{48}V, ^{46}Sc, $^{42;39}$Ar, ^{22}Na, and ^{7}Be from ^{nat}Zr are compared with the available experimental data in Figs. 67–75.

To illustrate the relative role of different reaction channels in the production of daughter nuclides, the contributions from the (p,d) and (p,np) channels to ^{96}Zr(p,x)^{95}Zr are shown in Fig. 50; the contributions from the (p,nα) channel to ^{92}Zr(p,x)^{88}Y is shown in Fig. 56; the contributions from the (p,nα), (p,2nα), (p,α), (p,npd), (p,2nd), (p,3np), (p,t), (p,nd), (p,2np), and (p,n2α) channels to the total yields of ^{86}Y, ^{87}Y, ^{88}Y, ^{88}Zr, ^{89}Zr, and ^{83}Rb from ^{91}Zr are shown, respectively, in Figs. 57 and 58; the contributions to the total yields of ^{88}Zr and ^{89}Zr from the channels (p,t), (p,nd), (p,2np), (p,d), and (p,np) in the reaction p+^{90}Zr are shown in Fig. 63; the contributions from the channels (p,α), (p,nα), (p,2nα), (p,^{3}He), (p,pd), and (p,n2p) to the total yields of $^{88-85}$Y are shown in Fig. 64, respectively.

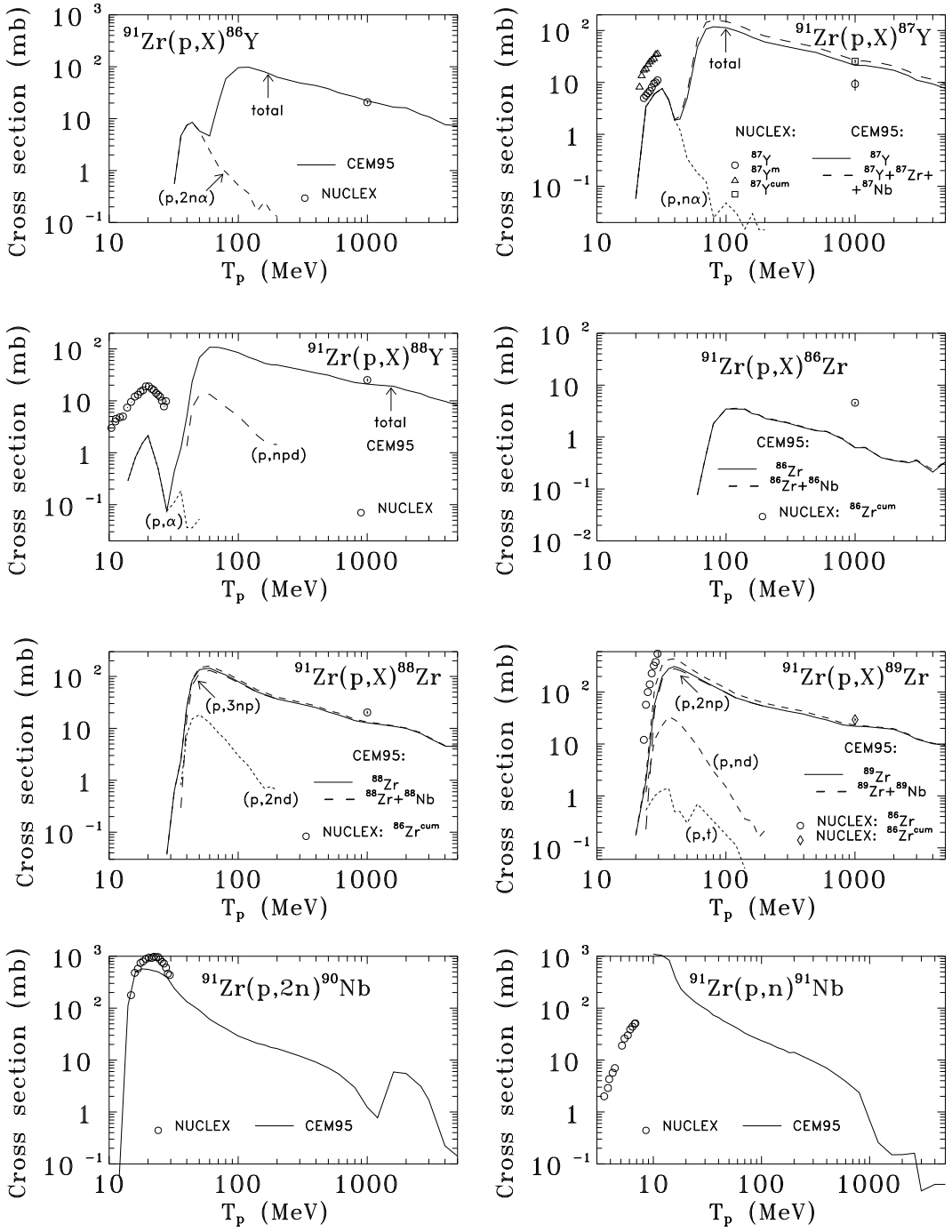

Fig. 57. Excitation functions for the production of ^{86}Y, ^{87}Y, ^{88}Y, ^{86}Zr, ^{88}Zr, ^{89}Zr, ^{90}Nb, and ^{91}Nb from p+^{91}Zr. The contributions from the channels (p,nα), (p,2nα), (p,α), (p,npd), (p,2nd), (p,3np), (p,t), (p,nd), and (p,2np) to the total CEM95 yields are shown by a dashed lines, as indicated. Experimental data labeled as NUCLEX are from the compilation [46, 47].

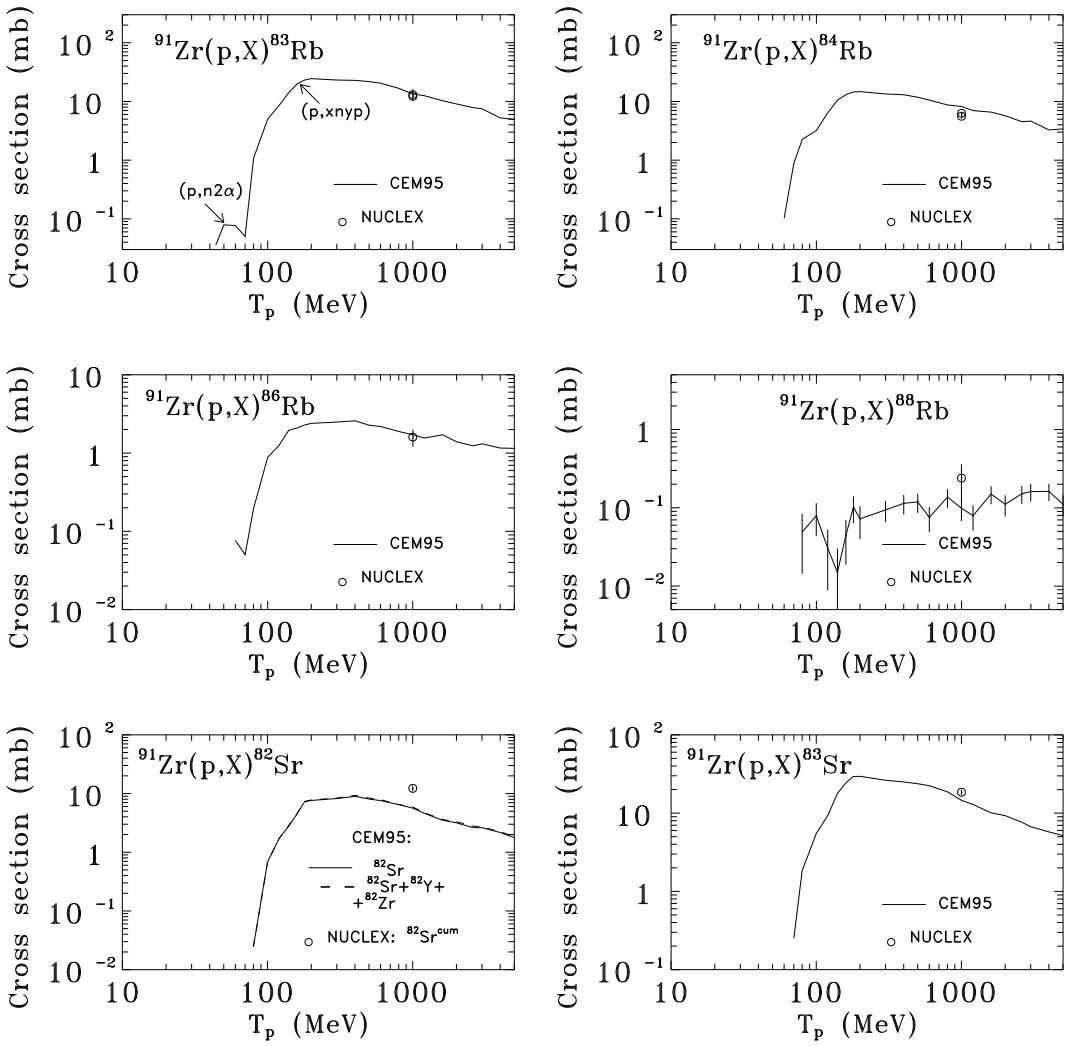

Fig. 58. Excitation functions for the production of ^{83}Rb, ^{84}Rb, ^{86}Rb, ^{88}Rb, ^{82}Sr, and ^{83}Sr from p+^{91}Zr. For ^{83}Rb, the contributions to the total CEM95 yield from the channels (p,n2α) and (p,xnyp) are shown separately, as indicated. Experimental data labeled as NUCLEX are from the compilation [46, 47].

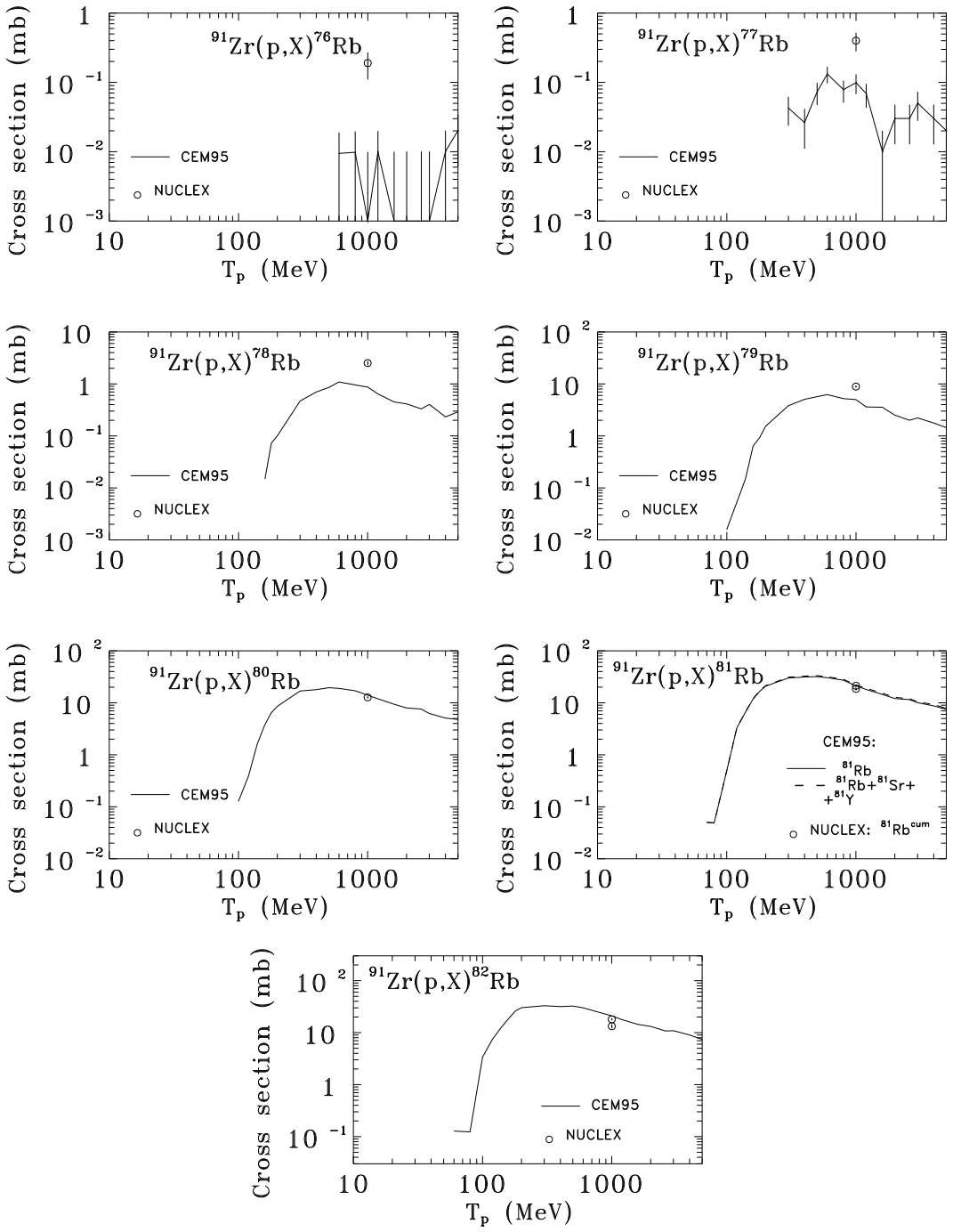

Fig. 59. Excitation functions for the production of ^{76}Rb, ^{77}Rb, ^{78}Rb, ^{79}Rb, ^{80}Rb, ^{81}Rb, and ^{82}Rb from p+^{91}Zr. Experimental data labeled as NUCLEX are from the compilation [46, 47].

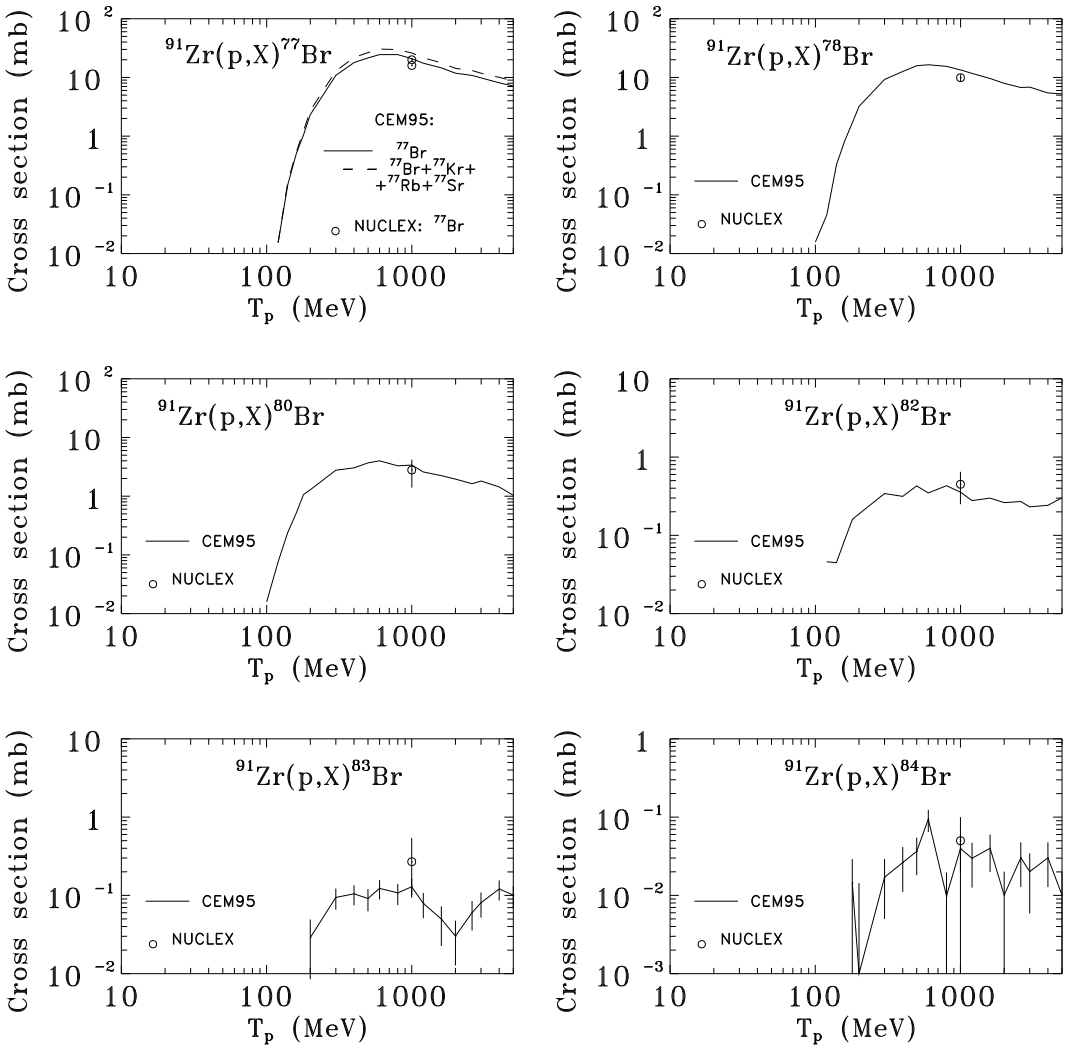

Fig. 60. Excitation functions for the production of ^{77}Br, ^{78}Br, ^{80}Br, ^{82}Br, ^{83}Br, and ^{84}Br from p+^{91}Zr. Experimental data labeled as NUCLEX are from the compilation [46, 47].

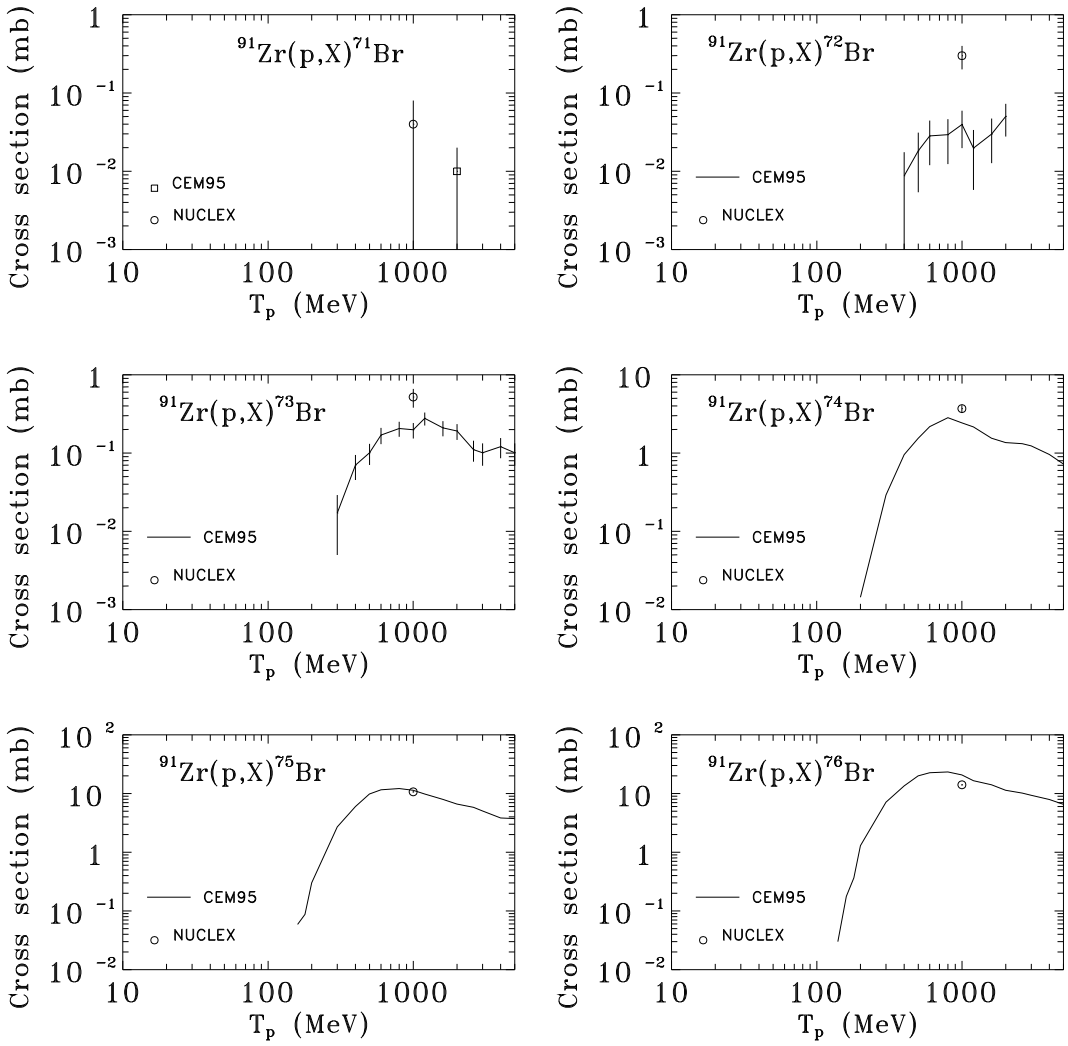

Fig. 61. Excitation functions for the production of ^{71}Br, ^{72}Br, ^{73}Br, ^{74}Br, ^{75}Br, and ^{76}Br from p+^{91}Zr. Experimental data labeled as NUCLEX are from the compilation [46, 47].

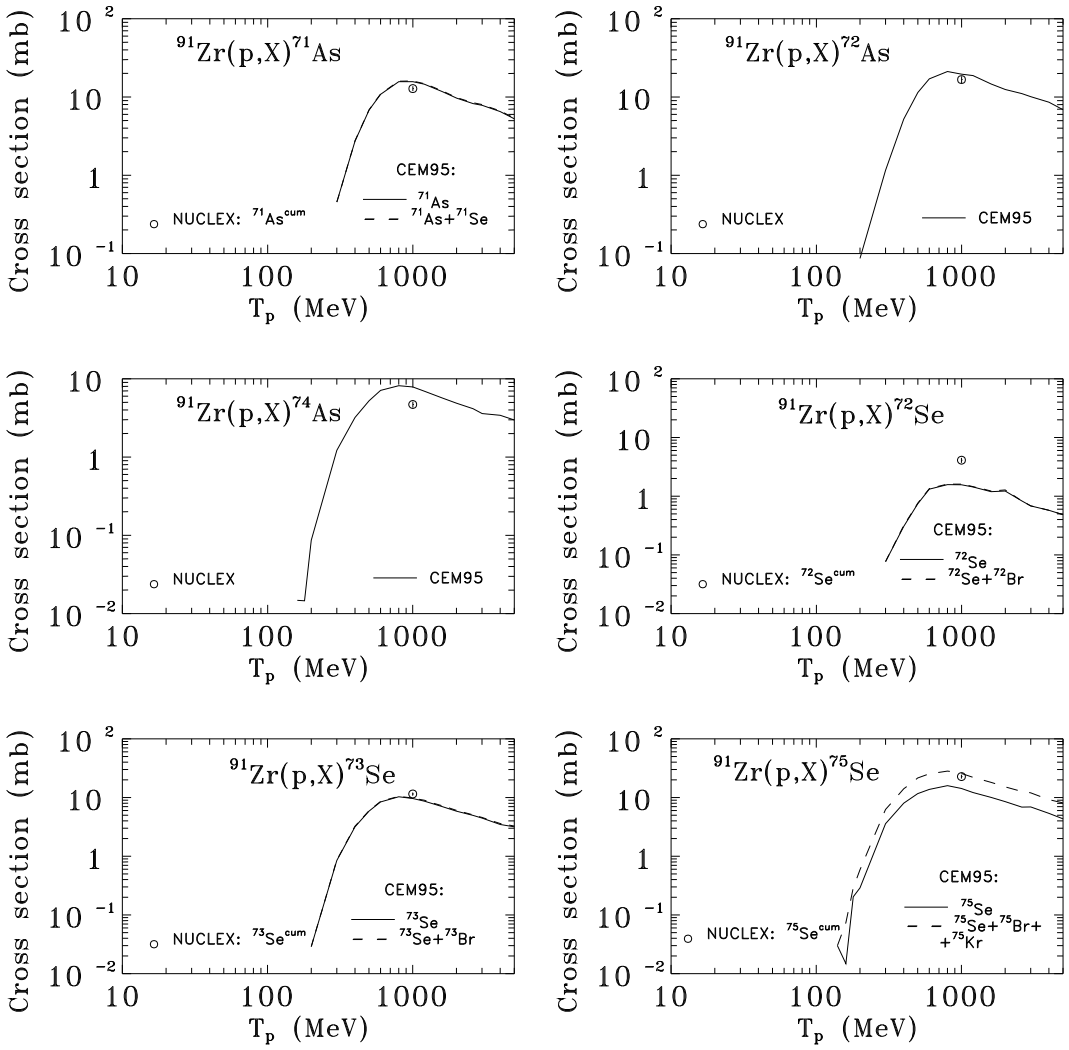

Fig. 62. Excitation functions for the production of ^{71}As, ^{72}As, ^{74}As, ^{72}Se, ^{73}Se, and ^{75}Se from p+^{91}Zr. Experimental data labeled as NUCLEX are from the compilation [46, 47].

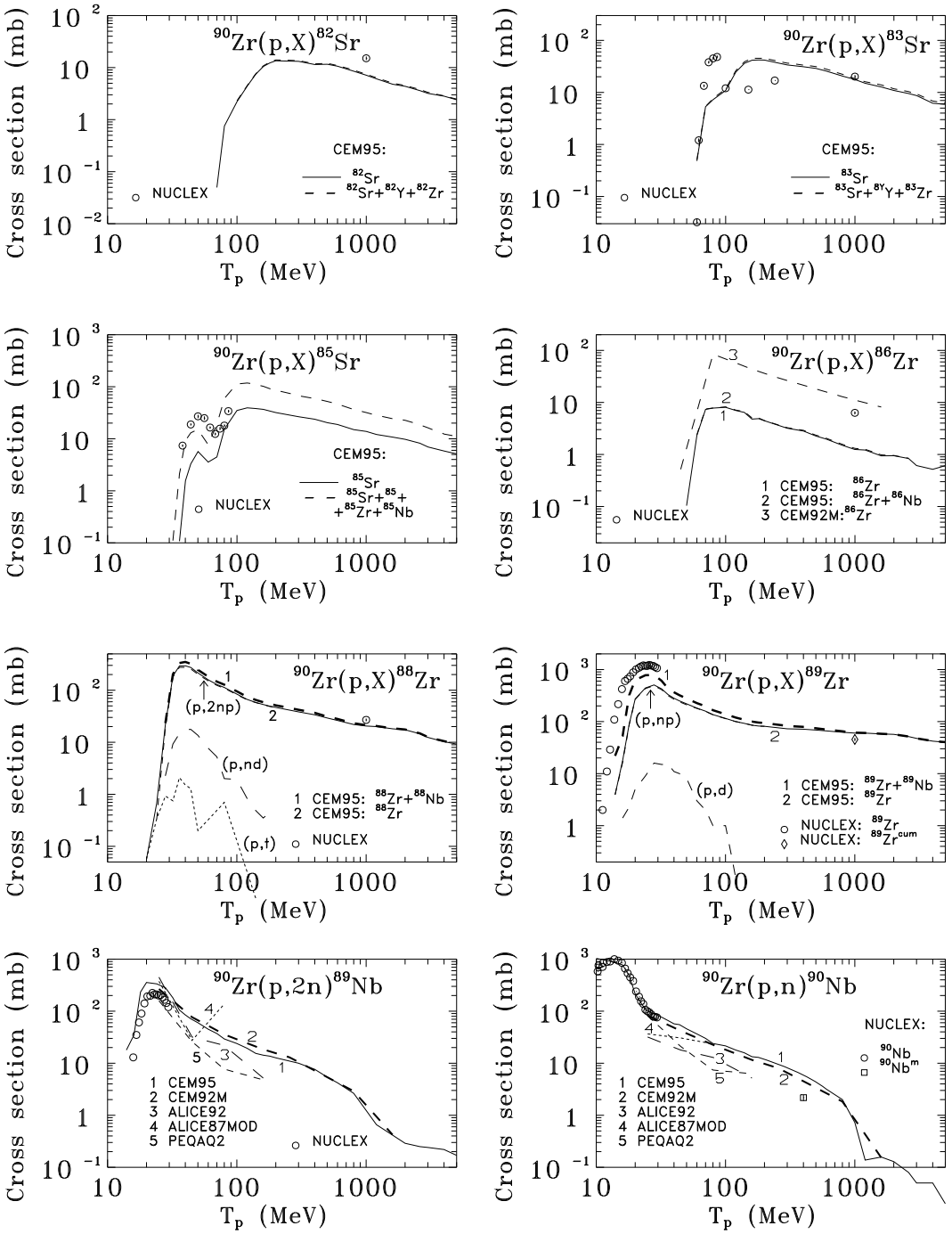

Fig. 63. Excitation functions for the production of ^{82}Sr, ^{83}Sr, ^{85}Sr, ^{86}Zr, ^{88}Zr, ^{89}Zr, ^{89}Nb, and ^{90}Nb from p+^{90}Zr. For ^{89}Nb and ^{90}Nb, predictions of the codes CEM92M [74], ALICE92 [147], ALICE87MOD [209], and PEQAQ2 [210] from the recent Intercomparison [48] are shown by dashed lines 2, 3, 4, and 5, respectively. For ^{88}Zr and ^{89}Zr, contributions to the total CEM95 yields from the channels (p,t), (p,nd), (p,2np), (p,d), and (p,np) are shown by dashed lines, as indicated. Experimental data labeled as NUCLEX are from the compilation [46, 47].

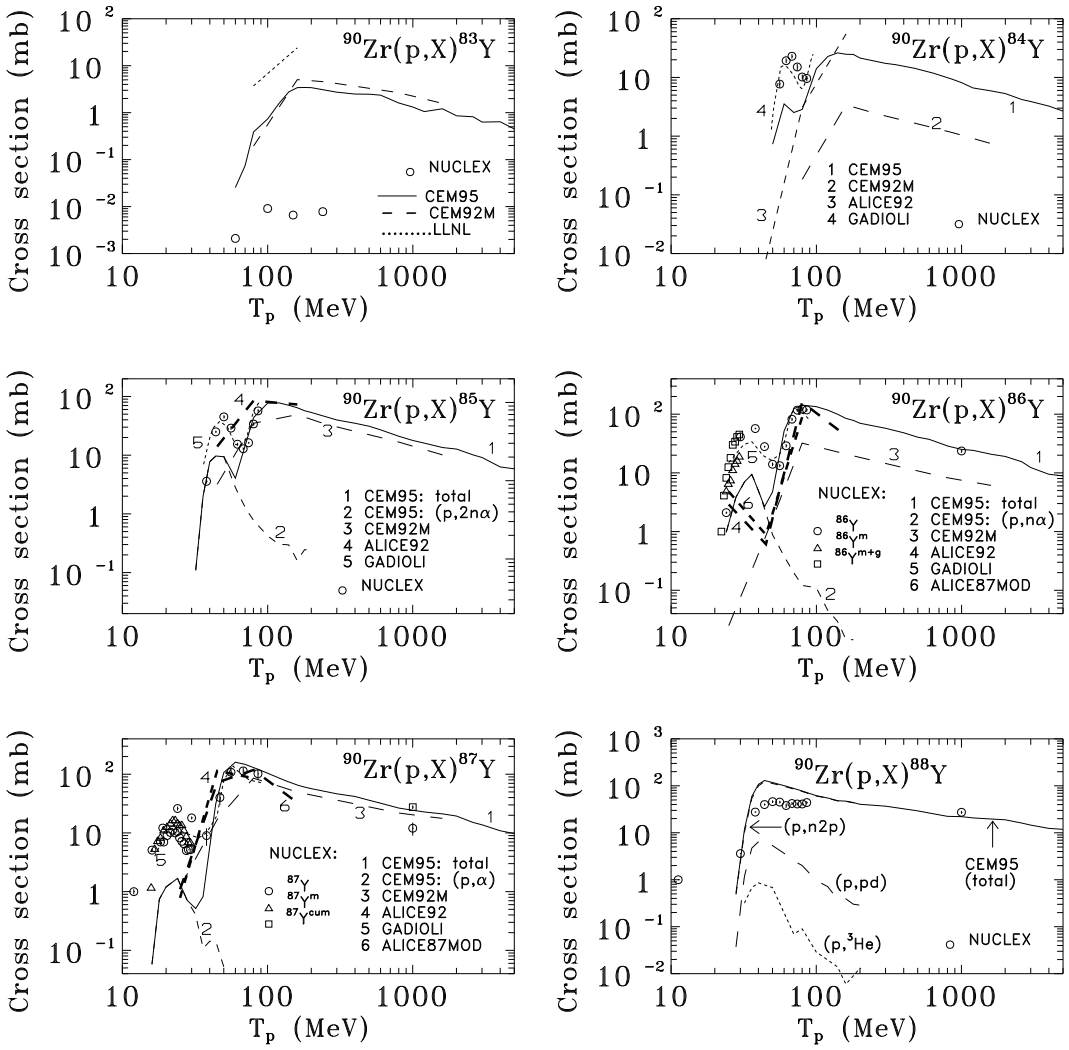

Fig. 64. Excitation functions for the production of ^{83}Y, ^{84}Y, ^{85}Y, ^{86}Y, ^{87}Y, and ^{88}Y from p+^{90}Zr. Predictions of the codes CEM92M [74], ALICE92 (labeled as ALICE92 and LLNL, for ^{83}Y) [147], ALICE87MOD [209], and of the exciton model with preformed α-particles by Gadioli et al. (labeled as GADIOLI) [102] are shown by dashed lines, as indicated. For ^{85}Y, ^{86}Y, ^{87}Y, and ^{88}Y, contributions to the total CEM95 yields from the channels (p,α), (p,nα), (p,2nα), (p,^{3}He), (p,pd), and (p,n2p) are shown by dashed lines, as indicated. Experimental data labeled as NUCLEX are from the compilation [46, 47].

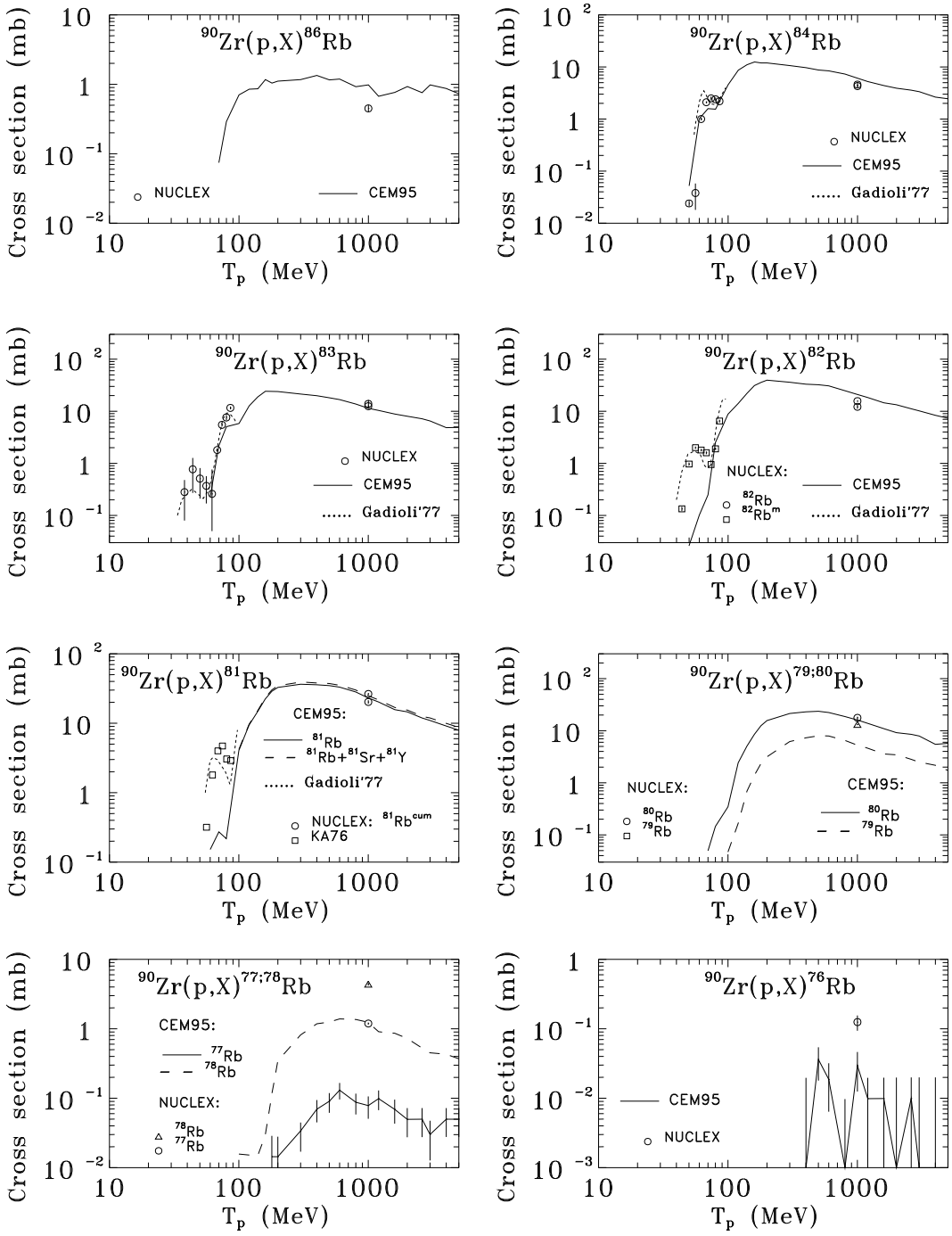

Fig. 65. Excitation functions for the production of ^{86}Rb, ^{84}Rb, ^{83}Rb, ^{82}Rb, ^{81}Rb, ^{80}Rb, ^{79}Rb, ^{78}Rb, ^{77}Rb, and ^{76}Rb from p+^{90}Zr. Dotted lines labeled as Gadioli'77 show predictions of the exciton model with preformed α-particles by Gadioli et al. [102]. Experimental data are labeled as: NUCLEX [46, 47] and KA76 [211].

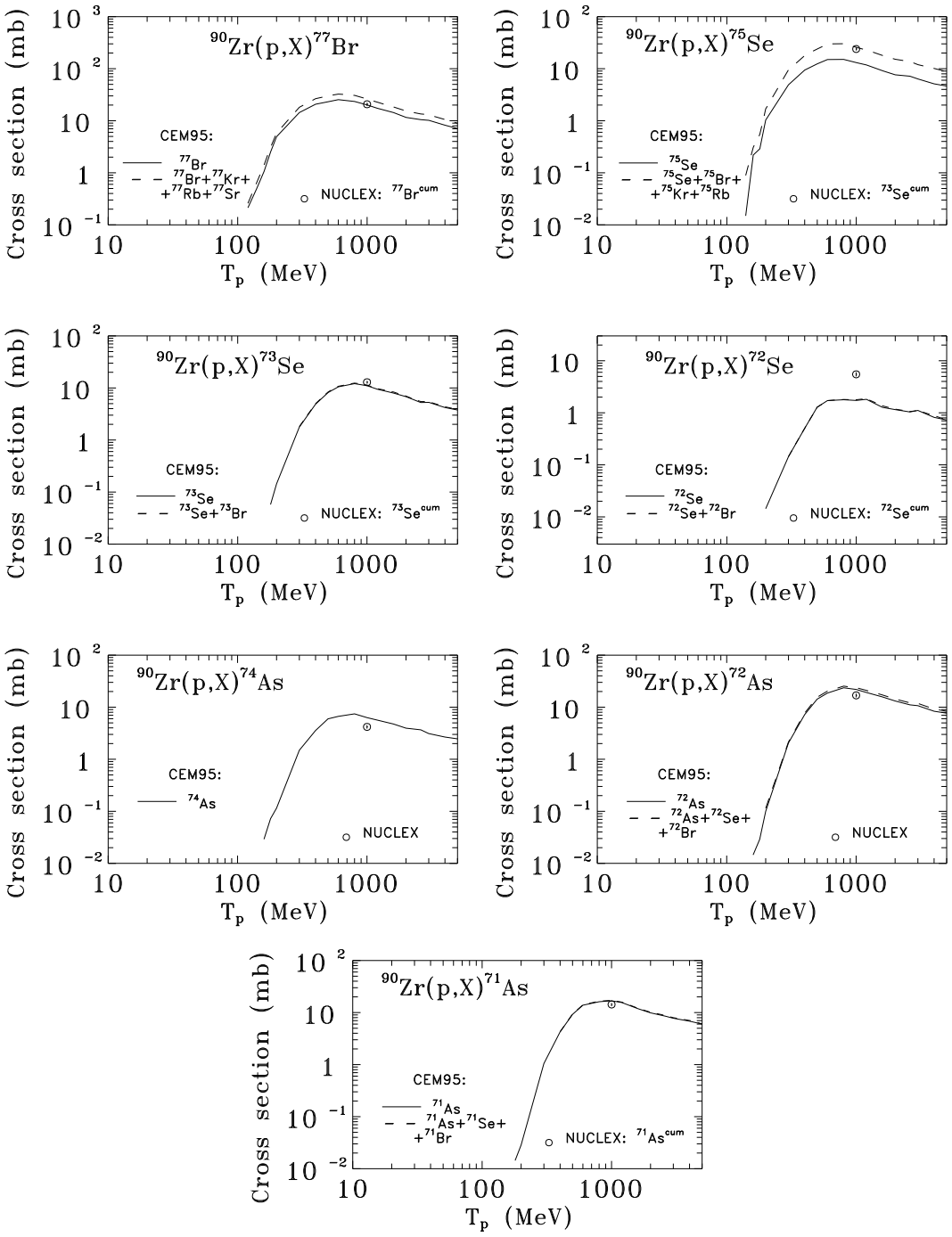

Fig. 66. Excitation functions for the production of ^{77}Br, ^{75}Se, ^{73}Se, ^{72}Se, ^{74}As, ^{72}As, and ^{71}As from p+^{90}Zr. Experimental data are labeled as: NUCLEX [46, 47].

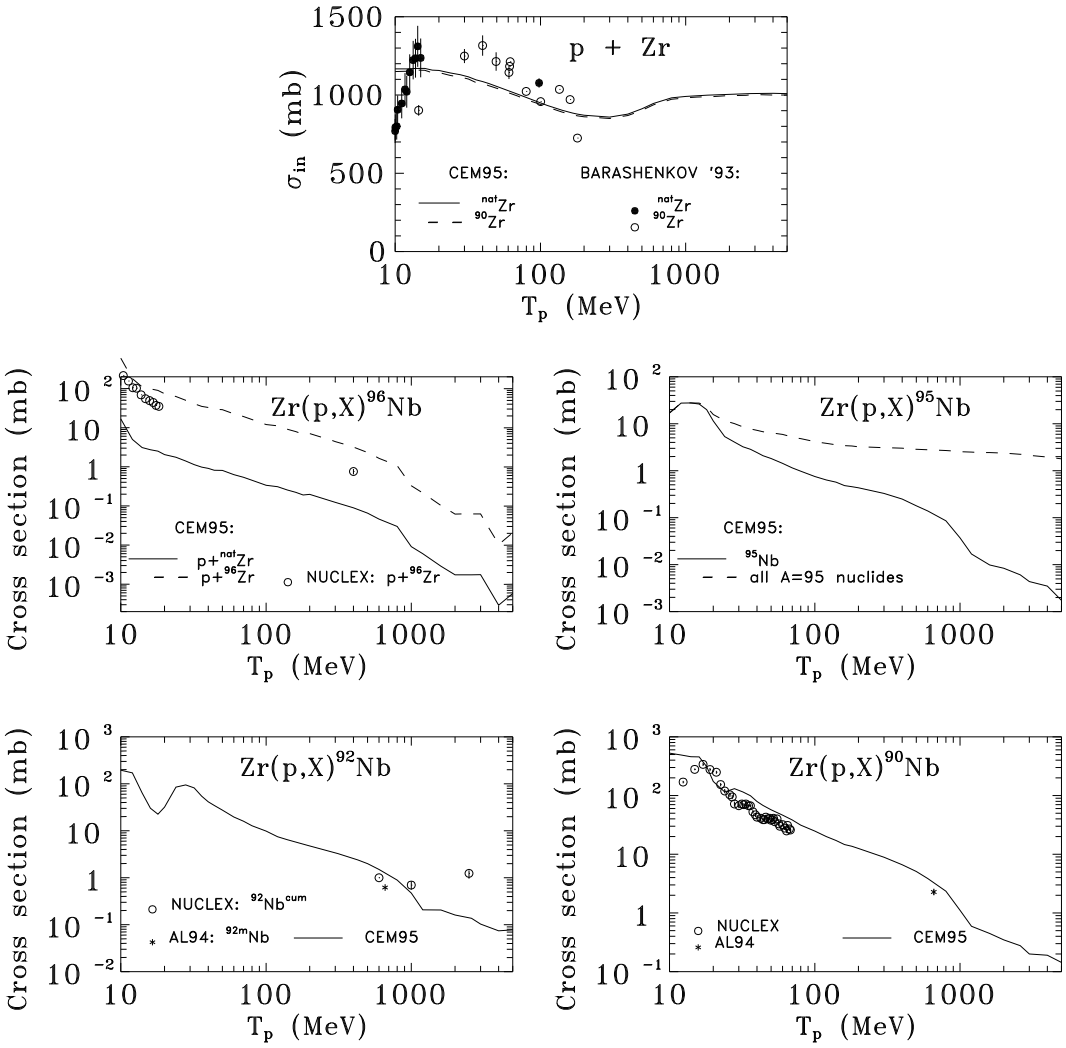

Fig. 67. Total inelastic cross section and excitation functions for the production of ^{96}Nb, ^{95}Nb, ^{92}Nb, and ^{90}Nb from p+^{nat}Zr. Experimental data are labeled as: BARASHENKOV'93 [158], NUCLEX [46, 47], and AL94 [212].

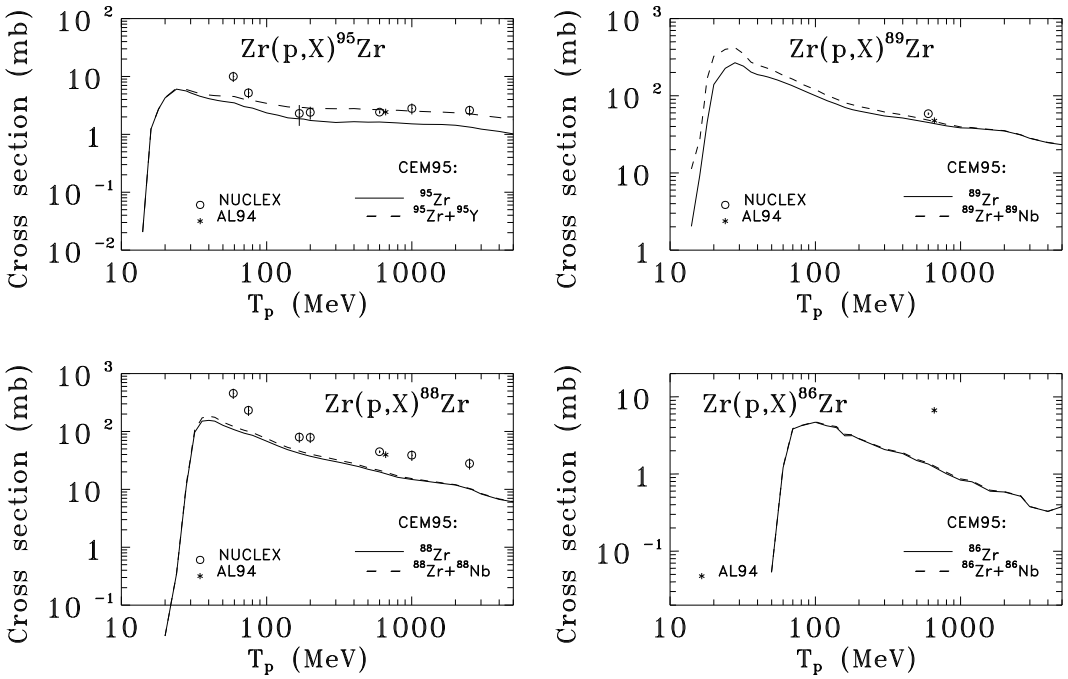

Fig. 68. Excitation functions for the production of ^{95}Zr, ^{89}Zr, ^{88}Zr, and ^{86}Zr from p+^{nat}Zr. Experimental data are labeled as: NUCLEX [46, 47] and AL94 [212].

From Figs. 51–75 one can see that all conclusions made above from the analysis of lighter targets are also valid for zirconium. On the whole, CEM95 reproduces satisfactorily most of the shapes and absolute values of measured excitation functions, especially at energies above $\sim$ 100 MeV. There are, nevertheless, some large discrepancies for several nuclides caused mainly by poor masses and binding energies used in the calculations of the corresponding nuclides. The CEM does not contain a model for fragmentation, therefore it cannot describe the production of ^{7}Be and other light fragments from zirconium; the CEM underestimates the production of ^{4}He, and therefore underestimates the corresponding parts of some excitation functions where α-emission plays an important role.

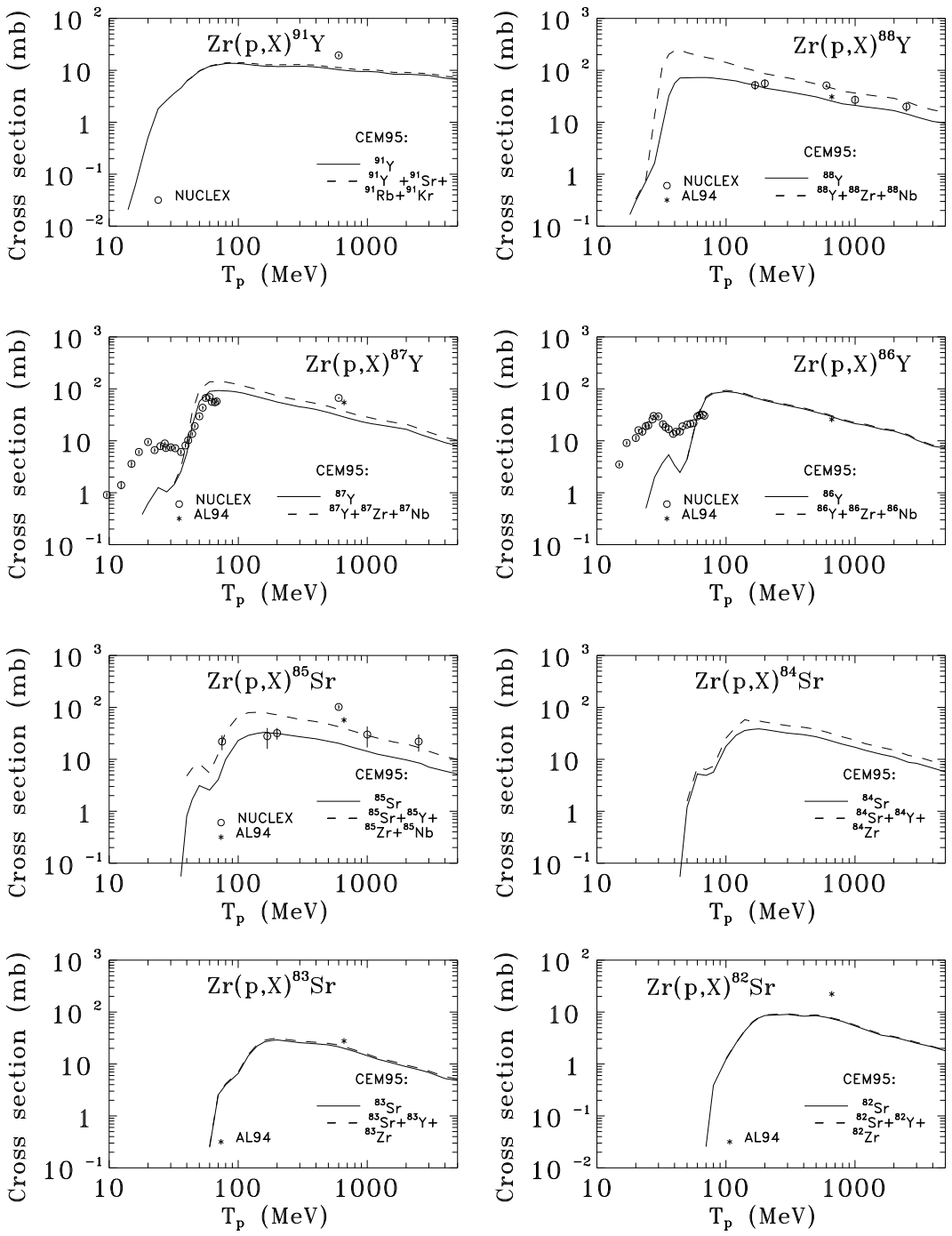

Fig. 69. Excitation functions for the production of ^{91}Y, ^{88}Y, ^{87}Y, ^{86}Y, ^{85}Sr, ^{84}Sr, ^{83}Sr, and ^{82}Sr from p+^{nat}Zr. Experimental data are labeled as: NUCLEX [46, 47] and AL94 [212].

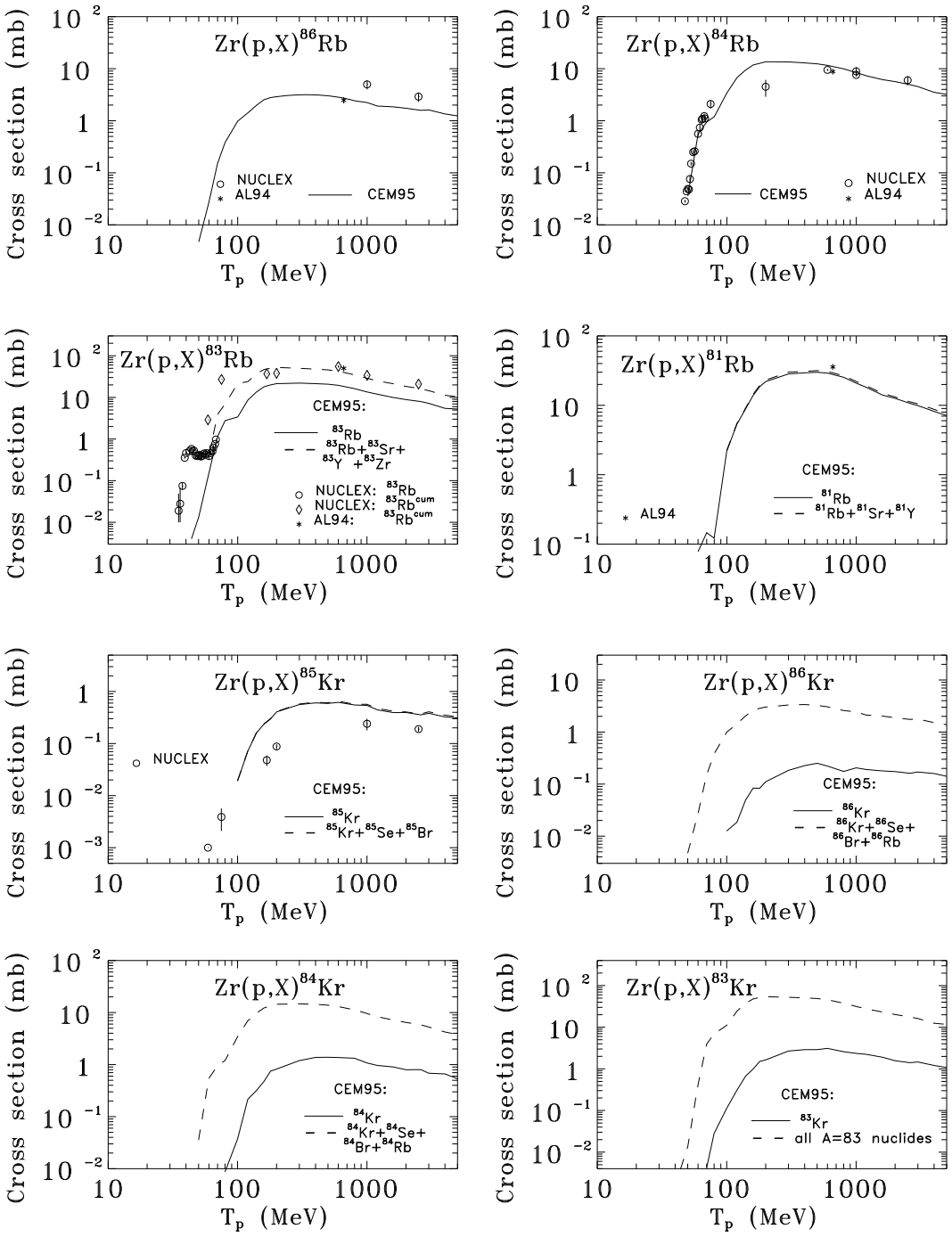

Fig. 70. Excitation functions for the production of ^{86}Rb, ^{84}Rb, ^{83}Rb, ^{81}Rb, ^{85}Kr, ^{86}Kr, ^{84}Kr, and ^{83}Kr from p+^{nat}Zr. Experimental data are labeled as: NUCLEX [46, 47] and AL94 [212].

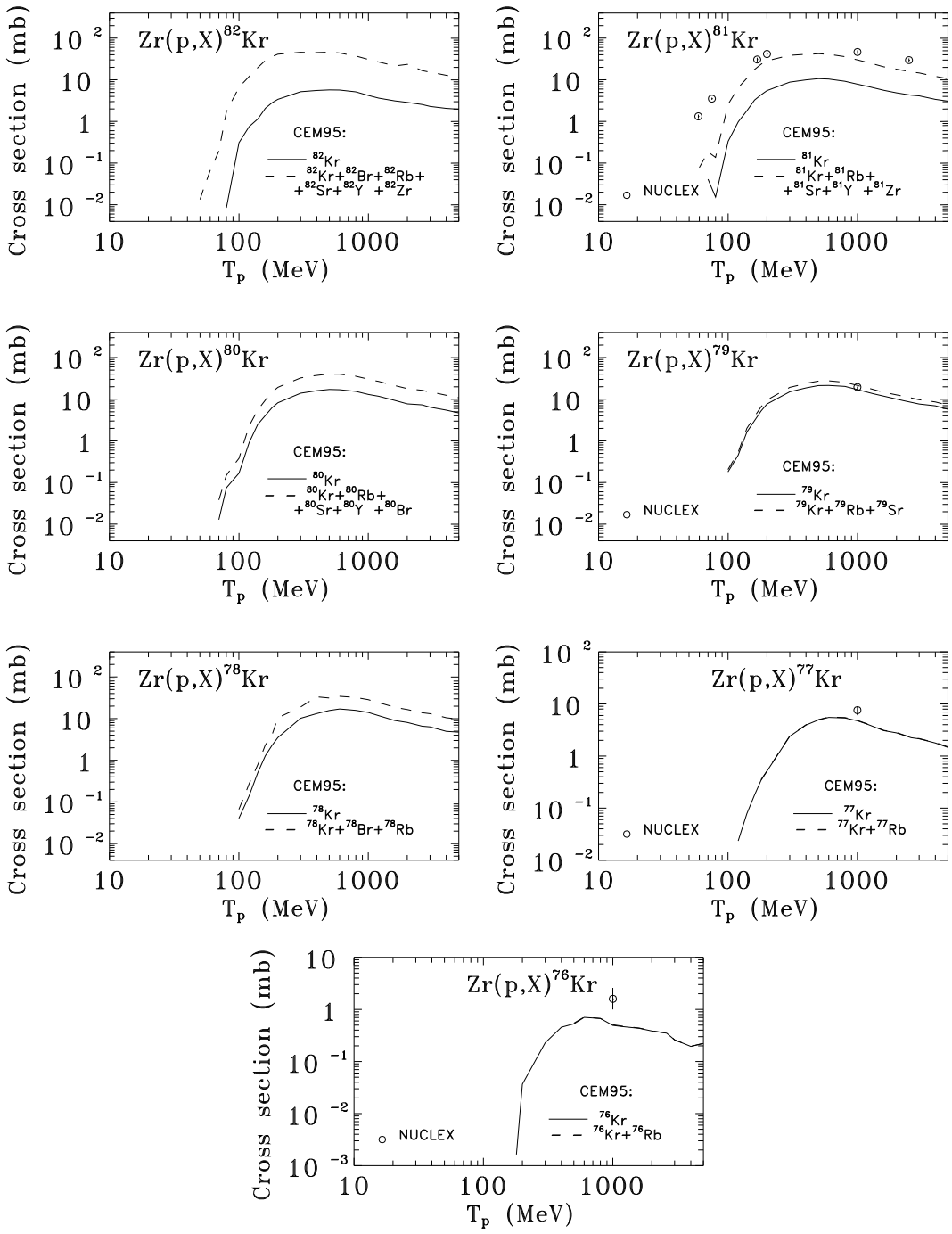

Fig. 71. Excitation functions for the production of ^{82}Kr, ^{81}Kr, ^{80}Kr, ^{79}Kr, ^{78}Kr, ^{77}Kr, and ^{76}Kr from p+^{nat}Zr. Experimental data are labeled as: NUCLEX [46, 47].

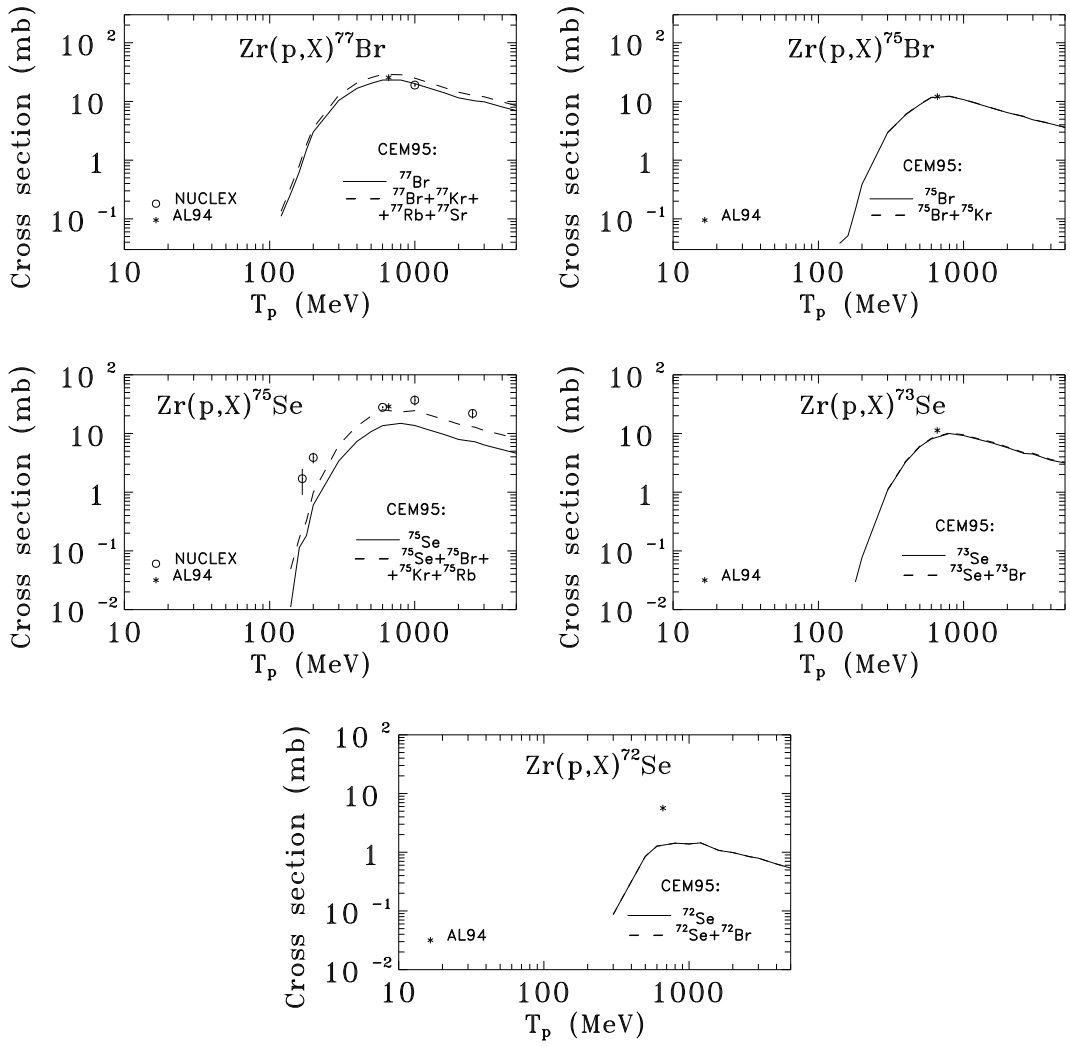

Fig. 72. Excitation functions for the production of ^{77}Br, ^{75}Br, ^{75}Se, ^{73}Se, and ^{72}Se from p+^{nat}Zr. Experimental data are labeled as: NUCLEX [46, 47] and AL94 [212].

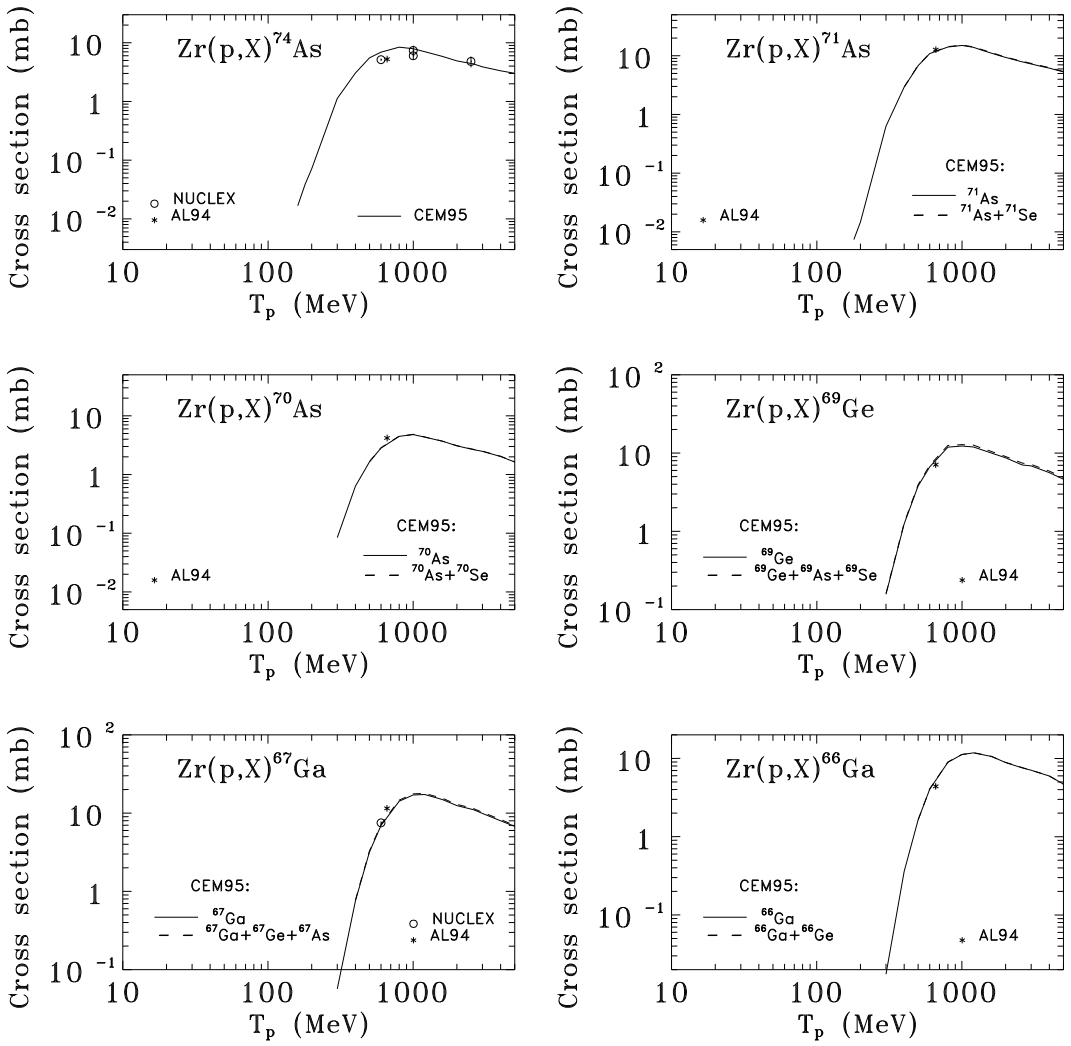

Fig. 73. Excitation functions for the production of ^{74}As, ^{71}As, ^{70}As, ^{69}Ge, ^{67}Ga, and ^{66}Ga from p+^{nat}Zr. Experimental data are labeled as: NUCLEX [46, 47] and AL94 [212].

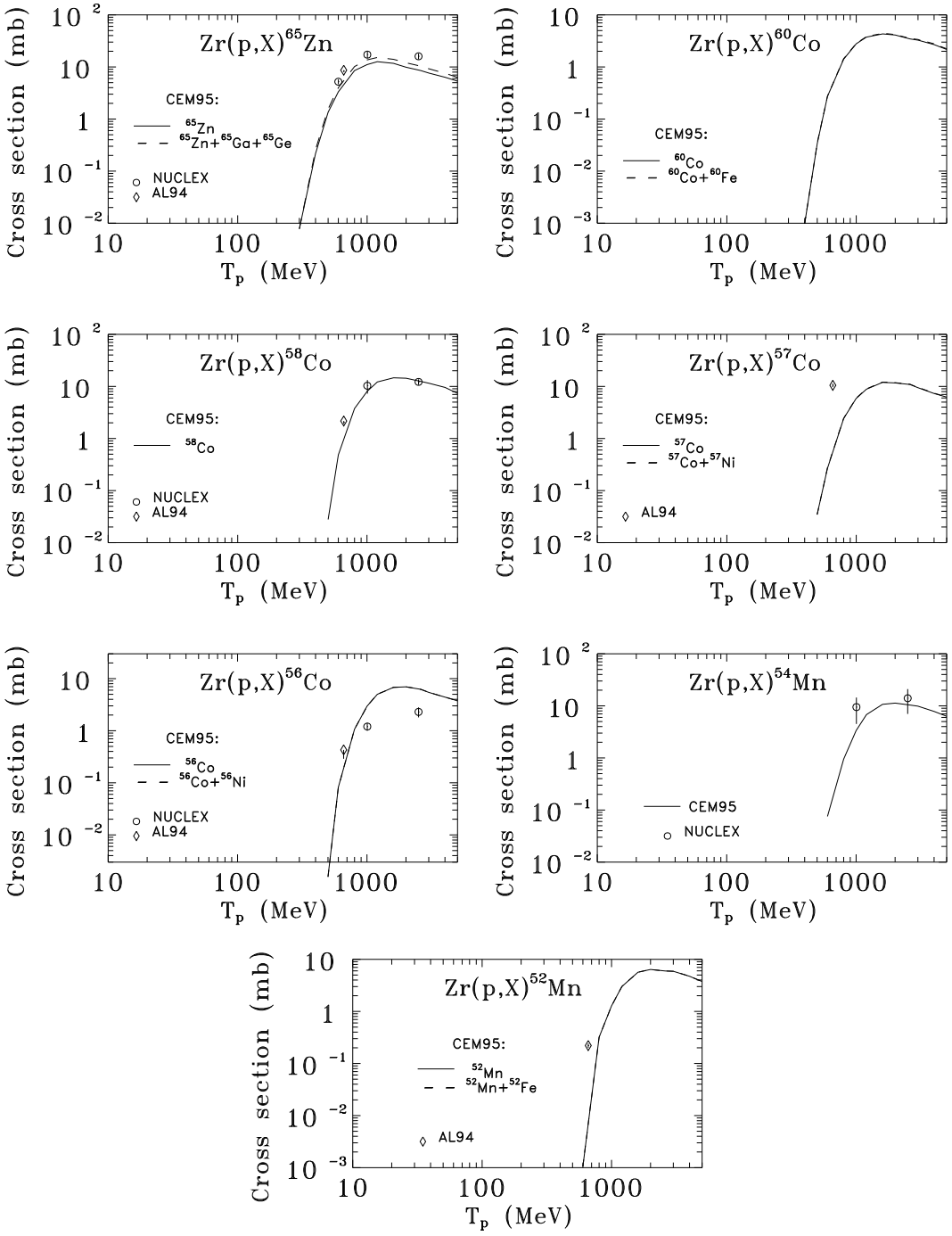

Fig. 74. Excitation functions for the production of ^{65}Zn, ^{60}Co, ^{58}Co, ^{57}Co, ^{56}Co, ^{54}Mn, and ^{52}Mn from p+^{nat}Zr. Experimental data are labeled as: NUCLEX [46, 47] and AL94 [212].

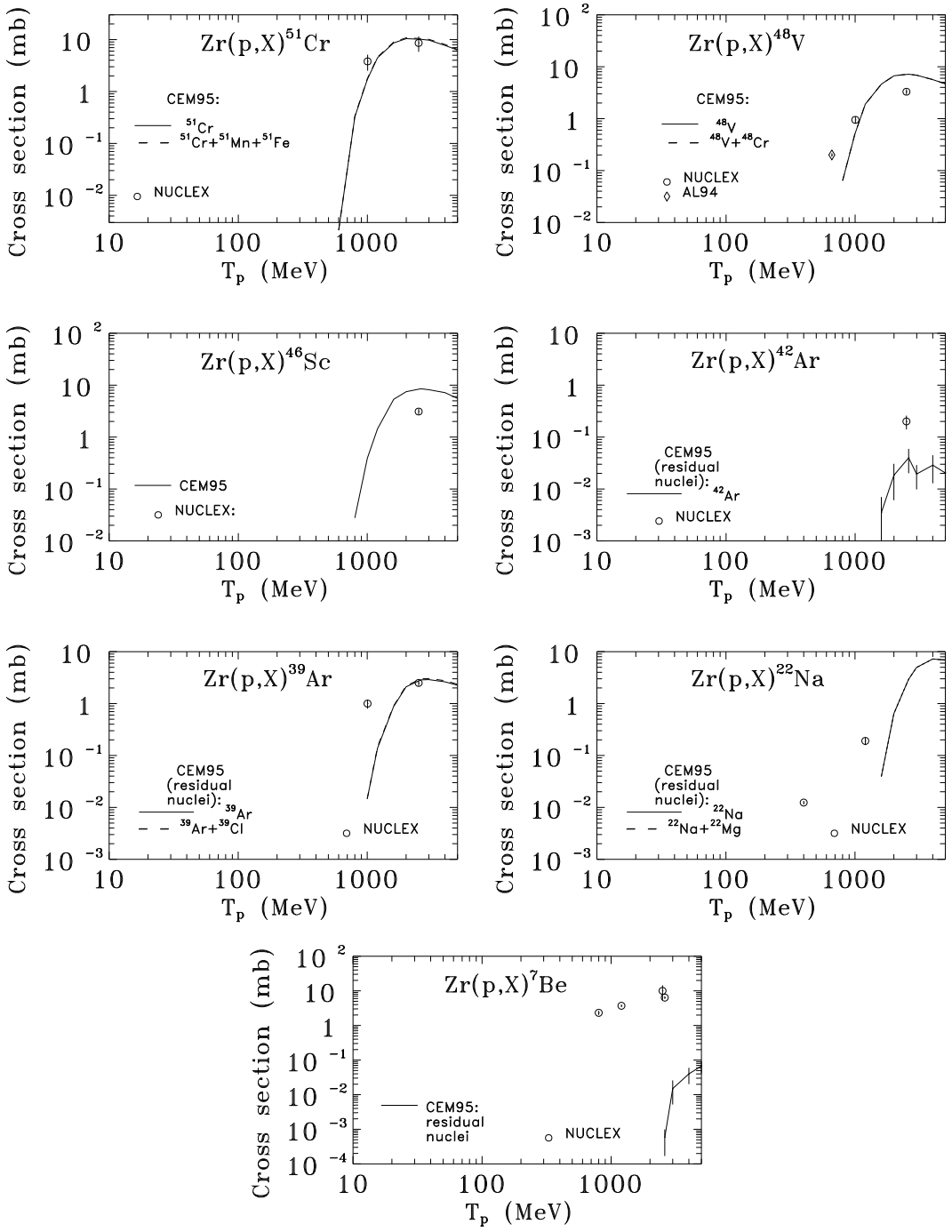

Fig. 75. Excitation functions for the production of ^{51}Cr, ^{48}V, ^{46}Sc, ^{42}Ar, ^{39}Ar, ^{22}Na, and ^{7}Be from p+^{nat}Zr. Experimental data are labeled as: NUCLEX [46, 47] and AL94 [212].

Let us return once again to the last problem. In our figures, a large underestimation of α-emission can be seen for the production of ^{88}Y from ^{92}Zr (Fig. 56), $^{88;87}$Y from ^{91}Zr (Fig. 57), ^{85}Sr and $^{87-85}$Y from ^{90}Zr (Figs. 63 and 64), and $^{87;86}$Y and ^{83}Rb from ^{nat}Zr (Figs. 69 and 70). Especially impressive are such discrepancies for ^{90}Zr(p,x)^{87}Y (Fig. 64) and ^{91}Zr(p,x)^{88}Y (Fig. 57), where in a limited region of incident energies, α-emission is the only mechanism for the production of ^{87}Y and ^{88}Y from these reactions. CEM95 reproduces correctly the position of the peaks connected with α-emission in these excitation functions, but the absolute values of the theoretical peaks are about one order of magnitude lower than the experimental data. Fortunately, as one can see from the experimental data, with increasing incident energy, the role of α-emission in the production of the final nuclides decreases, and at energies above about 80–100 MeV, this problem essentially no longer affects the calculated yields of daughter nuclides.

However, if we would like to calculate such excitation functions at lower energies, this problem has to be solved. As we mentioned above, this is a problem not only of the CEM, but also all other similar statistical Monte Carlo codes currently used in nuclear data evaluation; therefore, it has to be solved before using such codes to calculate excitation functions at low energies. As an example of how this problem might be solved, consider the Milan group's approach [102], where preformed α-clusters in nuclei are taken into account in a version of the exciton model of nuclear reactions (see a detailed discussion of this approach and many references in the recent book [103]). Gadioli et al. [102] have analyzed several excitation functions from p+^{90}Zr at energies below 100 MeV, and their results are shown, for comparison, for production of $^{87-84}$Y in Fig. 64, and for $^{84-81}$Rb, in Fig. 65. One can see that these results [102] agree very well with the data in the region of energy where α-emission is important.

An interesting comparison for excitation functions for production of ^{90}Nb, ^{89}Nb, ^{86}Zr, and $^{87-83}$Y from p+^{90}Zr is shown in Figs. 63 and 64. For these nuclides, the results from the first step of the Intercomparison [48] obtained with the codes CEM92M [74], ALICE92 [147], ALICE 87 MOD [209], and PEQAQ2 [210] are shown together with the experimental data and our present CEM95 calculations. The first step of the Intercomparison [48] aimed to test the predictive power of different models used to describe double differential cross sections of secondary nucleons. Apart from the required nucleon spectra, several contributors have presented, as a "byproduct", yields of residual nuclides. Just these "byproducts" published in a tabulated form in the Appendix III of the Report [48] are shown in our figures. To an extent, these results represent even better the general predictive powers of the compared models, as they were obtained as a byproduct, without a special fitting to the experimental excitation functions. Though the Intercomparison [48] required results for incident energies of only 25, 45, 80, 160, 256, 800, and 1600 MeV, which is not enough to trace all details in the energy dependence of the yields, some conclusions may be drawn. First, one can see very large discrepancies between results of different codes. None of these codes reproduces correctly the peaks connected with α-emission in these

excitation functions. The results labeled as CEM92M were obtained in the framework of the CEM [68] using a fixed value for the level density parameter, $a = 0.1A$, and a value of $\tilde{r}_0 = 1.3$ fm for the inverse cross sections in Eq. (22) (see details in Refs. [48, 74]). One can see that for $^{90;89}$Nb and $^{87;85;83}$Y, the predictions of CEM92M are very close to our present results obtained with CEM95, while, for ^{86}Zr and $^{86;84}$Y, the results of CEM92M are about an order of magnitude lower than both the present CEM95 results and the experimental data. This fact confirms once again the conclusions made in Section 3 that level density parameters, inverse cross sections, and shell and pairing corrections used in calculations may strongly affect theoretical yields of some nuclides; therefore, well tested approaches for the description of these values have to be used in calculations of excitation functions.

4.7. Target ^{197}Au

For ^{197}Au, we have used the compilation of experimental excitation functions from Ref. [46, 47]. Many new measurements on gold were performed recently by Michel's group (see Ref. [44]), but these new results appeared after we had finished our calculations. The experimental data on the total inelastic cross section is taken from the compilation [115], on the fission cross section, from Table 139 of Ref. [54], and on cross sections for the production of d, t, ^{3}He, and ^{4}He, from Table 121 of the same book by Barashenkov and Toneev [54].

Total inelastic and fission cross sections and excitation functions for production of $^{197;195-192;183}$Hg, $^{196-191;183}$Au, $^{195;194;191;189;188;178-175}$Pt, $^{195;194;192;190-184}$Ir, $^{191;185;183;182}$Os, $^{186;184-181}$Re, $^{183;182;177-175;173}$Ta, $^{175;173-170}$Hf, $^{174-169}$Lu, $^{169;166}$Yb, $^{168-165;154}$Tm, $^{153;152}$Er, $^{152;151}$Ho, ^{155}Dy, $^{156;153;151;149}$Tb, $^{153;151;149;147;146}$Gd, $^{149-145}$Eu, ^{138}Pr, ^{139}Ce, $^{133;131}$Ba, $^{127;122}$Xe, ^{124}I, ^{121}Te, ^{118}Sb, ^{113}Sn, ^{115}Cd, $^{113;110;106;105}$Ag, ^{109}Pd, $^{103-101}$Rh, $^{96;95}$Tc, ^{99}Mo, $^{98-95;92;90}$Nb, $^{97;95;89;88}$Zr, $^{88;87}$Y, $^{90;89;85;82}$Sr, $^{86;84;83}$Rb, $^{85;81}$Kr, $^{83;82;80}$Br, $^{75;72}$Se, $^{77;76;74;72;71}$As, $^{67;66}$Ge, $^{73;72;67;66}$Ga, $^{72;65}$Zn, $^{67;64}$Cu, $^{66;65}$Ni, $^{60;58;56}$Co, ^{59}Fe, $^{54;52}$Mn, ^{48}V, $^{48;46;44}$Sc, $^{42;39;37}$Ar, $^{33;32}$P, ^{28}Mg, $^{24;22}$Na, ^{24}Ne, ^{18}F, ^{7}Be, $^{4;3}$He, t, d, p, n, π^+, π^0, and π^- from p+^{197}Au are shown in Figs. 76–101.

It is convenient for us to divide these results, depending on production mechanisms of the final nuclides, into four different groups and to discuss them separately. Figures from 76 to approximately 88 show excitation functions for daughter nuclides in the spallation region. As an example, for production of ^{196}Au, ^{195}Au, and ^{194}Au, the contributions from the channels (p,d), (p,np), (p,t), (p,nd), (p,2np), (p,nt), (p,2nd), and (p,3np) to the total yields are shown separately in Fig. 77. One can see that as for previous targets (see Figs. 16, 20, 23, 31–33, 44, 50, 56–58, 63, 64), the main nuclide production mechanism in the spallation region is a successive emission of several nucleons, while emission of complex particles is of importance (and may be even the single mechanism for production of a given isotope in a limited range of incident energy, as it is shown in Figs. 57 and 64 for ^{88}Y and ^{87}Y) only at low incident energies, near the corresponding thresholds, while with increasing energy its relative

role quickly decreases. On the whole, CEM95 reproduces satisfactorily most of the measured excitation functions in this region, although some large discrepancies can be seen for several specific nuclides caused for the same reasons (poor masses and binding energies, underproduction of ^{4}He, poor shell and pairing corrections, and not well fitted inverse cross sections or level density parameters), as we discussed above for previous targets.

Let us state here another, not previously mentioned, reason for some possible discrepancies: the neglect in CEM95 of competition between γ emission and evaporation of particles (+ fission, for heavy nuclei) at the compound stage of the reactions. As was pointed out in a number of recent publications [145, 213], the neglect of competition between γ emission and evaporation in calculations with the hybrid model code ALICE92 [147] of interactions of nucleons with medium and heavy targets leads to false peaks in the calculated excitation functions near the thresholds. Due to the intranuclear cascade stage of the CEM (absent in the hybrid model), we do not think that this effect is of the same importance for CEM95 as for ALICE92, although a special analysis of this problem has not been done yet. Let us note that at the cascade and preequilibrium stages of reactions emission of hard photons is also possible, and such a phenomenon has been recently investigated both experimentally and theoretically [214]. We do not take into account such processes in CEM95 as the cross sections for gamma emission are very small and we do not expect that the neglect of such processes will affect perceptibly the calculated excitation functions, although an attempt to take into account such processes in the CEM has been already done [215].

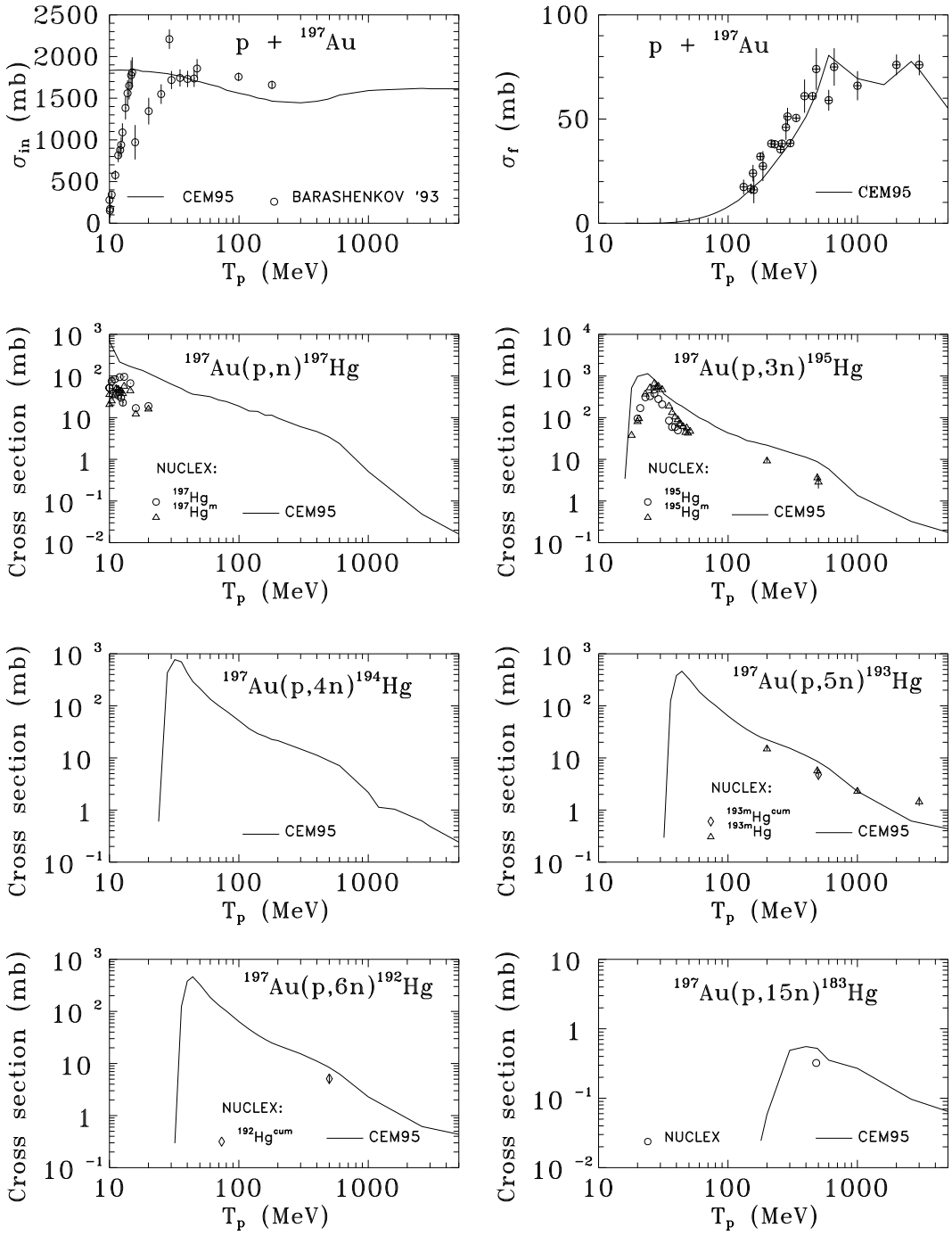

Fig. 76. Total inelastic and fission cross sections and excitation functions for the production of ^{197}Hg, ^{195}Hg, ^{194}Hg, ^{193}Hg, ^{192}Hg, and ^{183}Hg from p+^{197}Au. Experimental data are labeled as: BARASHENKOV'93 [158], and NUCLEX [46, 47]. Experimental fission cross sections (points) are taken from Table 139 of Ref. [54].

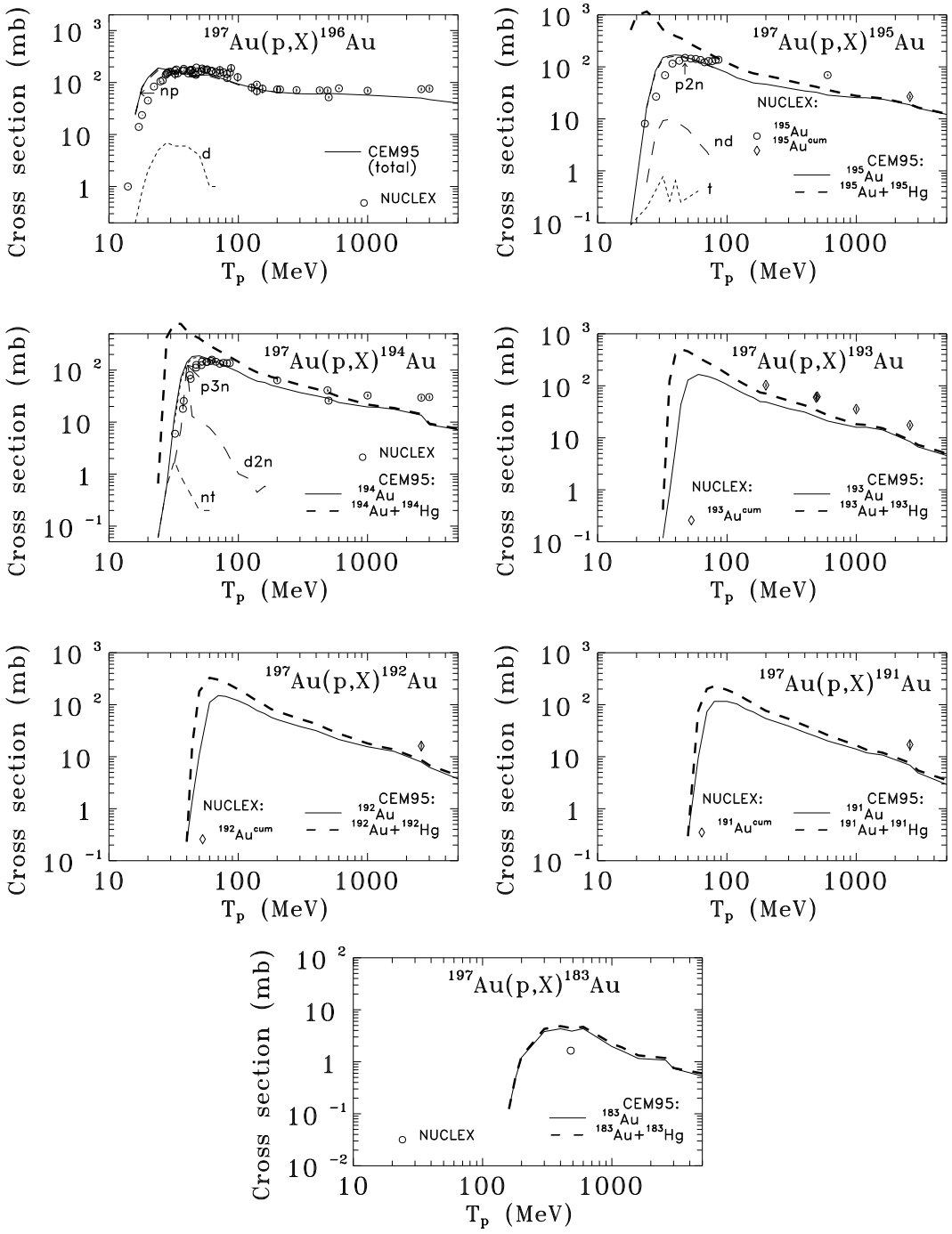

Fig. 77. Excitation functions for the production of ^{196}Au, ^{195}Au, ^{194}Au, ^{193}Au, ^{192}Au, ^{191}Au, and ^{183}Au from p+^{197}Au. For ^{196}Au, ^{195}Au, and ^{194}Au, contributions from the channels (p,d), (p,np), (p,t), (p,nd), (p,2np), (p,nt), (p,2nd), and (p,3np) to the total CEM95 yields are shown by dashed lines, as indicated. Experimental data labeled as NUCLEX are from the compilation [46, 47].

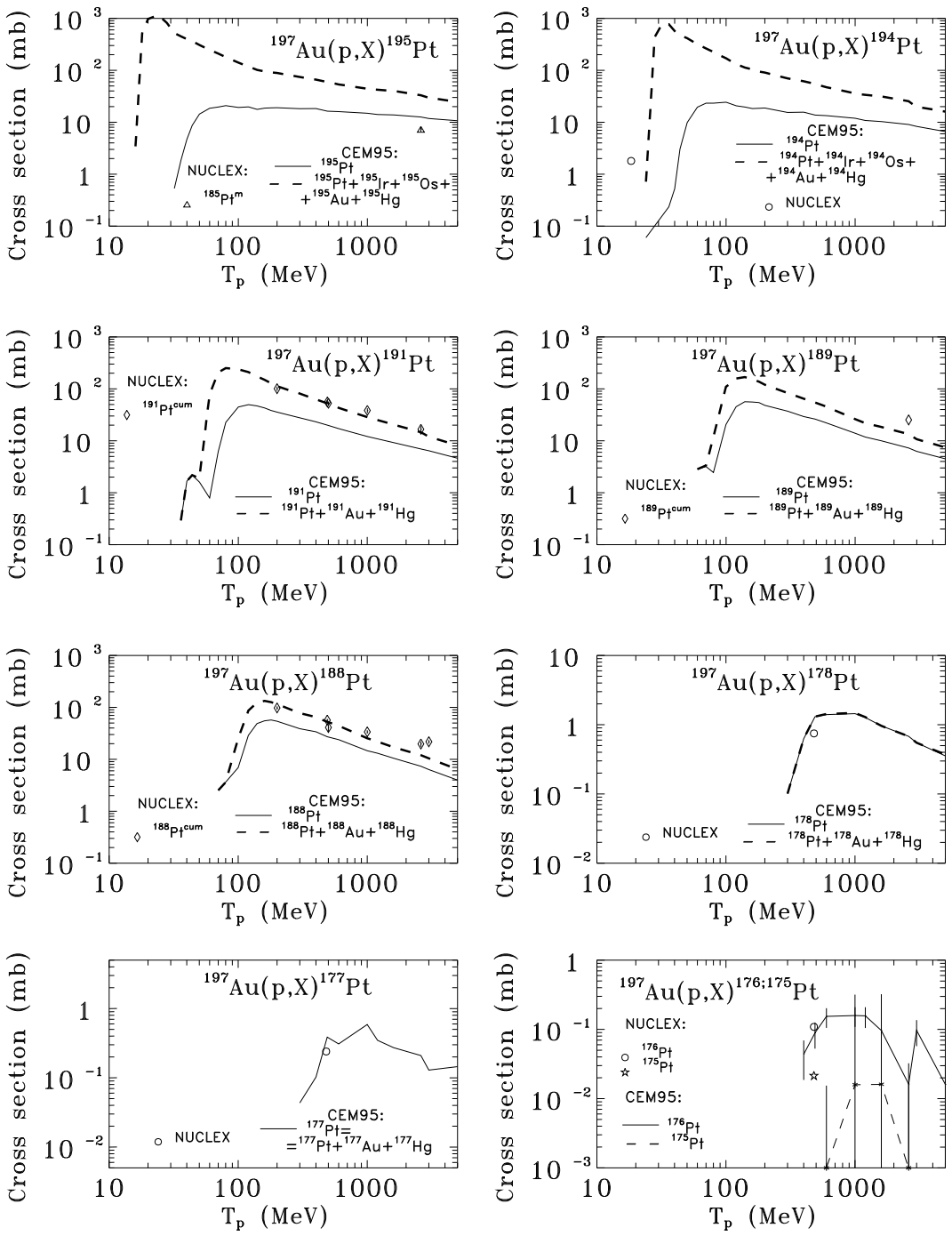

Fig. 78. Excitation functions for the production of ^{195}Pt, ^{194}Pt, ^{191}Pt, ^{189}Pt, ^{188}Pt, ^{178}Pt, ^{177}Pt, ^{176}Pt, and ^{175}Pt from p+^{197}Au. Experimental data labeled as NUCLEX are from the compilation [46, 47].

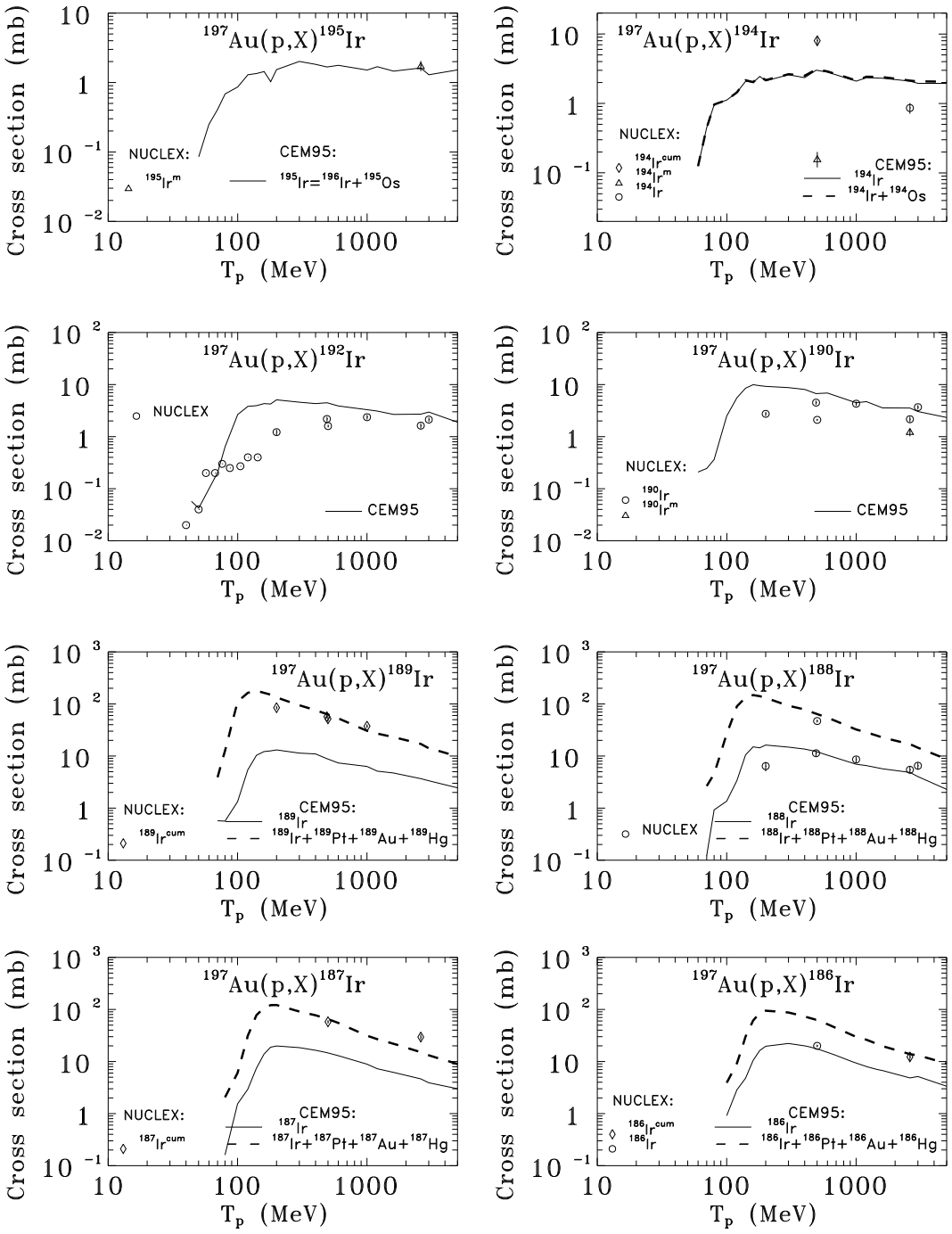

Fig. 79. Excitation functions for the production of ^{195}Ir, ^{194}Ir, ^{192}Ir, ^{190}Ir, ^{189}Ir, ^{188}Ir, ^{187}Ir, and ^{186}Ir from p+^{197}Au. Experimental data labeled as NUCLEX are from the compilation [46, 47].

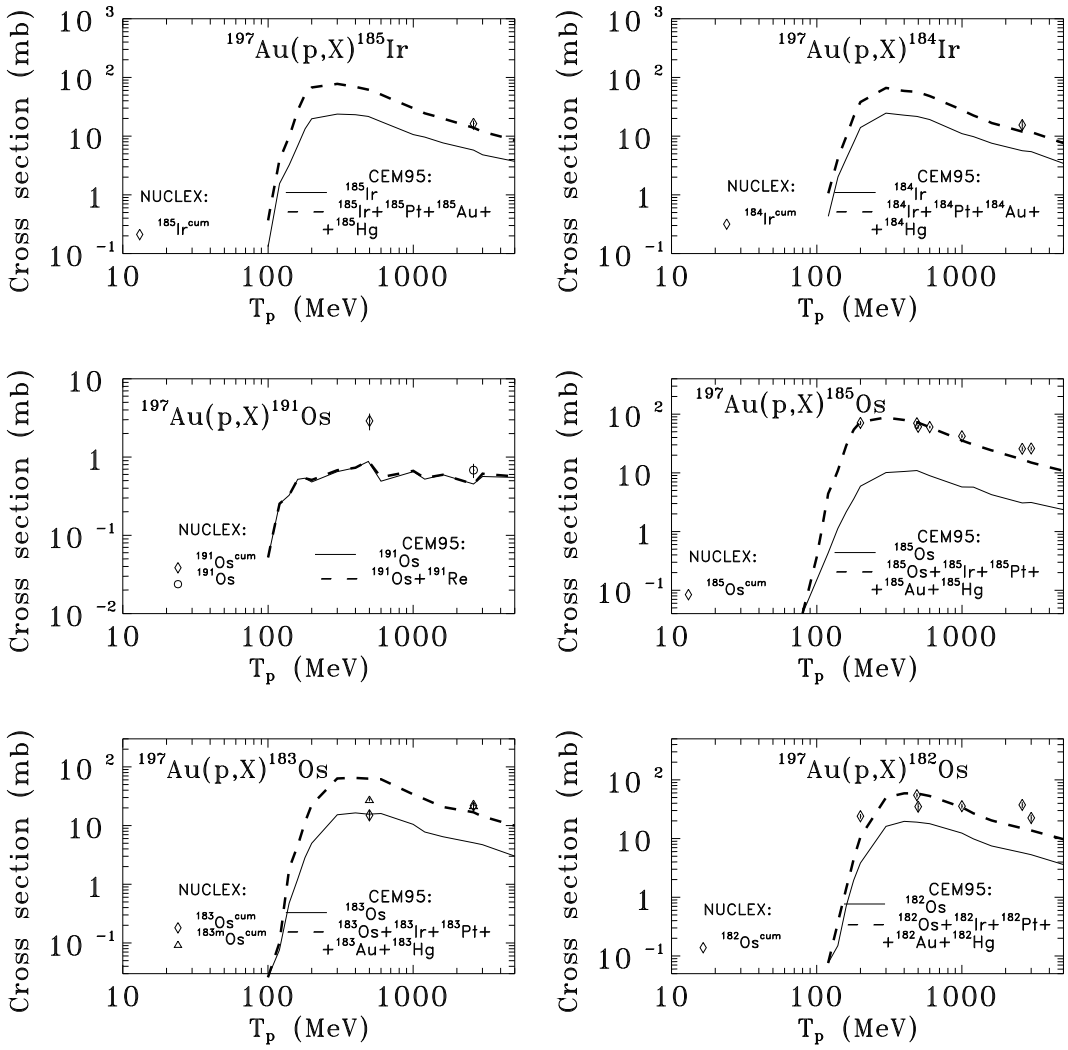

Fig. 80. Excitation functions for the production of ^{185}Ir, ^{184}Ir, ^{191}Os, ^{185}Os, ^{183}Os, and ^{182}Os from p+^{197}Au. Experimental data labeled as NUCLEX are from the compilation [46, 47].

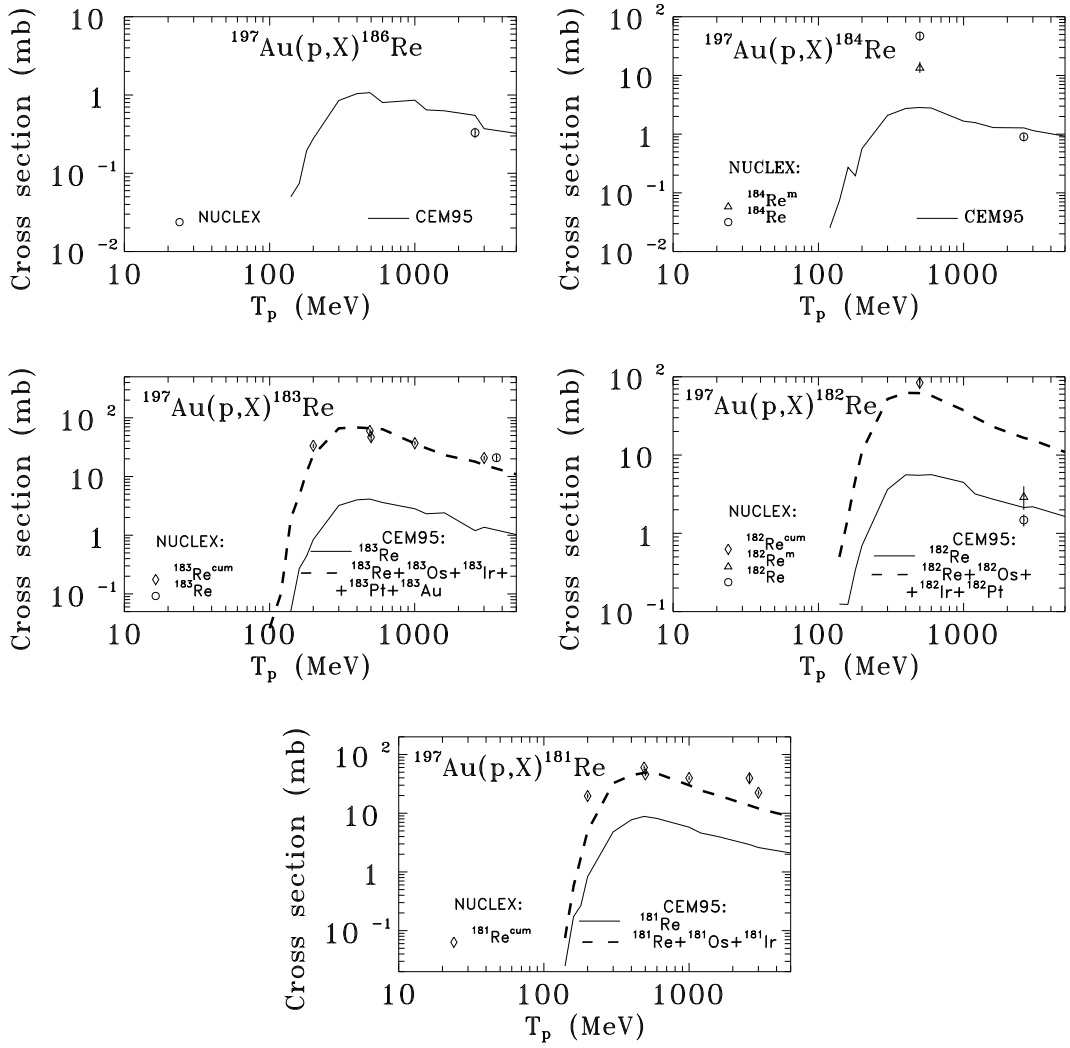

Fig. 81. Excitation functions for the production of ^{186}Re, ^{184}Re, ^{183}Re, ^{182}Re, and ^{181}Re from p+^{197}Au. Experimental data labeled as NUCLEX are from the compilation [46, 47].

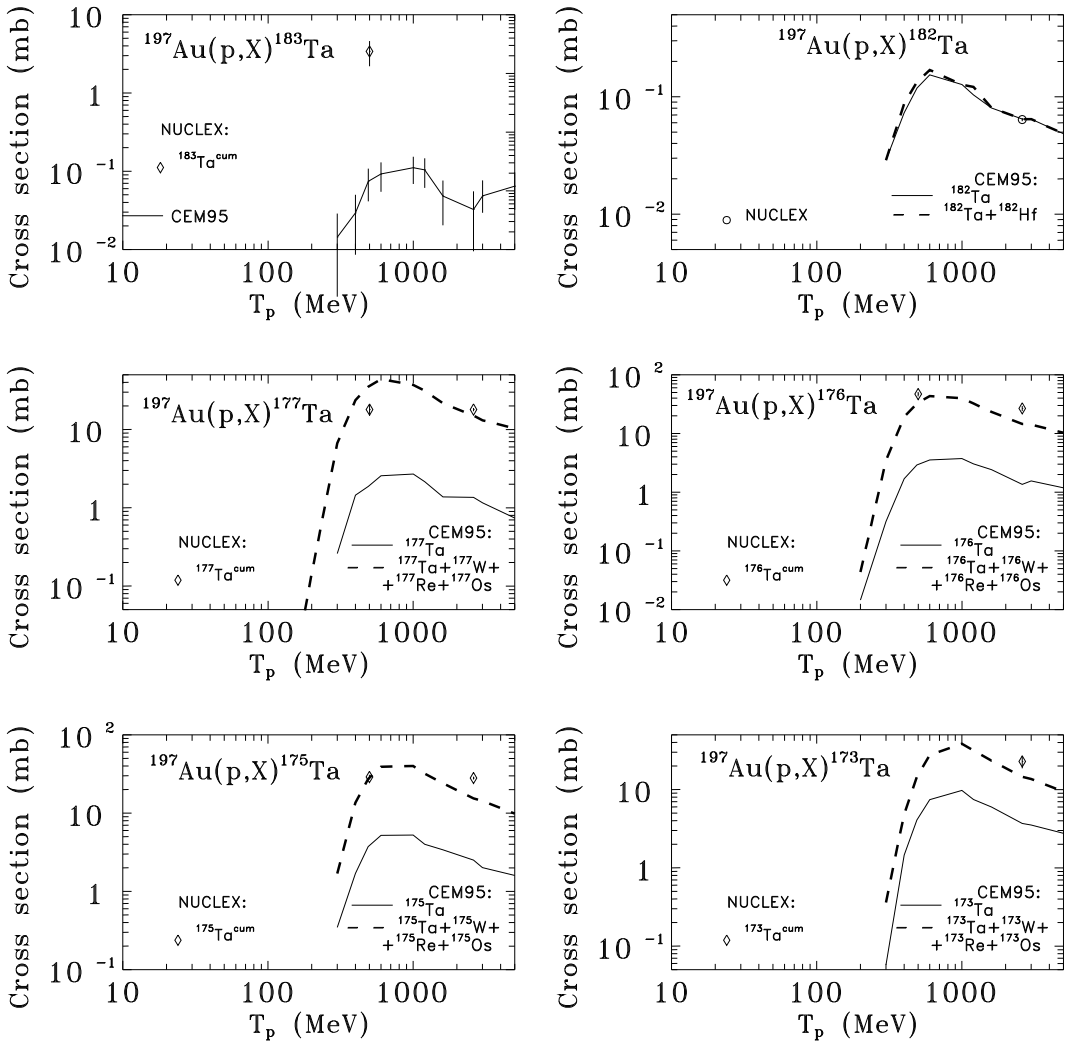

Fig. 82. Excitation functions for the production of ^{183}Ta, ^{182}Ta, ^{177}Ta, ^{176}Ta, ^{175}Ta, and ^{173}Ta from p+^{197}Au. Experimental data labeled as NUCLEX are from the compilation [46, 47].

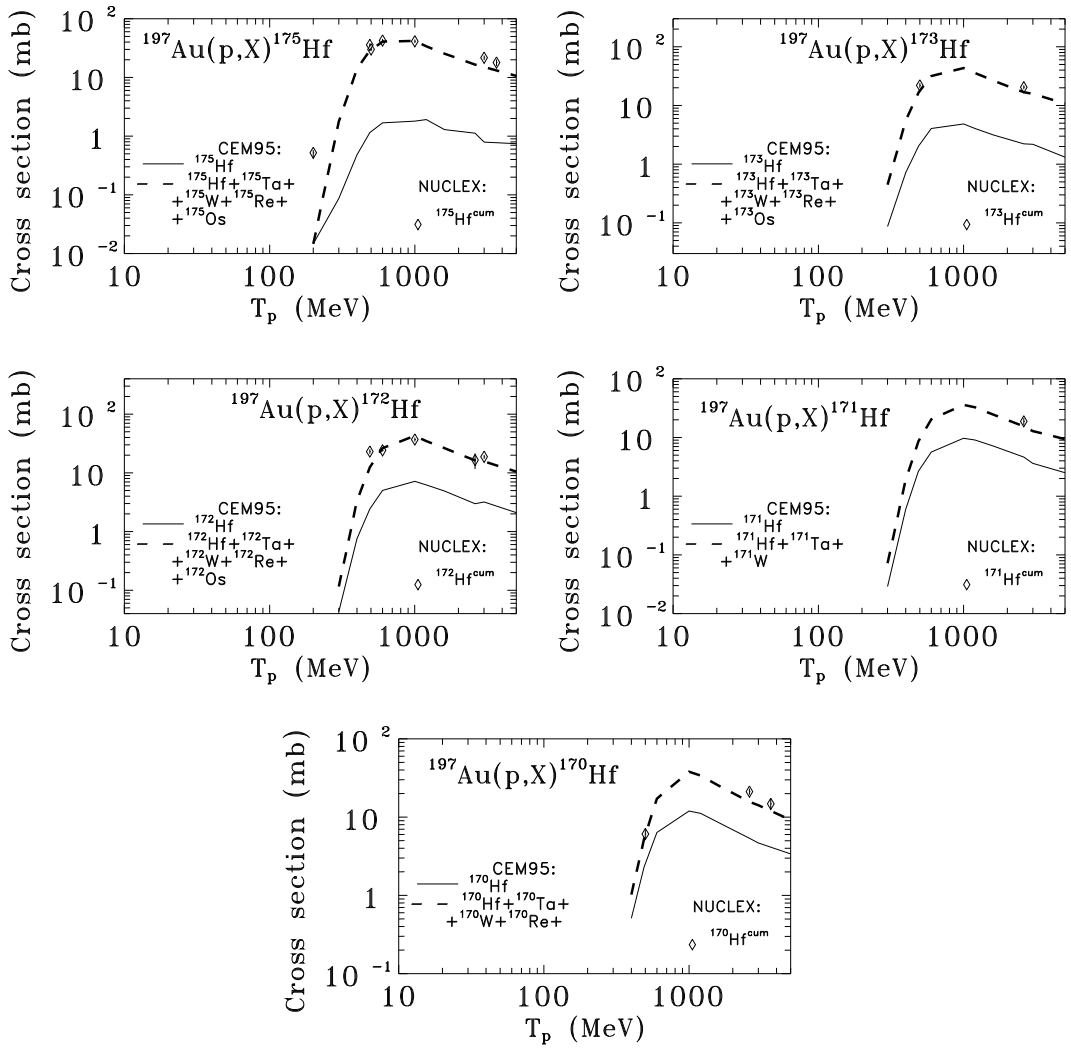

Fig. 83. Excitation functions for the production of ^{175}Hf, ^{173}Hf, ^{172}Hf, ^{171}Hf, and ^{170}Hf from p+^{197}Au. Experimental data labeled as NUCLEX are from the compilation [46, 47].

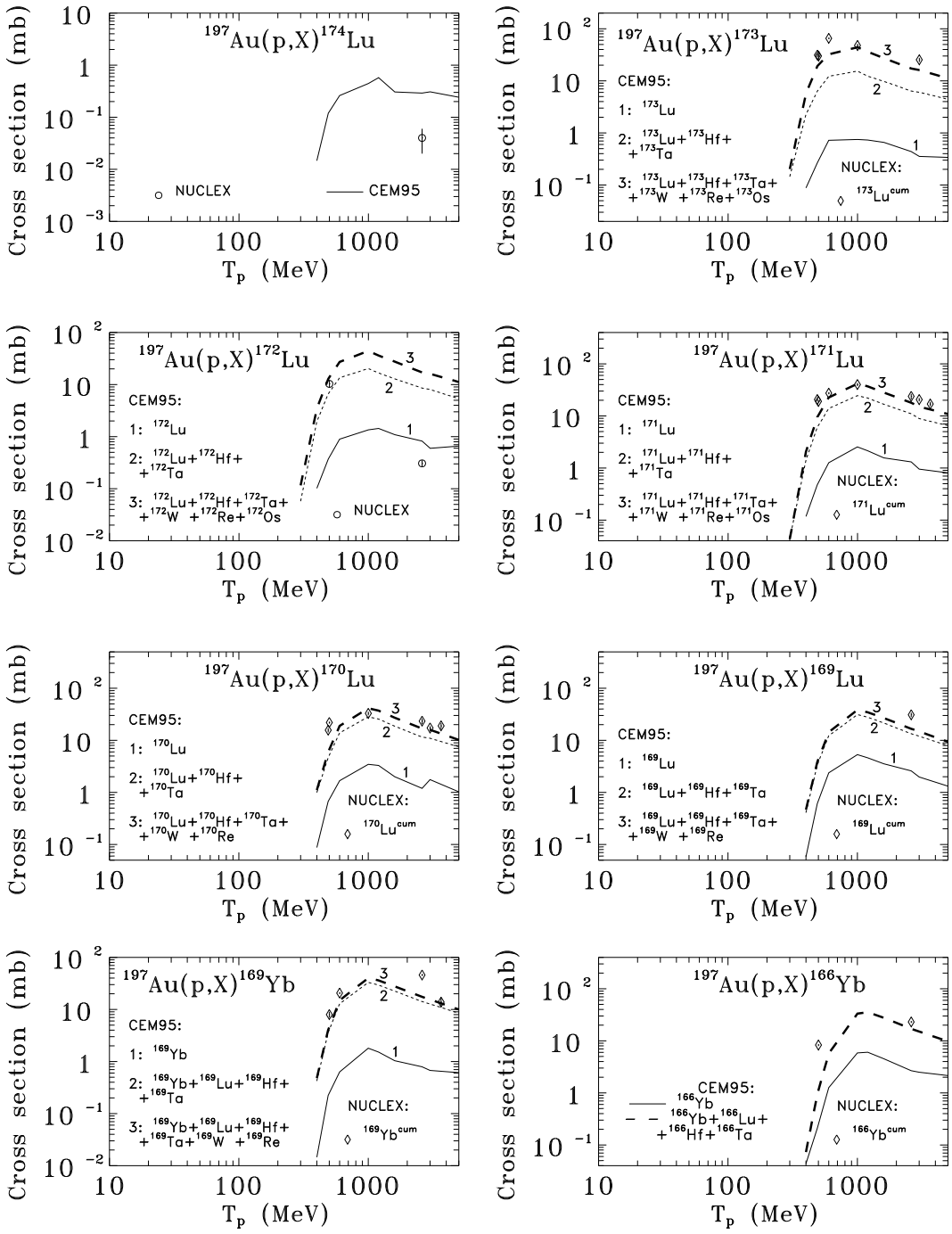

Fig. 84. Excitation functions for the production of ^{174}Lu, ^{173}Lu, ^{172}Lu, ^{171}Lu, ^{170}Lu, ^{169}Lu, ^{169}Yb, and ^{166}Yb from p+^{197}Au. Experimental data labeled as NUCLEX are from the compilation [46, 47].

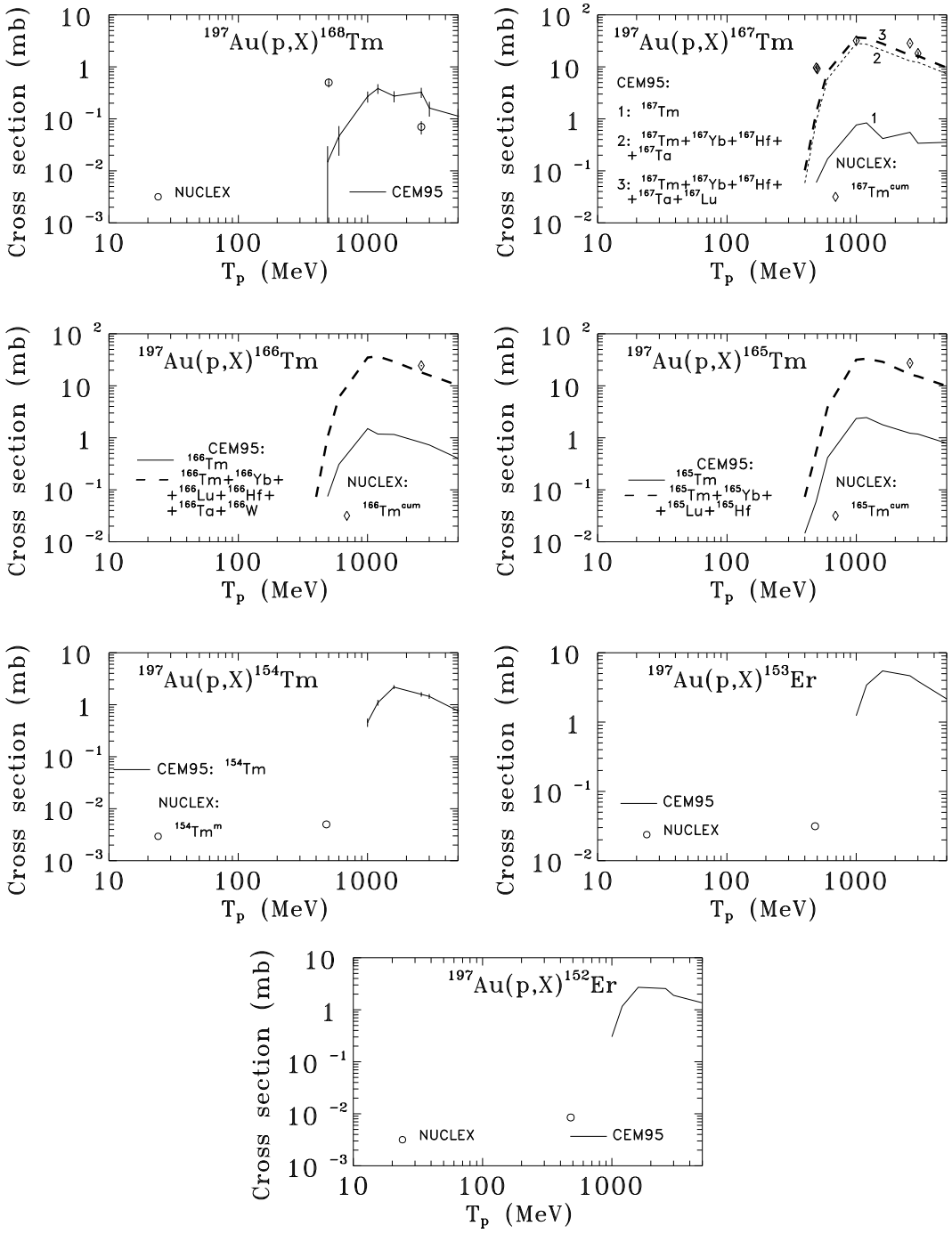

Fig. 85. Excitation functions for the production of ^{168}Tm, ^{167}Tm, ^{166}Tm, ^{165}Tm, ^{154}Tm, ^{153}Er, and ^{152}Er from p+^{197}Au. Experimental data labeled as NUCLEX are from the compilation [46, 47].

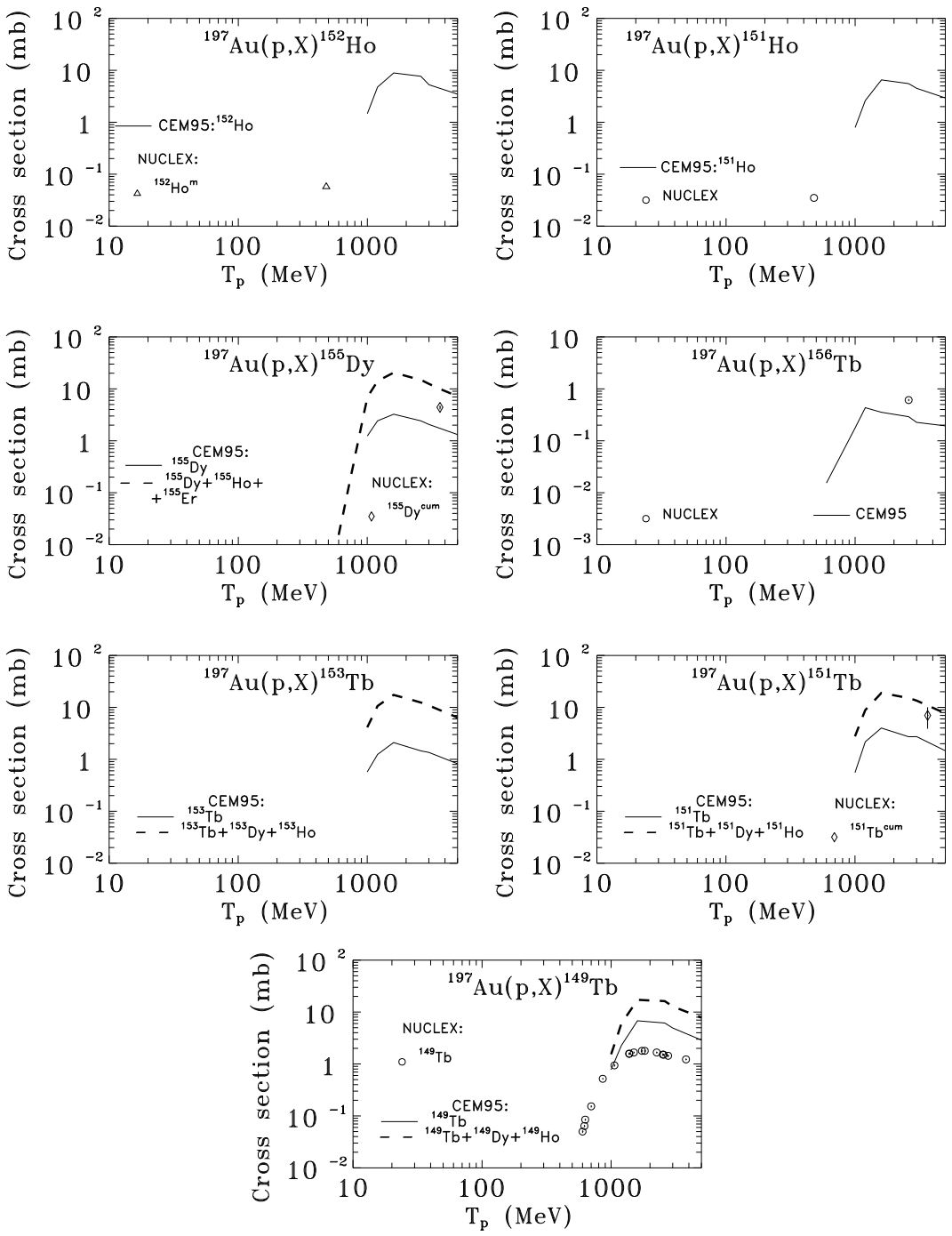

Fig. 86. Excitation functions for the production of ^{152}Ho, ^{151}Ho, ^{155}Dy, ^{156}Tb, ^{153}Tb, ^{151}Tb, and ^{149}Tb from p+^{197}Au. Experimental data labeled as NUCLEX are from the compilation [46, 47].

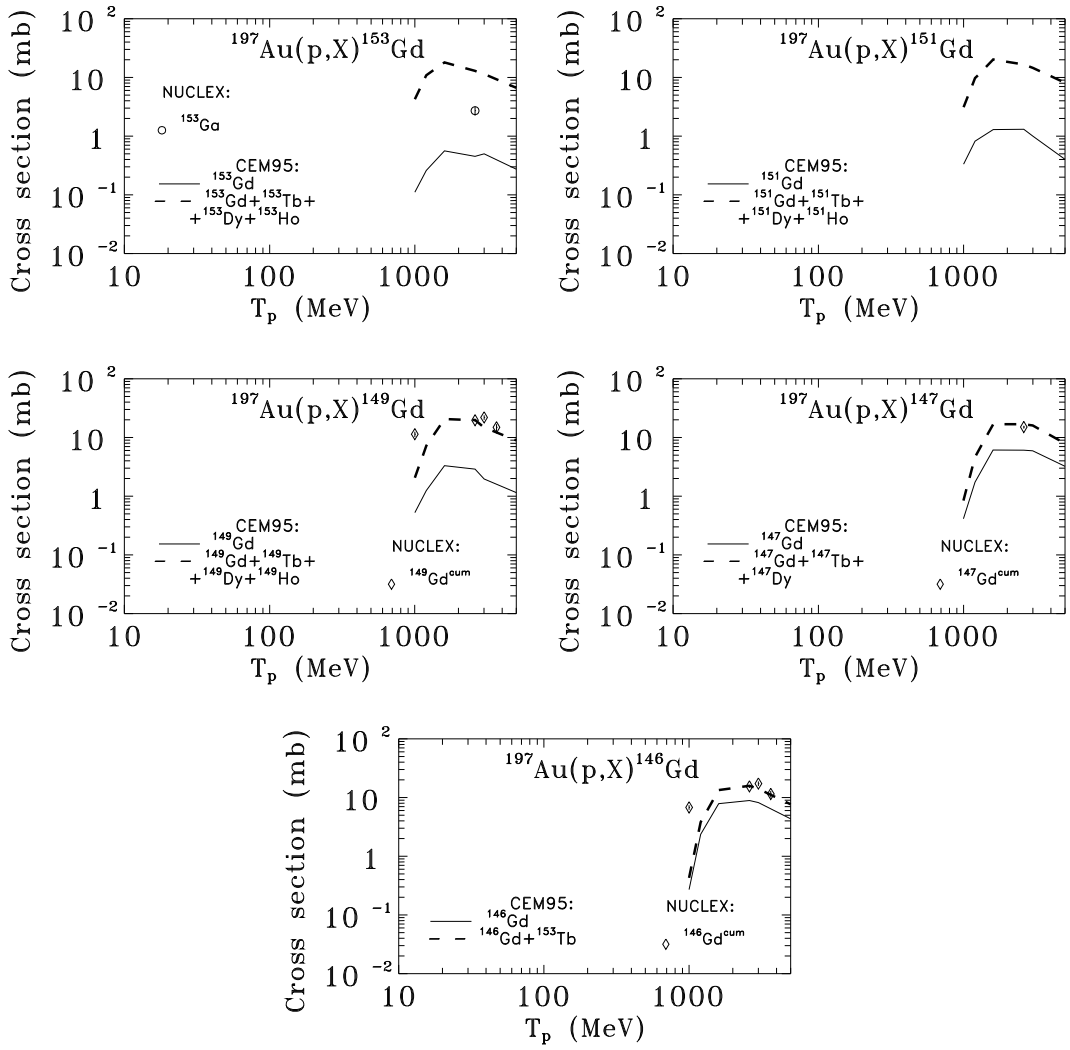

Fig. 87. Excitation functions for the production of ^{153}Gd, ^{151}Gd, ^{149}Gd, ^{147}Gd, and ^{146}Gd from p+^{197}Au. Experimental data labeled as NUCLEX are from the compilation [46, 47].

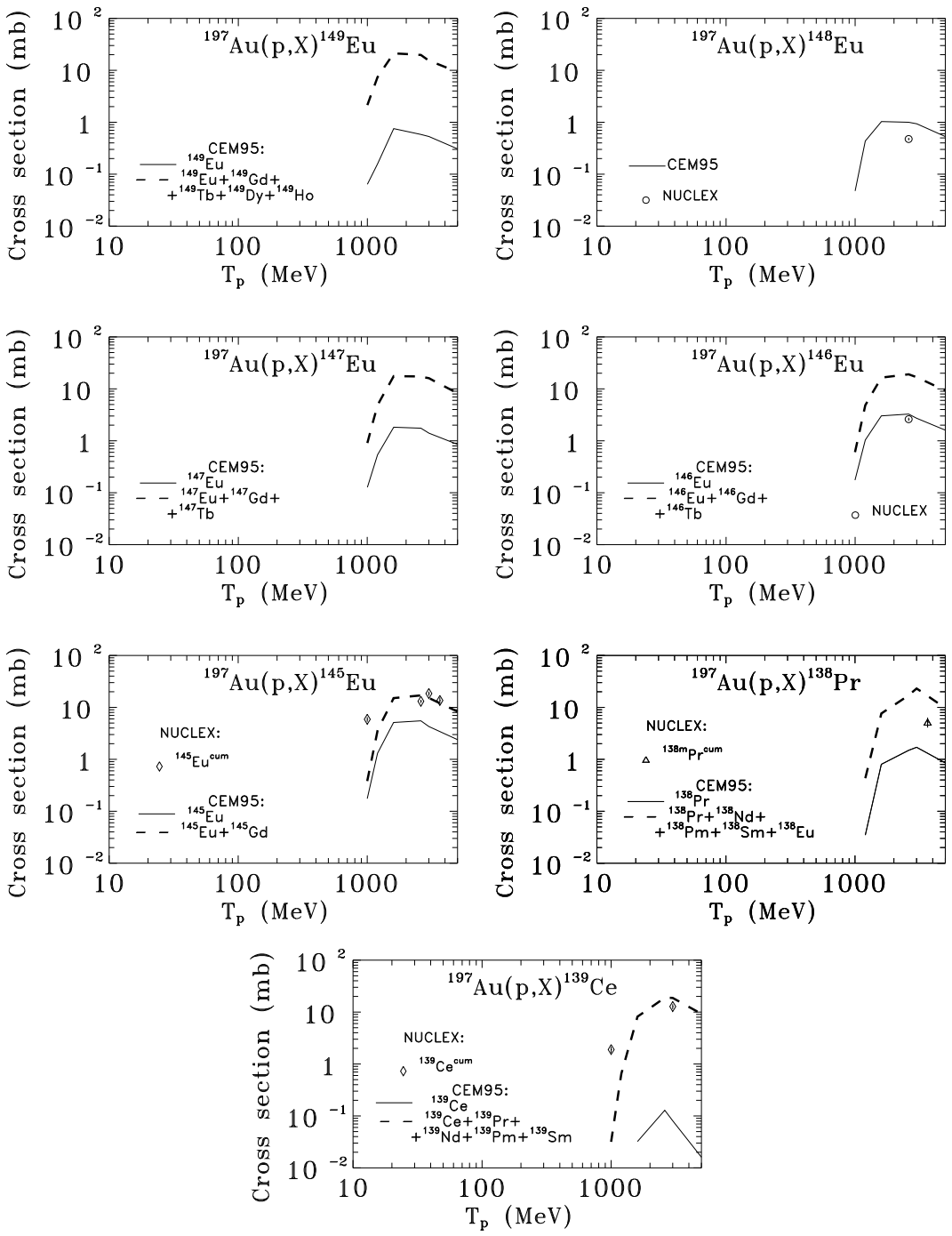

Fig. 88. Excitation functions for the production of ^{149}Eu, ^{148}Eu, ^{147}Eu, ^{146}Eu, ^{145}Eu, ^{138}Pr, and ^{139}Ce from p+^{197}Au. Experimental data labeled as NUCLEX are from the compilation [46, 47].

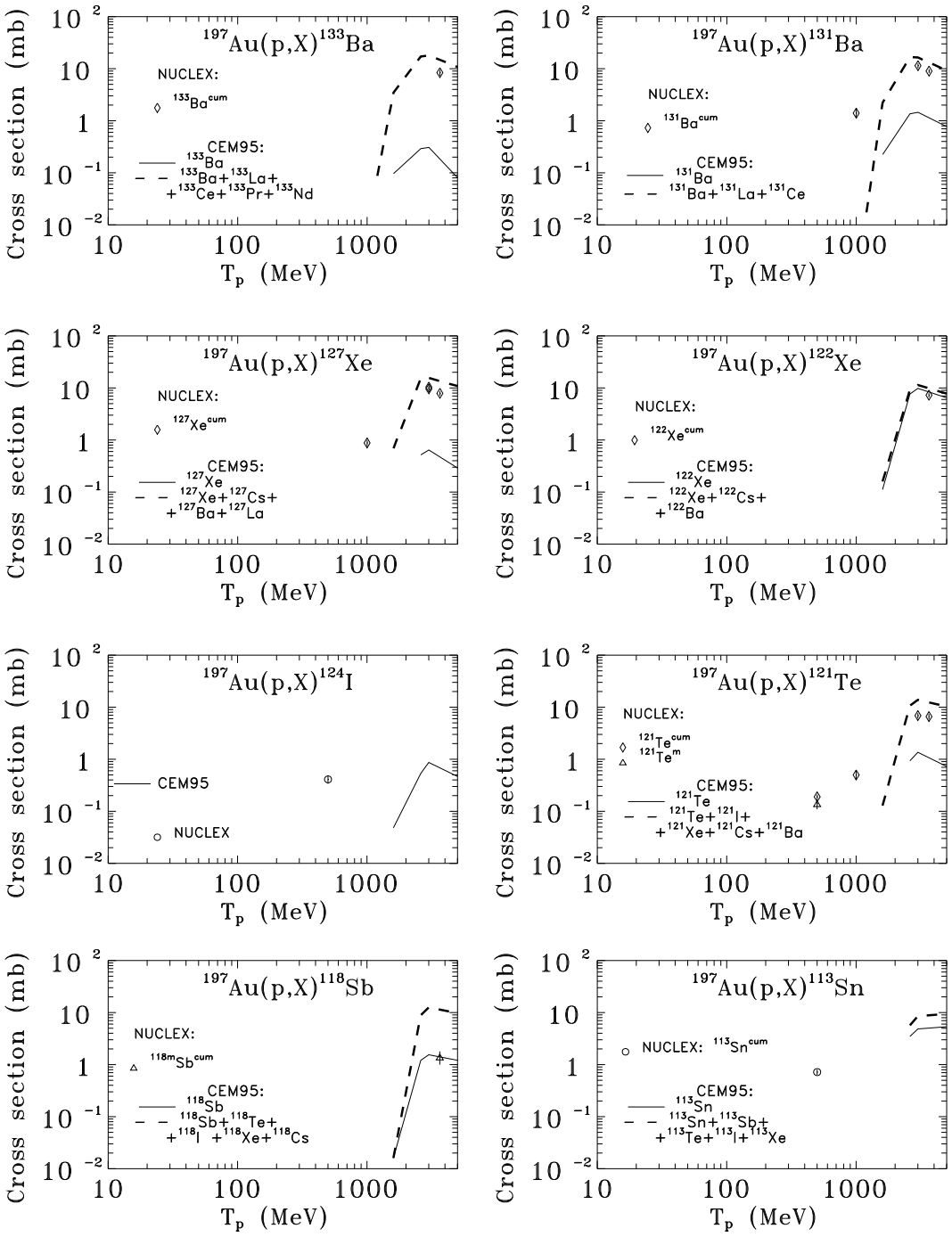

Fig. 89. Excitation functions for the production of ^{133}Ba, ^{131}Ba, ^{127}Xe, ^{122}Xe, ^{124}I, ^{121}Te, ^{118}Sb, and ^{113}Sn from p+^{197}Au. Experimental data labeled as NUCLEX are from the compilation [46, 47].

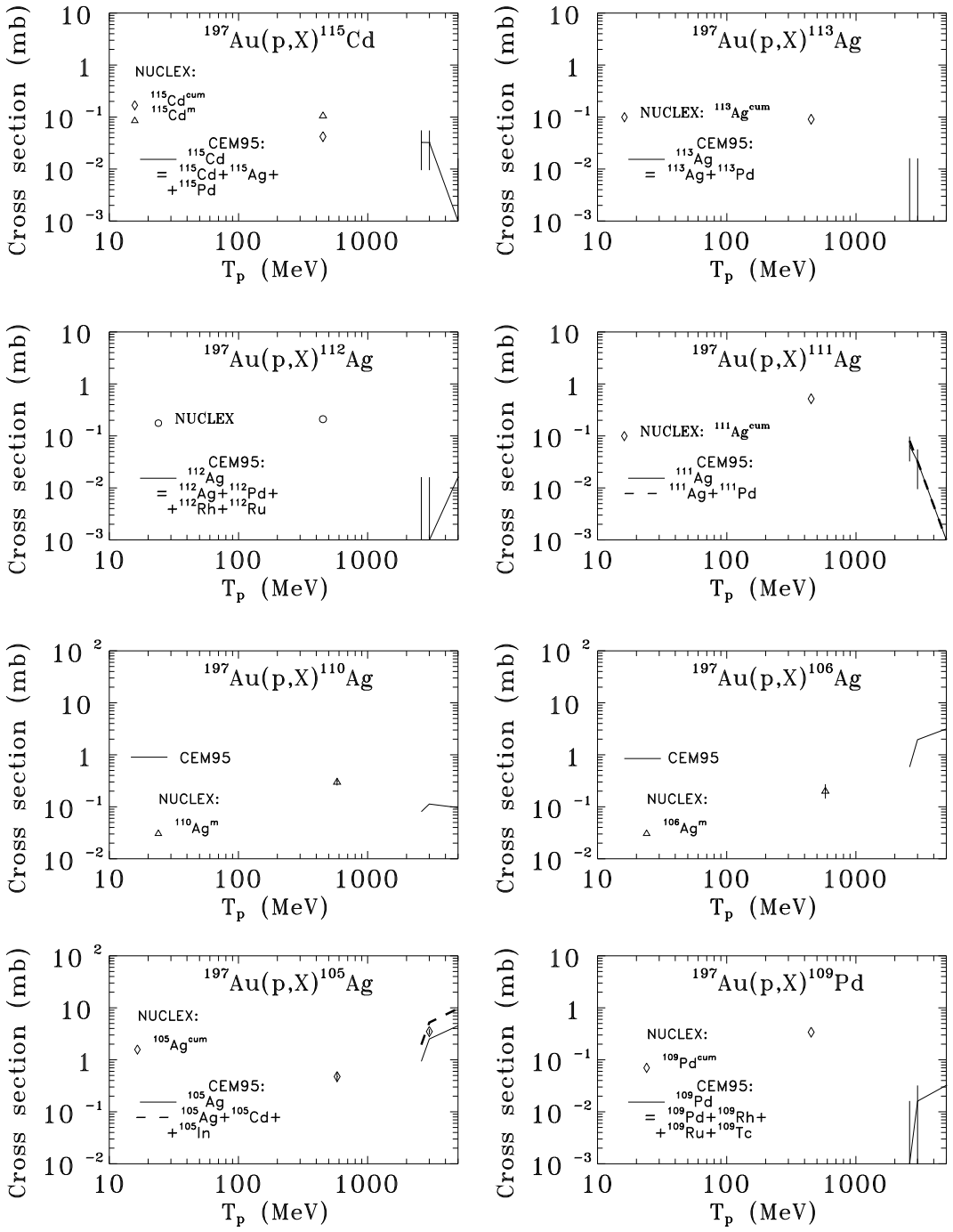

Fig. 90. Excitation functions for the production of ^{115}Cd, ^{113}Ag, ^{112}Ag, ^{111}Ag, ^{110}Ag, ^{106}Ag, ^{105}Ag, and ^{109}Pd from p+^{197}Au. Experimental data labeled as NUCLEX are from the compilation [46, 47].

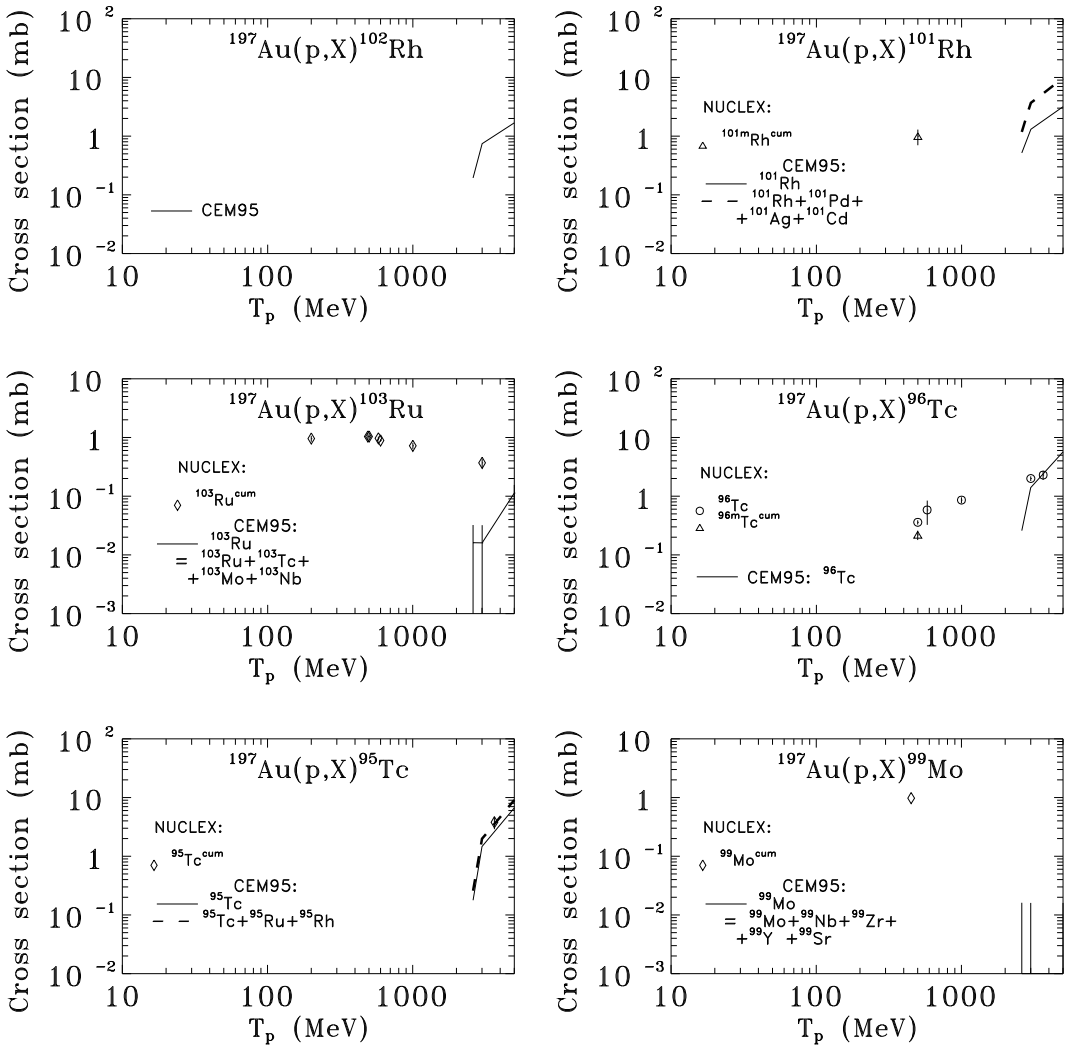

Fig. 91. Excitation functions for the production of ^{102}Rh, ^{101}Rh, ^{103}Ru, ^{96}Tc, ^{95}Tc, and ^{99}Mo from p+^{197}Au. Experimental data labeled as NUCLEX are from the compilation [46, 47].

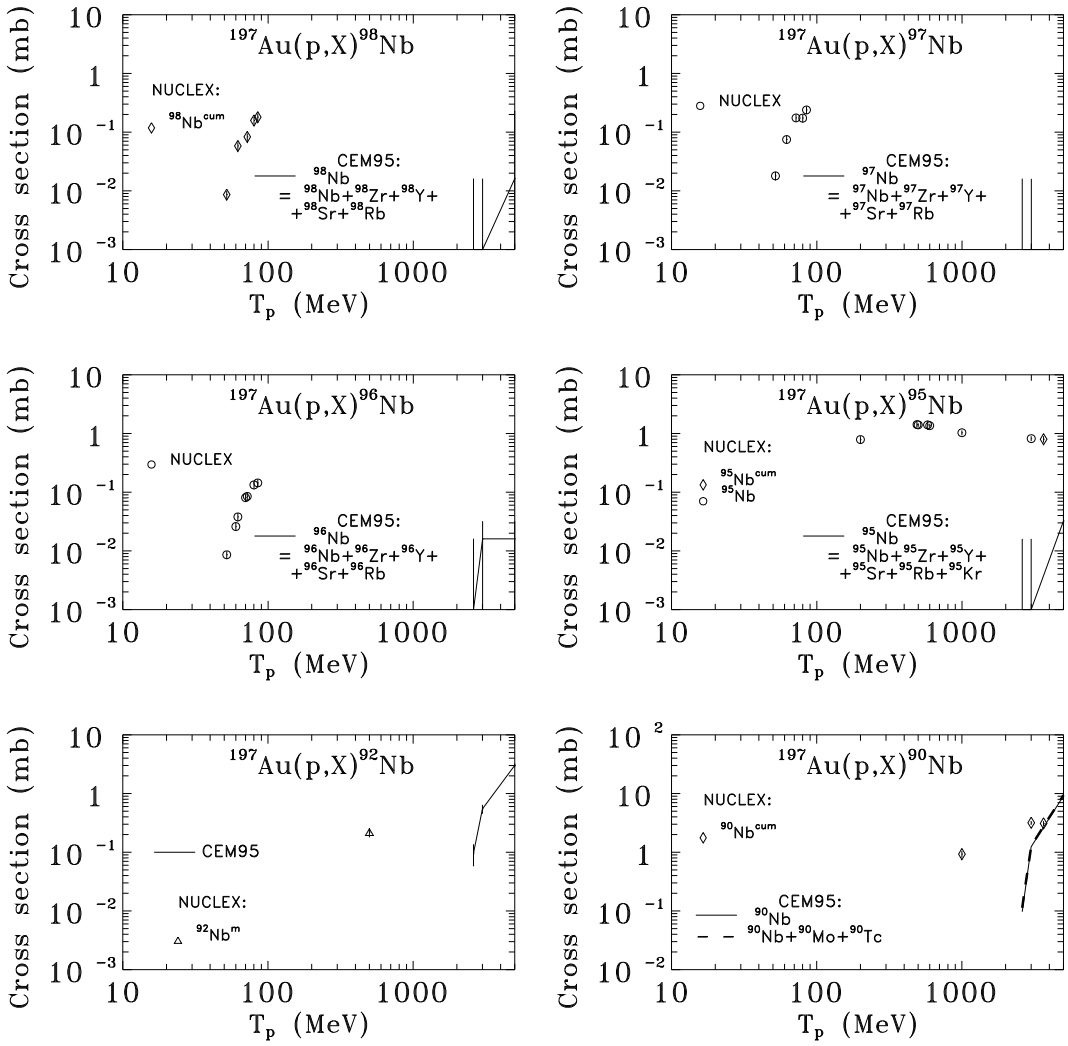

Fig. 92. Excitation functions for the production of ^{98}Nb, ^{97}Nb, ^{96}Nb, ^{95}Nb, ^{92}Nb, and ^{90}Nb from p+^{197}Au. Experimental data labeled as NUCLEX are from the compilation [46, 47].

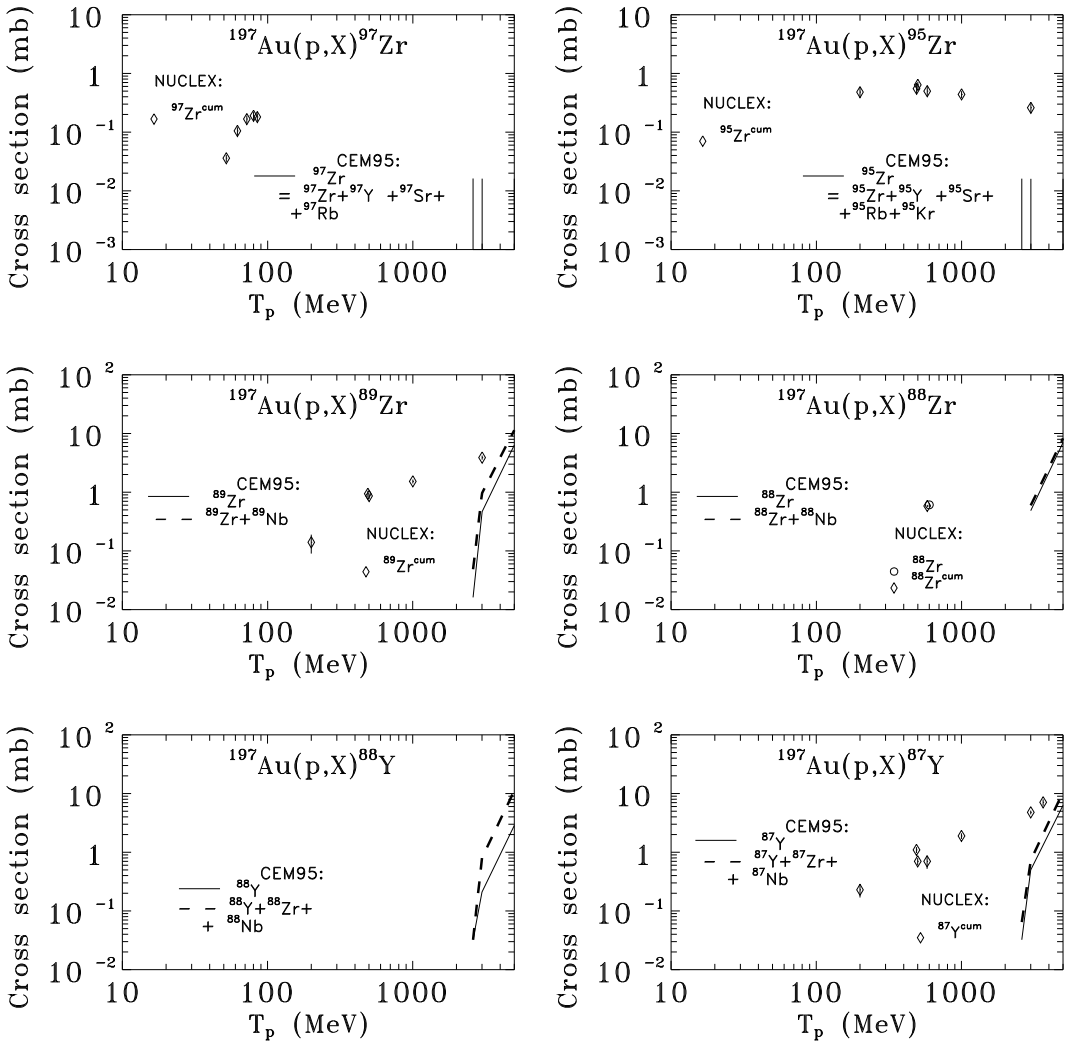

Fig. 93. Excitation functions for the production of ^{97}Zr, ^{95}Zr, ^{89}Zr, ^{88}Zr, ^{88}Y, and ^{87}Y from p+^{197}Au. Experimental data labeled as NUCLEX are from the compilation [46, 47].

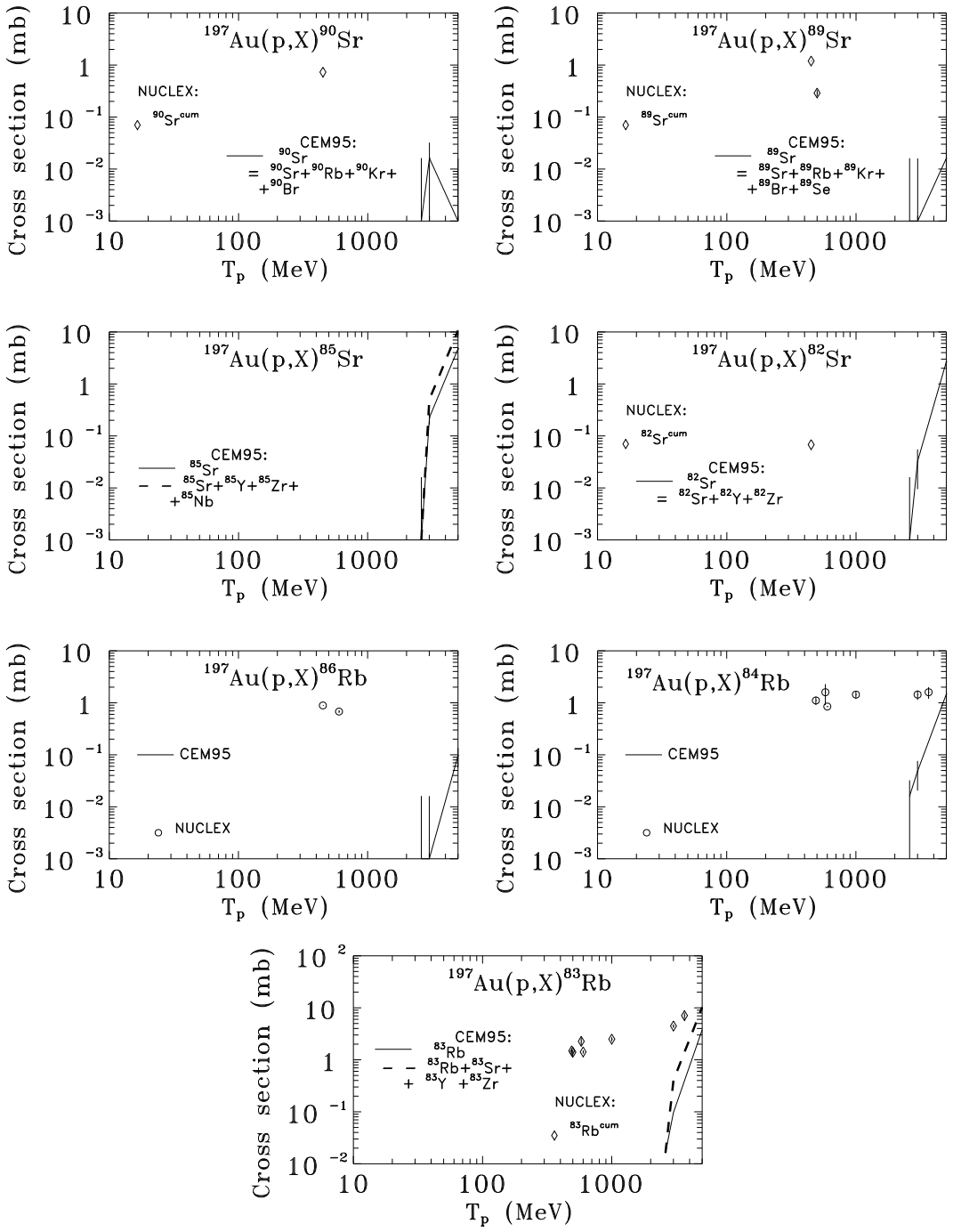

Fig. 94. Excitation functions for the production of ^{90}Sr, ^{89}Sr, ^{85}Sr, ^{82}Sr, ^{86}Rb, ^{84}Rb, and ^{83}Rb from p+^{197}Au. Experimental data labeled as NUCLEX are from the compilation [46, 47].

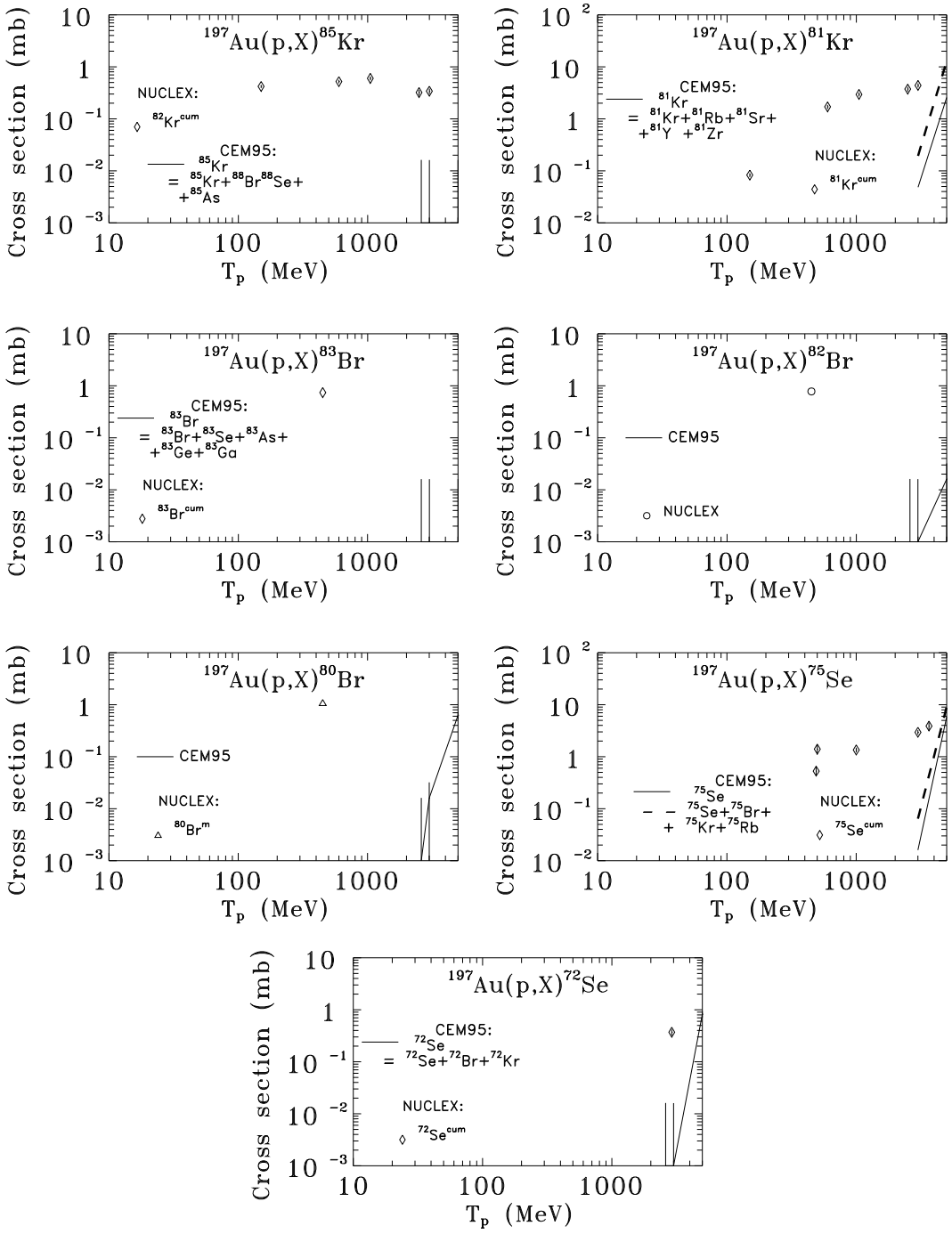

Fig. 95. Excitation functions for the production of ^{85}Kr, ^{81}Kr, ^{83}Br, ^{82}Br, ^{80}Br, ^{75}Se, and ^{72}Se from p+^{197}Au. Experimental data labeled as NUCLEX are from the compilation [46, 47].

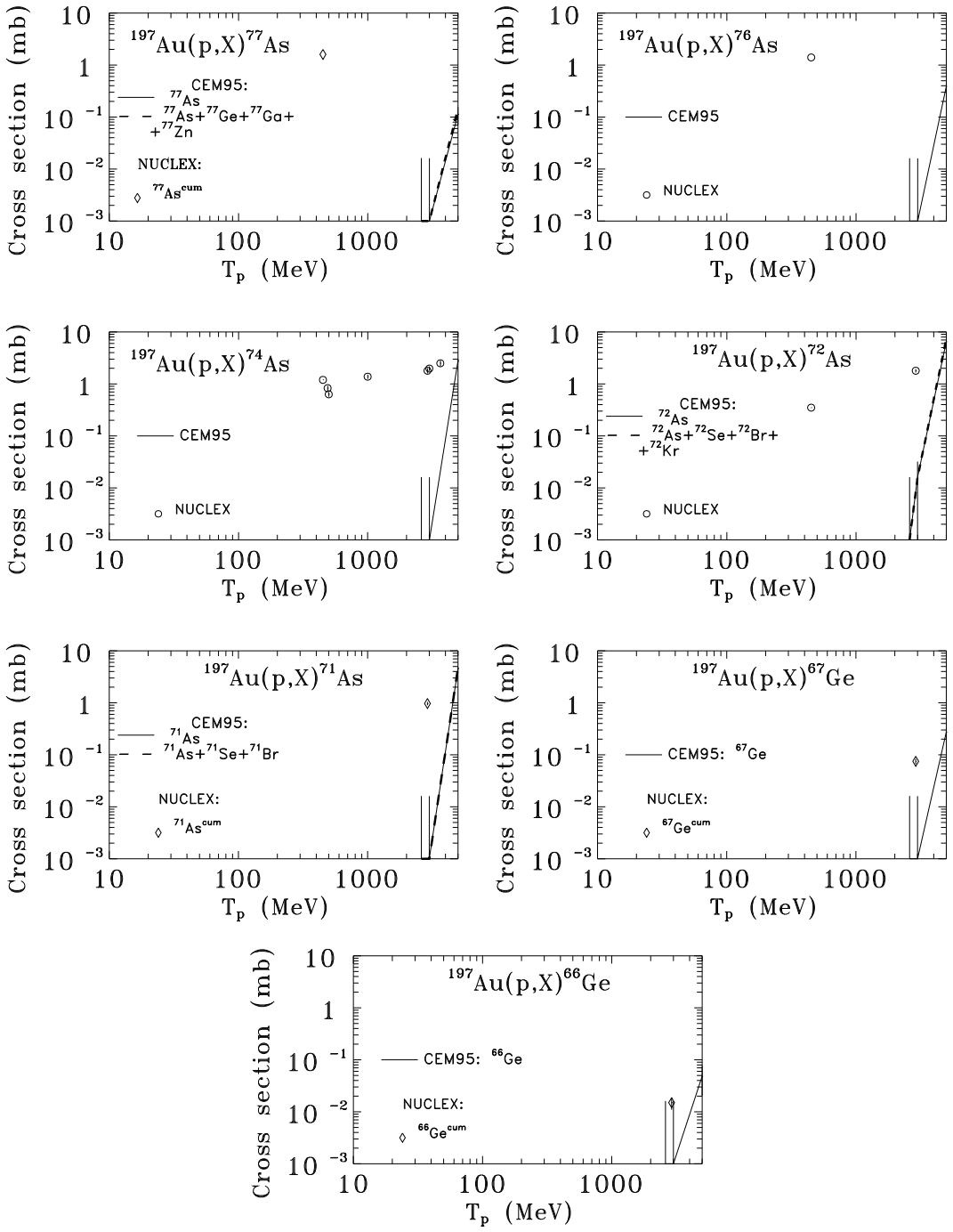

Fig. 96. Excitation functions for the production of ^{77}As, ^{76}As, ^{74}As, ^{72}As, ^{71}As, ^{67}Ge, and ^{66}Ge from p+^{197}Au. Experimental data labeled as NUCLEX are from the compilation [46, 47].

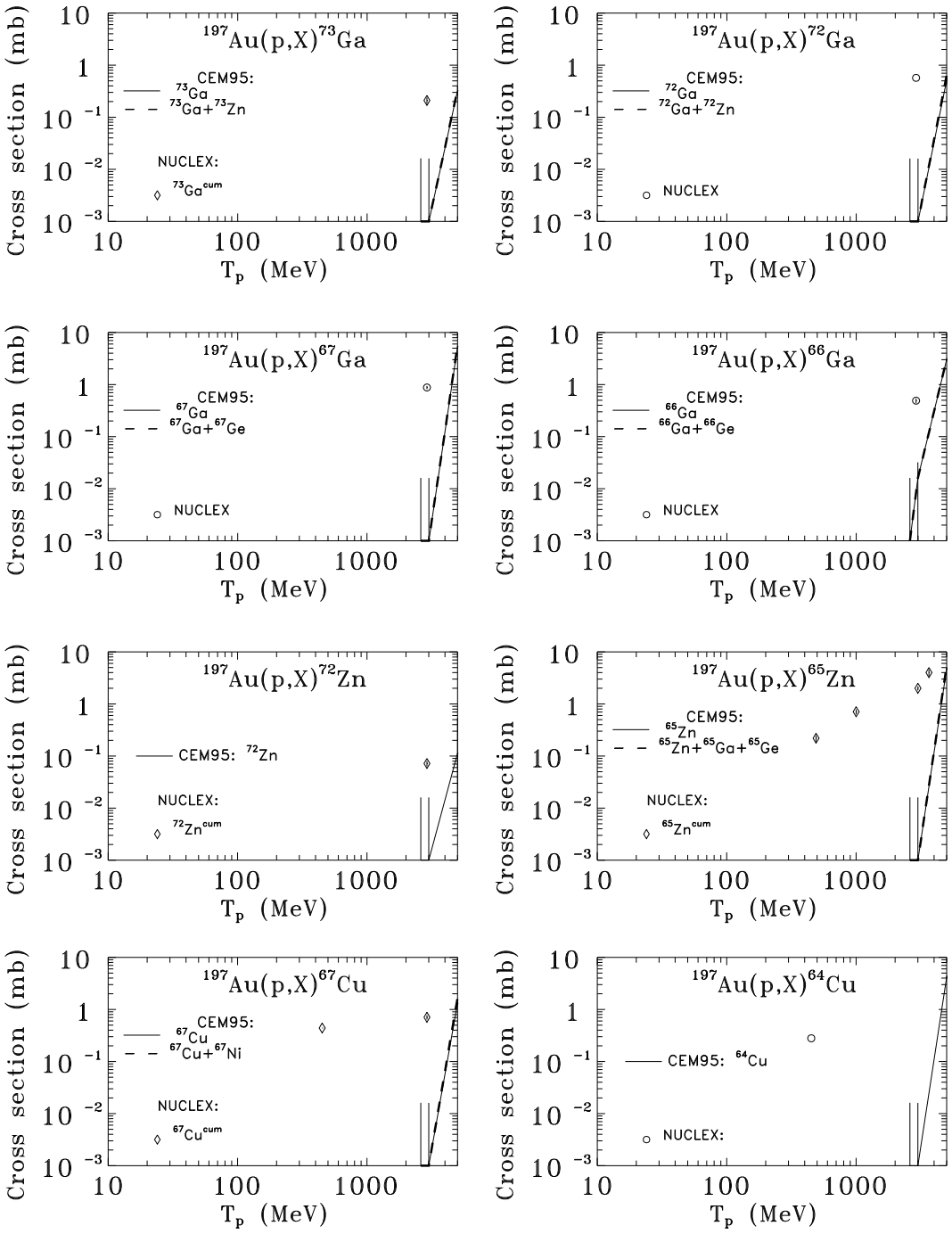

Fig. 97. Excitation functions for the production of ^{73}Ga, ^{72}Ga, ^{67}Ga, ^{66}Ga, ^{72}Zn, ^{65}Zn, ^{67}Cu, and ^{64}Cu from p+^{197}Au. Experimental data labeled as NUCLEX are from the compilation [46, 47].

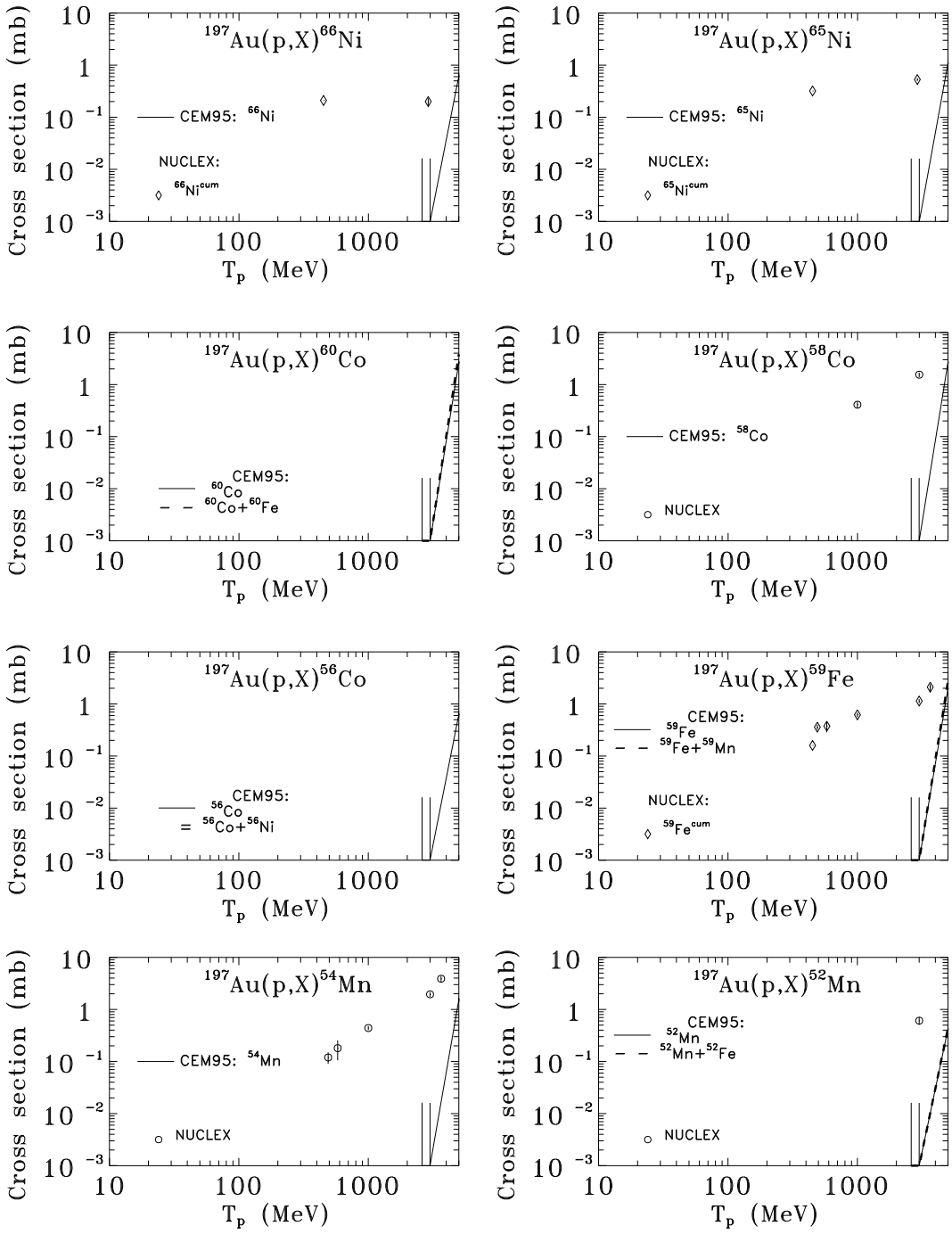

Fig. 98. Excitation functions for the production of ^{66}Ni, ^{65}Ni, ^{60}Co, ^{58}Co, ^{56}Co, ^{59}Fe, ^{54}Mn, and ^{52}Mn from p+^{197}Au. Experimental data labeled as NUCLEX are from the compilation [46, 47].

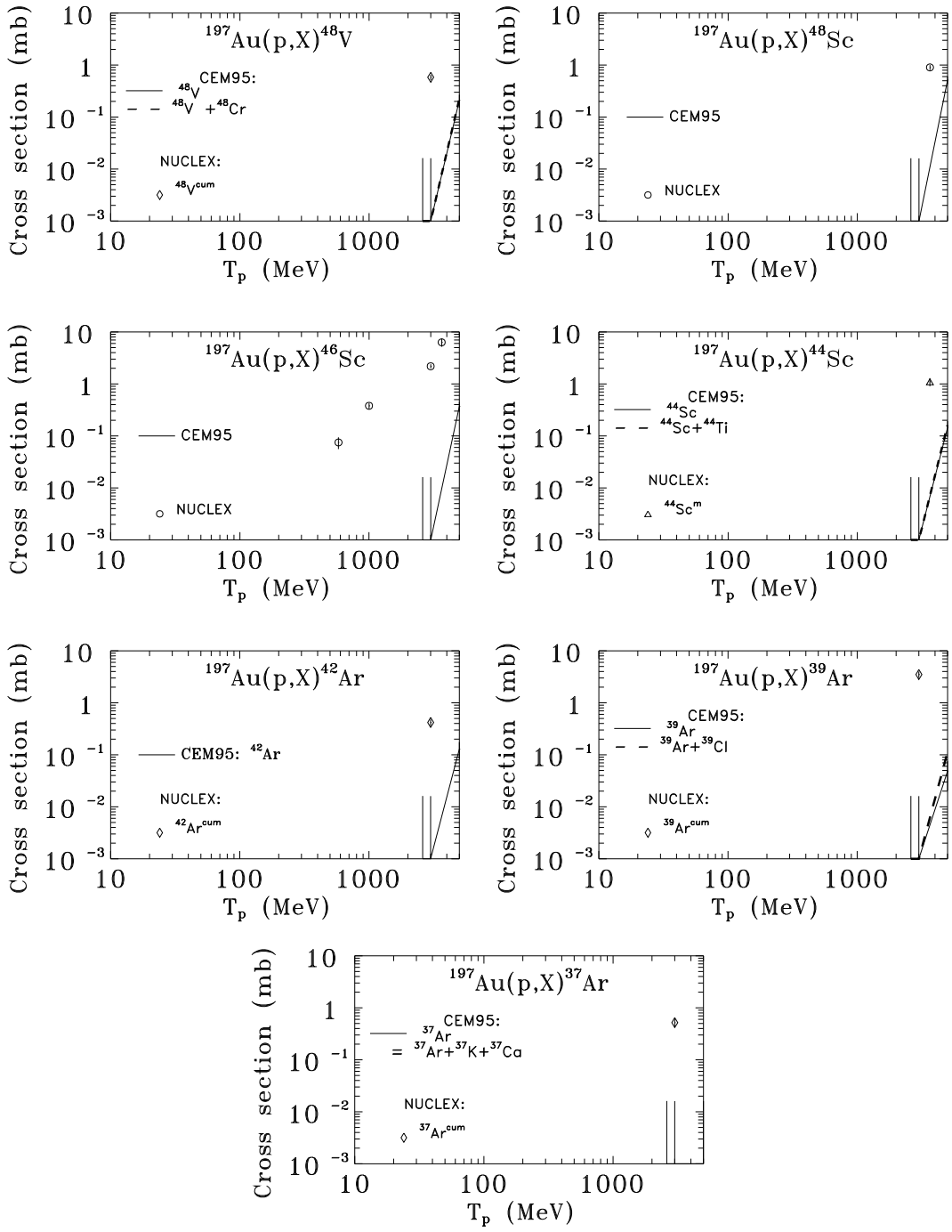

Fig. 99. Excitation functions for the production of ^{48}V, ^{48}Sc, ^{46}Sc, ^{44}Sc, ^{42}Ar, ^{39}Ar, and ^{37}Ar from p+^{197}Au. Experimental data labeled as NUCLEX are from the compilation [46, 47].

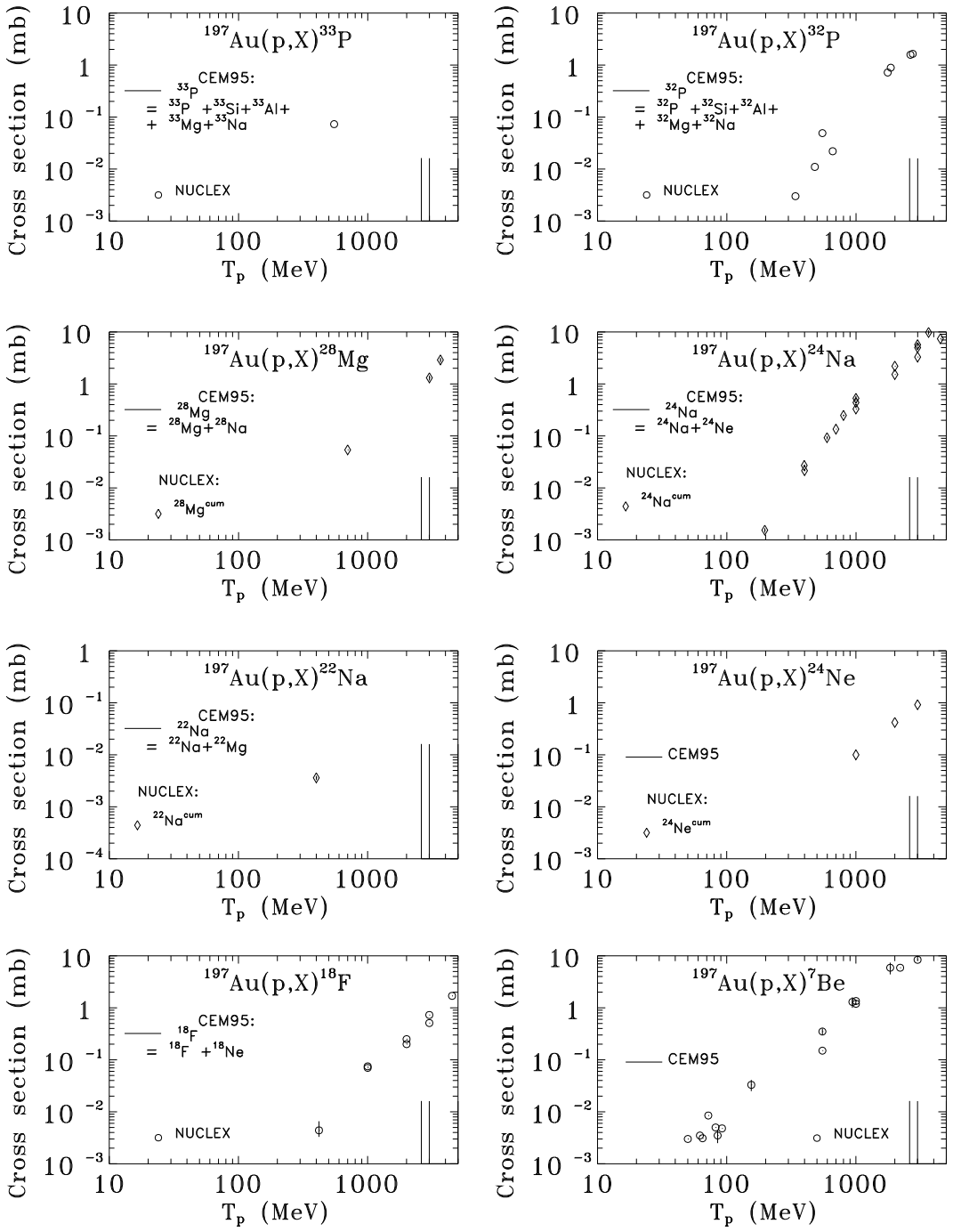

Fig. 100. Excitation functions for the production of ^{33}P, ^{32}P, ^{28}Mg, ^{24}Na, ^{22}Na, ^{24}Ne, ^{18}F, and ^{7}Be from p+^{197}Au. Experimental data labeled as NUCLEX are from the compilation [46, 47].

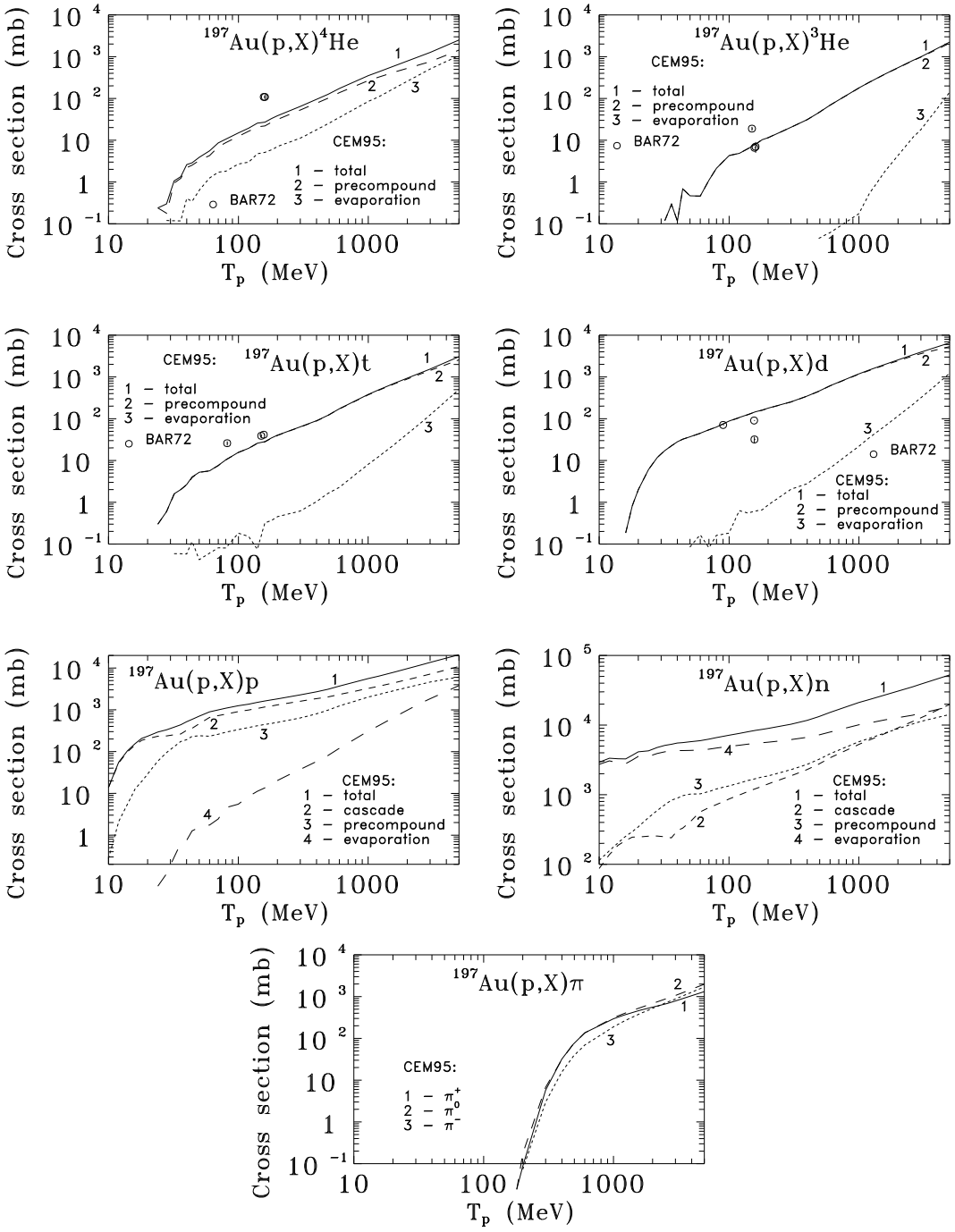

Fig. 101. Excitation functions for the production of ^{4}He, ^{3}He, t, d, p, n, π^+, π^0, and π^- from p+^{197}Au. The contributions to the total yields from cascade (for nucleons), pre-equilibrium emission, and evaporation are shown separately by dashed lines, as indicated. Experimental data labeled as BAR72 are taken from Ref. [54].

We show separately for all nuclides the independent and cumulative calculated yields in our figures. One can see that for gold, in contrast to the previous light and medium targets, the role of contributions from radioactive precursors to the measured yields is more important. For some nuclides (see, e.g., Figs. 84 and 85), the cumulative yields are up to two orders of magnitude higher than the independent ones. Therefore, for heavy targets, an especially careful calculation of cumulative yields and their comparison with the measured data are needed.

The next group of lighter nuclides from gold shown in Figs. 89 to 99 are mainly products of fission. CEM95 takes into account competition between evaporation and fission (see Section 2) and allows us to calculate fission cross sections and nuclear fissilities. Fig. 76 shows a comparison of fission cross section calculated according to Eq. (27) with the experimental data compiled in Ref. [54]. These calculations are performed with the code CEM95 using for the macroscopic fission barriers the Yukawa-plus-exponential modified LDM of Krappe, Nix and Sierk [119], and Cameron's shell and pairing corrections [111] for the ground state and Barashenkov et al. [115] corrections for the saddle-point masses for microscopic fission barriers; the third Iljinov's et al. systematics for the level density parameters [110], with shell corrections by Cameron et al. [112], without taking into account the dependence of fission barriers on angular momenta, and with the dependence of fission barriers on excitation energy proposed in Ref. [122]. A fixed value of 1.100 is used for the ratio a_f/a_n for all incident energies from 10 to 600 MeV. But to describe the decrease of fission cross section with increasing proton energy at about 1 GeV, with a possible minimum at about 2 GeV, which seems to be observed in experiment (see Fig. 76), we have to fit the ratio a_f/a_n, and the values of 1.080, 1.073, 1.064, 1.053, 1.045, and 1.004 are used at proton energies of 1.0, 1.2, 1.6, 2.6, 3.0, and 5.0 GeV, respectively.

As one can see from Fig. 76, with this set of parameters, CEM95 reproduces well the experimental fission cross section. But our code does not calculate the process of fission itself, and does not provide fission fragments and a further possible evaporation of particles from them. When, during the Monte Carlo simulation of a compound stage of a reaction, from evaporation and fission widths, we have to simulate a fission, we simply remember this event (that permits us to calculate fission cross section and fissility) and finish the calculation of this event without a real subsequent calculation of fission fragments and a further possible evaporation of particles from them. Therefore, our results in Figs. 89–99 show the contribution to the total yields of these nuclides only from deep spallation processes of successive emission of particles from the target, but do not contain fission products. One can see that the spallation mechanism for production of nuclides in this region provides only a very small part of the measured yields, and only for high incident energies, above 1–3 GeV. To be able to describe nuclide production in the fission region, CEM95 has to be extended by incorporating a model of high energy fission. For example, the Fong statistical model of fission [216] realized in different Monte Carlo codes, e.g., at JINR [217, 218], ORNL [219], BNL [220], PINP, Gatchina [221] may be used for this purpose. A similar approach based on the thermodynamical model of fis-

sion was developed in Moscow at ITEP by Stepanov [222] and was realized in the code INUCL [175]. A more sophisticated and physically grounded, but at the same time, more complicated and time consuming approach for this may be the dynamical "Diffusion Model of Fission" [223] realized as a Monte Carlo code at INR, Moscow by Mebel with co-authors [224, 82]. On the other hand, several much simpler approaches based on phenomenological distributions of fragments, such as Atchinson's model [225], Nakahara's model [226], and the recent Rubchenya model [227] are also used in a number of codes. Finally, in a number of current works, high energy fission and fragmentation is calculated in a single statistical model of sequential binary decays, realized in the code GEMINI [228].

Fig. 100 shows excitation functions for the third group of nuclides, in the region of fragmentation. These light nuclides are produced either via a very asymmetric fission, or by fragmentation or sequential fission of primary fission products. As the CEM does not contain any of these mechanisms of fragmentation, it cannot describe these nuclides at all. The vertical bars shown in Fig. 100 give an estimate of the upper limit to the total yields of these fragments estimated from a single calculated case of deep spallation, where such a fragment is produced as a residual nucleus at the end of a reaction. One can see that even this upper limit for the spallation mechanism of fragment production from gold is several order of magnitude lower than experimental data. To be able to describe fragment production, CEM95 has to be extended by incorporating a model of fragmentation. Good reviews of available models of fragmentation may be found in Refs. [54, 55, 82, 229, 230, 231]. Let us note here that besides the popular models of fragmentation based on statistical decay, like the Berlin model [232], the Moscow model of multifragmentation [233], the Copenhagen model [234], or models based on liquid-gas instability, like Cugnon's model [235], Friedman's model [236] and other sophisticated approaches reviewed in Refs. [55, 82, 229, 230, 231] and widely used in the literature, a much simpler systematics based on the liquid-gas phase-transition model was successfully incorporated [237] in the JAERI version of HETC.

It should also be noted that a possible mechanism of light fragment production from medium and heavy nuclei may be evaporation of fragments with $A > 4$ from compound nuclei, as was proposed and realized in a number of papers many years ago (see references in Ref. [54]). Another similar mechanism which would be simple to incorporate into CEM95, may be the emission of fragments with $A > 4$ at the preequilibrium stage of a reaction, as was realized recently for ^{7}Be in Ref. [238]. Another mechanism not taken into account here for the production of light fragments appropriate for medium and heavy targets, is the coalescence of fragments from particles emitted at the cascade (and maybe also the preequilibrium) stage of a reaction. As was shown in Ref. [71], incorporation in the CEM of the coalescence mechanism of complex particle production improves significantly the agreement of calculated spectra with experimental data, though it does not provide the total measured yields, and additional mechanisms of fragment production have to be incorporated in the model.

As a first attempt to solve at once both problems of fission and fragmentation, we have tried in the present work to use in CEM95 after the preequilibrium stage of reactions the well known code GEMINI [228] which has the advantage of treating the evaporation, fragmentation and fission processes in a consistent way. Our first preliminary results on this exercise are unsatisfactory and work in this direction will be continued.

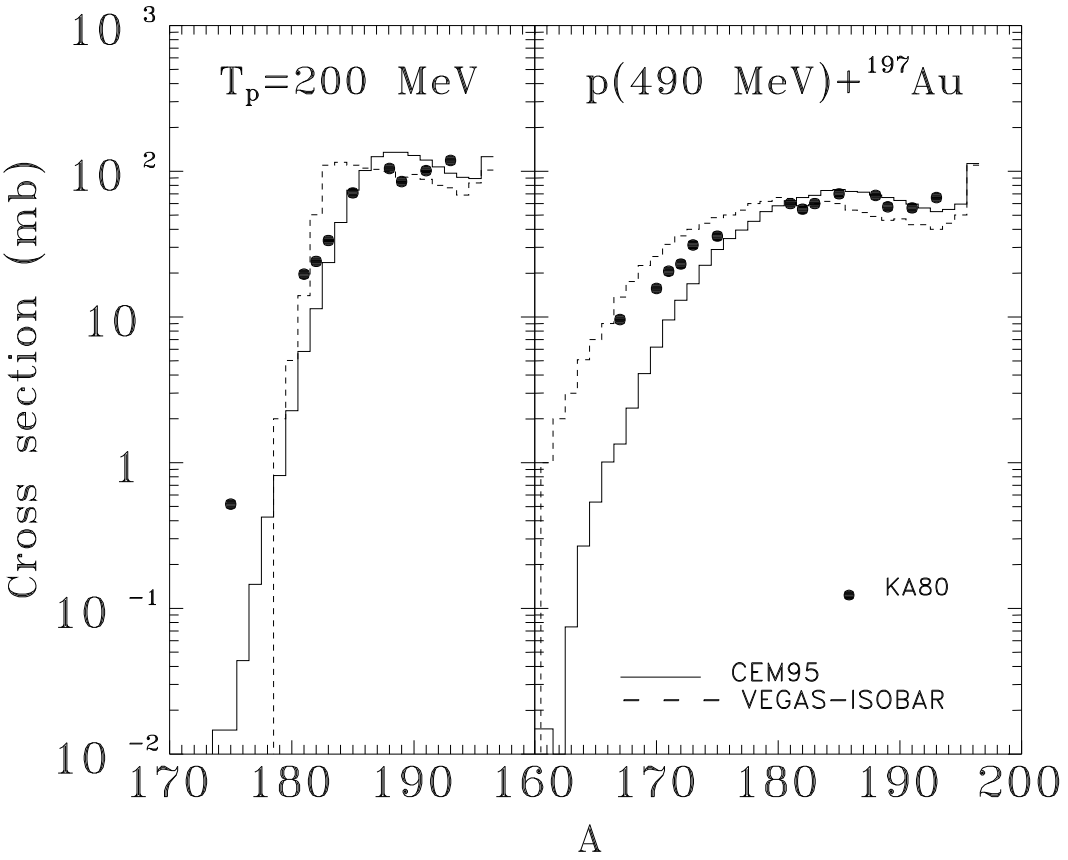

Fig. 102. Mass-yield distributions of residual nuclei from p+^{197}Au at 200 and 490 MeV. Solid histograms are calculated in the present work, dashed histograms show results of calculations with the Brookhaven National Laboratory and Columbia University version of the INC realized in the code VEGAS-ISOBAR [239] from Ref. [240]. Experimental data for cumulative yields of several nuclides labeled as KA80 are taken from Ref. [240].

Fig. 101 shows the excitation functions for the 4th group of the final products, i.e., particles emitted at different stages of reaction. One can see that the CEM reproduces satisfactorily the few available experimental yields of d, t, and ^{3}He, but, as for previous targets, it underestimates significantly the production of ^{4}He. To illustrate the relative role of different production mechanisms, the contributions to the total yields from cascade (for nucleons), preequilibrium emission, and evaporation are shown in Fig. 101 separately. A comparison of these results with similar ones given

above for previous targets (Figs. 17, 22, 26, 43, and 48) shows that the relative roles of different mechanisms of complex particle production change significantly both with changing the atomic mass of the target and with increasing incident energy, and these roles are different for different particles. The relative contribution of preequilibrium particle emission increases with increasing atomic mass of the target for the entire energy interval. For ^{197}Au, the preequilibrium emission provides almost the whole yield of complex particles in the CEM, while evaporation from compound nuclei is strongly suppressed by the Coulomb barrier, and does not provide even 10% of the total yields. The situation is just the opposite in the case of light targets like ^{12}C (Fig. 17) and ^{16}O (Fig. 22). Besides, for light targets, so much spallation takes place that a significant contribution to the total yields of complex particles comes from residual nuclei remaining after emission of other particles at the end of reactions. So, for targets of ^{12}C (Fig. 17) and ^{16}O (Fig. 22), this mechanism becomes predominant for the production of ^{3}He even at quite low energies. It is interesting to note that this "residual nucleus" mechanism does not decrease very quickly with increased mass targets. Even for Fe (Fig. 43) and Co (Fig. 48) one can see small contributions from such processes to the total yields of complex particles.

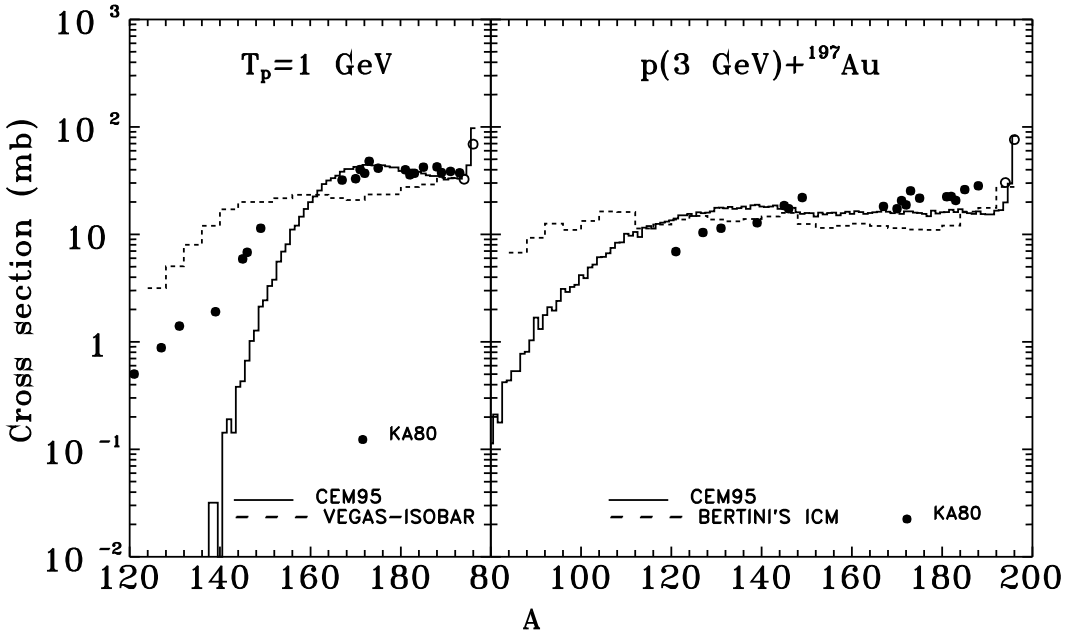

Fig. 103. Mass-yield distributions of residual nuclei from p+^{197}Au at 1 and 3 GeV. Solid histograms are calculated in the present work, dashed histograms show results of calculations with the Brookhaven National Laboratory and Columbia University version of the INC realized in the code VEGAS-ISOBAR [239] (for T_p = 1 GeV) and with the Oak Ridge National Laboratory version of the INC [241] (for T_p = 3 GeV) from Ref. [240]. Experimental data for cumulative yields of several nuclides labeled as KA80 are taken from Ref. [240].

A general summarizing overview on the capability of CEM95 to describe nuclide production from gold is given in Figs. 102 and 103, where mass-yield distributions of residual nuclei at 0.2, 0.49, 1.0, and 3.0 GeV calculated in the present work are compared with the results of calculations with the Brookhaven National Laboratory and Columbia University version of the INC realized in the code VEGAS-ISOBAR [239], with the Oak Ridge National Laboratory version of the INC [241], and with experimental data from Ref. [240]. One can see that for all these energies, CEM95 describes quite well the data in the spallation region, providing a better agreement with the measured cross sections than VEGAS-ISOBAR [239] or Bertini's INC [241] does. But with decreasing masses of measured nuclides and passing into the fission region, the disagreement with the data increases, and CEM95 has to be extended by incorporating a model of high energy fission to be able to describe nuclide production in this region as well.

Of course, many other reasons not discussed above might also cause some of the observed discrepancies. Different features of the CEM and of other similar models may be improved, which could result in a significant change of their predictions. Let us enumerate here several possible improvements of the CEM and further problems to be solved:

- use accurate nuclear densities and potential energy functions in the ICM,
- model the effects of refraction and reflection on the cascade particles as they move from one potential zone of the nucleus into another,
- use realistic velocity-dependent potentials,
- take into account not only the coordinates of elementary interactions but also their times,
- account for "trawling" (local reduction of nuclear density) of nuclei by fast cascade particles,
- incorporation of clusters in the ICM (see, e.g., [242]),
- model knock-out and pick-up processes,
- use of new, more precise experimental data for the cross sections of the elementary interactions,
- take into account nuclear medium effects on the properties of hadrons and their interactions inside a nucleus (see, e.g., Ref. [243]),
- take into account explicitly resonances (such as Δ, etc.) as cascade participants,
- ...

All these problems are very complicated and interconnected and have yet to be included together in a complete study, as fragmentary results obtained previously in the literature are often unexpected and/or contradictory. Unfortunately, inclusion of a separate refinement in nuclear models used in ICM calculations does not always lead to improved agreement with experimental data. So, Chen, et al. [84] have found that for incident energies below 200 MeV, especially for medium and heavy nuclei, the agreement with experimental data was better when refraction and reflection of cascade nucleons were neglected than when these effects were included (see the third paper in Ref. [84]). Further, the same authors have found (see the second paper in Ref. [84]) that the introduction of a velocity-dependent potential consistent with optical-model analyses of nuclear data does not lead to greatly improved agreement between intranuclear cascade calculations and experimental data. Only when in a following study (see the first paper in Ref. [84]), when the authors have included in their ICM effects of short-range nucleon correlations along with refraction and reflection at potential boundaries together with a velocity-dependent potential was the agreement with experimental data improved.

5. Summary

We have performed detailed analyses of more than 600 excitation functions for interactions of protons with energies from 10 MeV to 5 GeV with nuclei of ^{12}C, ^{14}N, ^{16}O, ^{27}Al, ^{31}P, ^{40}Ca, ^{54}Fe, ^{56}Fe, ^{57}Fe, ^{58}Fe, ^{nat}Fe, ^{59}Co, ^{90}Zr, ^{91}Zr, ^{92}Zr, ^{94}Zr, ^{96}Zr, ^{nat}Zr, and ^{197}Au in the framework of an extended version of the cascade-exciton model of nuclear reactions. We have compared our results with all reliable experimental data available to us and with predictions of other models realized in several codes: ALICE LIVERMORE 87 [171], HETC/KFA-2 [165], ALICE91 [180], LAHET [136], ALICE-F [179], NUCLEUS [152], MCEXCITON [181], ALICE82 [189], DISCA2 [166], CASCADE [167], HETC [174], INUCL [175], ALICE75 [207], ALICE LIVERMORE 82 [208], ALICE 87 MOD [209], PEQAQ2 [210], ALICE92 [147], CEM92M [74], with the Milan version of the exciton model of nuclear reactions with preformed α-clusters in nuclei [102], and with calculations using phenomenological systematics from Refs. [57]–[60].

Our analyses have shown that several different mechanisms participate in the production of most final nuclides. Their relative roles change significantly with changing atomic mass of targets, with increasing incident energy, and are different for different final nuclides. The main nuclide production mechanism in the spallation region is the successive emission of several nucleons, while emission of complex particles is important (and may be even the only mechanism for production of a given isotope in a limited range of incident energy) only at low incident energies, near the corresponding thresholds, while with increasing energy its relative role decreases quickly.

For medium and especially for heavy targets, the contribution from radioactive precursors to the measured yields of many nuclides is very important. The cumulative yields of some nuclides are up to two orders of magnitude higher than the independent ones. Therefore, for heavy targets, an especially careful calculation of cumulative yields and their comparisons with the measured data are needed.

Our analyses have shown that nuclear structure effects are very important in production of some nuclides and manifest themselves strongly even at an incident energy of 5 GeV. Therefore, reliable and well fitted approaches for shell and pairing corrections, level density parameters, and especially for nuclear masses and consequent binding energies and Q-values have to be used in calculations.

The extended version of the cascade-exciton model realized in the code CEM95 describes satisfactorily with a fixed set of input parameters the shapes and absolute values of the majority of measured excitation functions for production of nuclides in the spallation region and for the emission of secondary nucleons and complex particles. We feel that the yields of both nuclides in the spallation region and secondary particles of $A < 4$ predicted by CEM95 are at least as reliable, and in many cases more so, than those of the models and phenomenological systematics mentioned above.

For target nuclei from ^{27}Al to ^{197}Au, CEM95 describes the majority of experimental excitation functions in the spallation region to within a factor of 2. For lighter

targets than ^{27}Al, the agreement with the experimental data is worse, and the CEM, like the majority of other models, has to be improved to be able to describe excitation functions from light targets. CEM95 does not contain a special mechanism for fragmentation, underestimates production of ^{4}He, and does not include a model of high energy fission. These mechanisms of nuclear reactions should be incorporated into the CEM.

In rare cases, in the same spallation region, CEM95 underestimates or overestimates some individual measured excitation functions, sometimes up to an order of magnitude. This is mainly a result of the poor nuclear masses and binding energies used in CEM95. Other possible causes of such discrepancies were discussed in Sections 3 and 4.

One may conclude that the extended version of the cascade-exciton model realized in the code CEM95 is suitable for a rough evaluation of excitation functions in the spallation region. But for a better description of the measured yields in this region and for an extension of the range of its applicability into the fission and fragmentation regions, it should be developed further. Among improvements of the CEM which are of highest priority we consider the following:

- incorporation of recent experimental nuclear mass tables, and new reliable theoretical mass formulas for unmeasured nuclides,
- development and incorporation of an appropriate model of high-energy fission,
- modeling the emission of gammas competing with the evaporation of particles at the compound stage,
- treating more accurately α-emission at the preequilibrium stage,
- incorporation of a model for fragmentation of medium and heavy nuclei, and the Fermi breakup model, for highly excited light nuclei,
- modeling the evaporation of fragments with $A > 4$ from not too light excited nuclei (incorporation of such processes at the preequilibrium stage may also be important),
- modeling the coalescence of light fragments from fast emitted particles,
- improvement of the approximations for inverse cross sections, and
- use of new, more precise experimental data for the cross sections of elementary interactions at the cascade stage.

Such a development and improvement of the CEM is possible, and work in this direction is already in progress. We hope that a proper incorporation of the above improvements in the code will not destroy the present wholeness of CEM95 and its good predictive power for the spectra of secondary particles.

There are a number of other possible and desirable improvements of the CEM discussed in Section 4, justified from a physical point of view. Unfortunately, inclusion of separate refinements in nuclear models used in ICM calculations does not always lead to improved agreement with experimental data.

The problems discussed above are typical not only of the CEM, but also for all other similar models and codes, where they are not solved yet. Excitation functions are a very "difficult" characteristic of nuclear reactions as they involve together the different and complicated physics processes of spallation, evaporation, fission, and fragmentation of nuclei. A lot of work is still necessary to be done by theorists and code developers before a reliable complex of codes able to satisfactorily predict arbitrary excitation functions in a wide range of incident energies/projectiles/targets/final nuclides will be available. At present, we are still very far from the completion of this difficult task.

In the meantime, to evaluate excitation functions needed for science and applications, it is necessary to use and analyze together the available experimental data, and for each region of incident energies/projectiles/targets/final nuclides, the predictions of phenomenological systematics, and the results of calculations with the most reliable codes. Our present study has shown that for proton-induced reactions in the spallation region, not too low incident energies and not too light targets, CEM95 is such a reliable code.

Acknowledgements

We wish to thank N. M. Sobolevsky for kindly supplying us with experimental data from the compilation [46, 47]. We are very grateful to T. Fukahori for providing us with results of calculations of excitation functions with the codes ALICE91, ALICE-F, MCEXCITON, and NUCLEUS from the JAERI Benchmark [62, 63] and we thank H. Takada for sending us new, more refined [191] results of calculations with the codes NUCLEUS and HETC/3STEP (as compared to those published in [190]). It is a pleasure to acknowledge M. Blann, V. P. Eismont, L. M. Krizhansky, R. Michel, P. Nagel, and Yu. E. Titarenko for useful discussions on spallation physics which have stimulated us to carry out this research. One of the authors (S. G. M.) thanks CEA, Bruyères-le-Châtel and ORNL, Oak Ridge for kind hospitality and excellent conditions during his work in February–August 1996 at Bruyères-le-Châtel and in July–August 1995 at Oak Ridge, where most of this study was done. He is also grateful to M. B. Chadwick, R. E. MacFarlane, D. G. Madland, P. Möller, R. E. Prael, L. Waters, and P. G. Young of LANL for fruitful discussions and support.

This study was completed under the auspices of the U.S. Department of Energy by the Los Alamos National Laboratory under contract no. W-7405-ENG-36.

References

[1] *"Proc. 11th Int. Conf. on Ultra-Relativistic Nucleus-Nucleus Collisions (Quark Matter '95),"* *Nucl. Phys. A*, **590**, Nos. 1,2 (1995).

[2] *"Proc. 7th Int. Conf. on Nuclear Reaction Mechanisms,"* Varenna, June 6–11, 1994, E. GADIOLI, Ed., Università degli Studi di Milano (1994).

[3] *"Proc. Int. Conf. on Nuclear Data for Science and Technology,"* Gatlinburg, Tennessee, May 9–13, 1994, Vols. 1 and 2, J. K. DICKENS, Ed., American Nuclear Society (1994).

[4] *"Proc. Int. Conf. on Nuclear Data for Science and Technology,"* Jülich, Germany, May 13–17, 1991, S. M. QAIM, Ed., Springer-Verlag (1992).

[5] *"Proc. Int. Conf. on Nucl. Data for Science and Technology,"* Mito, Japan, May 30–June 3, 1988, S. IGRASI, Ed., JAERI (1988).

[6] A. J. KONING, "Requirements for an Evaluated Nuclear Data File for Accelerator-Based Transmutation," ECN-C-93-041, Petten (June 1993).

[7] "Overview of Physics Aspect of Different Transmutation Concepts," NEA / NSC / DOC (94) 11, OECD Nuclear Energy Agency (1994).

[8] J. P. SCHAPIRA, "Transmutation of Nuclear Wastes, A working report to Nupecc," I.P.N. Report IPNO DRE 94-04, Orsay (1994).

[9] K. D. TOLSTOV, "Perspectives of Electronuclear Method of Energy Generation and Nuclear Waste Transmutation," *JINR Rapid Communications*, **5[62]**, 5 (1993); see also "Simulation of Electronuclear Method of Atomic Energy Production and Radioactive Waste Transmutation," *JINR 18-92-303*, Dubna (1992); see also I. V. CHUVILO, G. V. KISELEV, B. R. BERGELSON, and B. P. KOCHUROV, "Nuclear Fuel Cycle Using Nuclear Power Facilities Based on Subcritical Blankets Driven by the Proton Accelerator," *Proc. Int. Conf. and Technol. Exposition on Future Nucl. Systems: Emerging Fuel Cycle and Waste Disposal Options, GLOBAL'93*, Seattle, Washington, September 12–17, 1993, p. 924.

[10] F. VENNERI, C. D. BOWMAN, and S. A. WENDER, "The Physics Design of Accelerator-Driven Transmutation Systems," *Proc. Int. Conf. on Evaluation of Emerging Nucl. Fuel Cycle Systems, GLOBAL'95*, Versailles, France, September 11–14, 1995, p. 474; see also T. TAKIZUKA, T. NISHIDA, T. SASA, H. TAKADA, S. MEIGO, M. MIZUMOTO, and K. HASEGAWA, "Research and Development on Proton Accelerator Based Transmutation of Nuclear Waste," *ibid.*, pp. 489–496; see also H. TAKAHASHI and H. RIEF, "Concept of Accelerator Based Transmutation Systems," *Proc. Specialists' Mtg. on*

Accelerator-Based Transmutation, Villigen, PSI, Switzerland, March 24–26, 1992, p. 2.

[11] *"Proc. of the Second Specialists' Meeting on High Energy Nuclear Data,"* JAERI, Tokai, Japan, January 26–27, 1995, JAERI-Conf, 95-016, INDC(JPN)-174/U, T. FUKAHORI and N. KISHIDA, Eds., JAERI (1995).

[12] *"Proc. of the 1995 Symposium on Nuclear Data,"* JAERI, Tokai, Japan, November 16–17, 1995, JAERI-Conf, 96-008, INDC(JPN)-175/U, T. IGUCHI and T. FUKAHORI, Eds., JAERI (1996).

[13] *"Proc. of the 1994 Symposium on Nuclear Data,"* JAERI, Tokai, Japan, November 17–18, 1994, JAERI-Conf, 95-008, INDC(JPN)-173/U, M. KAWAI and T. FUKAHORI, Eds., JAERI (1995).

[14] *"Proc. of the 1993 Symposium on Nuclear Data,"* JAERI, Tokai, Japan, November 18–19, 1993, JAERI-M, 94-019, INDC(JPN)-169/L, M. KAWAI and T. FUKAHORI, Eds., JAERI (1994).

[15] *"Proc. of the 1992 Symposium on Nuclear Data,"* JAERI, Tokai, Japan, November 26–27, 1992, JAERI-M, 93-046, NEA/NSC/DOC(93)2, INDC(JPN)-163/L, M. BABA and T. NAKAGAWA, Eds., JAERI (1993).

[16] *"Proc. of the 1991 Symposium on Nuclear Data,"* JAERI, Tokai, Japan, November 28–29, 1991, JAERI-M, 92-027, INDC(JPN)-157/L, M. BABA and T. NAKAGAWA, Eds., JAERI (1992).

[17] *"Proc. of the 1990 Symposium on Nuclear Data,"* JAERI, Tokai, Japan, November 29–30, 1990, JAERI-M, 91-032, NEANDC(J)-160/U, INDC(JPN)-148/L, M. IGASHIRA and T. NAKAGAWA, Eds., JAERI (1991).

[18] *"Proc. of the 1989 Symposium on Nuclear Data,"* JAERI, Tokai, Japan, November 16–17, 1989, JAERI-M, 90-025, NEANDC(J)-149/U, INDC(JPN)-136/L, Y. NAKAJIMA and M. IGASHIRA, Eds., JAERI (1990).

[19] *"4th Int. Information Exchange Meeting on Actinide and Fission Product Partitioning and Transmutation,"* Mito, Japan, September 11–13, 1996.

[20] *"Second Int. Conf. on Accelerator-Driven Transmutation Technologies and Applications,"* Kalmar, Sweden, June 3–7, 1996.

[21] *"Proc. Int. Workshop on Nucl. Methods for Transmutation of Nuclear Wastes: Problems, Perspectives, Cooperative Research,"* Dubna, Russia, May 29–31, 1996, M. Kh. KHANKHASAYEV, Zh. B. KURMANOV, and H. PLENDL, Eds., World Scientific, Singapore (1997).

[22] *"Proc. of the 3rd OECD-NEA Information Exchange Meeting on Actinide and Fission Product Partitioning and Transmutation,"* Cadarache, France, December 12–14, 1994.

[23] *"Special Scientific Programme on Use of High Energy Accelerators for Transmutation of Actinides and Power Production,"* IAEA General Conference, Vienna, Austria, September 21, 1994, **INIS-mf-14423**, IAEA (1994).

[24] *"Int. Conf. on Accelerator-Driven Transmutation Technologies and Applications,"* Las Vegas, USA, 1994, AIP Conference Proceedings No. 346, D. EDWARD, A. RODRIGUEZ, and S. O. SCHRIBER, Eds., AIP Press (1995).

[25] *"Proc. II Int. Sem. on Proton Accelerator Based Transmutation of Long-Lived Radioactive Wastes and Utilization of Weapon Plutonium,"* Moscow, Russia, May 23–27, 1994, ITEP, Moscow, Parts I and II, 1994.

[26] *"Proc. of the Information Exchange Meeting on Actinide and Fission Product Separation and Transmutation,"* Argonne National Laboratory, Argonne, Illinois, USA, November 11–13, 1992, NEA/P&T Report No. 7, OECD/NEA (1993).

[27] *"Workshop on Nuclear Transmutation of Long-Lived Nuclear Power Radiowastes,"* Obninsk, Russia, July 1–5, 1991.

[28] *"Proc. of the Information Exchange Meeting on Actinide and Fission Product Separation and Transmutation,"* Mito City, Japan, November 6–8, 1990, NEA/P&T Report No. 2, OECD/NEA (1991).

[29] W. GUDOWSKI, "Accelerator-Driven System — Survey of the Research Programs in the World," pp. 3–28 in Ref. [21].

[30] C. D. BOWMAN, "Accelerator-Driven Transmutation Technologies for Resolution of Long-Term Nuclear Waste Concerns," pp. 257–270 in Ref. [21].

[31] C. RUBBIA, "The Energy Amplifier: a Solid-Phase, Accelerator Driven, Sub Critical TH/233 U Breeder for Nuclear Energy Production with Minimal Actinide Waste," pp. 1065–1071 in Ref. [3]; see also "High Energy Particle Accelerators for Bulk Transformation of Elements and Energy Generation," pp. 13–35 in Ref. [23]; see also "Heavy-Ion Accelerators for Inertial Fusion," *Nuovo Cim. A*, **106**, 1429 (1993); see also C. RUBBIA, J. A. RUBIO, S. BUONO, F. CARMINATI, N. FIÉTIER, J. GALVEZ, C. GELÈS, Y. KADI, R. KLAPISCH, P. MANDRILLON, J. P. REVOL, and C. ROCHE, "Conceptual Design of a Fast Neutron Operated High Power Energy Amplifier," CERN Report CERN/AT/95-44(ET), 29 September 1995.

[32] A. N. SISAKIAN, "Elaboration of Physical Conception of Electronuclear Power Generation," p. T/B 27 in Ref. [20].

[33] V. S. BARASHENKOV, A. N. SOSNIN, S. Yu. SHMAKOV, N. G. GOLEMINOV, and A. POLANSKI, "Mathematical Simulation of Radiational Damages of Microelectronic Devices," *Fiz. Element. Chast. At. Yad.*, **24**, 246 (1993) [*Phys. Part. Nucl.*, **24**, 107 (1993)]; see also C. J. GELDERLOOS, R. J. PETERSON, M. E. NELSON, and J. F. ZIEGLER, "Pion-Induced Soft Upsets in 16 Mbit DRAM Chips," NPL-1139, University of Colorado (April 18, 1997).

[34] K. KITAO, "Production and Radiological Impact of Argon-39," pp. 249–256 in Ref. [16].

[35] R. M. WHITE, M. B. CHADWICK, W. P. CHANDLER, C. L. HARTMANN SIANTAR, and C. K. WESTBROOK, "Advances in Nuclear Data and All-Particle Transport for Radiation Oncology," pp. 1023–1028 in Ref. [3].

[36] A. HASHIZUME, "Radioisotope Productions for Medical Use," pp. 1067–1073 in Ref. [5]; see also S. N. DMITRIEV and N. G. ZAITSEVA, "Radionuclides for Biomedical Studies. Nuclear Data and Production Methods in Charged-Particle Accelerators," *Fiz. Elem. Chastis At. Yadra*, **27**, 977 (1996) [*Phys. Part. Nucl.*, **27**, 403 (1996)].

[37] G. F. STEYN, B. R. S. SIMPSON, S. J. MILLS, and F. M. NORTIER, "The Production of ^{55}Fe with Medium-Energy Protons," *Appl. Radiat. Isot.*, **43**, 1323 (1992).

[38] E. A. EDMONDS, "Radiation Scattering Techniques," in *Radioisotope Technique for Problem-Solving in Industrial Process Plants*, J. S. CHARLTON, Ed., Leonard Hill, Glasgow, p. 247 (1986).

[39] R. MICHEL, I. LEYA, and L. BORGES, "Production of Cosmogenic Nuclides in Meteorites: Accelerator Experiments and Model Calculations to Decipher the Cosmic Ray Record in Extraterrestrial Matter," *Nucl. Instr. Meth. B*, **113**, 434 (1996).

[40] R. BODEMANN, H.-J. LANGE, I. LEYA, R. MICHEL, T. SCHIENKEL, R. RÖSEL, U. HERPERS, H. J. HOFMANN, B. DITTRICH, M. SUTER, W. WÖLFLI, B. HOLMQVIST, H. CONDÉ, and P. MALMBORG, "Production of Residual Nuclei by Proton-Induced Reactions on C, N, O, Mg, Al and Si," *Nucl. Instr. Meth. B*, **82**, 9 (1993).

[41] R. MICHEL and R. STÜCK, "On the Production of Cosmogenic Nuclides in Meteorites by Primary Galactic Particles: Cross Sections and Model Calculations," *J. Geophys. Res. B*, **89**, 673 (1984).

[42] R. MICHEL, "Proton-Induced Spallation at 600 MeV," *Analyst*, **114**, 287 (1989).

[43] R. MICHEL, M. GLORIS, H.-J. LANGE, I. LEYA, M. LÜPKE, U. HERPERS, B. DITTRICH-HANNEN, R. RÖSEL, Th. SCHIEKEL, D. FILGES, P. DRAGOVITSCH, M. SUTER, H.-J. HOFMANN, W. WÖLFLI, P.-W. KUBIK, H. BAUR, and R. WIELER, "Nuclide Production by Proton-Induced Reactions on Elements ($6 \leq Z \leq 29$) in the Energy Range from 800 to 2600 MeV," *Nucl. Instr. Meth. B*, **93**, 183 (1995).

[44] R. MICHEL, R. BODEMANN, H. BUSEMANN, R. DAUNKE, M. GLORIS, H.-J. LANGE, B. KLUG, A. KRINS, I. LEYA, M. LÜPKE, S. NEUMANN, H. REINHARDT, M. SCHNATZ-BÜTTGEN, U. HERPERS, Th. SCHIENKEL, F. SUDBROCK, B. HOLMQVIST, H. CONDÉ, P. MALMBORG, M. SUTER, B. DITTRICH-HANNEN, P.-W. KUBIK, H.-A. SYNAL, and D. FILGES "Cross Sections for the Production of Residual Nuclides by Low- and Medium-Energy Protons from the Target Elements C, N, O, Mg, Al, Si, Ca, Ti, V, Mn, Fe, Co, Ni, Cu, Sr, Y, Zr, Nb, Ba, and Au," *Nucl. Instr. Methods B*, **129**, 153 (1997); see also the Web page at:**http://sun1.rrzn-user.uni-hannover.de/zsr/survey.htm#url=overview.htm.**

[45] J. HUDIS, "Spallation Reactions: Experimental Results, 1967–1975," pp. 9–25 in *Spallation Nuclear Reactions and Their Applications*, **Astrophysics and Space Science Library, vol. 59**, B. S. P. SHEN and M. MERKER, Eds., D. Reidel Publishing Company, Dordrecht-Holland (1976).

[46] A. S. ILJINOV, V. G. SEMENOV, M. P. SEMENOVA, N. M. SOBOLEVSKY, and L. V. UDOVENKO, "Production of Radionuclides at Intermediate Energies," Springer Verlag, Landolt-Börnstein, New Series, subvolumes **I/13a** (1991), **I/13b** (1992), **I/13c** (1993), and **I/13d** (1994).

[47] V. I. IVANOV, N. M. SOBOLEVSKY, and V. G. SEMENOV, "NUCLEX — an IBM PC Version of Handbook on Radionuclide Production Cross Section at Intermediate Energies," pp. 387–388 in Ref. [50].

[48] M. BLANN, H. GRUPPELAR, P. NAGEL, and J. RODENS, *International Code Comparison for Intermediate Energy Nuclear Data*, NEA OECD, Paris (1994).

[49] P. NAGEL, J. RODENS, M. BLANN, and H. GRUPPELAR, "Intermediate Energy Nuclear Reaction Code Intercomparison: Application to Transmutation of Long-Lived Reactor Wastes," *Nucl. Sci. Eng.*, **119**, 97 (1995).

[50] "Intermediate Energy Nuclear Data: Models and Codes," *Proc. Specialists' Mtg.*, Issy-les-Moulineaux, France, May 30–June 1, 1994, OECD, Paris (1994).

[51] J. J. SCHMIDT, "Nuclear Data — Their Importance and Application in Fission Reactor Physics Calculations," Workshop on the Computation and Analysis of Nuclear Data Relevant for Nuclear Energy and Safety, Trieste, Italy, 10 February–13 March 1992, H4.SMR 614/2 (1992).

[52] "Summary and Conclusion of the Specialists' Meeting on Shielding Aspects of Accelerators, Targets, and Irradiation Facilities," Arlington, Texas, 28–29 April, 1994, NEA/NSC/DOC(94)17, OECD Nuclear Energy Agency, (May 1994).

[53] A. J. KONING, "Review of High Energy Data and Model Codes for Accelerator-Based Transmutation," ECN-C-93-005, Petten (January 1993).

[54] V. S. BARASHENKOV and V. D. TONEEV, *Interaction of High Energy Particles and Nuclei with Atomic Nuclei*, (in Russian) Atomizdat, Moscow (1972).

[55] J. HÜFNER, "Heavy Fragments Produced in Proton-Nucleus and Nucleus-Nucleus Collisions at Relativistic Energies," *Phys. Rep.*, **125**, 129 (1985).

[56] T. A. GABRIEL and S. G. MASHNIK, "Semiempirical Systematics for Different Hadron-Nucleus Interaction Cross Sections," JINR Preprint E4-96-43, Dubna (1996).

[57] G. RUDSTAM, "Systematics of Spallation Yields," *Z. Naturforsch. A*, **21**, 1027 (1966).

[58] B. K. GUPTA, S. DAS, and M. M. BISWAS, "Cross Sections for the Production of Nuclides from Medium-Weight Elements by High-Energy Proton Bombardment," *Nucl. Phys. A*, **155**, 49 (1970).

[59] M. FOSHINA, J. B. MARTINS, and O. A. P. TAVARES, "Systematics of Spallation Yields with a Four-Parameter Formula," *Radiochim. Acta*, **35**, 121 (1984).

[60] A. Yu. KONOBEYEV and Yu. A. KOROVIN, "Tritium Production in Materials from C to Bi Irradiated with Nucleons of Intermediate and High Energies," *Nucl. Instr. Meth. B*, **82**, 103 (1993).

[61] R. SILBERBERG, C. H. TSAO, and M. M. SHAPIRO, "Semiempirical Cross Sections, and Applications to Nuclear Interactions of Cosmic Rays," pp. 49–81 in *Spallation Nuclear Reactions and Their Applications*, **Astrophysics and Space Science Library, vol. 59**, B. S. P. SHEN and M. MERKER, Eds., D. Reidel Publishing Company, Dordrecht, Holland (1976).

[62] T. FUKAHORI, S. CHIBA, H. TAKADA, N. KISHIDA, Y. WATANABE, and N. YAMAMURO, "Benchmark Calculations of Theoretical Calculation Codes

for Nuclear Data Evaluation in the Intermediate Energy Region," pp. 57–71 in Ref. [15].

[63] T. FUKAHORI, S. CHIBA, H. TAKADA, N. KISHIDA, Y. WATANABE, and N. YAMAMURO, "Comparison of Isotope Production Cross Section in the Intermediate Energy Region Calculated by Various Theoretical Calculation Codes for Nuclear Data Evaluation," JAERI Preliminary Report Distributed to Participants of Gatlinburg '94 Int. Conf. on Nucl. Data for Sci. and Technology; to be published.

[64] "International Code Comparison for Intermediate Energy Nuclear Data *The Thick Target Benchmark*," Report NSC/DOC(95) 2, D. FILGES, P. NAGEL, and R. D. NEEF, Eds., NEA OECD (1995).

[65] N. SOBOLEVSKY, "Conclusions of International Code Comparison for Intermediate Energy Nuclear Data *Thick Target Benchmark for Lead and Tungsten, Report NSC/DOC(95)2*," Report NSC/DOC(96)-15, NEA OECD (1996).

[66] R. MICHEL and P. NAGEL, "Specification for an International Codes and Model Intercomparison for Intermediate Energy Activation Yields," *NEA/NSC/DOC(95)8*, NEA OECD, 30 May 1995.

[67] R. MICHEL and P. NAGEL, *International Codes and Model Intercomparison for Intermediate Energy Activation Yields*, NSC/DOC(97)-1, NEA/P/&T No 14, OECD, Paris (1997); see also the Web page at: **http://www.nea.fr/html/science/pt/ieay**.

[68] K. K. GUDIMA, S. G. MASHNIK, and V. D. TONEEV, "Cascade-Exciton Model of Nuclear Reactions," *Nucl. Phys. A*, **401**, 329 (1983).

[69] K. K. GUDIMA, S. G. MASHNIK, and V. D. TONEEV, "Cascade-Exciton Model of Nuclear Reactions: Model Formulation," *JINR Communication P2-80-774*, Dubna (1980); "Cascade-Exciton Model of Nuclear Reactions: Comparison with Experiment," *JINR Communication P2-80-777*, Dubna (1980).

[70] S. G. MASHNIK, "The Cascade-Exciton Approach for Intermediate Energy Nuclear Reactions," pp. 100–109 in Ref. [2]; see also S. G. MASHNIK and S. A. SMOLYANSKY, "The Cascade-Exciton Approach to Nuclear Reactions (Foundation and Achivements)," pp. 137–159 in *Dynamics of Transport in Plasmas and Charged Beams*, G. MAINO and M. OTTAVANI, Eds., World Scientific, Singapore (1996).

[71] S. G. MASHNIK, "Neutron-Induced Particle Production in the Cumulative and Noncumulative Regions at Intermediate Energies," *Nucl. Phys. A*, **568**, 703 (1994); K. O. OGANESYAN, M. I. GOGOLEV, S. I. GOSTKIN, S. I. MERZLYAKOV, E. A. PASYUK, S. Yu. POROKHOVOY, N. SCINTEE, and

S. G. MASHNIK, "Proton-Induced Production of Protons and Deuterons on Copper and Gallium in the 300–400 MeV Energy Range," *Int. Nuclear Phys. Conf.*, Beijing, China, August 21–26, 1995, Book of Abstracts, p. 5.6–9, and to be published.

[72] S. G. MASHNIK, "How Many Nucleons Are Required for Nuclear Pion Absorption?" *Yad. Fiz.*, **58**, 1772 (1995) [*Phys. At. Nucl.*, **58**, 1672 (1995)]; see also "Low- and Intermediate-Energy Pion-Nucleus Interactions in the Cascade-Exciton Model," *Acta Phys. Pol. B*, **24**, 1685 (1993); see also "Stopped Pion Absorption by Nuclei in the Cascade-Exciton Model," *Rev. Roum. Phys.*, **37**, 179 (1992).

[73] T. GABRIEL, G. MAINO, and S. G. MASHNIK, "Analysis of Intermediate Energy Photonuclear Reactions," JINR Preprint E2-94-424, Dubna (1994); see also Proc. XII Int. Sem. on High Energy Probl. *Relativistic Nucl. Phys. & Quantum Chromodynamics*, Dubna, Russia, 12–17 September, 1994.

[74] S. G. MASHNIK, "Physics of the CEM92M Code," pp. 107–120 in Ref. [50];

[75] S. G. MASHNIK, "Analysis of Excitation Functions of Proton-Nucleus Reactions within the Cascade-Exciton Model," *Izv. Rossiiskoi Akad. Nauk, ser. fiz.*, **60**, 73 (1996) [*Bull. Russian Acad. Sci.: Physics*, **60**, 58 (1996)].

[76] Yu. E. TITARENKO, E. I. KARPIKHIN, A. F. SMOLYAKOV, M. M. IGUMNOV, S. G. MASHNIK, T. A. GABRIEL, N. V. STEPANOV, V. D. KAZARITSKY, V. F. BATYAEV, and O. V. SHVEDOV, "Experimental and Theoretical Study of Radionuclide Production on the Electronuclear Plant Target and Construction Materials Irradiated by 1.5 GeV and 130 MeV Protons," pp. 207–215 in Ref. [21].

[77] Yu. E. TITARENKO, E. I. KARPIKHIN, A. F. SMOLYAKOV, M. M. IGUMNOV, S. G. MASHNIK, T. A. GABRIEL, N. V. STEPANOV, V. D. KAZARITSKY, V. F. BATYAEV, and O. V. SHVEDOV, "Experimental and Theoretical Study of Radionuclide Production on the Electronuclear Plant Target and Construction Materials Irradiated by 1.5 GeV and 130 MeV Protons," *Proc. II Int. Conf. on Accelerator-Driven Transmutation Technologies and Applications*, Kalmar, Sweden, June 3–7, 1996.

[78] Yu. E. TITARENKO, E. I. KARPIKHIN, A. F. SMOLYAKOV, M. M. IGUMNOV, O. V. SHVEDOV, N. V. STEPANOV, V. D. KAZARITSKI, V. F. BATYAEV, S. G. MASHNIK, and T. A. GABRIEL "Experimental and Calculational Study of Radionuclide Production — Products of Target and Construction Materials for Electronuclear Facilities Irradiated by 1.5 GeV and 130 MeV Protons," *Intl. Seminar on Precise Mesurements in Nucl. Spectrometry "TlYaS-XI"*, Sarov (Arzamas-16), Russia, September 2–5, 1996, *Voprosy*

Atomnoi Nauki i Techniki, Seriya: Fizika Yadernykh Reaktorov, TlYaS-XI, Special Issue, p184 (1997) (in Russian).

[79] Yu. E. TITARENKO, O. V. SHVEDOV, M. M. IGUMNOV, R. MICHEL, S. G. MASHNIK, E. I. KARPIKHIN, V. D. KAZARITSKY, V. F. BATYAEV, A. B. KOLDOBSKY, V. M. ZHIVUN, A. N. SOSNIN, R. E. PRAEL, M. B. CHADWICK, T. A. GABRIEL, and M. BLANN, "Experimental and Theoretical Study of the Yields of Radionuclides Produced in ^{209}Bi Thin Target Irradiated by 1500 MeV and 130 MeV Protons," to be published in *Nucl. Instr. Meth. B, 1997*.

[80] V. A. KONSHIN, "Calculation of Neutron and Proton Induced Reaction Cross Sections for Actinides in the Energy Region from 10 MeV to 1 GeV," *JAERI-Research 95-036*, JAERI (1995); see also "Calculations of Neutron and Proton Induced Reaction Cross Sections for Actinides in the Energy Region from 10 MeV to 1 GeV," pp. 57–69 in Ref. [11]; see also "Calculation of Nuclear Data for Reactions of Neutrons and Protons with Heavy Nuclei at Energy from 1 MeV up to 2 GeV," pp. 29–35 in Ref. [13].

[81] V. S. BARASHENKOV, A. S. ILJINOV, N. M. SOBOLEVSKII, and V. D. TONEEV, "Interaction of Particles and Nuclei of High and Ultrahigh Energy with Nuclei," *Usp. Fiz. Nauk*, **109**, 91 (1973) [*Sov. Phys.-Usp.*, **16**, 31 (1973)].

[82] A. S. ILJINOV, M. V. KAZARNOVSKY, and E. Ya. PARYEV, *Intermediate-Energy Nuclear Physics*, CRC Press, Boca Raton, Florida (1994).

[83] H. W. BERTINI, "Low-Energy Intranuclear Cascade Calculation," *Phys. Rev.*, **131**, 1801 (1963); see also *Phys. Rev.*, **138**, AB2 (1965); see also "Intranuclear Cascade Calculation of the Secondary Nucleon Spectra from Nucleon-Nucleus Interactions in the Energy Range 340 to 2900 MeV and Comparison with Experiment," *Phys. Rev.*, **188**, 1711 (1969).

[84] K. CHEN, G. FRIEDLANDER, G. D. HARP, and J. M. MILLER, "Effects of Nucleon-Pair Correlations on Monte Carlo Intranuclear-Cascade Simulations," *Phys. Rev. C*, **4**, 2234 (1971); K. CHEN, G. FRIEDLANDER, and J. M. MILLER, "Effects of Using a Velocity-Dependent Potential in a Monte Carlo Simulation of Intranuclear Cascades," *Phys. Rev.*, **176**, 1208 (1968); see also K. CHEN, Z. FRAENKEL, G. FRIEDLANDER, J. R. GROVER, J. M. MILLER, and Y. SHIMAMOTO, "VEGAS: A Monte Carlo Simulation of Intranuclear Cascades," *Phys. Rev.*, **166**, 948 (1968).

[85] V. S. BARASHENKOV, H. W. BERTINI, K. CHEN, G. FRIEDLANDER, G. D. HARP, A. S. ILJINOV, J. M. MILLER, and V. D. TONEEV,

"Medium Energy Intranuclear Cascade Calculations: a Comparative Study," *Nucl. Phys. A*, **187**, 531 (1972).

[86] K. KIKUCHI and M. KAWAI, *Nuclear Matter and Nuclear Reactions*, North-Holland, Amsterdam, (1968).

[87] N. METROPOLIS, R. BIVINS, M. STORM, A. TURKEVICH, J. M. MILLER, and G. FRIEDLANDER, "Monte Carlo Calculations on Intranuclear Cascades. I. Low-Energy Studies," *Phys. Rev.*, **110**, 185 (1958).

[88] F. D. BECCHETTI, Jr. and G. W. GREENLESS, "Nucleon-Nucleus Optical-Model Parameters, $A > 40$, $E < 50$ MeV," *Phys. Rev.*, **182**, 1190 (1969).

[89] J. J. H. MENET, E. E. GROSS, J. J. MALANIFY, and A. ZUCKER, "Total-Reaction-Cross-Section Measurements for 30-60-MeV Protons and the Imaginary Optical Potential," *Phys. Rev. C*, **4**, 1114 (1971).

[90] H. MARSHAK, A. LANGSFORD, T. TAMURA, and C. Y. WONG, "Total Neutron Cross Section of Oriented ^{165}Ho from 2 to 135 MeV," *Phys. Rev. C*, **2**, 1862 (1970).

[91] K. K. GUDIMA, S. G. MASHNIK, and V. D. TONEEV, "Preequilibrium Emission in Hadron-Nucleus Reactions at $T_0 \leq$ 1–2 GeV," Proc. Europhysics Topical Conf. *Neutron Induced Reactions*, Smolenice, June 21–25, 1982, *Physics and Applications*, **10**, 347 (1982).

[92] N. YOSHIZAWA, K. ISHIBASHI, and H. TAKADA, "Development of High Energy Transport Code HETC-3STEP Applicable to the Nuclear Reaction with Incident Energies above 20 MeV," *J. Nucl. Sci. Techn.*, **32**, 601 (1995).

[93] K. K. GUDIMA, G. A. OSOSKOV, and V. D. TONEEV, "Model for Pre-Equilibrium Decay of Excited Nuclei," *Yad. Fiz.*, **21**, 260 (1975) [*Sov. J. Nucl. Phys.*, **21**, 138 (1975)].

[94] S. G. MASHNIK and V. D. TONEEV, "MODEX — the Program for Calculation of the Energy Spectra of Particles Emitted in the Reactions of Pre-Equilibrium and Equilibrium Statistical Decays," *JINR Communication P4-8417*, Dubna (1974).

[95] T. ERICSON, "The Statistical Model and Nuclear Level Densities," *Adv. in Physics*, **9**, 425 (1960).

[96] F. C. WILLIAMS Jr., "Intermediate State Transition Rates in the Griffin Model," *Phys. Lett. B*, **31**, 184 (1970).

[97] F. C. WILLIAMS Jr., Particle-Hole State Density in the Uniform Spacing Model," *Nucl. Phys. A*, **161**, 231 (1971).

[98] I. RIBANSKY, P. OBLOZINSKY, and E. BETAK, "Pre-Equilibrium Decay and the Exciton Model," *Nucl. Phys. A*, **205**, 545 (1973).

[99] G. MANTZOURANIS, H. A. WEIDENMÜLLER, and D. AGASSI, "Generalized Exciton Model for the Description of Preequilibrium Angular Distributions," *Z. Phys. A*, **276**, 145 (1976).

[100] E. BETAK, "Complex Particle Emission in the Exciton Model of Nuclear Reactions," *Acta Phys. Slov.*, **26**, 21 (1976).

[101] J. R. WU and C. C. CHANG, "Complex-Particle Emission in the Pre-Equilibrium Exciton Model," *Phys. Rev. C*, **17**, 1540 (1978).

[102] E. GADIOLI, E. GADIOLI ERBA, and J. J. HOGAN, "Preequilibrium Decay of Nuclei with $A \simeq 90$ at Excitation Energies to 100 MeV," *Phys. Rev. C*, **16**, 1404 (1977).

[103] E. GADIOLI and P. E. HODGSON, *Pre-Equilibrium Nuclear Reactions*, Oxford University Press, New York (1992).

[104] V. F. WEISSKOPF and D. H. EWING, "On the Yield of Nuclear Reactions with Heavy Elements," *Phys. Rev.*, **57**, 472 (1940).

[105] N. BOHR and J. A. WHEELER, "The Mechanism of Nuclear Fission," *Phys. Rev.*, **56**, 426 (1939).

[106] A. V. MALYSHEV, *Level Density and Structure of Atomic Nuclei*, (in Russian) Atomizdat, Moscow (1969).

[107] A.V. IGNATYUK, G. N. SMIRENKIN, and A. S. TISHIN, "Phenomenological Description of the Energy Dependence of the Level Density Parameter," *Yad. Fiz.*, **21**, 485 (1975) [*Sov. J. Nucl. Phys.*, **21**, 255 (1975)].

[108] A. V. IGNATYUK, M. G. ITKIS, V. N. OKOLOVICH, G. N. SMIRENKIN, and A. S. TISHIN, "Fission of Pre-Actinide Nuclei. Excitation Functions for the (α, f) Reaction," *Yad. Fiz.*, **21**, 1185 (1975) [*Sov. J. Nucl. Phys.*, **21**, 612 (1975)].

[109] E. A. CHEREPANOV and A. S. ILJINOV, "Statistical Calculation of Nuclear Level Densities," (in Russian) Preprint INR AS USSR, P-0064, Moscow (1977); *Nucleonika*, **25**, 611 (1980).

[110] A. S. ILJINOV, M. V. MEBEL, N. BIANCHI, E. De SANCTIS, C. GUARDALO, V. LUCHERIINI, V. MUCCIFORA, E, POLLI, A. R. REOLON, and P. ROSSI, "Phenomenological Statistical Analysis of Level Densities, Decay Width and Lifetimes of Excited Nuclei," *Nucl. Phys. A*, **543**, 517 (1992).

[111] A. G. W. CAMERON, "A Revised Semiempirical Atomic Mass Formula," *Can. J. Phys.*, **35**, 1021 (1957).

[112] J. W. TRURAN, A. G. W. CAMERON, and E. HILF, "Construction of Mass Formulas Designed to be Valid for Neutron-Rich Nuclei," *Proc. Int. Conf. on the Properties of Nuclei Far From the Region of Beta-Stability*, Leysin, Switzerland, 1970, v. 1, p. 275.

[113] W. D. MYERS and W. S. SWIATECKI, "Anomalies in Nuclear Masses," *Ark. Fysik.* **36**, 343 (1967).

[114] S. G. MASHNIK, "Statistical Model Calculations of Nuclear Level Density with Different Systematics for the Level Density Parameter," *Acta Phys. Slovaca*, **43**, 86 (1993).

[115] V. S. BARASHENKOV, A. S. ILJINOV, V. D. TONEEV, and F. G. GEREGHI, "Fission and Decay of Excited Nuclei," *Nucl. Phys. A*, **206**, 131 (1973).

[116] V. S. BARASHENKOV and F. G. GEREGHI, "Systematics of Fission Barriers," (in Russian) *Communication JINR, P4-10781*, Dubna (1977).

[117] H. C. PAULI and T. LEDERGERBER, "Fission Threshold Energies in the Actinide Region," *Nucl. Phys. A*, **175**, 545 (1971).

[118] H. J. KRAPPE and J. R. NIX, "Modified Definition of the Surface Energy in the Liquid Drop Formula," *Proc. 3rd IAEA Symp. on the Phys. and Chemistry of Fission*, Rochester, New York, 1973 (IAEA-SM-174/12, Vienna, 1974), v. 1, p. 159.

[119] H. J. KRAPPE, J. R. NIX, and A. J. SIERK, "Unified Nuclear Potential for Heavy-Ion Elastic Scattering, Fusion, Fission, and Ground-State Masses and Deformations," *Phys. Rev. C*, **20**, 992 (1979).

[120] A. J. SIERK, "Macroscopic Model of Rotating Nuclei," *Phys. Rev. C*, **33**, 2039 (1986).

[121] V. M. KUPRIYANOV, K. K. ISTEKOV, B. I. FURSOV, and G. N. SMIRENKIN, "Simple Description of the Dependence of the Fission Barriers and the Ratio Γ_n/Γ_f on the Nucleonic Composition for Transuranium Nuclei," *Yad. Phys.*, **32**, 355 (1980) [*Sov. J. Nucl. Phys.*, **32**, 184 (1980)].

[122] V. S. BARASHENKOV, A. S. ILJINOV, V. D. TONEEV, and F. G. GEREGHI, "Inelastic Interactions of High Energy Nucleons with Heavy Nuclei," *Nucl. Phys. A*, **222**, 204 (1974).

[123] G. SAUER, H. CHANDRA, and U. MOSEL, "Thermal Properties of Nuclei," *Nucl. Phys. A*, **264**, 221 (1976).

[124] V. M. STRUTINSKIĬ, "Form of the Fissioning Nucleus at the Saddle Point and the Liquid-Drop Model," *Yad. Fiz.*, **1**, 821, (1965) [*Sov. J. Nucl. Phys.*, **1**, 588, (1965)].

[125] S. COHEN and W. J. SWIATECKI, "The Deformation Energy of a Charged Drop. Part V: Results of Electronic Computer Studies," *Ann. Phys. (N.Y.)*, **22**, 406 (1963).

[126] S. G. MASHNIK, "Optimal Systematics of Single-Humped Fission Barriers for Statistical Calculations," *Acta Phys. Slovaca*, **43**, 243 (1993).

[127] A. S. ILJINOV and V. D. TONEEV, "Calculation of Successive Particle Emission from a Highly Excited Nucleus with High Angular Momentum," *Yad. Fiz.*, **9**, 48 (1968) [*Sov. J. Nuc. Phys.*, **9**, 30 (1969)]; see also "Analysis of Excitation Functions in Heavy Ion Reactions," (in Russian) *Acta Phys. Polonica B*, 173 (1973).

[128] A. S. ILJINOV, E. A. CHEREPANOV, and S. E. CHIGRINOV, "Probability of Nuclear Fission Induced by Moderate-Energy Particles," *Yad. Fiz.*, **32**, 322 (1980) [*Sov. J. Nucl. Phys.*, **32**, 166 (1980)].

[129] E. A. CHEREPANOV, "Statistical Model for Calculating the Characteristics of Heavy Ion Nuclear Reactions Based on the Monte-Carlo Method," *Proc. Int. Symp. on In-Beam Nuclear Spectroscopy*, Debercen, Hungary, May 14–18, 1984, p. 499.

[130] I. DOSTROVSKY, Z. FRANKEL, and G. FRIEDLANDER, "Monte Carlo Calculations of Nuclear Evaporation Processes. III. Application to Low-Energy Reactions," *Phys. Rev.*, **116**, 683 (1959).

[131] M. TRABANDT, W. SCOBEL, M. BLANN, B. A. POHL, R. C. BYRD, C. C. FOSTER, and R. BONETTI, "Preequilibrium Neutron Emission in the Reactions ^{90}Zr, ^{208}Pb(p, xn) with 80 MeV Projectiles," *Phys. Rev. C*, **39**, 452 (1989).

[132] A. A. COWLEY, A. VAN KENT, J. J. LAURIE, S. V. FORTSCH, D. M. WHITTAL, J. V. PILCHER, F. D. SMIT, W. A. RICHTER, R. LINDSAY, I. J. HEERDEN, R. BONETTI, and P. E. HODGSON, "Preequilibrium Proton Emission Induced by 80 and 120 MeV Protons Incident on ^{90}Zr," *Phys. Rev. C*, **43**, 678 (1991).

[133] P. W. LISOWSKI, A. GAVRON, W. E. PERKER, J. L. ULLMANN, S. J. BALESTRINI, A. D. CARLSON, O. A. WASSON, and N. W. HILL,

"Fission Cross Sections in the Intermediate Energy Region," *Proc. of a Specialists' Meeting on Neutron Cross Section Standards for the Energy Region Above 20 MeV*, Uppsala, Sweden, May 21–23, 1991, p. 177.

[134] V. P. EISMONT, A. V. PROKOFYEV, A. A. RIMSKI-KORSAKOV, A. N. SMIRNOV, H. CONDÉ, K. ELMGREN, S. HULTQVIST, J. NILSSON, N. OLSSON, E. RAMSTRÖM, T. RÖNNQVIST, and E. TRANÉUS, "Neutron-Induced Fission Cross Sections of ^{209}Bi and ^{238}U in the Intermediate Energy Region," pp. 360–362 in Ref. [3].

[135] H. CONDÉ, K. ELMGREN, S. HULTQVIST, J. NILSSON, N. OLSSON, T. RÖNNQVIST, E. TRANÉUS, V. P. EISMONT, A. V. PROKOFYEV, and A. N. SMIRNOV, "A Facility for Measurement of Fission Cross Sections at Intermediate Energies," *Uppsala University Neutron Physics Report, UU-NF 94/#6*, January 1994.

[136] R. E. PRAEL and H. LICHTENSTEIN, "User Guide to LCS: The LAHET Code System," *LA-UR-89-3014*, Los Alamos National Laboratory (September 1989); see also R. E. PRAEL, "A Review of Physics Models in the LAHET^{TM} Code," pp. 145–157 in Ref. [50]; see also L. S. WATERS, "Status of the LAHET^{TM} Code System," *Simulating Accelerator Radiation Environments 2 (SARE2) proceedings*, CERN, Geneva, October 9–13, 1995; see also R. E. PRAEL and M. BOZOIAN, "Adaptation of the Multistage Preequilibrium Model for the Monte Carlo Method (I)," *LA-UR-88-3238*, Los Alamos National Laboratory (September 1988); see also R. E. PRAEL, "LAHET Benchmark Calculation of Differential Neutron Production Cross Sections for 113 and 256 MeV Protons," *LA-UR-89-3347*, Los Alamos National Laboratory (1989); see also R. E. PRAEL, "LAHET Benchmark Calculation of Neutron Yield from Stopping-Length Target for 113 MeV and 256 MeV Protons," *LA-UR-90-1620*, Los Alamos National Laboratory (1990); see also R. E. PRAEL, "LAHET^{TM} Benchmark Calculation of Differential Neutron Production Cross Sections for 597 and 800 MeV Protons," *LA-UR-95-2142*, Los Alamos National Laboratory (1995); see also R. E. PRAEL, "Model Cross Section Calculation Using LAHET," *LA-UR-92-3404*, Los Alamos National Laboratory (1992); the majority of documents on LAHET are presently available on the Web at: **http://www-xdiv.lanl.gov/XTM/**.

[137] R. MICHEL, F. PEIFFER, and R. STÜCK, "Measurement and Hybrid Model Analysis of Integral Excitation Functions for Proton-Induced Reactions on Vanadium, Manganese and Cobalt up to 200 MeV," *Nucl. Phys. A*, **441**, 617 (1985).

[138] O. V. SHVEDOV, Yu. E. TITARENKO, E. I. KARPIKHIN, I. V. FEDOROV, V. D. KAZARITSKY, V. F. BATYAEV, Yu. V. KOCHEVALIN, and

N. V. STEPANOV, "Experimental and Calculating Research of Deep Spallation Reactions on ^{59}Co Induced by 1.2 GeV Protons. Chapter 2. Calculated Results," Preprint ITEP 30-94, Moscow (1994).

[139] A. P. VINOGRADOV, A. K. LAVRUKHINA, and L. D. REVINA, (in Russian) *Geokhimiya*, **11**, 955 (1961).

[140] A. K. LAVRUKHINA, L. D. REVINA, V. V. MALYSHEV, and L. M. SATAROVA, "Spallation of Fe Nuclei Induced by 150 MeV Protons," *Jurnal Exp. Teor. Fiz.*, **44**, 1429 (1963).

[141] G. RUDSTAM, P. C. STEVENSON, and R. L. FOLYER, "Nuclear Reactions of Iron with 340 MeV Protons," *Phys. Rev.*, **87**, 358 (1963).

[142] Yu. V. ALEKSANDROV, S. K. VASILJEV, R. B. IVANOV, L. M. KRIZHANSKY, and V. P. PRIKHODTZEVA, "Cross Section for the Production of Radionuclides from an Iron Target Irradiated with 660 MeV Protons," (in Russian), *Int. Conf. on Nucl. Spectroscopy and Nucl. Structure*, St.-Petersburg, June 27–30, 1995, Book of Abstract, St. Petersburg, 1995, p. 244.

[143] M. HONDA and D. LAL, "Spallation Cross Sections for Long-Lived Radionuclides in Iron and Light Nuclei," *Nucl. Phys.*, **51**, 363 (1964).

[144] Yu. N. SHUBIN, V. P. LUNEV, and A. Yu. KONOBEEV, "Role of Nuclear Level Density in Description of Cross Sections of Nuclear Reactions with Multiple Emission of Particles." (in Russian), Proc. Int. Conf. on Nucl. Phys. *"XLVI Meeting on Nucl. Specrtoscopy and Structure of At. Nucl."*, Moscow, June 18–21, 1996, Book of Abstracts, St. Petersburg, 1996, p. 116, and to be published in *Bull. Russian Acad. Sci.: Physics*.

[145] N. V. KURENKOV, V. P. LUNEV, and Yu. N. SHUBIN, "Influence of Nuclear Level Density on Calculations of Excitation Functions for the Production of Radionuclides Cs, Xe, I, Pb, Tl, and Bi," (in Russian), Preprint FEI-2390, Obninsk (1994).

[146] V. A. KONSHIN, "Neutron Cross-Section Calculations Using Optical, Statistical and Pre-Equilibrium Models," Workshop on the Computation and Analysis of Nuclear Data Relevant for Nuclear Energy and Safety, Trieste, Italy, 10 February–13 March 1992, H4.SMR 614/3 (1992).

[147] M. BLANN, "ALICE 92," pp. 158–160 in Ref. [48]; see also LLNL Report UCRL-JC-109050, November 1991.

[148] A. V. IGNATYUK, "Contribution of Collective Motions in the Density of Excited States of a Nucleus," *Yad. Fiz.*, **21**, 20 (1975) [*Sov. J. Nucl. Phys.*, **21**, 10 (1975)]; see also A. I. BLOKHIN, A. V. IGNATYUK, A. B. PASHCHENKO,

Yu. V. SOKOLOV, and Yu. N. SHUBIN, "Analysis of Excitation Functions of Threshold Reactions in the Generalized Superfluid Model," *Izv. AN SSSR, Ser. Fiz.*, **49**, 962 (1985); see also A. I. BLOKHIN, A. V. IGNATYUK, and Yu. N. SHUBIN, "Vibrational Enhancement of the Level Density of Nuclei in the Iron Region," *Yad. Fiz.*, **48**, 371 (1988) [*Sov. J. Nucl. Phys.*, **48**, 232 (1988)]; see also A. V. IGNATYUK, J. L. WEIL, S. RAMAN, and S. KAHANE, "Density of Discrete Levels in ^{116}Sn," *Phys. Rev. C*, **47**, 1504 (1993).

[149] T. FUKAHORI, "Review of Evaluation in the Medium Energy Region," pp. 106–123 in Ref. [17].

[150] V. S. RAMAMURTHY, M. ASGHAR, and S. K. KATARIA, "Mean Distribution of Single-Particle Levels in Thin-Skinned Potential Wells and the Macroscopic Level Density Parameters of Nuclei," *Nucl. Phys. A*, **398**, 544 (1983).

[151] T. NISHIDA and Y. NAKAHARA, "Analysis of Spallation Product Yields for Proton-Induced Reactions," pp. 975–978 in Ref. [5].

[152] T. NISHIDA, Y. NAKAHARA, and T. TSUTSUI, "Development of a Nuclear Spallation Simulation Code Calculation of Primary Spallation Products," *JAERI-M-86-116* (1986) (in Japanese); see also T. NISHIDA, H. TAKADA, and Y. NAKAHARA, "NUCLEUS," pp.152–157 in Ref. [48]; see also H. TAKADA, Y. NAKAHARA, T. NISHIDA, K. ISHIBASHI, and N. YOSHIZAWA, "Microscopic Cross Section Calculations with NUCLEUS and HETC-3STEP," pp. 121–136 in Ref. [50].

[153] K. J. Le COUTEUR, "The Evaporation Theory of Nuclear Disintegrations," *Proc. Phys. Soc. (London)*, **A63**, 259 (1950).

[154] T. NISHIDA, Y. NAKAHARA, and T. TSUTSUI, "Analysis of the Mass Formula Dependence of the Spallation Product Distribution," *JAERI-M-87-088* (1987);

[155] R. MICHEL, G. BRINKMANN, H. WEIGEL, and W. HERR, "Measurement and Hybrid Model Analysis of Proton-Induced Reactions on V, Fe, and Co," *Nucl. Phys. A*, **322**, 40 (1979).

[156] Yu. V. ALEKSANDROV, A. I. BOGDANOV, S. K. VASILJEV, R. B. IVANOV, M. A. MIKHAILOVA, T. I. POPOVA, and V. P. PRIKHODTZEVA, "Cross Section for the Production of Radionuclides from Interaction of 1 GeV Protons with Medium Atomic Number Nuclei," *Izv. AN SSSR, Ser. Fiz.*, **54**, 2249 (1990).

[157] N. G. ZAITSEVA, C. DEPTULA, O. KNOTEK, KIM SEN KHAN, S. MIKOLAEWSKI, P. MIKEC, E. RURARZ, V. A. KHALKIN, V. A. KONOV, and

L. M. POPINENKOVA, "Cross Sections for the 100 MeV Proton-Induced Nuclear Reactions and Yields of some Radionuclides Used in Nuclear Medicine," *Radiochimica Acta*, **54**, 57 (1991).

[158] V. S. BARASHENKOV, *Cross Sections of Interaction of Particles and Nuclei with Nuclei*, (in Russian) JINR, Dubna (1993); see also the Web page at: **http://www.nea.fr/html/dbdata/bara.html**.

[159] F. YIOU, M. BARIL, J. DUFAURE DE CITRES, and P. FONTES, "Mass-Spectrometric Measurement of Lithium, Beryllium, and Boron Isotopes Produced in ^{16}O by High-Energy Protons and some Astrophysical Implications," *Phys. Rev.*, **166**, 968 (1968).

[160] B. S. AMIN, S. BISWAS, D. LAL, and B. L. K. SOMAYAJULU, "Radiochemical Measurements of ^{10}Be and ^{7}Be Formation Cross Sections in Oxygen by 135 and 550 MeV Protons," *Nucl. Phys. A*, **195**, 311 (1972).

[161] S. SUDÁR and S. M. QAIM, "Excitation Functions of Proton and Deutron Induced Reactions on Iron and Alpha-Particle Induced Reaction on Manganese in the Energy Region up to 25 MeV," *Phys. Rev. C*, **50**, 2408 (1994).

[162] R. W. MILLS, M. F. JAMES, and D. R. WEAVER, "The JEF2 Fission Product Yield Evaluation," *Proc. of a Specialists' Meeting on Fission Product Nuclear Data*, Tokai, Japan, May 25–27, 1992, NEA/NSC/DOC(92)9, p. 358; see also H. O. DENSCHLAG, "Measurement of Cumulative and Independent Fission Yields," *ibid.*, pp. 256–270; see also A. C. WAHL, "Nuclear-Charge Distribution and Delayed-Neutron Yields for Thermal-Neutron-Induced Fission of ^{235}U, ^{233}U, and ^{239}Pu and for Spontaneous Fission of ^{252}Cf," *At. Data and Nucl. Data Tab.*, **39**, 1 (1988).

[163] N. G. GUSEV and P. P. DMITRIEV, *Radioactive Chains: Handbook*, (in Russian) 2d Edition, Energoatomizdat, Moscow (1988).

[164] C. M. LEDERER and V. S. SHIRLEY, *Table of Isotopes*, 7th Edition, John Wiley, New York (1978); see also E. BROWNE and R. B. FIRESTONE, *Table of Radioactive Isotopes*, V. S. SHIRLEY, Ed., John Wiley & Sons, New York (1986).

[165] P. CLOTH, D. FILGES, R. D. NEEF, G. STERZENBACH, C. REUL, T. W. ARMSTRONG, B. L. COLBORN, B. ANDERS, and H. BRÜCKMANN, "HERMES A Monte Carlo Program System for Beam-Material Studies," KFA-Report *KFA-IRE-EAN/12/88*, Jül-2203 (1988); see also "HETC/KFA2," pp. 134–136 in Ref. [48].

[166] A. Yu. KONOBEEV, Yu. A. KOROVIN, and V. N. SOSNIN, "Neutron Displacement Cross-Sections for Structural Materials Below 800 MeV,"

J. Nucl. Materials, **186**, 117 (1992); see also "A Nuclear Data Library for Structural Material Radiation Damage Calculation at High Energies," *Kerntechnik*, **57**, 188 (1992); see also A. Yu. KONOBEEV and Yu. A. KOROVIN, "The Cross Section Library "BISERM" for Calculation of the Helium, Hydrogen Production and Damage Rate in Structural Materials Irradiated with Nucleons at the Energies from 15 MeV to 800 MeV," (in Russian) *Voprosy Atomnoi Nauki i Tekhniki, Series: Yadernye Konstanty*, **4**, 92 (1991).

[167] V. S. BARASHENKOV, LE VAN NGOK, L. G. LEVCHUK, Zh. Zh. MUSULMANBEKOV, A. N. SOSNIN, V. D. TONEEV, and S. Yu. SHMAKOV, "CASCADE Program Complex for Monte-Carlo Simulation of Nuclear Processes Initiated by High Energy Particles and Nuclei in Gaseous and Condensed Matter," (in Russian) JINR Preprint P2-85-173, Dubna (1985).

[168] Th. SCHIEKEL, R. RÖSEL, U. HERPERS, I. LEYA, M. GLORIS, R. MICHEL, B. DITTRICH-HANNEN, P. W. KUBIK, H.-A. SYNAL, and M. SUTER, "Cross Sections for the p-Induced Production of Longlived Radionuclides for the Interactions of Cosmogenic Nuclides," pp. 344–346 in Ref. [3].

[169] B. DITTRICH, U. HERPERS, H. J. HOFMANN, W. WÖLFLI, R. BODERMANN, M. LÜPKE, R. MICHEL, P. DRAGOVITSCH, and D. FILGES, "AMS Measurements of Thin-Target Cross Sections for the Production of ^{10}Be and ^{26}Al by High-Energy Protons," *Nucl. Instrum. Methods B*, **52**, 588 (1990).

[170] E. M. RIMMER and P. S. FISHER, "Resonances in the (p,n) Reaction on ^{12}C," *Nucl. Phys. A*, **108**, 561 (1968).

[171] M. BLANN, *Alice Livermore 87 Code*, Private Communication (1987), Citation under Ref. [169].

[172] G. AUDI and A. H. WAPSTRA, "The 1993 Atomic Mass Evaluation (I). Atomic Mass Table," *Nucl. Phys. A*, **565**, 1 (1993); see also "The 1995 Update to the Atomic Mass Evaluation," *Nucl. Phys. A*, **595**, 409 (1995).

[173] P. MÖLLER, J. R. NIX, W. D. MYERS, and W. J. SWIATECKI, "Nuclear Ground-State Masses and Deformations," *Atomic Data and Nuclear Data Tables*, **59**, 185 (1995); see also J. DUFLO and A. P. ZUKER, "Microscopic Mass Formulas," *Phys. Rev. C*, **52**, R23 (1995).

[174] T. W. ARMSTRONG and K. C. CHANDLER, "HETC — A High Energy Transport Code," *Nucl. Sci. Eng.*, **49**, 110 (1972).

[175] G. A. LOBOV, N. V. STEPANOV, A. A. SIBIRTZEV, and Yu. V. TREBUKHOVSKI, "Statistical Simulation of Interaction of Hadrons and Light Nuclei with Nuclei. Intranuclear Cascade Model," (in Russian) ITEP Preprint

ITEP-91, Moscow (1983); see also A. A. SIBIRTZEV, N. V. STEPANOV, and Yu. V. TREBUKHOVSKI, "Interaction of Particles with Nuclei: Evaporation Model," (in Russian) ITEP Preprint ITEP-129, Moscow (1985); see also N. V. STEPANOV, "Statistical Simulation of High-Excited Nuclei Fission. I. Model Formulation," (in Russian) ITEP Preprint ITEP-81, Moscow (1987); see also N. V. STEPANOV, "Statistical Simulation of High-Excited Nuclei Fission. II. Calculation and Comparison with Experiment," (in Russian) ITEP Preprint ITEP-55, Moscow (1988).

[176] Th. SCHIEKEL, F. SUDBROCK, U. HERPERS, M. GLORIS, H.-J. LANGE, I. LEYA, R. MICHEL, B. DITTRICH-HANNEN, H.-A. SYNAL, M. SUTER, P. W. KUBIK, M. BLANN, and D. FILGES, "Nuclide Production by Proton-Induced Reactions on Elements ($6 \leq Z \leq 29$) in the Energy Range from 200 MeV to 400 MeV," *Nucl. Instr. Meth. B*, **114**, 91 (1996).

[177] M. BLANN, *AREL Code*, Private Communication (1996), Citation under Ref. [176].

[178] T. FUKAHORI had kindly supplied S. Mashnik with files: **/pub/he-benchmark/upto1gen/calc/al.alice-f**; **al.alice91**; **fe.alice-f**; **fe.alice91**; **mcexciton**; and **nucleus** with results of the recent JAERI Benchmark [62, 63].

[179] T. FUKAHORI, "ALICE-F Code System," pp.164–167 in Ref. [48]; see also T. FUKAHORI, "ALICE-F Calculation of Nuclear Data up to 1 GeV," *JAERI-M 92-039*, 114 (1992); see also S. PEARLSHTEIN, "Medium-Energy Nuclear Data Libraries: A Case Study, Neutron- and Proton-Induced Reactions in ^{56}Fe," *Astrophys. J.*, **346**, 1049 (1989). *Alice Livermore 87 Code*, Private Communication (1987), Citation under Ref. [169].

[180] *ALICE91 Code*, Private Communication (1991), Citation under Ref. [178].

[181] N. KISHIDA and H. KADOTANI, "On the Validity of the Intranuclear-Cascade and Evaporation Model for High-Energy Proton Induced Reactions," pp. 1209–1212 in Ref. [5]; see also Y. NAKAHARA and T. NISHIDA, "Monte Carlo Alogarithms for Simulating Particle Emission from Preequilibrium States During Nuclear Spallation Reactions," JAERI-M 86-074 (1986).

[182] F. BAROS and S. REGNIER, "Measurement of Cross Sections for ^{22}Na, $^{20-22}$Ne and $^{36-42}$Ar in the Spallation of Mg, Al, Si, Ca and Fe Production Ratios of some Cosmogenic Nuclides in Meteorites," *J. Phys. (Paris)*, **45**, 855 (1984).

[183] R. H. BIERI and W. RUTSCH, "Erzeugungsquerschnitte für Edelgase aus Mg, Al, Fe, Ni, Cu und Ag bei Bestrahlung mit 540 MeV Protonen," *Helv. Phys. Acta*, **33**, 553 (1962).

[184] K. GOEBEL, H. SCHULTES, and J. ZÄHRINGER, "Production Cross-sections of Tritium and Rare Gases in Various Elements," CERN-64-12, Geneve (1964).

[185] R. MICHEL, F. PEIFFER, S. THEIS, F. BEGEMANN, H. WEBBER, P. SIGNER, R. WIELER, P. CLOTH, P. DRAGOVITSCH, D. FILGES, and P. ENGELERT, "Production of Stable and Radioactive Nuclides in Thick Stony Targets (R=15 and 25 cm) Isotropically Irradiated with 600 MeV Protons and Simulation of the Production of Cosmogenic Nuclides in Meteorites," *Nucl. Instrum. Methods B*, **42**, 76 (1989).

[186] Y. TAKAO, Y. KANADA, S. ITADANI, T. TAKAHASHI, H. EIFUKU, M. MORINAGA, and A. IWASAKI, "Measurements of Helium Production Cross Sections of Aluminum Irradiated by Protons," pp. 226–232 in Ref. [18].

[187] O. F. NEMETS and Yu. V. GOFMAN, *Handbook of Nuclear Physics*, (in Russian) Naukova Dumka, Kiev (1975).

[188] M. C. LAGUNAS-SOLAR and R. P. HAFF, "Theoretical and Experimental Excitation Functions for Proton Induced Nuclear Reactions on $Z = 10$ to $Z = 82$ Target Nuclides," *Radiochimica Acta*, **60**, 57 (1993).

[189] M. BLANN and T. A. KOMOTO, "Alert I and II, Hauser-Feshbach Codes for Nuclei at High Excitation and Angular Momenta," LLNL Report # UCID-19390 (1982).

[190] H. TAKADA, Y. NAKAHARA, T. NISHIDA, K. ISHIBASHI, and N. YOSHIZAWA, "Microscopic Cross Section Calculations with NUCLEUS and HETC-3STEP," pp. 121–136 in Ref. [50].

[191] Dr. H. TAKADA had kindly sent S. Mashnik files with new and revised results, (as compared with the ones published in Ref. [190]) of calculations with the codes NUCLEUS [152] and HETC-3STEP [92].

[192] R. L. BRODZINSKI, L. A. RANCITELLI, J. A. COOPER, and N. A. WOGMAN, "High-Energy Proton Spallation of Iron," *Phys. Rev. C*, **4**, 1257 (1971).

[193] G. V. S. RAYUDU, "Formation Cross Sections of Various Radionuclides from Ni, Fe, Si, Mg, O, and C for Protons of Energies Between 130 and 400 MeV," *Can. J. Chem.*, **42**, 1149 (1964).

[194] G. V. S. RAYUDU, "Formation Cross Sections of Various Radionuclides from Ni, Fe, Si, Mg, O, and C for Protons of Energies Between 0.5 and 2.9 GeV," *J. Inorg. Nucl. Chem.*, **30**, 2311 (1964).

[195] M. HONDA and D. LAL, "Spallation Cross Sections for Long-Lived Radionuclides in Iron and Light Nuclei," *Nucl. Phys.*, **51**, 363 (1964).

[196] D. FINK, M. PAUL, G. HOLLOS, S. THEIS, S. VOGT, R. STUECK, P. ENGLARD, and R. MICHEL, "Measurements of ^{41}Ca Spallation Cross Sections and ^{41}Ca Concentrations in the Grant Meteorite by Accelerator Mass Spectrometry," *Nucl. Instr. Meth. B*, **29**, 275 (1987).

[197] K. F. CHACKETT, "Yields of Potassium Isotopes in High Energy Bombardments of Vanadium, Iron, Cobalt, Nickel, Copper and Zinc," *J. Inorg. Nucl. Chem.*, **27**, 2493 (1965).

[198] O. A. SCHAEFFER and J. ZÄEHRINGER, "High-Sensitivity Mass Spectrometric Measurements of Stable Helium and Argon Isotopes Produced by High-Energy Protons in Iron," *Phys. Rev.*, **113**, 674 (1959).

[199] A. CHENG, Thesis, Stony Brook (1972).

[200] M. BAKLOUTI, Thesis, Bordeaux (1975).

[201] S. REGNIER, M. BAKLOUTI, M. SIMONOFF-LAGARDE, and G. N. SIMONOFF, "Production of ^{36}Cl by High Energy Spallation," *Phys. Lett. B*, **68**, 202 (1977).

[202] A. K. LAVRUKHINA, R. I. KUZNETSOVA, and L. M. SATAROVA, "Rate of Formation of Radioactive Isotopes in Chondrites by Cosmic-Ray Reactions," *Geokhimya*, **12**, 1219 (1964) [*Geochemistry International*, **6**, 1129 (1964)].

[203] M. LÜPKE, R. MICHEL, B. DITTRICH, U. HERPERS, P. DRAGOVITSCH, D. FILGES, H. J. HOFMANN, W. WÖLFLI, "Proton-Induced Spallation Between 600 and 2600 MeV," pp. 702–704 in Ref. [4].

[204] G. M. RAISBECK, C. MENNINGA, R. BRODZINSKI, and N. WOGMAN, "Cross Sections for the production of ^{26}Al from Targets of Si, Al, and Fe Irradiated by Protons of 60 MeV," *Proc. 15th Int. Cosmic Ray Conf.*, Plovdiv, Bulgaria, August 13–26, 1977, vol. 2, p. 116, Bulgarian Academy of Science (1977).

[205] P. PAILLARD, "Production of ^{26}Al by Spallation of Fe, Si, Al Nuclei," (in French) Thesis (D. 3e Cycle), Centre d'Etudes Nucleares, Bordeaux-1 Univ. (1977).

[206] J. DEDIEUX, "Cross Section Measurements for Long-Lived Isotopes and their Interest in Astrophysics," (in French) Thesis (D. 3e Cycle) Centre d'Etudes Nucleares, Bordeaux-1 Univ. (1979).

[207] M. BLANN, *Overlaid ALICE Code*, CCO/3494-29, Rochester (1975).

[208] M. BLANN, *Alice Livermore 82 Code*, Private Communication (1982), Citation under Ref. [137].

[209] M. BLANN and V. P. LUNEV, "ALICE 87," pp. 161–163 in Ref. [48]; see also Reports UCID-19614, UCID-20169.

[210] E. BETAK, "PEQAG2 (extended)," pp. 168–170 in Ref. [48]; see also Report INDC(CSR)-016/LJ, IAEA, Vienna (1989); see also Report FU SAV 89/5, Inst. Phys., Bratislava (1989).

[211] M. V. KANTELO and J. J. HOGAN, "Charged-Particle Emission in Reactions of ^{90}Zr with 10–86 MeV Protons," *Phys. Rev. C*, **14**, 64 (1976); see also M. V. KANTELO, Ph. D. Thesis, McGill University, Montreal, Quebec, Canada (1975).

[212] Yu. V. ALEKSANDROV, S. K. VASILJEV, R. B. IVANOV, L. M. KRIZHANSKY, M. A. MIKHAILOVA, T. I. POPOVA, V. P. PRIKHODTZEVA, V. P. EISMONT, A. F. NOVGORODOV, and R. MISIAK, "Cross Section for Spallation Production of Radioactive Nuclides by 660 MeV Protons," *Izv. Rossiiskoi Akad. Nauk, ser. fiz.*, **59**, 206 (1995) [*Bull. Russian Acad. Sci.: Physics*, **59**, 895 (1996)]; see also Yu. V. ALEKSANDROV, V. P. EISMONT, R. B. IVANOV, L. M. KRIZHANSKY, M. A. MIKHAILOVA, T. I. POPOVA, V. P. PRIKHODTZEVA, S. K. VASILJEV, A. F. NOVGORODOV, and R. MISIAK, "Cross Section for the Production of Residual Radionuclides by Proton-Induced Spallation at 660 MeV Protons," pp. 371–373 in [3].

[213] M. BLANN, V. P. LUNEV, V. S. MASTEROV, and Yu. N. SHUBIN, "Effect of Gamma Emission Competition on the Excitation Function Description for the Reactions Induced by Medium Energy Nucleons," pp. 539–541 in Ref. [3].

[214] H. NIFENECKER and J. A. PINSTON, "High Energy Photon Production in Nuclear Reactions," *Annu. Rev. Part. Sci.*, **40** 113 (1990); see also "High Energy Gamma-Ray Production in Nuclear Reactions," *Prog. Part. Nucl. Phys.*, **23** 271 (1989).

[215] S. G. MASHNIK, Ye. S. GOLUBEVA, and A. S. ILJINOV, "Gamma Emission Calculations in the Cascade-Exciton Model," *Proc. Int. Conf. on Perspectives for the Interacting Boson Model on the Occasion of its 20th Anniversary*, Padova, Italy, June 13–17, 1994, R. F. CASTEN, A. VITTURI, A. B. BALANTEKIN, B. R. BARRETT, J. N. GINOCCHIO, G. MAINO, and T. OTSUKA, Eds., World Scientific, Singapore (1994), p. 726.

[216] P. FONG, *Statistical Theory of Nuclear Fission*, Gorgon and Breach Science Publishers, New York (1969).

[217] V. D. TONEEV, "Interaction of Fast Nucleons with Nuclei. III. Calculation of Nuclear Fission," (in Russian) *JINR Report B1-2812*, Dubna (1966) ; see also V. S. BARASHENKOV, V. M. MALTSEV, and V. D. TONEEV, "Interaction

of Fast Protons with Heavy-Nuclei," *Izv. AN SSSR, ser. fiz.*, **30**, 322 (1966) [*Bull. USSR Acad. Sci., Phys. Ser.*, **30**, 327 (1966)]; see also "Calculation of Fission of Nuclei Induced by Fast Particles," *Izv. AN SSSR, ser. fiz.*, **30**, 337 (1966) [*Bull. USSR Acad. Sci., Phys. Ser.*, **30**, 342 (1966)].

[218] V. S. BARASHENKOV and S. Yu. SHMAKOV, "Nuclear Fission Induced by High-Energy Protons," *JINR Communication E2-12902*, Dubna (1979).

[219] F. S. ALSMILLER, R. G. ALSMILLER, Jr., T. A. GABRIEL, R. A. LILLIE, and J. BARISH, "A Phenomenological Model for Particle Production from the Collisions of Nucleons and Pions with Fissile Elements at Medium Energies," *Nucl. Sci. Eng.*, **79**, 147 (1981); see also R. G. ALSMILLER, Jr., T. A. GABRIEL, J. BARISH, and F. S. ALSMILLER, "Neutron Production by Medium-Energy ($\leq$ 1.5 GeV) Protons in Thick Uranium Targets," *Nucl. Sci. Eng.*, **79**, 166 (1981).

[220] H. TAKAHASHI, "Analysis of Neutron Yields from High-Energy Proton Bombardment of Uranium Targets," *Nucl. Sci. Eng.*, **87**, 432 (1984)

[221] M. M. NESTEROV, V. F. PETROV and N. A. TARASOV, "The Role of Shell Effects in Fission of Nuclei by Fast Protons," *Yad. Fiz.*, **35**, 1131 (1982) [*Sov. J. Nucl. Phys.*, **35**, 662 (1982)].

[222] N. V. STEPANOV, "Statistical Simulation of Fission of Excited Atomic Nuclei. I. Model Formulation," *Institute of Theoretical and Experimental Physics (ITEP) Preprint 81*, Moscow (1987) (in Russian); see also "Statistical Simulation of Fission of Excited Atomic Nuclei. II. Calculation and Comparison with Experiment," *ITEP Preprint 55-88*, Moscow (1988) (in Russian).

[223] G. D. ADEEV, I. I. GONCHAR, V. V. PASHKEVICH, N. I. PISCHASOV, and O. I. SERDYUK, "Diffusion Model of Formation of Fission-Fragment Distributions," *Fiz. Elem. Chastits At. Yadra*, **19**, 1229 (1988) [*Sov. J. Part. Nucl.*, **19**, 529 (1988)]; see also I. I. GONCHAR, "Langevin Fluctuation-Dissipation Dynamics of Fission of Excited Atomic Nuclei," *Fiz. Elem. Chastits At. Yadra*, **26**, 932 (1995) [*Phys. Part. Nucl.*, **26**, 394 (1995)].

[224] G. D. ADEEV, A. S. BOTVINA, A. S. ILJINOV, M. V. MEBEL, N. I. PISCHASOV, and O. I. SERDYUK, "Method of Calculation of Mass-Energy Distributions of Fragments of Fission of Nuclei by Intermediate Energy Particles," *Preprint INR 816/93*, Moscow (1993).

[225] F. ATCHINSON, "Spallation and Fission in Heavy Metal Nuclei under Medium Energy Proton Bombardment," *Proc. Meeting on Targets for Neutron Beam Spallation Sources*, KFA Jülich, Germany, June 11–12, 1979, Report Jül-Conf-34, 17 (1980); see also "A Treatment of Fission for HETC," pp. 199–218 in Ref. [50].

[226] Y. NAKAHARA and T. TSUTSUI "NMTC/JAERI A Simulation Code System for High Energy Nuclear Reactions and Nucleon-Meson Transport Processes," *JAERI-M 82-198*, JAERI (1982) [in Japaness]; see also Y. NAKAHARA, "Evaluation of Computational Models for Fission and Spallation Reactions Used in Accelerator Breeding and Transmutation Analysis Code," *J. Nucl. Sci. Technol.*, **20**, 511 (1983).

[227] P. P. JAUHO, A. JOKINEN, M. LEINO, J. M. PARMONEN, H. PENTTILÄ, J. ÄYSTÖ, K. ESKOLA, and V. A. RUBCHENYA, "Isotopic Product Distributions in Near Symmetric Mass Region in Proton Induced Fission of ^{238}U," *Phys. Rev. C*, **49**, 2036 (1994).

[228] R. J. CHARITY, M. A. McMAHAN, G. J. WOZNIAK, R. J. McDONALD, L. G. MORETTO, D. G. SARANTITES, L. G. SOBOTKA, G. GUARINO, A. PANTALEO, L. FIORE, A. GOBBI, and K. D. HILDENBRAND, "Systematics of Complex Fragment Emission in Niobium-induced Reactions," *Nucl. Phys. A*, **483**, 371 (1988).

[229] J. CUGNON, "Nuclear Multifragmentation. Antiprotons versus Protons and Heavy Ions," *Yad. Fiz.*, **57**, 1705 (1994) [*Phys. At. Nucl.*, **57**, 1635 (1994)].

[230] D. H. E. GROSS and K. SNAPPEN, "Statistical Multifragmentation: Comparison of Two Quite Successful Models," *Nucl. Phys. A*, **567**, 317 (1994).

[231] J. P. BONDORF, A. S. BOTVINA, A. S. ILJINOV, I. N. MISHUSTIN, and K. SNEPPEN, "Statistical Multifragmentation of Nuclei," *Phys. Rep.*, **257**, 133 (1995).

[232] D. H. E. GROSS, "Statistical Decay of Very Hot Nuclei — the Production of Large Clusters," *Rep. Progr. Phys.*, **53**, 605 (1990).

[233] A. S. BOTVINA, A. S. ILJINOV, and I. N. MISHUSTIN, "Multifragmentation Breakup of Nuclei by Intermediate-Energy Protons," *Nucl. Phys. A*, **507**, 649 (1990).

[234] J. P. BONDORF, "Chaotic Fragmentation of Nuclei," *Nucl. Phys. A*, **387**, 25c (1982).

[235] J. CUGNON, "Possible Fragmentation Instability in a Nuclear Expanding Firebale," *Phys. Lett. B*, **135**, 374 (1984).

[236] W. A. FRIEDMAN, "Rapid Massive Cluster Formation," *Phys. Rev. C*, **42**, 667 (1990).

[237] N. SHIGYO, T. NAKAMOTO, and K. ISHIBASHI, "Fragmentation Cross Sections by HETC," pp. 272–277 in Ref. [12]; see also "Systematics of Fragmentation Reaction and their Incorporation into HETC," pp. 217–220 in Ref. [13]; see

also *J. Nucl. Sci. Technol.*, **32**, 1 (1995); see also N. SHIGYO, K. ISHIBASHI, and Y. WAKUTA, "Systematics of the Fragmentation Cross Sections for Incident Proton Energies up to 3 GeV," pp. 351–361 in Ref. [14]; see also S. SAKAGUCHI, K. ISHIBASHI, T. NAKAMOTO, Y. WAKUTA, and Y. NAKAHARA, "Systematics of the Fragmentation Cross Section for 1–3 GeV Proton Induced Spallation Reactions," pp. 237–248 in Ref. [16]

[238] A. Yu. KONOBEEV and Yu. A. KOROVIN, "Emission of ^{7}Be from Nuclei with Atomic Number $Z \geq 13$ by Intermediate Energy Protons," *Kerntechnik*, **60(4)**, 147 (1995).

[239] K. CHEN, Z. FRAENKEL, G. FRIEDLANDER, J. R. GROVER, J. M. MILLER, and Y. SHIMAMOTO, "VEGAS: A Monte Carlo Simulation of Intranuclear Cascades," *Phys. Rev.*, **166**, 948 (1968); see also G. D. HARP, K. CHEN, G. FRIEDLANDER, Z. FRAENKEL, and J. M. MILLER, "Intranuclear Cascade Studies of Low-Energy Pion-Induced Nuclear Reactions: Possible Effects of the Finite Lifetime of the (3,3) Isobar," *Phys. Rev. C*, **8**, 581 (1973); see also J. N. GINOCCHIO, "Deep Inelastic Pion-Induced Nuclear Reactions in the Isobar Model," *Phys. Rev. C*, **17**, 195 (1978).

[240] S. B. KAUFMAN and E. P. STEINBERG, "Cross-Section Measurements of Nuclides Formed by the Reaction of 0.20–6.0 GeV Protons," *Phys. Rev. C*, **22**, 167 (1980).

[241] H. W. BERTINI, "Nonelastic Interactions of Nucleons and π Mesons with Complex Nuclei at Energies Below 3 GeV," *Phys. Rev. C*, **6**, 631 (1972).

[242] K. ISHIBASHI, H. TAKADA, T. SAKAE, Y. NAKAHARA, and T. NISHIDA, "Improvement on Intranuclear Cascade Model Calculation for an Energy Range 500–1000 MeV," pp. 1143–1146 in Ref. [5].

[243] E. SUETOMI, N. KISHIDA, and H. KADOTANI, "An Analysis of the Intranuclear Cascade Evaporation Model with In-Medium Nucleon-Nucleon Cross Sections," *Phys. Lett. B*, **333**, 22 (1994).